

An exploration of neural network activity within the limb-associated somatosensory cortex of the healthy and stroke injured brain of mice

by

Mischa V. Bandet

A thesis submitted in partial fulfillment of the requirements for the degree of

Doctor of Philosophy

Neuroscience
University of Alberta

© Mischa V. Bandet, 2022

Abstract

Altered somatosensation is a hallmark of incomplete recovery from stroke. Although the basic mechanisms of limb-associated somatosensation have been well studied in primates, comparatively little literature exists on the limb-associated somatosensory system of rodents. Rodent models are the primary animal models used to study post-stroke plasticity and cortical network function. Further study into the basic function of the limb-associated somatosensory system in the healthy and stroke injured brain of rodents may provide insight into therapeutic targets to improve recovery after stroke. The data presented in this thesis contributes to the literature by defining the response properties of the limb-associated somatosensory cortex of mice to various frequencies of mechanical stimuli often used in stroke research without prior knowledge on the expected cortical responses in the uninjured brain. It further elucidates longitudinal changes in cell activity, functional connectivity, and neural network architecture in the peri-infarct and distal regions of the limb-associated somatosensory cortex of awake behaving head-fixed mice after stroke.

The somatosensory cortex of mice has often been a focus for studies measuring the effect of stroke on sensory-evoked cortical activation. Most of these studies have looked at widescale activity across the entire limb-associated somatosensory cortex as a marker of post-stroke plasticity and changes in cortical excitability. A limited number of studies have looked at changes in the activity of individual neurons post-stroke within the limb associated somatosensory cortex. However, these studies have not thoroughly defined why the particular stimulation parameters were chosen, if the somatosensory cortex of mice can reliably respond to the multi-modal features of the stimuli, and if the cortical representations of the stimuli would

change based on different stimulus frequencies or durations. The goal of Chapter 2 of this thesis was to assess if the somatosensory cortex of mice can differentially represent distinct stimuli with unique patterns of activity, even if they have overlapping features, and provide fundamental insight into sensory-evoked response properties of the limb-associated somatosensory cortex that can be applied to future studies examining these same patterns after stroke. To do this, we utilized widefield flavoprotein autofluorescence imaging to map the somatosensory cortex of anesthetized C57BL/6 mice, then used *in vivo* two-photon Ca^{2+} imaging to define patterns of neuronal activation during mechanical square-wave stimulation of the contralateral forelimb or hindlimb at various frequencies from 3-300Hz. We discovered that the variation in cortical response to different square-wave stimuli can be represented by the population pattern of supra-threshold Ca^{2+} transients, the magnitude and temporal properties of the evoked activity, and the structure of the stimulus-evoked correlation between neurons.

After having studied the representation of artificial mechanical limb stimuli in the limb-associated somatosensory cortex of the uninjured brain, we shifted to a model in which we could repeatedly measure network activity of the limb-associated somatosensory cortex at the single neuron level over the course of recovery from focal forelimb stroke. We noted that despite substantial recent progress in mapping the trajectory of network plasticity resulting from focal ischemic stroke, questions remained about the state of neuronal excitability and activity within the peri-infarct cortex of mice. Mounting evidence pointed to a deficit in sensory-evoked cortical activation after stroke despite multiple markers of impaired inhibitory neurotransmission and a potential for epileptogenic hyperexcitability. However, most of these findings had come from anesthetized animals, acute tissue slices, or immunoassays on extracted tissue and may not

reflect cortical activity dynamics in the intact, awake cortex after stroke. To provide further insight on this discrepancy, we used *in vivo* two-photon Ca^{2+} imaging of awake head-fixed mice in a floating homecage at baseline and weekly for 2 months to longitudinally examine patterns of neural activity, network functional connectivity, and neural assembly architecture within the peri-infarct and distal cortex. We combined these observations with behavioral testing on a tapered beam task, string pull task, and in monitoring animal movement within the mobile homecage during imaging to monitor behavioral recovery in concert with the weekly imaging sessions. In Chapter 3, we provided the first evidence of a significant deficit in neural network functional connectivity and assembly architecture concurrent with a trend towards reduced neuronal firing within the peri-infarct cortex 1 week after stroke. We could not detect these network deficits a short distance outside the peri-infarct cortex in the distal region. Finally, we demonstrated that deficits in peri-infarct neural function and network architecture occur concurrently with a transient behavioral deficit in the tapered beam task within the same timeframe.

In summary, the work presented in this thesis elucidates patterns by which different frequencies of artificial sensory stimuli applied to the limbs are represented within the mouse limb-associated somatosensory cortex under anesthetized conditions in the uninjured brain. It further reveals longitudinal alterations to cortical network activity and functional network structure within the peri-infarct cortex after a focal photothrombotic stroke to the forelimb somatosensory cortex. These data increase our knowledge on the basic function of the limb-associated somatosensory cortex in the healthy and injured cortex of mice, and provide insight at the neural network and behavioral level for the plastic recovery of network function after stroke.

Preface

This thesis is an original work by Mischa V. Bandet. All animal research was conducted in accordance with Canadian Council on Animal Care guidelines. All animal use protocols were approved by the University of Alberta Animal Care and Use Committee (AUP361).

Chapter 2 of this thesis has been published as M.V. Bandet, B. Dong, and I.R. Winship (2021) “Distinct patterns of activity in individual cortical neurons and local networks in primary somatosensory cortex of mice evoked by square-wave mechanical limb stimulation”. PLoS ONE, 16(4): e0236684. doi: 10.1371/journal.pone.0236684. B. Dong and I were responsible for surgical preparations. I was responsible for the data collection and analysis as well as the manuscript composition. I.R. Winship was the supervisory author and was involved with experimental design, concept formation, manuscript composition and manuscript edits.

For data presented in Chapter 3, I was involved in concept formation, data collection, analysis, and manuscript composition. I.R. Winship was the supervisory author and gave feedback on concept formation, experimental design, and was involved in manuscript edits.

Acknowledgments

First and foremost, my deepest gratitude and thanks goes out to my supervisor, Dr. Ian Winship, for his guidance, patience and encouragement throughout my PhD. To my committee members, Dr. Clayton Dickson and Dr. Simon Gosgnach, for their questions and comments that stumped me at times, but ultimately led to my growth as a scientist and researcher. I extend thanks to my past and present lab mates, Bernice, Sam, Anna, Eszter, Junqiang, John (Wes), Somnath, Hossein, Sima, Celestina, Ron, Faith, Grant, Rayyan, and An for their support, curiosity and friendship throughout the course of my graduate studies. Finally, I want to thank my family for their constant and unconditional support and encouragement throughout the years; I couldn't have done this without them.

Table of Contents

Abstract	ii
Preface	v
Acknowledgments	vi
List of Figures	xi
List of Abbreviations and Symbols	xiii
Chapter 1: An introduction to stroke, the limb-associated somatosensory system, and plastic changes in the structure and function of the post-stroke brain	1
Our current understanding of the limb-associated somatosensory pathway in the undamaged brain	4
Cutaneous afferents and their associated mechanoreceptors	5
Proprioceptive afferents and their associated mechanoreceptors	7
Subcortical pathways on the way to the primary somatosensory cortex	8
Cortical areas involved in somatosensory processing	11
Multimodal interactions within somatosensory cortical areas.....	17
Structural plasticity within post-stroke cortical networks	21
The role glutamate and its ionotropic receptors in post-stroke plasticity	25
The role GABA and its ionotropic receptors in post-stroke plasticity	29
Post-stroke regional and cellular remapping, and alterations in functional activation	35
Deficits in sensory-evoked somatosensory activity despite purported network hyperexcitability after stroke	38
Thesis outline and aims	43

Chapter 2: Distinct patterns of activity in individual cortical neurons and local networks in primary somatosensory cortex of mice evoked by square-wave mechanical limb stimulation45

Abstract..... 46

Introduction..... 47

Materials and Methods..... 50

 Animals 50

 Identification of forelimb and hindlimb somatosensory cortex representations..... 50

 Calcium imaging 52

 Two-photon image processing and determination of responding neurons 54

 Stimulus-evoked cell-cell correlation analysis 56

 Statistical analysis..... 57

Results 58

 Stimulus frequency preference within somatosensory cortex neurons..... 58

 Patterns of activation to somatosensory stimuli within S1 cortex are distinct 59

 Mean population Ca²⁺ response characteristics do not scale linearly with the number of oscillations in a stimulus..... 60

 Stimulus-evoked pairwise correlations vary as a function of the square-wave stimulus frequency..... 61

 Frequency or quantity representations in cortical Ca²⁺ transients 63

 Longer stimuli evoke more consistent patterns of activity in somatosensory neuronal networks 64

Discussion..... 66

Chapter 2: Figures 73

Chapter 3: Photothrombotic stroke is associated with reduced cortical activity, deficits in functional connectivity and alterations in neural assembly architecture at early time points within the peri-infarct cortex as measured in awake behaving animals.....90

Abstract..... 91

Introduction..... 92

Methods..... 96

Animals 96

Chronic cranial window implantation..... 96

Tapered beam task habituation, testing and analysis 97

String pull task habituation, testing and analysis..... 98

Mobile floating homecage habituation and measurement of movement parameters 100

Identification of forelimb and hindlimb somatosensory cortex representations using widefield Ca²⁺ imaging of sensory-evoked responses 101

Calcium imaging..... 102

Photothrombotic stroke and sham procedure..... 103

Two-photon image processing and analysis of neuronal activity 103

Ca²⁺ trace deconvolution to determine neuron firing..... 104

Neuron-neuron correlation analysis and functional connectivity 104

Determination of neural assemblies and their activity patterns 105

Statistical analysis..... 106

Results 107

Photothrombotic stroke results in forelimb representation remapping onto adjacent areas of cortex and altered sensory-evoked widefield Ca²⁺ response properties at 8 weeks post-stroke..... 108

Behavioral tracking in the mobile homecage does not detect a deficit after stroke 110

Tapered beam task depicts a transient behavioral deficit at 1 week post-stroke 111

String pull task does not detect a behavioral deficit after stroke 111

Neuron firing rate trends towards a transient decrease at 1 week post-stroke in the peri-infarct imaging region..... 113

Average neuron correlation with animal movement is not altered by stroke	114
Neural population functional connectivity measurements indicate a transient loss of functional connections and connection strength at 1 week post-stroke in the peri-infarct imaging region	116
Neural assembly architecture is affected at 1 week post-stroke in the peri-infarct imaging region	117
No detectable change in the correlation between assembly activations and movement after stroke	119
Correlation among neural assemblies is increased in the peri-infarct imaging region after stroke.....	120
Discussion.....	121
Chapter 3: Figures	134
Chapter 4: Conclusions	161
References	171

List of Figures

Figure 2.1. Imaging protocols and experimental methods	74
Figure 2.2. Neuronal and population response selectivity to stimulus frequency within the limb associated somatosensory cortex	76
Figure 2.3. Mean population Ca ²⁺ response characteristics do not scale linearly with the number of oscillations in a stimulus	78
Figure 2.4. Stimulus-evoked pairwise correlations vary as a function of the stimulus frequency	80
Figure 2.5. Frequency or quantity representations in cortical Ca ²⁺ transients	82
Figure 2.6. Longer stimuli evoke more consistent patterns of activity in somatosensory neuronal networks	84
Figure S2.1. Visual example of the structural similarity (SSIM)-based method for trial-by-trial comparisons of correlational map similarity	86
Figure S2.2. Short duration, high frequency stimuli lead to differential cortical activity from long duration, low frequency stimuli	88
Figure 3.1. Experimental timeline and methods	135
Figure 3.2. Photothrombotic stroke results in forelimb representation remapping onto adjacent areas of cortex and altered sensory-evoked widefield Ca ²⁺ response properties at 8 weeks post-stroke	137
Figure 3.3. Behavioral tracking in the mobile homepage does not detect a deficit after stroke	139
Figure 3.4. Tapered beam task depicts a behavioral deficit at 1 week post-stroke.....	141
Figure 3.5. String pull task does not detect a behavioral deficit after stroke	143
Figure 3.6. Example Ca ²⁺ deltaF/F ₀ traces and spike rasters for a peri-infarct imaging region depicting a transient decrease in firing at 1 week post-stroke	145
Figure 3.7. Neuron firing rate trends towards a decrease at 1 week in the peri-infarct imaging region after stroke	147
Figure 3.8. Average neuron correlation with animal movement is not detectably altered by stroke	149
Figure 3.9. Example cellular GCaMP6S Ca ²⁺ fluorescence images and population functional	

connectivity plots	151
Figure 3.10. Neural population functional connectivity measurements indicate a loss of functional connections and connection strength at 1 week post-stroke in the peri-infarct imaging region	153
Figure 3.11. Neural assembly architecture is affected at 1 week post-stroke in the peri-infarct region	155
Figure 3.12. Correlation between assembly activations and movement is not detectably affected by stroke	157
Figure 3.13. Correlation among neural assemblies is increased in the peri-infarct region	159

List of Abbreviations and Symbols

ACSF: Artificial cerebral spinal fluid
AMPA: α -amino-3-hydroxy-5-methyl-4-isoxazolepropionic acid
APC: Anterior parietal cortex
ATP: Adenosine tri-phosphate
AUC: Area under the curve
BDNF: Brain derived neurotrophic factor
BOLD: Blood oxygen level dependent
CCAO: Common carotid artery occlusion
cFL: Contralateral forelimb
cHL: Contralateral hindlimb
CNS: Central nervous system
CSF: Cerebral spinal fluid
DCN: Dorsal column nuclei
DMSO: Dimethyl sulfoxide
EEAC1: Excitatory amino acid carrier 1
EPSP: Excitatory post-synaptic potential
ET-1: Endothelin-1
FA: Flavoprotein autofluorescence
FL: Forelimb
GABA: Gamma aminobutyric acid
GABA_AR: GABA_A receptor
GAT: GABA transporter
GECI: Genetically encoded calcium indicator
GEVI: Genetically encoded voltage indicator
GLT-1: Glutamate transporter-1
GTO: Golgi tendon organ
HL: Hindlimb
ICA: Internal carotid artery
IOS: Intrinsic optical signal imaging

ISI: Interstimulus interval
KCC2: K-Cl (Potassium Chloride) Cotransporter 2
LPC: Lateral parietal cortex
LTP: Long-term potentiation
M1: Primary motor cortex
MCA: Middle cerebral artery
MCAO: Middle cerebral artery occlusion
MP: Multi-photon
MRNA: Messenger ribonucleic acid
NMDA: N-methyl-D-aspartate
OGB-1: Oregon green BAPTA-1
OGD: Oxygen-glucose deprivation
PC: Pacinian Corpuscle
PCA: Principle component analysis
PM: Parietal medial area
PPC: Posterior parietal cortical area
PV: Parvalbumin
PVA: Parietal ventral area
RA1: Rapidly adapting type 1
RA2: Rapidly adapting type 2
RFs: Receptive Fields
ROIs: Regions of interest
S1: Primary somatosensory
S2: Secondary somatosensory cortex
SA1: Slowly adapting type 1
SA2: Slowly adapting type 2
SEM: Standard error mean
SD: Standard deviation
SMA: Supplementary motor area
SOM: Somatostatin
SR101: Sulforhodamine 101

SSIM: Structural similarity index

TCR: Thalamocortical relay

VGAT: Vesicular GABA transporter

VIP: Vasoactive intestinal peptide

VPL: Ventroposterior lateral

VPS: Ventroposterior superior

VSD: Voltage sensitive dye

Chapter 1: An introduction to stroke, the limb-associated somatosensory system, and plastic changes in the structure and function of the post-stroke brain

Over 15 million people across the globe suffer a stroke each year (Ding et al., 2021; Feigin et al., 2014). In North America, stroke is the leading cause of acquired adult disability and the third leading cause of death (Murphy and Corbett, 2009). Current rehabilitative therapies permit only limited functional recovery, and up to 94% of stroke survivors continue to experience sensory motor deficits despite these rehabilitative therapies (Carey et al., 1993; Julkunen et al., 2005). Cortical damage and dysfunction from stroke results from disturbances of blood flow to the brain (Doyle et al., 2008; Green, 2003; Hossmann, 2006). Stroke may be global, such that blood flow is disrupted to the entire brain, or focal, such that only a localized area of the brain is damaged. Strokes can be classified as hemorrhagic or ischemic. Hemorrhagic strokes are far less common than ischemic and occur when an artery in the brain ruptures or leaks (Green, 2003). Ischemic stroke accounts for approximately 87% of all stroke cases and results from vascular occlusion due to a blood clot (Virani et al., 2021). Mortality rate for ischemic stroke at thirty-days has been estimated at around 15% in high income countries (Feigin et al., 2009; Ganesh et al., 2016; Gattringer et al., 2019; Saposnik et al., 2011). Despite decades of research into new therapeutics targeted at neuroprotection during stroke or augmenting post-stroke plasticity and recovery, few have shown strong clinical success in human patients (Kuriakose and Xiao, 2020). Indeed, the gold standard treatment leading to the least pathophysiology remains attempting to reperfuse cortical tissue within the first 6 hours of stroke onset (Jones and Adkins, 2015; Saver and Yafeh, 2007), a timeframe when the treatment is most effective and least likely to lead to hemorrhagic transformation (Adeoye et al., 2011; Fang et al., 2010). This is, however, dependent on the stroke being discovered within the short treatment window, and reperfusion therapies being clinically accessible (Fang et al., 2010; Kuriakose and Xiao, 2020). Unfortunately, only approximately 15-32% of patients arrive to the hospital within

a 3 hour window of symptom onset, and only 40-50% are eligible for thrombolytic therapy (Fang et al., 2010). Thus, most stroke survivors are left with permanent brain injury that accounts for their chronic disability. Upper limb disability is one of the most common persistent impairments after stroke. In human stroke patients, damage to the somatosensory cortex leads to impairments that include the inability to sense vibration frequency, object texture, and direction of movement across the skin. Many also present with deficits in stimulus localization due to enlarged receptive field sizes, inability to identify shape and form by touch (stereognosis), and with impaired proprioception (Carey and Matyas, 2011; Connell et al., 2008; Kwakkel et al., 2004; Patel et al., 2000; Tyson et al., 2008). Combinations of these deficits often lead to a decrease in the ability to control fine aspects of motor behavior, such as skilled movement of the hand and arm necessary for reaching and grasping movements (Carey and Matyas, 2011; Connell et al., 2008; Kwakkel et al., 2004; Patel et al., 2000; Tyson et al., 2008). Fortunately, the nervous system has the capacity to partially compensate for injury via “adaptive plasticity” (Carmichael, 2006; Murphy and Corbett, 2009; Winship and Murphy, 2009). Understanding the basic properties of the somatosensory system in the healthy brain and the adaptive plasticity that alters the brain’s function and connectivity after stroke has tremendous clinical value for the development of new therapies to augment brain repair, reduce impairment and improve rehabilitation. While the fundamental mechanisms of sensory processing within the limb-associated somatosensory cortex have been well studied in non-human primates, little information exists on the sensory processing of somatic stimuli within the limb-associated somatosensory cortex of rodents, the primary animal model used for stroke research. Furthermore, minimal research exists on how stroke alters patterns of neural activity within the limb-associated somatosensory area of awake behaving rodents. An understanding of the limb-

associated somatosensory pathway in both the undamaged and injured brain may be critical to understand the adaptive processes that lead to recovery.

Our current understanding of the limb-associated somatosensory pathway in the undamaged brain

The pathway for limb-associated somatosensation has primarily been studied in non-human primates. Although the vibrissae somatosensory system of rodents has been extensively examined (for review, see (Adibi, 2019; Ebner and Kaas, 2015; Petersen, 2019)), the limb-associated somatosensory pathway of mice is comparatively poorly studied. Our proprioceptive sense allows us to know the position of the limbs in space and maintain posture, whereas our tactile sense provides information on object contact and shape. Dynamic interactions between the skin and objects, combined with proprioceptive information, is a necessity for the complex use of tools and optimal mobility within our environment. In both proprioceptive and tactile sensation, mechanoreceptors found within the limbs are activated by the deformation of skin, muscles, tendons, ligaments or joints and relay the properties of those deformations via peripheral nerves to the central nervous system (CNS). Within the CNS, the important elements of these peripheral signals give rise to percepts of our body and the external environment to inform the progression of motor commands during behavior. Indeed, human patients with a deficit in somatosensation due to large-fiber sensory neuropathy are known to show movement deficits, especially those related to multi-joint coordination (Sainburg et al., 1995). Furthermore, the elimination of tactile sensation via local anesthetic delivered to the skin severely impairs the ability for object grasping and manipulation (Augurelle et al., 2003; Johansson and Flanagan, 2009; Witney et al., 2004).

Cutaneous afferents and their associated mechanoreceptors

To understand sensory-evoked activation patterns of the limb-associated somatosensory cortex and how stroke may affect these patterns, an understanding of the mechanoreceptors that generate signals at the periphery, and the afferent pathways that modulate these signals as they pass through the somatosensory hierarchy, is required. Most tactile and proprioceptive fibers, other than pain associated c-tactile fibers, are large, myelinated, and have high conduction velocities necessary for rapidly fine-tuning motor behavior. On the glabrous skin, four classes of mechanoreceptors and their associated fibers are present and are split into two categories. Slowly adapting afferents maintain a sustained response to continual skin indentation, with activity that declines slowly over time. Rapidly adapting afferents respond only to onset and offset of an indentation. Slowly adapting type 1 (SA1) fibers branch and innervate multiple clusters of Merkel receptors found in close proximity to the surface of the skin with small receptive fields (Nakatani et al., 2015). As a population, SAI afferents convey information related to bars, edges, gratings, and stationary or slow moving textural properties of a stimulus (Johansson et al., 1982a; Phillips and Johnson, 1981). Rapidly adapting type 1 (RA1) fibers innervate multiple Meissner's corpuscles with small receptive fields. Each Meissner's corpuscle receives convergent input from multiple RA1 fibers, resulting in complex receptive fields (Cauna, 1956; Cauna and Ross, 1960; Nolano et al., 2003). RA1 afferents are tuned to dynamic deformation of the skin at intermediate frequencies between 5-50Hz, and are silent during sustained skin deformation (Freeman and Johnson, 1982a; Johansson et al., 1982b; Muniak et al., 2007). RA1 fibers convey a poorly defined spatial image of patterns indenting the skin (Phillips et al., 1992), and as a population convey information related to stroking, slip and flutter across the dermal surface (Delhayé et al.,

2018). Slowly adapting type 2 (SA2) fibers innervate individual Ruffini corpuscles found deep within the skin. SA2 fibers have large receptive fields and respond to tension and skin stretch that activate Ruffini corpuscles within the deep skin (Knibestöl, 1975). SA2 fibers also densely innervate Ruffini corpuscles found within the border of fingernails in humans to sense tension applied by the fingertips (Birznieks et al., 2009). Rapidly adapting type 2 (RA2) fibers innervate a single Pacinian corpuscle each. RA2 fibers have large receptive fields stemming from the Pacinian corpuscle's depth under the skin surface and from their exquisite sensitivity to rapid, submicron-scale vibrations (40-400Hz) propagating from large distances across the skin surface (Bell et al., 1994; Freeman and Johnson, 1982a; Johansson et al., 1982b; Muniak et al., 2007). RA2 fibers convey information related to surface texture as surfaces are swept across the skin (Weber et al., 2013) and mediate somatosensation of vibrations at a distance during tool use (Brisben et al., 1999). The cutaneous modalities of rodents are believed to be largely homologous to those of primates, however with less densely populated glabrous skin and with more contribution from hair follicles covering the majority of the rodent body (Ebner and Kaas, 2015). It has also recently been shown in mice that Pacinian Corpuscles are sparsely present, and primarily found within the deep tissue associated with joints and bones (Prsa et al., 2019). Hair follicle afferents convey information on hair bending with rapidly adapting responses and large receptive fields for the relatively crude localization of stimuli on the hairy skin (Abraira and Ginty, 2013; Vallbo et al., 1995), and C-tactile afferents from hairy skin are also thought to play a role in affective touch (Ackerley et al., 2014; Löken et al., 2009).

Proprioceptive afferents and their associated mechanoreceptors

Afferent information from proprioceptive pathways is a necessity for the control of the limbs, coordination of multi-joint movements and for the maintenance of posture (Sainburg et al., 1995). Indeed, case reports in human stroke patients of selective thalamic damage that impairs the transmission of proprioceptive information to the cortex indicates symptoms that included contralesional weakness and an inability to walk, despite normal tactile sensation of the skin (Gutrecht et al., 1992; Sacco et al., 1987). In mice, the absence of proprioceptive afferent information has also been shown to cause deficits in limb coordination and locomotion (Akay et al., 2014). Three groups of proprioceptive afferents sense muscle and joint movements. Primary and secondary spindle afferents innervate intrafusal muscle spindle fibers. Primary spindle afferents are more sensitive to dynamic length changes, whereas secondary spindle afferents are more sensitive to continual muscle tension (Cheney and Preston, 1976; Edin and Vallbo, 1990a). Due to muscle spindle innervation by gamma motor fibers, the responsiveness of spindle afferents can be tuned during active movements based on behavioral demands (Dimitriou and Edin, 2008a, 2008b). Golgi tendon organ (GTO) afferents respond to tension within the tendon and respond vigorously during isometric contractions and with muscle stretching (Edin and Vallbo, 1990a, 1990b; Matthews, 1933). Joint receptor afferents innervate the joint capsule and nearby ligaments where they sense pressure applied to the joint, joint movements, and dynamic pressure changes due to contraction of muscles inserting into the capsule (Grigg and Greenspan, 1977). Ruffini-like corpuscles, Pacinian-like corpuscles, and Golgi organs located in the ligaments give rise to afferent signals in the joint receptor afferents (Zimny, 1988). Joint afferents are thought to primarily be involved in sensing impending joint damage as they exhibit

slowly adapting responses primarily when the joint is in hyperextension or hyperflexion, and therefore may play a very minor role in active proprioception (Burke et al., 1988; Grigg and Greenspan, 1977). Similar to primates, rodents have muscle spindles, GTOs, and joint associated Ruffini corpuscles subserving their proprioceptive sense (Ebner and Kaas, 2015).

Subcortical pathways on the way to the primary somatosensory cortex

To understand sensory-evoked cortical activation and the representation of somatic stimuli in the somatosensory cortex, it is necessary to understand how these signals are first modulated in subcortical structures prior to reaching the primary somatosensory (S1) cortex. Although it was once believed that multimodal somatosensory information was primarily segregated within subcortical pathways on the way to the neocortex, it is now believed that many subcortical structures may be activated by complex multimodal combinations of somatic information before transmitting a modulated form of the information that they received to higher order sensory structures (Jörntell et al., 2014). Indeed, interneurons within the spinal cord may be the first point where a degree of multimodal convergence from the limbs occurs (Abraira and Ginty, 2013; Bourane et al., 2015; Bui et al., 2015; Johansson and Flanagan, 2009; Jörntell et al., 2014; Kim et al., 2015; Li et al., 2011; Shishido and Toda, 2017). Axons of afferent fibers from the dorsal root ganglia terminate on three different locations. They may terminate onto alpha motor neurons or interneurons at the same level of the spinal cord, higher and lower nearby levels of the spinal cord, or they can ascend in somatotopically organized fascicles in the dorsal column tract (Smith and Deacon, 1984). S1 cortex is believed to only be activated by inputs from the dorsal column tracts as complete lesions of the dorsal columns leads to an abolishment of S1

activation (Jain et al., 1997; Makous et al., 1996). Sensory integration in these spinal interneurons plays a role not only in reflex loops within the spinal cord, but also in the modulation of motor neurons that receive corticospinal innervation (Bui et al., 2015). Indeed, loss of different populations of spinal interneurons that integrate tactile signals leads to distinct deficits in motor control on different tasks (Bourane et al., 2015; Bui et al., 2013, 2015). A subset of spinal interneurons, dI1, project via the spinocerebellar tracts to feedback sensory information to the cerebellum for correcting movement and for motor learning (Bui et al., 2015). Afferents projecting rostrally from spinal interneurons follow the dorsal column tract or the dorsolateral tracts (spinomedullothalamic and spinocervicothalamic) and also synapse within the dorsal column nuclei (Delhaye et al., 2018), thereby suggesting they may play a role in the modulation of afferent signals within higher order subcortical and cortical structures as afferent information flows towards the cortex.

The dorsal column nuclei (DCN) are the first major station for receiving and processing somatosensory afferents, mainly those from first order sensory afferents emanating from the dorsal root ganglion. The cuneate nucleus and external cuneate nucleus receive projections from the upper body and the gracile nucleus receives projections from the lower body. Cutaneous afferents from the upper body are believed to synapse primarily on the cuneate nucleus, whereas proprioceptive inputs are believed to synapse primarily on the external cuneate nucleus (Dykes et al., 1982; Fyffe et al., 1986; Hummelsheim et al., 1985). The DCN are somatotopically organized along the mediolateral axis from lower limb to head (Xu and Wall, 1996, 1999). Similar to primates, afferents from muscle spindles and joints of the forelimb (FL) in rodents travel via the cuneate fasciculus to the external cuneate nucleus (Bolton and Tracey, 1992; Li et

al., 2012), whereas proprioceptive afferents of the hindlimb (HL) leave the gracile fasciculus at thoracic levels to terminate in Clark's column – the dorsal nucleus of the spinal cord – prior to ascending and innervating nucleus Z rostral to the gracile nucleus, as well as the cerebellum (Li et al., 2012; Low et al., 1986). Similar to primates, dorsal column transection in rodents highly diminishes the responsiveness of neurons within the dorsal column nuclei as well as contralateral somatosensory cortex to FL and HL stimulation (Massey et al., 2006), and leads to impairments in behavioral tasks requiring reaching and grasping (Kaas et al., 2008; McKenna and Whishaw, 1999).

Neurons of the DCN were once believed to be simple relays with efferents being sent to the contralateral ventroposterior complex of the thalamus via medial lemniscal projections (Rasmussen and Peyton, 1948). More recently, it's been shown that cuneate neurons undertake feature extraction of somatic information (Bengtsson et al., 2013; Hayward et al., 2014; Jörntell et al., 2014). DCN neurons also receives modulatory descending input from the sensorimotor cortex (Bentivoglio and Rustioni, 1986; Cheema et al., 1983). During active touch, descending fibers provide an efference copy, also named corollary discharge, to subcortical networks, thereby allowing the somatosensory system to differentiate somatic signals of active from passive touch (Brooks and Cullen, 2019; Claxton, 1975; Gurtubay-Antolin et al., 2018; Nelson, 1996; Yu et al., 2016). Thus, the DCN can be seen as the first major neuronal structure that undertakes a representational processing of somatosensory information prior to sending that modified information to the thalamus.

Within the primate thalamus, the ventroposterior lateral (VPL) nucleus receives primarily

cutaneous input from the cuneate nucleus, whereas the ventroposterior superior (VPS) nucleus receives primarily proprioceptive input (Krubitzer and Kaas, 1992). These inputs are somatotopically organized and mapped (Qi et al., 2011). Their projections to other brain regions are highly convergent, divergent, and are modulated by cortical feedback from cortical S1 neurons (Alitto and Usrey, 2003; Alloway et al., 2008, 2009; Briggs and Usrey, 2008; Kaas, 2004; Künzle, 1977; Smith et al., 2022), thereby demonstrating that thalamic sensory neurons are also more than simple relay stations for sensory afferents. However, neurons in the somatosensory thalamic areas do not seem to be modulated by high level processing features such as attention or the demands of cognitive tasks, unlike neurons of the primary somatosensory cortex (Bushnell and Duncan, 1987; Camarillo et al., 2012; Chapman et al., 1987; Vázquez et al., 2012). Similar to primates, rodents display a VPL and VPS nucleus, however the VPL can further be divided into 3 zones in rodents; a rostral zone, that shows mainly proprioceptive/large receptive fields (RFs) related to muscle and joint movement, a middle zone, that has small precise somatotopic RFs related to cutaneous sensation input via the lemniscal pathway, and a caudal zone, that has large RFs that include both somatotopic touch and visceral pain inputs (Francis et al., 2008). Within all regions of the ventroposterior thalamus, however, it's often noted that many cells are responsive to both touch and noxious stimuli (Guilbaud et al., 1980).

Cortical areas involved in somatosensory processing

After somatosensory information has undergone subcortical modulation while passing through the dorsal column nuclei and thalamus, it is sent via thalamocortical fibers to the primary somatosensory cortex. To understand the representation of these modulated signals in the cortical

hierarchy of the healthy brain, and how these representations may be disrupted by stroke, it is necessary to understand how sensory features are parcellated and/or combined in hierarchical somatosensory areas. Importantly, the primate brain is notably different in its parcellation of somatic signals in comparison to what is known of the rodent brain, and as such the representation of afferent signals in S1 cortex between the species likely dissimilar. In primates, the anterior parietal cortex (APC) is the primary recipient of tactile and proprioceptive signals from the periphery. The APC in primates contains four cytoarchitectonically defined areas; Areas 3a, 3b, 1 and 2. Neurons in area 3a are responsive primarily to proprioceptive information (Iwamura et al., 1985, 1993; Krubitzer et al., 2004; Taoka et al., 2000). RFs in area 3a vary in size from a single digit, to multiple digits or even the entire hand (Krubitzer et al., 2004), potentially resulting from convergent input from multiple afferents or from single afferents innervating multi-joint muscles. Area 3a makes reciprocal connections with area 2, M1, supplementary motor area (SMA), and area 1 (Darian-Smith et al., 1993; Huerta and Pons, 1990; Huffman and Krubitzer, 2001; Jones et al., 1978; Stepniewska et al., 1993). Approximately 15% of neurons within area 3a are also corticomotoneuronal cells that innervate motoneurons of the hand within the spinal cord (Rathelot and Strick, 2006). Neurons of area 3b respond primarily to cutaneous stimulation (Hyvärinen and Poranen, 1978; Iwamura et al., 1993; Seelke et al., 2012; Taoka et al., 2000). Neurons in area 3b are organized into cortical columns with similar receptive fields, yet most receive convergent input from multiple submodalities (Pei et al., 2009). RF size within the columns of 3b increase as information passes from granular layer 4 to supragranular layers 1-3 (DiCarlo et al., 1998). Area 1 and 2 have larger receptive fields and more complex response properties than those of areas 3a and 3b. Neurons of area 1 have reciprocal connections with areas 3a, 3b, 2, primary motor cortex, lateral parietal cortex and posterior parietal area 5

(Burton and Fabri, 1995; Jones et al., 1978; Krubitzer and Kaas, 1990; Pons and Kaas, 1986; Stepniewska et al., 1993). Neurons of area 1 demonstrate preferential activation by the particular texture of a somatic stimulus (Carlson, 1981; Randolph and Semmes, 1974). Neurons of area 2 show responses to both cutaneous and proprioceptive inputs (Hyvärinen and Poranen, 1978; Iwamura et al., 1993; Kim et al., 2015; Seelke et al., 2012; Taoka et al., 2000) and are tuned to the particular size and shape of the somatic stimulus as a potential initial step in stereognosis of objects (Felleman and Van Essen, 1991; Iwamura, 1998; de Lafuente and Romo, 2006; Pack and Bensmaia, 2015). Neurons of area 2 have large RFs comprising multiple fingers with blurred somatotopical features (Pons et al., 1985). Lesions of area 2 impair the coordination of finger movement and shape and size discrimination of grasped objects. Area 2 makes reciprocal connections with areas 3a, 3b, area 1, M1 (Jones et al., 1978; Pons and Kaas, 1986; Stepniewska et al., 1993), the anterior pulvinar of the thalamus (Padberg et al., 2009), and projects to lateral and posterior parietal cortex (Pons and Kaas, 1986).

Area 3b in primates is believed to be homologous to S1 cortex of other mammals, such as rodents (Kaas, 1983). Unlike primates, S1 cortex in rodents is not currently divided into multiple sub-regions. Instead, rodent S1 displays granular and dysgranular divisions (Krubitzer et al., 2011). Granular S1 contains densely packed neurons in cortical layers II/III and IV that are predominantly responsive to cutaneous stimuli, similar to area 3b in primates, whereas dysgranular S1 contains neurons predominantly activated by proprioceptive joint and muscle movements, similar to area 3a of primates (Chapin and Lin, 1984; Dawson and Killackey, 1987; Francis et al., 2008; Kim and Lee, 2013; Krubitzer et al., 2011). The middle nucleus of the rodent ventroposterior thalamus relays information related to SA and RA receptors to granular

S1. Lesions of both the granular and dysgranular cortex of S1 produce deficits in FL and HL placement on a behavioral placing test (Ryck et al., 1992). Rodent S1 contains a somatotopic map of the contralateral body and RFs of neurons in rodent S1 are smaller than RFs in other somatosensory areas (Angel and Lemon, 1975; Chapin and Lin, 1984; Hall and Lindholm, 1974; Koralek et al., 1990; Wallace, 1987; Welker, 1971, 1976; Woolsey, 1967). Similar to granular S1 cortex, dysgranular S1 also shows a degree of somatotopic mapping (Chapin et al., 1987; Kim and Lee, 2013). No studies exist on the parcellation of features such as object texture, size, shape or movement within S1 cortex or surrounding cortex to potentially define higher order cortical areas similar to areas 1 and 2 in primates. It is possible that similar feature extraction to areas 1 and 2 has already taken place within the hierarchical cortical layers of S1 cortex of rodents, however this has yet to be shown. It may also be possible that cortical areas such as the secondary somatosensory (S2) or parietal medial (PM) cortex near to S1 cortex in rodents could also play this role of higher order representation of more complex sensory stimuli features, however this has also not been shown.

The lateral parietal cortex (LPC) in primates, found directly lateral to the tongue representation of the APC, encompasses secondary somatosensory cortex and parietal ventral area (PVA). Both S2 and PVA contain mirrored somatotopic body maps (Burton and Carlson, 1986; Disbrow et al., 2000; Krubitzer et al., 1995). Sandwiched between the two areas are neurons that exhibit primarily cutaneous responses, whereas neurons within the areas respond to either cutaneous or proprioceptive inputs, or both (Fitzgerald et al., 2004; Krubitzer et al., 1995; Taoka et al., 2016). Few S2 neurons are responsive to the orientation of bars indented onto the digits, and instead require more complex features such as object curvatures in their tuned

direction (Yau et al., 2013). RFs on neurons within the LPC are larger, encompassing multiple fingers, bilateral inputs from both limbs (Burton and Carlson, 1986; Fitzgerald et al., 2006; Iwamura et al., 1994; Poranen and Hyvärinen, 1982; Ruben et al., 2001; Sinclair and Burton, 1993) and even multiple regions of the body (Taoka et al., 2016). The LPC receives input from all areas of the APC (Burton et al., 1995; Garraghty et al., 1990; Krubitzer and Kaas, 1990; Pons et al., 1987, 1992; Qi et al., 2002), as well as having reciprocal connections with the APC, thalamus, insula, and contralateral somatosensory regions (Delhaye et al., 2018). Due to its high level of interconnection with other somatosensory areas, lesions to the LPC lead to impairment in tests of texture and shape discrimination in primates (Murray and Mishkin, 1984; Suzuki et al., 2008). Neuronal activity in the LPC is strongly modulated by both the attentional state (Burton et al., 1997; Chapman and Meftah, 2005; Hsiao et al., 1993; Meftah et al., 2002; Salinas et al., 2000) and behavioral outcome of a task (Hernández et al., 2010; Jiang et al., 1997; de Lafuente and Romo, 2006; Romo et al., 2002; Salinas et al., 2000). Subsets of neurons within the LPC respond directly to, or have their activity modulated by, visual (Agnew and Wise, 2008; Hihara et al., 2015) and auditory (Meftah et al., 2009; Ro et al., 2013) stimuli, thereby further defining the LPC as an area of higher order associative cortical processing.

Holding a degree of similarity to primate LPC, S2 cortex in rodents receives inputs from both the granular and dysgranular S1 cortex, and displays a somatotopy that is a mirror reversal of S1 along the S1-S2 border (Ebner and Kaas, 2015; Kim and Lee, 2013). S2 in rodents is relatively small in comparison to S1 and does not show the same degree of cortical somatotopic magnification seen in rodent S1. RFs of S2 are also larger, and less responsive in anesthetized animals than S1 (Krubitzer et al., 2011). While very little is known about the exact function of

S2 for limb-associated sensory processing in rodents, the whisker associated S2 has been more thoroughly studied. Whisker S2 demonstrates supra-linear multi-whisker integration over longer time periods (Goldin et al., 2018), and shows poor temporal accuracy for encoding stimulus frequency (Melzer et al., 2006). Whisker S2 has also been shown to persistently encode stimulus information for reference and comparison to new information within S1 cortex (Condylis et al., 2020). In line with the role of S2 being a higher order region for multisensory integration as seen in primates, parts of S2 in rats responds to both somatosensory as well as auditory stimuli (Brett-Green et al., 2003, 2004). It has also been suggested that a distinct multisensory zone be classified apart from S2 cortex to delineate the region of S2 responsive to multisensory integration (Menzel and Barth, 2005).

The parietal medial (PM) area in rodents is also thought to be homologous to the posterior parietal cortical area (PPC) of primates, an area for the integration of somatosensory, visual, auditory and vestibular modalities involved in sensorimotor planning, guidance, and haptic exploration (Delhaye et al., 2018). Neurons within the PM area of rodents receive convergent input primarily from dysgranular zone neurons of rodent S1 (Akers and Killackey, 1978; Fabri and Burton, 1991; Lee et al., 2011), and show large receptive fields with very coarse, but complete, representation of the body (Krubitzer et al., 2011). PM is believed to be a high order association area for the convergence of somatosensory and visual information required for generating frames of reference for spatial navigation within its environment (Bucci, 2009; Nitz, 2009; Reep and Corwin, 2009; Torrealba and Valdés, 2008), and for directing attention to salient environmental cues (King and Corwin, 1993; Reep and Corwin, 2009). It has also been proposed that area PM in rodents resembles area 1 plus area 2 in primates, however lesions to PM impairs

navigation and spatial orientation in the water maze (Kolb and Walkey, 1987), and results in hemi-neglect to multisensory cues in the contralateral field (King and Corwin, 1993; Reep and Corwin, 2009), thereby suggesting that the function of textural processing and stereognosis assigned to area 1 and 2, respectively, may take place within upstream area S1, S2/PV, or other areas yet to be discovered in the rodent somatosensory cortex.

Multimodal interactions within somatosensory cortical areas

Much of previous research on the various somatosensory areas has, perhaps incorrectly, focused primarily on defining the responses of individual cells to stimuli predicted to primarily target specific mechanoreceptor classes within restricted RFs. Vibratory stimuli applied to single locations on the glabrous skin of primates has extensively been used to depict properties of somatic processing for stimulus frequency. Responses of primary sensory afferents to periodic vibratory stimuli have been found to be reliably phase locked to the stimulus frequency (Birznieks and Vickery, 2017; Freeman and Johnson, 1982a, 1982b; Mackevicius et al., 2012; Talbot et al., 1968). APC neurons have also been found to demonstrate phase locking to low frequency sinusoids, but with highly decreasing fidelity as frequency increases. While many cells of primate S1 cortex can entrain to 1 Hz stimuli within their RF, only a very small percentage are capable of following frequencies up to 300 Hz or more (Harvey et al., 2013; Hernández et al., 2000; Mountcastle et al., 1969). For low frequency stimuli, firing rate of APC neurons increases systematically and interburst interval decreases systematically with increasing frequency, thereby suggesting that information on frequency is conveyed in the firing rate and temporal patterning of the responses (Hernández et al., 2000; Salinas et al., 2000). At high frequencies, however,

firing rate loses its dependency on frequency and instead a subpopulation of neurons displays phase locked activity temporally modulated by the stimulus frequency (Harvey et al., 2013). Because the firing rate of tactile fibers is dependent not only on frequency but also on the amplitude of a stimulus, the intensity of a given stimulus is believed to be encoded by the entire population of primary afferent fibers activated by a stimulus, and weighted by fiber type (Muniak et al., 2007). All responsive cells of S1 cortex have been found to faithfully encode increasing stimulus amplitude by increasing their burst firing rate, regardless of the frequency of the stimulus applied (Harvey et al., 2013).

Due to different relative strengths of input from each somatosensory modality, somatosensory cortical neurons vary in their frequency response profile. The responses to skin vibrations of these neurons is primarily linearly dependent on RA1 and SA1 input, whereas the precise timing of responses is modulated by RA2 input (Saal et al., 2015). Studies in cats have shown that 25Hz vibrations applied to the glabrous skin of the paw (believed to more strongly activate SA1 and RA fibers), result in strong localized excitation within S1 cortex as measured by intrinsic optical signal imaging, whereas 200Hz vibrations (believed to more strongly excite RA2 fibers) produce shorter excitatory responses and stronger, more spatially extended after-inhibition (Tommerdahl et al., 1999, 2005). In rodents, S1 cortical neurons responding to sinusoidal indentations applied to the paws have demonstrated that inhibitory S1 neurons are more broadly tuned in their responsiveness to a range of stimulus frequencies (Hayashi et al., 2018), potentially reflecting increased non-selective input integration from surrounding excitatory cells (Bock et al., 2011; Harris and Mrsic-Flogel, 2013; Hofer et al., 2011; Kerlin et al., 2010; Khan et al., 2018; Scholl et al., 2015), whereas excitatory neurons display sharper

selectivity to stimulus frequency (Hayashi et al., 2018). Similar to primates, the temporal precision of spike timing of S1 neurons in rats has been found to convey information on sensory features such as stimulus location on the skin (Foffani et al., 2004, 2008).

A more recent view of somatosensory areas of the cortex has formed in the scientific community whereby neurons, even at low levels on the cortical somatosensory hierarchy such as those in primate areas 3a and 3b, display responses modulated by multimodal features of both cutaneous and proprioceptive inputs (Kim et al., 2015; Saal and Bensmaia, 2014; Saal et al., 2015). Not only do receptive fields of area 3b neurons show excitatory receptive fields surrounded by inhibitory fields (Delhaye et al., 2018), but neurons in area 3b demonstrate orientation tuning due to their oblong receptive fields (Bensmaia et al., 2008; DiCarlo et al., 1998), and temporally delayed inhibitory RFs that overlap their excitatory RFs (DiCarlo and Johnson, 2000). The majority of neurons of areas 1 and 2 of the APC, and a subset of neurons of area 3b, display responses that are also dependent on the direction and magnitude of shear forces (Fortier-Poisson et al., 2016; Salimi et al., 1999a, 1999b, 1999c), potentially to encode information about surface friction (Fortier-Poisson and Smith, 2016). On a behavioral level, neurons within the somatosensory areas may respond only to passive or only to active movements of the limb (London and Miller, 2013; Soso and Fetz, 1980), and may only respond to static posture of the animal or during active movement of the limbs (Gardner and Costanzo, 1981; Soso and Fetz, 1980; Yumiya et al., 1974). Further, neurons within the somatosensory cortex may also display RFs dependent on multi-joint interactions, yielding preferred combinations of joint postures not predicted by the linear combination of joint angles (Costanzo and Gardner, 1981). Interestingly, less than 50% of neurons in the APC of primates display

attentional modulation (Burton and Sinclair, 2000; Hsiao et al., 1993; Meftah et al., 2002), compared to 60-80% of higher order LPC neurons (Burton et al., 1997; Hsiao et al., 1993; Meftah et al., 2002). These features of behavioral relevance are not believed to be processed by neurons in the early stages of somatosensory processing in primates. Neuronal responses in the VPL of the thalamus have not been shown to be modulated by attention to the stimulus (Camarillo et al., 2012; Tremblay et al., 1993; Vázquez et al., 2012). However, high order sensory integration and attentional modulation may occur at earlier stages within the somatosensory hierarchy of rodents. It has recently been shown that activity within S1 cortex of mice can tightly correlate with, and even precede, the onset and speed of locomotion in freely moving mice (Karadimas et al., 2020), potentially suggesting that higher order sensory integration for motor output is already taking place within S1 cortex of rodents.

In summary, the afferent information for somatic stimuli from the limbs undergoes multiple stages of signal convergence and feature extraction prior to its representation within S1 cortex, thereby suggesting that cortical representations of stimuli in S1 cortex appear to be highly multimodal and high order in the healthy brain. The properties of cells within neural networks undergoing plastic re-organization of structure and function within the somatosensory cortex after stroke, for which the next sections will examine, must therefore be considered in the context of these high order representations.

Structural plasticity within post-stroke cortical networks

At the onset of stroke, insufficient oxygen delivery impairs oxidative phosphorylation and ATP generation leading to excitotoxicity and necrotic cell death (Doyle et al., 2008; Murphy and Corbett, 2009). This subsequently leads to the formation of a well-defined stroke core within only three hours of stroke onset (Carmichael, 2006). Surrounding the core is a penumbral area of hypo-perfused tissue undergoing evolving infarction. Cells within the penumbra will undergo apoptotic processes over the hours and days after stroke unless reperfusion occurs within the first few hours following stroke (Murphy and Corbett, 2009). As structural and functional connections between interconnected brain regions are disrupted, diaschisis occurs within the cortex, potentially leading to dysfunction and degeneration in areas distal to the stroke core (Carrera and Tononi, 2014). Unilateral damage to the sensorimotor cortex often results in disuse of the affected limb and compensatory reliance on the unaffected limb (Luke et al., 2004; Murphy and Corbett, 2009). The extent of behavioral modification is dependent on the degree to which the ipsilesional and contralesional cortices are able to undergo re-organization of neuronal structure and re-connection via redundant connections to compensate for the lost tissue (Murphy and Corbett, 2009; Winship and Murphy, 2009). Zhang et al. (2005) found that after moderate ischemia (~50% of control blood flow) in mice induced by endothelin-1 (ET-1), synaptic spines of layer 5 somatosensory neurons within the penumbral area are stable over the first 5 hours. At times greater than 7 hours, apoptotic and necrotic processes result in the gradual breakdown of cellular and dendritic membranes. More severe reductions in blood flow (<20% of control) induced by photothrombosis result in blebbing of dendrites and complete loss of dendritic spines within the first 30 minutes after occlusion. Spontaneous reperfusion due to break-up of the

photothrombotic clot within 20-60 mins results in restoration of dendrites and spines, but these later degenerate through apoptotic processes occurring slowly during the following 24 hours (Zhang et al., 2005). Dendritic damage is non-uniform within single neurons and is greater with increasing proximity to ischemic zones (Brown and Murphy, 2008; Brown et al., 2008; Enright et al., 2007; Zhang and Murphy, 2007), with dendritic tufts of layer 5 neurons appearing to be most affected (Enright et al., 2007). In mice, two-photon imaging of dendritic spines revealed that stable spines were normally found within 13um from small flowing vessels after ischemia, but that dendritic structure could be maintained by flowing vessels as far as 80um away (Zhang and Murphy, 2007). This suggest that within the acute period after the onset of ischemia, cortical cells are differentially affected based on the length of time they are deprived of oxygen and nutrients, as well as their proximity to flowing vessels.

Neurons may undergo morphological changes over time to adapt and compensate for connections lost in the apoptotic/necrotic core. Brown et al. (2010) found that before stroke in mice, the shape of dendritic arbors of layers 2/3, 5 and 6 are stable and there is very little retraction or growth of dendritic tips. After photothrombotic lesion to the somatosensory cortex, the amount of tip extension and retraction increases considerably, especially within the first 2 weeks post-lesion. The growth and retraction follows a homeostatic mechanism whereby the net arbor length does not change over time; retractions of dendritic tips found most proximal to the lesion border are balanced by extensions of tips most distal to the border. The amount of dendritic remodeling follows a linear relationship with the neuron's distance to the lesion border, whereby neurons that are closer to the lesion undergo greater net amounts of proximal dendritic retraction and distal dendritic extension. These neurons are believed to be attempting to re-

establish synaptic connections in order to improve efficacy and function of remaining synaptic networks in the ipsilesional hemisphere (Brown et al., 2010). Although this relationship may hold true for the ipsilesional hemisphere, it is potentially mediated by local induction of genes and signaling molecules in partially ischemic penumbral tissue and may therefore be spatially limited to the ipsilesional cortex. Surprisingly, unilateral ET-1 induced lesion of the forelimb (cFL) cortex was correlated with enhanced synaptogenesis in the contralesional layer 5 motor cortex and increased performance of the contralesional unimpaired cFL over that of sham animals as early as 5-7 days post-lesion (Luke et al., 2004). This increase in synaptogenesis was also coupled with an increase in the number of both perforated and multisynaptic boutons, suggesting an increase in complexity of the synaptic network in cortex contralesional to stroke (Luke et al., 2004). Although this observation proposes that stroke directly increases plasticity in the contralateral cortex, an opposing interpretation is that increased behavioral reliance on the unaffected cFL results in increased contralesional motor cortex synaptic plasticity. In support of this interpretation, two-photon imaging of apical dendrites of layer 5 pyramidal neurons in mice without post-stroke reach training indicates that the contralesional somatosensory area shows no change in the rate of dendritic remodeling or spine turnover, and no change in the area of cFL mediated cortical activation, as measured by intrinsic optical signal imaging, for either distal MCAO or photothrombotic stroke to the opposite S1FL somatosensory cortex (Johnston et al., 2013).

In the peri-infarct area (<250um from lesion) 6 weeks after stroke, Brown et al. (2007) demonstrated that surviving dendrites are found to run in parallel with flowing vessels and radiate out from the site of infarction. Regions far (500-800um) from the lesion border, and

control animals, do not show the same parallel organization. This parallel organization increases over time, concurrent with increased vascular density due to angiogenesis that occurs within the peri-infarct region (Brown et al., 2007). The increase in parallel organization of dendrites and vessels may occur as dendrites extend away from the site of infarct and follow newly generated vessels providing the needed metabolic supply in the mildly ischemic peri-infarct zone (Brown and Murphy, 2008). The remodeling of dendritic spines is also up-regulated in an attempt to reform synaptic connections within the peri-infarct tissue (Murphy and Corbett, 2009). Acutely, golgi staining at 2, 6 and 24 hours after photothrombotic lesion to the cFL cortex of mice indicates that penumbral spines that remain intact within <200um from the core in all cortical layers became 25% longer on average 6 hours post-occlusion (Brown et al., 2008). On a more chronic scale in mice, Brown et al. (2007) demonstrated that photothrombotic lesion of the cFL cortex results in an increase in the rate of spine turnover of layer 5 neuron apical tufts within the peri-infarct area. At 1-2 weeks after lesion, turnover is up to 8 times greater than controls, and remains elevated at 6 weeks post-lesion. In contrast, spine turnover in controls is constant over extended periods of time. At distances greater than 1.5mm from the lesion core in the ipsilesional hemisphere, turnover rates are not changed, further indicating that local signals near the infarct site give rise to the increased plasticity (Brown et al., 2007). This increased plasticity may underlie compensation and functional rewiring of the lost cFL somatosensory representation to the peri-infarct cortex. Indeed, the combination of rehab therapy with plasticity enhancing therapies has been shown to increase spine survival and decrease spine turnover, leading to an increase in spine density in perilesional tissue in a mouse model of cortical stroke (Mascaro et al., 2019).

The role glutamate and its ionotropic receptors in post-stroke plasticity

Shortly after the onset of ischemia, a complex cascade of intra- and extra-cellular signaling (Carmichael, 2003a, 2006; Carmichael et al., 2005; Li and Carmichael, 2006; Li et al., 2010) ultimately leads to re-organization of the microarchitecture of surviving peri-infarct tissue, whether adaptive or maladaptive (Murphy and Corbett, 2009; Winship and Murphy, 2009). These signalling cascades can either potentiate the neuroplastic events leading to re-wiring and recovery of neocortical function post-stroke, or be detrimental to its progression, such as by establishing a physical or neurochemical barrier that impedes growth and plasticity (Carmichael, 2003a, 2006; Carmichael et al., 2005; Li and Carmichael, 2006; Li et al., 2010). During the acute phase of ischemia (first 24hrs), the release of signaling molecules from neuronal or glial tissue can occur through several mechanisms; (1) Disruption of the plasma membrane allowing the signal to leak out, (2) release via reversal of function of signal specific membrane transporters due to loss of ion gradient, and/or loss of energy reserves, or (3) by augmented exocytosis from synaptic vesicles (Saransaari and Oja, 2008). At more chronic time points, modification of signal release is thought to depend on alterations in gene expression, and/or changes in the activity of proteins responsible for the formation of signaling molecules and their respective receptors (Saransaari and Oja, 2008).

During the acute period after the initiation of ischemia, the release of glutamate is mediated primarily by the reversal of neuronal glutamate re-uptake transporters which normally act by using the K^+ gradient to drive $3Na^+$, Glu^- and H^+ into the cell (Rossi et al., 2000). Studies using intracerebral microdialysis in rats have shown that extracellular glutamate concentrations

may be increased over 500% for the first 10-15 mins after the onset of 10 minute transient global ischemia induced by a neck cuff (Benveniste et al., 1984). On a longer time scale, rats subject to 1hr transient occlusion via monofilament middle cerebral artery occlusion (MCAO) displayed reduced neuronal EAAC1 and glial GLT-1 glutamate transporters mRNA and protein expression at 24 and 72 hours within the ipsilesional hemisphere compared to the contralesional cortex or sham treatments (Rao et al., 2001). This down-regulation may disrupt the clearance of glutamate from the extracellular space, thereby contributing to increased neurotoxicity within the first 72 hours after stroke (Rao et al., 2001). NMDA antagonists have been found to provide neuroprotection during the acute period after the onset of ischemia, but show efficacy only when given before or within the first 30-60 mins of ischemic onset (Rod and Auer, 1989). After this time point, NMDA antagonism reduces plastic processes and impairs behavioral recovery (Rod and Auer, 1989), and has led to worse clinical outcome in several human studies due mainly to the long delay before treatment (6-24hrs) and treatment that lasted too long (3-7 days) (Ginsberg, 2008; Hoyte et al., 2004).

In mice, infarction just lateral to the cFL and cHL somatosensory region induced by thermocoagulation of the right MCAO resulted in an increase in bilateral NMDA receptor density 1 month after the lesion as indicated by increased [³H]MK-801 autoradiographic binding (Qü et al., 1998a). Further, bilateral levels of both [³H]kainate and [³H]AMPA binding were unchanged, whereas [³H]muscimol binding was reduced, indicating the selective up-regulation of NMDA-Rs and down-regulation of GABA_ARs at 1 month post-stroke (Qü et al., 1998a). As expected with a loss of cortical tissue within the lesion core after infarction, all receptor binding in the core was decreased (Qü et al., 1998a). Photothrombotic infarct to the cHL somatosensory

region of rats demonstrated a time dependence for NMDA-R upregulation; NMDA-Rs were up-regulated primarily at 30 days in the ipsilesional cortex, whereas NMDA-Rs were up-regulated as early as 14 days in the contralesional cortex (Que et al., 1999). These results have been contested by other studies demonstrating a decrease in [³H]MK-801 binding in the neocortex of rats at 14 and 30-40 days after 90 minute transient MCAO using the monofilament model (Dhawan et al., 2010) and a reduction of AMPA receptor (AMPA-R) GluR1-4 subunits mRNA and reduced NMDA NR1 subunit mRNA by 24 hours after permanent monofilament MCAO (Friedman et al., 2000). Potentiation of NMDA signaling by d-cycloserine has been found to increase fMRI BOLD response in the ipsilesional hemisphere when given a single time 24 hours after monofilament induced 90 min transient MCAO in rats, and measured at 7, 14, and 30 days (Dhawan et al., 2011). This was seen to improve memory in a novel object recognition task back to baseline levels at 7, 14 and 30 days, and did not cause an increase in infarction size measured at 30 days (Dhawan et al., 2011). As d-cycloserine has a half-life of approximately 10-12 hours (Kalisch et al., 2009), these results may suggest that potentiation of plastic processes mediated by increasing NMDA-R signaling improves functional re-wiring within the first several days (Dhawan et al., 2011). Despite the conflicting finding on the expression pattern of the NMDA receptor after infarct, the NMDA receptor is known to be involved in use dependent enlargement of lesion volume due to forced overuse of the affected forelimb (Humm et al., 1999), thereby suggesting that the NMDA receptor plays a dual role in both plastic processes, as well as contributing to damage when over-stimulated. Activation of NMDA receptors during MCAO has also been found to downregulate KCC2 and δ containing GABA_ARs, potentially playing a role in increasing post-stroke motor recovery, but also acting as a potential contributor to post-stroke epileptogenesis (Jaenisch et al., 2016).

AMPA-Rs have also been found to be involved in plasticity and motor recovery after stroke. Clarkson et al. (2011) demonstrated that an AMPA-R antagonist, CFM2, started at 5 days after photothrombotic stroke to the forelimb somatosensory area in mice results in more foot faults on a grid walking test, less successful reaching behavior and more behavioral reliance on the unaffected forelimb. In contrast, potentiating AMPA-R signaling using the high-impact ampakine CX1837 increases the release of BDNF and results in greater TrkB BDNF receptor phosphorylation in the ipsilesional, but not contralesional cortex, thereby increasing behavioral recovery on a grid walking task and decreased reliance on the unaffected forelimb. These behavioral improvements were seen to be reliant on TrkB signaling as a BDNF ligand decoy, TrkB-Fc, stops the increase in TrkB phosphorylation induced through increased BDNF, and eliminates the increase in behavioral recovery mediated through CX1837's potentiation of AMPA-Rs. This potentiation of recovery by CX1837 was also found to be time dependent, whereby early administration of CX1837 during the time of the stroke potentiated neurotoxicity and led to increased infarct size, whereas CX1837 started at 5 days does not (Clarkson et al., 2011). The rise of BDNF is potentiated by rehabilitative therapies such as running exercise and skilled reaching practice started 3 days after endothelin-1 induced MCAO in rats, and is known to aid in functional recovery within the first 28 days (Ploughman et al., 2009). Likewise, recovery is reduced when antisense-BDNF oligonucleotide is used to silence BDNF gene expression during this time (Ploughman et al., 2009). These results suggest that increased cortical activity and induction of augmented BDNF signaling may be mediated, in part, by an increase in AMPA-R mediated cortical excitability after ischemia. Similarly, 20 minute transient oxygen-glucose deprivation (OGD) of hippocampal neuronal cultures *in vitro* results in a decrease in the expression of GluR2 containing AMPA receptors at synaptic sites, resulting in an

increase in miniature EPSC amplitudes (Liu et al., 2006). As the loss of GluR2 subunits also confers increased Ca^{2+} permeability to synapses between these neurons, there is a higher likelihood that Ca^{2+} may mediate intracellular signals for increased pro-plasticity gene expression in an activity dependent manner (Liu et al., 2006).

The role GABA and its ionotropic receptors in post-stroke plasticity

During the acute period after the initiation of ischemia, the release of GABA is potentiated in two steps; First through exocytotic Ca^{2+} dependent release mechanisms as neurons depolarize and trigger N-type voltage dependent Ca^{2+} channels (VDCCs) (Saransaari and Oja, 2008). Second, by non-vesicular release mechanisms as ionic homeostasis is lost and a reversal of Na^+ and Cl^- dependent GABA transporters occurs (Saransaari and Oja, 2008). The initial Ca^{2+} dependent vesicular GABA release is further potentiated by pre-synaptic NMDA and AMPA autoreceptors (Saransaari and Oja, 2008), but may also be reduced by metabotropic glutamate autoreceptors (Green et al., 2000). After 1 hour of transient left hemisphere ischemia due to monofilament occlusion of the left internal carotid artery (ICA) of male spontaneously hypertensive rats, the left hemisphere shows a progressive reduction in the expression of the vesicular GABA/glycine transporter (VGAT) mRNA and protein levels over the next 3-72 hours, whereas the contralateral hemisphere showed no reduction (Vemuganti, 2005). Further, no change in mRNA levels for vesicular monoamine transporters (VMAT1/2), vesicular acetylcholine transporter (VAChT) or vesicular glutamate transporters (VGluT1/2) occurred within the first 24hrs after ischemia in either the ipsilateral or contralateral hemispheres, thereby indicating that a specific down-regulation of VGAT gene expression or selective destruction of

VGAT expressing cells occurs over the first 72hrs after ischemia (Vemuganti, 2005). A progressive decrease in VGAT expression in peri-infarct tissue over 72hrs would decrease the rate of GABA/glycine packaging into synaptic vesicles and may thereby potentiate the excitotoxic damage due to a decrease in inhibitory neurotransmission over this period (Vemuganti, 2005). Interestingly, it has also been proposed that a potential reduction of GABAergic neurotransmission during the acute ischemic phase may mediate reduced neuronal swelling via a reduction of Cl⁻ entry during excitotoxic events during the acute phase of ischemia, thereby reducing the osmotic force driving water into the cell and reducing the risk of cell bursting (Allen et al., 2004).

Although the exact protective or detrimental role of GABA mediated Cl⁻ entry into the post-synaptic cell during early ischemia is still debated, enhancing GABAergic inhibitory signalling during the acute phase of stroke has been proposed as a logical intervention in the attempt to decrease glutamate mediated neuronal excitotoxicity during the ischemic episode (Green et al., 2000). Pharmacological interventions that increase GABA release or synthesis, or that are GABA receptor agonists or positive allosteric modulators, act as neuroprotective agents when given before the onset of cerebral ischemia (Green et al., 2000; Lyden and Hedges, 1992). Unfortunately, due to the inherent nature of reduced or complete lack of blood flow to the ischemic region of the brain during cerebral vessel occlusion, many of these compounds have little or no effect if given after the onset of ischemia as they are unable to reach ischemic tissue in sufficient concentration to promote neuroprotection (Green et al., 2000; Lie et al., 2018). Further, there is a critical window in which an increase in GABA signalling promotes rather than deters recovery from stroke (Lazar et al., 2002). Benzodiazepines given to human stroke patients

at late time points after the occurrence of their stroke (7 days to 6 years) caused an increase in the re-emergence of stroke related syndromes (Lazar et al., 2002). Likewise, a decrease in GABA has been measured in the brains of human stroke patients using magnetic resonance spectroscopy and has shown that increased recovery during constraint-induced movement therapy correlated with decreases in ipsilesional GABA levels (Blicher et al., 2015). This suggests an alternate role for GABAergic inhibition in plasticity and functional recovery in the chronic period after the onset of stroke.

GABA_ARs are known for their role as the primary mediators of post-synaptic ionotropic inhibition (Glykys and Mody, 2007; Mody et al., 1994). The pharmacological and electrophysiological properties of these receptors are mainly mediated by expression of different α -subunit variants (Glykys and Mody, 2007; Sieghart et al., 1999). Phasic inhibition is primarily mediated via GABA_ARs at synaptic sites containing a combination of $\gamma 2$, $\alpha 1-3$ subunits and β_x subunits (Fritschy and Mohler, 1995). Tonic inhibition is mediated by extrasynaptic GABA_ARs containing $\alpha 4$ and $\alpha 6$ subunits, combined with δ and β_x subunits, which are continuously activated by low concentrations of ambient GABA in the extracellular space due to their high affinity for GABA and low rate of desensitization (Farrant and Nusser, 2005; Glykys and Mody, 2007; Nusser and Mody, 2002). Both phasic and tonic inhibition is also mediated by GABA_ARs containing the $\alpha 5$ subunit localized to synaptic and extrasynaptic sites (Glykys and Mody, 2007; Serwanski et al., 2006). Contradictory results have been observed for the expression of GABA_ARs after stroke. A number of studies have shown a downregulation in $\alpha 1$ containing GABA_ARs associated with phasic inhibition as early as 7 days post-stroke (Neumann-Haefelin et al., 1998, 1999; Redecker et al., 2002), while others have indicated an upregulation and an

increased efficacy of spontaneous and miniature inhibitory post-synaptic currents in pyramidal neurons associated with the $\alpha 1$ receptors (Hiu et al., 2016). Another study, has also shown a peak reduction of $\alpha 2$, $\alpha 5$ and $\gamma 2$ containing GABA_ARs in peri-lesional tissue 7 days after photothrombotic infarction in rats, and a return to baseline expression levels by 30 days (Redecker et al., 2002). It's contested as to whether the $\alpha 3$ containing GABA_AR is down-regulated after stroke (Redecker et al., 2000; Schmidt et al., 2012) or not (Redecker et al., 2002). Other studies, using autoradiography, have demonstrated a general reduction of GABA_ARs in both the ipsilesional and the contralesional hemisphere 7 days post-stroke (Qü et al., 1998b; Schiene et al., 1996). The contralesional cortex also shows a peak reduction in $\alpha 1$, $\alpha 2$ and $\alpha 5$, but not $\gamma 2$, 7 days after stroke, suggesting a period of reduced cortical inhibition in widespread cortical areas of the contralesional cortex at early time points after stroke (Redecker et al., 2002). However, this contralesional decrease in GABA receptors returns to control levels by 30 days post-stroke (Redecker et al., 2002). Interestingly, application of a non-competitive NMDA-R antagonist, MK-801, 30 mins prior to photochemical infarction in rats results in the complete abolishment of bihemispheric GABA_AR dysregulation measured at 7 days (Neumann-Haefelin et al., 1999). This result, combined with an apparent increase in mRNA synthesis of $\alpha 1$ and $\alpha 2$ subunits at 7 days in the peri-infarct region, indicates that hyperexcitability and Ca^{2+} entry mediated through NMDA-R activation may lead to a reduction of GABA_AR protein translation within the peri-infarct cortex within the first 7 days post-stroke (Neumann-Haefelin et al., 1999), which is then restored at later time points (Redecker et al., 2002). These changes also show age dependency, whereby old (24 month), but not young (3 month), rats display a substantial increase in $\alpha 5$ containing GABA_ARs in the peri-infarct cortex lateral to a photothrombotic infarction in the parietal cortex at 7 days (Schmidt et al., 2012). Taken together, these results

primarily indicate a decrease in phasic GABAergic inhibition between cells mediated through the alteration of GABA_AR levels found within the synapse of young rats (Redecker et al., 2002), and that this may contribute to increased neuronal excitability seen after stroke. Interestingly, enhancing phasic GABA inhibition using Zolpidem, a GABA_AR positive allosteric modulator with high affinity for $\alpha 1$ GABA_ARs (Che Has et al., 2016), has been shown to improve behavioral recovery from stroke (Hiu et al., 2016; Oh et al., 2018), potentially by upregulating BDNF (Oh et al., 2018), thereby suggesting that phasic GABAergic activity may play a role in promoting post-stroke plasticity-related recovery. Likewise, recent research using continuous theta burst stimulation to elevate phasic inhibition after photothrombotic stroke has also shown benefit in promoting functional recovery (Feng et al., 2020).

There is mounting evidence that extrasynaptic GABA_ARs also play a strong role in altering neuronal excitability after stroke. These extrasynaptic tonic GABA_ARs are known to set an excitability threshold for neurons (Clarkson et al., 2010; Glykys and Mody, 2006; Jaenisch et al., 2016; Lee and Maguire, 2014; Walker and Semyanov, 2008). At 3, 7, and 14 days after photothrombotic stroke, layer II/III cortical pyramidal neurons were found to have elevated tonic inhibition resulting from increased extracellular GABA due to a dysfunction of the GABA transporters 3 & 4 (GAT-3/4) (Clarkson et al., 2010). The expression of GAT-1 protein, but not mRNA, has also been shown to be down-regulated at 7 days lateral of a photothrombotic lesion to the cHL cortex of rats (Frahm et al., 2004). Blocking $\alpha 5$ containing GABA_ARs after stroke using the selective inverse agonist L655,708 (Clarkson et al., 2010; Lake et al., 2015) or S44819 (Wang et al., 2018) to decrease tonic inhibition has also been shown to dose dependently lead to an increase in behavioral recovery when started at 72hr (Wang et al., 2018), 3 days (Clarkson et

al., 2010) or 7 days (Lake et al., 2015) after infarction. Knockout of the $\alpha 5$ or δ gene also results in increased behavioral recovery after stroke, thereby indicating that a potential increase in tonic inhibition after stroke can reduce functional recovery (Clarkson et al., 2010). Unfortunately, the $\alpha 5$ antagonist S44819 has failed to improve clinical outcome in human patients after stroke (Chabriat et al., 2020).

Fast-spiking, parvalbumin-positive (PV+) GABAergic interneurons are known to play a powerful role in controlling cortical activity, plasticity, and sensory processing (Lehmann et al., 2012; Méndez and Bacci, 2011; Tremblay et al., 2016) and are highly metabolically active (Alia et al., 2021; Tremblay et al., 2016). In a mouse model of global ischemia induced with 5 minute common carotid arterial occlusion (CCAO) followed by reperfusion, the dendrites of PV neurons were rapidly damaged within 5 mins of ischemic onset, but were able to structurally recover within 5 mins after reperfusion (Xie et al., 2014). While optogenetically evoked PV neuron excitability was suppressed during transient ischemia, it recovered rapidly with reperfusion (Xie et al., 2014). However, PV neuron stimulation evoked GABAergic inhibition of network activity remained suppressed even 1 hour after reperfusion, suggesting a role for the downregulation of synaptic GABA receptors, or a decrease in presynaptic release post-stroke (Xie et al., 2014). Multiple studies have also found degeneration of parvalbumin-positive inhibitory interneurons and their dendrites in the peri-infarct zone up to 1mm from the lesion core of a photothrombotic infarct (Luhmann et al., 1995; Neumann-Haefelin et al., 1998), suggesting that structural alteration in PV cells may play a role in post-stroke network changes. It has also recently been discovered that inhibitory vasoactive intestinal peptide (VIP) expressing interneurons, that regulate the activity of PV and somatostatin (SOM) neurons (Chamberland et al., 2010; Jackson

et al., 2016; Pfeffer et al., 2013), show disrupted fidelity and predictability in evoked responses to somatic stimuli, and that this occurs within a subset of VIP neurons that were highly active prior to stroke (Motaharinia et al., 2021).

Post-stroke regional and cellular remapping, and alterations in functional activation

A complex pattern of intracellular signaling cascades and gene expression takes place after stroke that influences the rearrangement and function of somatosensory neural networks (Alia et al., 2021; Carmichael, 2003a; Carmichael et al., 2005; Li and Carmichael, 2006; Winship and Murphy, 2008, 2009). Plasticity within and between cortical structures leads to partial recovery of function but is proportional to both the extent of damage, as well as the form and quantity of rehabilitative therapy post-stroke (Murphy and Corbett, 2009; Xu et al., 2009). A critical period of highest plasticity begins shortly after the onset of stroke, is greatest during the first few weeks, and progressively diminishes over the weeks to months after stroke (Biernaskie et al., 2004; Brown et al., 2007, 2009; Carmichael et al., 2005; Cheatwood et al., 2008; Ploughman et al., 2009). The functional maps of the somatosensory and motor cortices exhibit remarkable use-dependent plasticity (Murphy and Corbett, 2009; Nudo et al., 1996; Winship and Murphy, 2009). Functional recovery after stroke is a thought to depend largely on the adaptive plasticity of surviving neurons that reinforce existing connections and/or replace the function of lost networks (Carmichael, 2003b, 2006; Dancause, 2005; Winship and Murphy, 2008, 2009). This neuronal plasticity leads to somatosensory and motor functional remapping to adjacent areas of the cortex and altered topographical organization (Carmichael, 2003b, 2006; Castro-

Alamancos and Borrell, 1995; Dancause, 2005; Dijkhuizen et al., 2001, 2003; Frost et al., 2003; Rossini, 2001; Rossini et al., 1998, 2007; Schaechter et al., 2006; Winship and Murphy, 2008, 2009). In human stroke patients, magnetoencephalography, functional magnetic resonance imaging (fMRI), and positron-emission tomography has been used to show that the somatosensory hand representation of the contralateral affected limb expands into ipsilesional regions not normally associated with hand somatosensation (Winship and Murphy, 2009). Increased activation within these novel ipsilesional sensorimotor areas is correlated with greater functional recovery in patients (Fridman et al., 2004; Johansen-Berg et al., 2002; Johansen-Berg et al., 2002). Remapping that occurs onto the contralesional cortex is considered a sign of less complete recovery from stroke, often due to extensive damage with limited viable tissue in the stroke affected hemisphere, and is usually present in patients with larger cortical strokes where fewer ipsilesional compensatory networks are able to form (Buetefisch, 2015; Calautti and Baron, 2003; Cramer, 2008; Schaechter, 2004; Ward et al., 2003). These findings have been corroborated in animal models of sensorimotor remapping, whereby contralesional activation due to stimulation of the stroke-affected limb, concurrent with a lack of somatosensory activation within the peri-infarct region, is only present in cases of poor functional recovery (Dijkhuizen et al., 2001, 2003; Weber et al., 2008). Indeed, in rats given small infarcts targeting the MCA with ET-1, ipsilesional cortical activity was a necessity for functional recovery on a pellet reaching task (Biernaskie et al., 2005). Further, rehabilitative training beginning 1 week after focal ET-1 infarct of the cFL somatosensory area of rats leads to improved motor recovery concurrent with restoration of cFL motor map size as measured by intracortical microstimulation (Nishibe et al., 2015).

On the level of individual neurons within the peri-infarct area, extracellular recordings of neurons during cutaneous somatic stimulation have shown that surviving neurons demonstrate enlarged receptive fields post-stroke (Fujioka et al., 2004; Jenkins and Merzenich, 1987; Reinecke et al., 2003). In rodents, photothrombotic infarct affecting the cHL somatosensory area leads to an enlargement of the cutaneous receptive field size of cHL neurons in both the ipsilesional cortex and contralesional cortex as early as 1 week post stroke (Reinecke et al., 2003). In primates, loss of the palm representation in the peri-lesional somatosensory cortex after electrocoagulatory lesion led to enlarged receptive fields of surviving neurons within area 3b at 1 month post-lesion (Jenkins and Merzenich, 1987). In rodents, previous research by Winship and Murphy (2008) demonstrated that prior to cFL targeted photothrombotic stroke, neurons within the limb-associated somatosensory cortical areas, mapped by intrinsic optical signal (IOS) imaging, demonstrate almost complete selectivity for their associated limb and a sharp border between cHL and cFL responsive neurons. At 1-2 weeks post stroke, diaschisis occurred in peri-infarct cortical tissue, leading to a loss of the sensory-evoked cFL IOS map and lack of evoked cFL neuronal Ca^{2+} responses, while cHL IOS map and neuronal Ca^{2+} responses were maintained. At 1 month post-stroke, the sensory-evoked cFL map re-emerged within the peri-infarct area, with its map partially overlapping that of the cHL. Neurons within the overlapping area were found to have lost selectivity in their responsiveness to a single limb. At 2 months post-stroke, sharp borders between cHL and cFL responsive maps were re-established, with the cFL representation having seized a portion of the area that had previously shown overlapping activation by both limbs (Winship and Murphy, 2008).

Deficits in sensory-evoked somatosensory activity despite purported network hyperexcitability after stroke

Patients surviving stroke often develop enhanced brain excitability and epileptic seizures (Witte and Freund, 1999). The peri-infarct cortex of rodents has also previously been found to be hyperexcitable after stroke (Carmichael, 2003b; Centonze et al., 2007; Luhmann et al., 1995; Mittmann et al., 1998; Neumann-Haefelin et al., 1995; Schiene et al., 1996). This hyperexcitability has been shown with peri-infarct multi-unit recordings demonstrating a 10-fold increase in spontaneous firing rates measured at early time points within 3-7 days post-stroke (Schiene et al., 1996). This increase in spontaneous firing slowly diminished over a 2 month period after stroke, yet remaining elevated relative to control animals even at 4 months after stroke (Schiene et al., 1996). In cortical tissue slices taken from mice 3, 28 or 6 months after permanent MCAO, low-intensity orthodromic stimulation of peri-infarct pyramidal cells resulted in epileptiform extracellular field potential responses and intracellular EPSPs that were much longer in duration than controls, especially at 28 days post-stroke (Mittmann et al., 1998). However, the peak amplitude of the early postsynaptic potential was lower than controls, and with a higher late onset post-synaptic potential (Mittmann et al., 1998). This late EPSP component was found to be dependent on NMDA receptor activity and was blocked by NMDA antagonism (Mittmann et al., 1998). Notably, multiphasic long-latency field potential and EPSP activity was also measured at a late time point over 1 year after stroke and was found alongside repetitive synaptic activity bursts at a frequency of 5-10 Hz that were also blocked by NMDA antagonism (Luhmann et al., 1995). After photothrombotic lesions in rats, induction of LTP between layers 4 and 2/3 is also enhanced in the ipsilesional cortex, but not contralesional cortex

(Hagemann et al., 1998). Infarcted animals also show diminished inhibitory postsynaptic potentials (Neumann-Haefelin et al., 1995), and reduced paired pulse inhibition within the perilesional cortex (Buchkremer-Ratzmann and Witte, 1997; Domann et al., 1993; Fujioka et al., 2004) and contralesional cortex (Buchkremer-Ratzmann and Witte, 1997), indicating a deficit in inhibitory functional connections within the cortex post-stroke. Epileptogenic hyperexcitability may also occur after stroke due to a downregulation of KCC2 and an impairment in Cl⁻ extrusion from neurons (Jin et al., 2005; Khirug et al., 2021; Martín-Aragón Baudel et al., 2017; Schulte et al., 2018).

Despite this purported hyperexcitability and diminished inhibitory functional connections within post-stroke cortex, studies have shown that somatosensory activity evoked by limb stimulation shows deficits in magnitude and temporal fidelity after stroke. Sigler et al. (2009) demonstrated that before stroke, activation of the cortex imaged using VSD in mice indicates that the forelimb somatosensory area is activated within 10ms of a single 5ms contralateral forelimb pulse. 20-80 minutes after photothrombotic lesion to the forelimb cortex of mice, little ipsilesional cFL activation is seen within the original cFL area from contralateral cFL stimulation. Instead, activation within 20-30ms is thinly spread posterior to the cFL representation into the more anterior edges of the cHL representation, and reaches its maximum signal amplitude with delayed kinetics within this region. This area of activation was within 200-500um of the lesion core, thereby indicating the penumbral/peri-infarct area that maintained partial function (Sigler et al., 2009). Within one week of stroke, most of the remaining sensory-evoked cFL VSD response disappears, indicating diaschisis in remaining cortical networks (Brown et al., 2009; Lim et al., 2014). After 8 weeks recovery, responses to cFL stimulation re-

appear in cortical tissue surrounding the infarct within 20ms of stimulation, indicating remapping of the cFL somatosensory response to peri-infarct tissue (Brown et al., 2009; Lim et al., 2014). Compared to non-lesioned controls, this response was found to have decreased amplitude (~35% of control), increased time to peak (>100% longer), and shows greatly prolonged signal responses (300-400% longer), potentially indicating profound deficits in the temporal dynamics of cortical information processing within the peri-infarct cortex (Brown et al., 2009; Lim et al., 2014). It has, however, been suggested that the slower kinetics of excitation at late time points 2-3 months after stroke in remapped sensory circuits may enhance the probability of Hebbian forms of synaptic strengthening (Brown et al., 2009; Murphy and Corbett, 2009), although direct evidence for this has not been shown. VSD imaging has also been used to determine the interstimulus interval (ISI) necessary to elicit significant sensory-evoked somatosensory responses to two concurrent cFL deflections 3 months after photothrombotic infarct when measured in S1 and S2 cortex of mice. Sweetnam and Brown (2013) found that the remapped forelimb representation required longer ISIs in order to show distinct activation to each stimulus. cFL S1 cortex in controls could reliably respond to stimuli with ISIs of 100ms, whereas the remapped cFL S1 cortex required ISIs of 200ms or greater in order to elicit reliable responses. The first stimulus elicited cFL S1 activation with the same amplitude as controls, but with slightly longer time to peak and greater half-width. Interestingly, the cFL S2 cortex in lesioned animals displayed increased signal amplitudes relative to control and had similar time to peak and half-width as controls, thereby potentially suggesting increased reliance on S2 cortex for responding to cFL associated stimuli (Sweetnam and Brown, 2013). These results are distinct from previous experiments done within the first 1-6 hours after photothrombotic infarct in rats that demonstrated that at short time points the cortex is hyper-responsive to repeated stimuli,

even with ISIs as short as 10-100ms (Fujioka et al., 2004).

Deficits in thalamo-cortical function may underlie some of the discrepancy between studies measuring cortical hyperexcitability and those measuring sensory evoked activation of the somatosensory cortex after stroke. Focal stroke is associated with retrograde degeneration, gliosis, and a reduction in size of the thalamic VP nucleus resulting from VP thalamic neuronal atrophy and a loss of thalamo-cortical projections (Carmichael et al., 2001). Dysfunction of thalamo-cortical relay (TCR) neurons may also result from dysfunction of the reticular thalamic nucleus (nRT) after stroke. The nRT is a web-like layer of GABAergic neurons that covers the surface of the lateral thalamic nuclei. These inhibitory cells act as gates that modify the transmission of sensory information as it is relayed through the thalamus to the cortex, and between the various cortical areas (Deleuze and Huguenard, 2006; Velayos et al., 1989). In a photothrombotic model of stroke, lesion to the somatosensory cortex did not induce nRT cell loss but resulted in modification of their morphology from their normal fusiform shape into a circular shape, a decrease in dendritic length, and decreased synaptic connections between the nRT and the VPM and VPL thalamic nuclei (Paz et al., 2010). This morphologic change was also accompanied at 4-6 days post-lesion by a loss of nRT innervation from TCR fibers and a loss of innervation from cortico-thalamic fibers within the first hours to days after the lesion (Paz et al., 2010). Although neuronal loss occurs within the neocortex within the first hours to days after lesion to the somatosensory cortex, greatest losses of TCR cells is delayed until 4-6 days post-lesion and is most prominent within the VPL nucleus (Paz et al., 2010).

Several lines of research suggest that the fidelity of transmission through the thalamus

may be impaired after stroke. Tennant et al. (2017) demonstrated that thalamocortical projections to the peri-infarct somatosensory cortex are diminished from 1-5 weeks after stroke. Further, Tennant et al. (2017) showed that there is a substantial decrease in remaining thalamocortical boutons that are responsive to forelimb stimuli from 1-4 weeks after stroke (Tennant et al., 2017). When using VSD to measure sensory-evoked cortical activation of the peri-lesional cFL area at 1 and 8 weeks after stroke, and comparing it to VSD responses resulting from optogenetic stimulation, sensory-evoked stimulation yielded weak cortical VSD responses whereas optogenetic stimulation gave stronger than expected VSD responses, a result suggesting that reduced sensory-evoked cortical activation may be due to deficits in thalamo-cortical circuits (Lim et al., 2014). Cells within the nRT itself are also interconnected, thereby providing complex patterns of inhibition of inhibition (Battaglia et al., 1994; Raos and Bentivoglio, 1993). The anterior third of the nRT is mainly responsible for bilateral thalamic projections through the interthalamic adhesion (Chen et al., 1992; Raos and Bentivoglio, 1993). After photothrombotic lesion in the somatosensory cortex, nRT cells near the lesion core display a decrease in burst firing while those found far (>300um) from the lesion retain their instantaneous burst firing rates (Paz et al., 2010). If nRT neurons within the anterior third of the nRT are found far from the somatosensory lesion, their ability to inhibit the contralateral nRT after stroke may be augmented by intra-nuclei dis-inhibited resulting from the loss of GABAergic projections from more medial areas of the nRT (Mohajerani et al., 2011). At short time frames (<2hr) after stroke, these bihemispheric nRT interactions are thought play a role in increased contralesional somatosensory activation due to ipsilateral limb stimulation (Mohajerani et al., 2011), however these effects have not been shown on chronic time scale after stroke.

Thesis outline and aims

The somatosensory cortex of mice has often been a focus for studies measuring the effect of stroke on sensory-evoked cortical activation. Most of these studies have looked at widescale activity across the entire limb-associated somatosensory cortex as a marker of post-stroke plasticity and changes in cortical excitability. A limited number of studies have looked at changes in the activity of individual neurons post-stroke within the limb associated somatosensory cortex, however these studies had not thoroughly defined why the particular stimulation parameters had been chosen, if the somatosensory cortex of mice could even reliably respond to the multi-modal features of the stimuli, and if the cortical representations of the stimuli would change based on different stimulus frequencies or durations.

In Chapter 2 of this thesis, I examine the ability of the somatosensory cortex of mice in responding to and differentially representing artificial forms of limb stimulation often used in these previous studies. To do this, I employed piezo-electric bending actuators attached to the cFL and cHL of mice and varied the stimulus frequency from 3-300 Hz as well as the stimulus duration while imaging their somatosensory cortex with calcium imaging.

Hypothesis of Chapter 2: The limb-associated somatosensory cortex will differentially represent different frequencies of limb stimulation, with the greatest somatosensory activity being driven by high frequency stimuli and the differential representation of stimuli most strongly depicted by different patterns of correlation between neurons within cortical networks.

In Chapter 3 of this thesis, I shift to a chronic post-stroke study in awake freely behaving mice in order to measure somatosensory activity before and after stroke. This was done to determine if awake measures of cortical activity match with alterations in cortical activity seen in

past studies of anesthetized animals, and determine the time course for recovery in network activity, functional connectivity and neural assembly architecture. We also measured behavioral recovery post-stroke with two novel automated methods for determining impairment, a tapered beam task and a string pull task, as well as by tracking indices of animal movement in the floating homecage where the awake imaging was done.

Hypothesis Chapter 3: The limb-associated somatosensory cortex will undergo diaschisis within the first two weeks after stroke, resulting in decreased cortical activity and an impairment on behavioral measures. The number of neural assemblies present within the somatosensory cortex will be reduced within the first month as neurons become less selective in their processing of information from the limbs.

Chapter 2: Distinct patterns of activity in individual cortical neurons and local networks in primary somatosensory cortex of mice evoked by square-wave mechanical limb stimulation

Abstract

Artificial forms of mechanical limb stimulation are used within multiple fields of study to determine the level of cortical excitability and to map the trajectory of neuronal recovery from cortical damage or disease. Square-wave mechanical or electrical stimuli are often used in these studies, but a characterization of sensory-evoked response properties to square-waves with distinct fundamental frequencies but overlapping harmonics has not been performed. To distinguish between somatic stimuli, the primary somatosensory cortex must be able to represent distinct stimuli with unique patterns of activity, even if they have overlapping features. Thus, mechanical square-wave stimulation was used in conjunction with regional and cellular imaging to examine regional and cellular response properties evoked by different frequencies of stimulation. Flavoprotein autofluorescence imaging was used to map the somatosensory cortex of anaesthetized C57BL/6 mice, and *in vivo* two-photon Ca^{2+} imaging was used to define patterns of neuronal activation during mechanical square-wave stimulation of the contralateral forelimb or hindlimb at various frequencies (3, 10, 100, 200, and 300 Hz). The data revealed that neurons within the limb associated somatosensory cortex responding to various frequencies of square-wave stimuli exhibit stimulus-specific patterns of activity. Subsets of neurons were found to have sensory-evoked activity that is either primarily responsive to single stimulus frequencies or broadly responsive to multiple frequencies of limb stimulation. High frequency stimuli were shown to elicit more population activity, with a greater percentage of the population responding and greater percentage of cells with high amplitude responses. Stimulus-evoked cell-cell correlations within these neuronal networks varied as a function of frequency of stimulation, such that each stimulus elicited a distinct pattern that was more consistent across multiple trials of the same stimulus compared to trials at different frequencies of stimulation. The variation in

cortical response to different square-wave stimuli can thus be represented by the population pattern of supra-threshold Ca^{2+} transients, the magnitude and temporal properties of the evoked activity, and the structure of the stimulus-evoked correlation between neurons.

Introduction

Investigations of how the somatosensory cortex responds to artificial forms of stimulation, and to what extent patterns of regional and cellular activity can distinguish between distinct stimuli with overlapping characteristics, is important in interpreting studies that use such stimuli to elicit cortical responses in the healthy brain, or as a measure of cortical excitability and plasticity during disease or after injury (Ashby et al., 2019; Brown et al., 2009; Sigler et al., 2009; Sweetnam and Brown, 2013; Winship and Murphy, 2008). While square-wave and sinusoidal patterns of mechanical limb stimulation have been used in studies after cortical injury, and those studies identified deficits in the amplitude and fidelity of evoked activity after damage to the somatosensory cortex (for example, see (Brown et al., 2009; Sweetnam and Brown, 2013; Winship and Murphy, 2008, 2009)), a more detailed investigation across multiple frequencies and intensities of stimulation has not been performed with mechanical square-wave stimuli. Mechanical square-wave stimulation allows precise control of the fundamental frequency (as with sinusoidal stimulation) but includes harmonic frequencies. These harmonics may overlap between different stimuli, and it may, therefore, be more challenging for the somatosensory system to distinguish between these stimuli. Whereas considerable literature exists for somatosensation within the healthy brain in non-human primates (for review, see (Delhaye et al., 2018; Mountcastle, 2005)), and the sensory-evoked response properties of the barrel cortex of rodents has been extensively studied (Adibi, 2019; Petersen, 2019), literature on the sensory

evoked response properties of limb associated somatosensory system of rodents is more limited. Given that rodents are a prominent animal model used to study recovery of reaching and upper limb use after central nervous system damage or disability (Balbinot et al., 2018; Klein et al., 2012), it is important to understand how different forms of somatic and movement related stimuli used in rodent research are processed in the rodent somatosensory cortex. Most current research on the limb-associated somatosensory cortex in rodents utilize artificial forms of mechanical (Foffani et al., 2008; Storchi et al., 2012; Tutunculer et al., 2006; Vardar and Güçlü, 2017, 2020; Winship and Murphy, 2008) or electrical stimuli (Humanes-Valera et al., 2014; Mc Larney et al., 2020; Morales-Botello et al., 2012; Park et al., 2021; Schroeter et al., 2017) to assess sensory-evoked responses using electrophysiology of individual cells or aggregate responses from large cortical regions. Artificial stimuli used for rodent research that may be thought of as relatively simple in comparison to naturalistic stimuli or movements, such as limb oscillation through a single axis of motion, still likely result in the generation of complex multimodal sensory information in the periphery. These multimodal signals may arise from activation of mechanoreceptors at the stimulator attachment site, the propagation of vibration at the fundamental and harmonic frequencies to distal Pacinian corpuscles closely associated with joints and bones (Prsa et al., 2019), the activation of proprioceptive receptors within the muscles and joints, and to a large potential array of signals arising due to deflections of hair follicle associated mechanoreceptors (for review, see (Abraira and Ginty, 2013)). Although particular subsets of cutaneous and proprioceptive mechanoreceptors have long been known in non-human primates to be tuned to characteristics such as stimulus intensity, frequency and receptive field location (Bolanowski et al., 1988; Delhaye et al., 2018; Gescheider et al., 2002; Johnson et al., 2000; Mountcastle, 2005; Mountcastle et al., 1972), the harmonics resulting from square-wave

oscillation of the entire forelimb or hindlimb of mice would likely elicit highly mixed activity in mechanoreceptor populations, with weighted preference to mechanoreceptor populations most sensitive to the particular frequencies and biomechanics of the stimulus.

Calcium imaging has been used as a method for studying activity within regional cortical networks (Kerr et al., 2005, 2007; Ohki et al., 2005; Stosiek et al., 2003; Winship and Murphy, 2008). Here, Ca^{2+} imaging was used to investigate how the limb-associated somatosensory cortex represents different frequencies of square-wave limb oscillation, and if differential patterns of activity in somatosensory neurons and local networks could be detected within the Ca^{2+} response. Flavoprotein autofluorescence imaging (Husson et al., 2007; Michael et al., 2014; Reinert et al., 2007; Shibuki et al., 2003; Weber et al., 2004) was first used to identify limb-associated regions of cortical activation during mechanical forelimb or hindlimb stimulation delivered with piezoelectric actuators (Winship and Murphy, 2008; Winship et al., 2007) (Fig 2.1a). *In vivo* two-photon Ca^{2+} imaging was used to optically record the response properties of individual neurons and local neuronal networks within these limb-associated somatosensory regions during multiple frequencies of contralateral forelimb (cFL) or contralateral hindlimb (cHL) oscillation (Fig 2.1b-d). Our data shows that the magnitude of the neuronal population response in somatosensory cortex is non-linearly related to the frequency of mechanical limb stimulation. High frequency 100Hz, 200Hz and 300Hz stimuli were found to elicit more responding neurons, a greater response strength, and higher average cross-correlation between neurons than lower frequency 3Hz and 10Hz stimuli. Whereas average population response magnitude within the low frequency and high frequency groups was not a strong differentiator of how populations represented stimuli within these groups, the pattern of responsive neurons

within the local neuronal network and differences observed in the cross-correlation maps for populations responding to these stimuli clearly differentiated between stimuli within and between stimulus groups.

Materials and Methods

Animals

Male, two to four month old C57BL/6 mice ($n=10$) were used in this study. Mice were group housed in standard laboratory cages in a temperature-controlled room (23°C), maintained on a 12 hr light/dark cycle, and given standard laboratory diet and water *ad libitum*. All experiments were approved by the University of Alberta's Health Sciences Animal Care and Use Committee and adhered to the guidelines set by the Canadian Council for Animal Care. Animals were euthanized through decapitation following the end of the imaging session.

Identification of forelimb and hindlimb somatosensory cortex representations

A surgical plane of anesthesia was achieved with 20% (w/v) urethane dissolved in saline and administered via intraperitoneal injection (1.25 g/kg; supplemented at 0.25 g/kg as needed). Body temperature was measured using a rectal probe and maintained at $37\pm 0.5^\circ\text{C}$. Mice were administered 0.15 mL of Ringer's solution every 2 hours to maintain hydration levels. The skull was exposed by midline scalp incision and the skin retracted. A metal plate was secured to the skull using cyanoacrylate glue and dental cement and then fastened to the surgical stage to prevent head movement during imaging. A 4 x 4 mm region of the skull overlying the right hemisphere somatosensory region was thinned to 25-50% of original thickness using a high-speed dental drill (~1-5mm lateral, +2 to -2 mm posterior to bregma). This thinned region was

covered with 1.3% low-melt agarose dissolved in artificial CSF (ACSF) at 37°C, then covered with a 3mm glass coverslip. Flavoprotein autofluorescence (FA) imaging was performed through this thin skull preparation before *in vivo* Ca²⁺ imaging to determine somatosensory limb regions on the cortex. These mapped regions were later used for OGB-1 indicator injection and for determination of imaging window coordinates for Ca²⁺ imaging following the FA mapping. For FA imaging, the cortical surface was illuminated with a xenon lamp (excitation band-pass filtered at 450-490nm). Autofluorescence emissions were long-pass filtered at 515nm and captured in 12-bit format by a Dalsa Pantera 1M60 camera mounted on a Leica SP5 confocal microscope. The depth of focus was set between 100-200 μm below the cortical surface.

Custom-made piezoceramic mechanical bending actuators were used to elicit oscillatory limb stimulation during FA and Ca²⁺ imaging. The piezo bending actuators comprised a piezo element (Piezo Systems # Q220-A4-203YB) attached to an electrically insulated metal shaft holding a metal U-bend at its end. The palm of the mouse paw was placed within the U-bend, and the U-bend bent to shape to lightly secure the palm. The metal U-bend made contact across a vertical rectangular area of approximately 3x1mm on the palmar and dorsal surface of the hand. Stimulators were driven with square-wave signals from an A-M Systems Model 2100 Isolated Pulse Stimulator. For FA imaging only, stimulation alternated between contralateral forelimb (cFL) and contralateral hindlimb (cHL) for a total of 40 trials of stimulation of each limb. Placement of actuators was on the glabrous skin of the forepaw or hindpaw, with consistent alignment relative to the flexion of wrist and ankle. Images were captured for 5.0s at 5 Hz (1s before and 4s after stimulus onset; interstimulus interval = 20s). 40 trials for each limb were averaged in ImageJ software (NIH). Frames 1-1.5s after stimulus onset were averaged and

divided by baseline frames 1s before stimulus onset to generate a response maps for each limb. Response maps were thresholded at 50% maximal response to determine limb associated response boundaries, merged, and overlaid on an image of surface vasculature to delineate the cFL and cHL somatosensory areas (Fig 2.1a). These areas were used as guides for Ca²⁺ indicator injections (Winship and Murphy, 2008), and were subsequently imaged.

Calcium imaging

Subsequent to FA imaging as described above, the coverslip and agarose were removed and a 3 x 3 mm craniotomy performed centering over the cFL and cHL functional areas, determined via FA imaging. A dental drill was used to progressively thin the overlying skull until the bone could be removed with forceps, leaving the dura intact. The exposed cortical surface was bathed in ACSF pre-heated to 37°C. Pressure injections of membrane-permeant Oregon Green BAPTA-1 (OGB-1) were made 180-200 µm below the cortical surface of the cFL and cHL cortical regions using glass micropipettes with resistances of 2-5 MΩ (Stosiek et al., 2003; Winship and Murphy, 2008). After OGB-1 injection, the cortex was incubated for 10min with sulforhodamine 101 (SR101) dissolved in DMSO to label astrocytes (Nimmerjahn et al., 2004; Stosiek et al., 2003; Winship and Murphy, 2008; Winship et al., 2007). The craniotomy was then covered with 1.3% agarose dissolved in ACSF and sealed with a glass coverslip.

Two-photon imaging was performed using a Leica SP5 MP confocal microscope equipped with a Ti:Sapphire Coherent Chameleon Vision II laser tuned to 810 nm for OGB-1 and SR101 excitation. A Leica HCX PL APO L 20x 1.0NA water immersion objective was used. Images were acquired using Leica LAS AF using two line-averages, a zoom of 1.7x and a frame-

rate of 25Hz. Images were acquired at 256x256 pixels over an area of 434x434 μm , yielding a resolution of 1.7 μm per pixel. Ca^{2+} fluctuations in neurons, astrocytes, and neuropil were imaged in response to 8 trials at each different frequency and duration of mechanical stimulation (3, 10, 100, 200, and 300Hz for 1s, 0.1s 100Hz & 0.05s 200Hz). While imaging the cHL somatosensory region mapped via FA imaging, only the cHL was stimulated. Likewise, only the cFL was stimulated during imaging of the cFL somatosensory region. The same custom piezo-electric stimulators used for FA imaging were used for calcium imaging. The order of the stimulation frequency was randomized at the beginning of each experiment for each animal. During stimulation, the entire limb underwent an oscillation with the following peak-peak amplitudes by frequency based on the limb weight loaded electromechanical properties of the bending actuator: 280 μm (3 & 10Hz), 335 μm (100Hz), 220 μm (200Hz), 170 μm (300Hz). To determine these peak-peak oscillation amplitudes, the movement of the limb was imaged using a Dalsa Pantera 1M60 camera mounted on a Leica SP5 microscope using a 2.5X objective. The limb was attached to the stimulator and placed on a black background to increase contrast of the limb relative to the background. Bending actuators were driven by an A-M Systems Model 2100 stimulator, an analog stimulator with 1 microsecond timing (250 ns jitter). Three different imaging frame rates and resolutions were recorded for each frequency of limb stimulus based on the limits imposed by the camera hardware: 58fps at 1024x1024 (17.24ms exposure), 100fps at 512x512 (10ms exposure) and 157fps at 256x256 (6.37ms exposure). As all of these imaging frame rates were undersampling relative to the Nyquist criterion for the 300Hz stimuli, we employed several measures to get an index of the peak-to-peak amplitude of the limb oscillation as follows. For all imaging framerates, we recorded extended video (approximately 5 minutes per recording), then used max intensity projections to determine the maximal bending amplitude of the stimulus at

each stimulus frequency. To confirm this method, we compared the max projection measurements and frame-per-frame measurements for low frequency stimuli and found them to be equal. Peak-to-peak deviation measurements from all three imaging framerates at all frequencies were compared and found not to be significantly different. To determine if the peak-to-peak bending amplitude was consistent across multiple stimulus trials, we repeated the video recordings multiple times and separately analyzed each trial. Bending amplitudes were consistent across trials of the same stimulus frequency. Fig 2.1c depicts the various oscillatory stimuli used throughout this study to elicit Ca^{2+} responses in cell populations. Fig 2.1d depicts an example timelapse montage of Ca^{2+} imaging during limb stimulation and example cell responses.

Two-photon image processing and determination of responding neurons

Using custom scripts written in Metamorph (Molecular Devices, California U.S.A.), a median filter (radius, 1 pixel) was applied to each of the image sequences of 8 trial sweeps at each frequency and duration of stimulation in order to remove photodetector related photon transfer noise (e.g. photon-shot noise) from the digitized images. The 8 sweeps at each stimulus frequency and duration were independently averaged. Regions of interest (ROIs) were drawn around visible neurons and astrocytes were excluded from analysis by removing ROIs that co-labelled astrocytes in the SR101 channel. Raw neuronal fluorescence traces were exported from Metamorph and were imported into Excel (Microsoft, Inc.). A 5-point moving triangular filter was applied to each neuronal trace to remove noise artifacts in the temporal domain. We found that this triangular filter did not affect the overall amplitude or main signal properties of our recorded Ca^{2+} traces, but did reduce single frame Ca^{2+} trace artifacts. $\Delta F/F_0$ traces were generated from the raw fluorescence traces as previously described (Winship and Murphy,

2008). Neuronal and neuropil Ca^{2+} signals were analyzed in Clampfit 10.0. Due to the large number of signal traces that required analysis (over 40,000 traces; over 6000 neurons; 10 mice), a range of threshold criteria, based on previous research (Kerlin et al., 2010; Ohki et al., 2005; Roth et al., 2012; Schummers et al., 2008; Winship and Murphy, 2008), were tested to differentiate responsive neuron Ca^{2+} transients from fluorescent noise. This range of threshold criteria was tested against manual annotation of Ca^{2+} responses gathered from multiple observers for a small subset of the experimental dataset from multiple animals. Positive identification of a Ca^{2+} transient from noise within the manual annotation was based on the expected Ca^{2+} transient waveform demonstrating fast rise on the leading edge of the fluorescence, and a slow decay back to baseline. The threshold criteria found to most effectively select Ca^{2+} transient waveforms that met this expected waveform shape was selected for identification of Ca^{2+} transients across all animals. A threshold criteria requiring the Ca^{2+} fluorescence of the cell, averaged from 8 trials, to increase by 3X the standard deviation of the baseline period $\Delta F/F_0$ (baseline defined as 1s before stimulus onset), and remain above this criteria for 160ms (4 successive frames), was used to differentiate the Ca^{2+} transient waveform of a response of the neuron from random noise fluctuations. The percentage of neurons that met an additional criteria of peak $\Delta F/F_0$ greater than 10% were deemed “strongly responsive” neurons (Fig 2.3d) based on previous studies associating >10% increases in OGB-1 $\Delta F/F_0$ with firing of multiple action potentials underlying the Ca^{2+} response (Kerr et al., 2005). Neuronal traces that met these criteria were included in subsequent analysis of peak amplitude and area under the curve (AUC) measurements. AUC was measured as the total area under the curve of the $\Delta F/F_0$ from when the stimulus began to when the $\Delta F/F_0$ returned to the baseline level. AUC was used as a measurement of the sum strength of the calcium transient response over the time course of that particular transient. Neuronal

response maps for visualization (Fig 2.2a) were generated by averaging the calcium imaging frames during the 1s stimulus period for each stimuli and dividing by the average of the 1s baseline frames prior to stimulus onset. Percent of overlapping responsive neurons for each pairwise stimulus comparison (Fig 2.2g) was calculated by counting the number of cells showing common responses between the pairwise stimuli and dividing by the combined total population responsive to the pairwise stimuli. Percent overlapping responsive neurons was averaged across all animals (N=10).

Stimulus-evoked cell-cell correlation analysis

In order to demonstrate a visual example of how the calcium fluorescence of a single cell may correlate with other pixels across an imaging window, a custom Matlab R2018a (Mathworks) script was used to generate an example seed-based stimulus-evoked neuronal correlation map (as shown in Fig 2.4a). With this script, filtered image sequences of $\Delta F/F_0$ were imported into Matlab and the signal trace for a chosen neuron was correlated with the $\Delta F/F_0$ of all pixels within the imaging field. A representative image during 1s 100Hz stimulus measured at a depth of 130 μ m in the cHL region is shown in Fig 2.4a. Using a separate custom written script in Matlab, Pearson product-moment correlation coefficients were calculated between the z-scored signal traces derived from each of our neuronal ROIs in a given optical section. Pairwise Pearson's r correlation coefficients were calculated between each pair of neurons in each optical section. These stimulus-evoked correlation coefficient maps (e.g. Fig 2.4b, 2.5, and 2.6) were created by plotting example matrices of these pairwise correlation coefficients at a specific region of S1 (cFL or cHL) during sensory stimulation of the limb. ROI location co-ordinates were exported from ROI in Metamorph and imported into Matlab in order to compute the

pairwise distance between each ROI. The stimulus-evoked pairwise correlation coefficient for each neuron pair was measured as a function of the distance between the pair (for each frequency of stimulation), and a line fit for regression analysis. Determination of stimulus-evoked correlation map equality was performed using the Jennrich test for correlation matrix equality (Jennrich, 1970) implemented in Matlab (with $p < 0.001$ considered as significant). A stationary bootstrapping procedure was used as a further test of the significance of the Pearson's r calculated between the $\Delta F/F_0$ of each neuron pair. Within the stationary bootstrapping procedure, 10000 iterations were run and a mean block length of 5 frames (200ms) was used based on previous studies indicating the minimum period of time between action potentials necessary to detect a calcium transient using OGB-1 (Tada et al., 2014). Pairwise r values greater than the 97.5th percentile of the stationary bootstrap are indicated by light blue pixels (Fig 2.4c) and the correlation map replotted to show only those correlations meeting the bootstrap criteria (Fig 2.4D). To further determine the degree of correlation map similarity, comparisons of correlation map similarity within repeated trials of the same stimulus, and between trials of different stimuli, were generated using custom Matlab based scripts based on the structural similarity index (SSIM). The SSIM score assessed the localized correlation value, contrast, and structure of correlation maps it was comparing. The SSIM score has a maximal value of 1 that indicates complete similarity between the two maps in comparison. An example of these within and between stimulus comparisons is shown in Fig S2.1. SSIM score results were averaged across all animals (N=10).

Statistical analysis

Univariate comparisons were made using ANOVA with *post hoc* Tukey's honestly

significant difference (HSD) tests for all statistical tests. Stimulus-evoked correlation between cells was analyzed using the Pearson r . Significance for the slope of the pairwise neuron correlation coefficient by distance was analyzed using multiple t-tests between the mean slope value for each stimulus condition and a no-slope null hypothesis, and adjusted using Bonferroni for multiple comparisons. Statistical analyses were performed in GraphPad Prism 6.0 windows version. A p value of ≤ 0.05 was considered statistically significant. A p value of ≤ 0.10 was considered a trend, however not statistically significant. Data are expressed as the mean \pm SEM.

Results

Stimulus frequency preference within somatosensory cortex neurons

To elucidate the effect of the frequency of oscillatory limb stimulation on Ca^{2+} response strength at the level of individual neurons within the population, Ca^{2+} transients evoked by square-wave mechanical limb oscillation were optically recorded during *in vivo* two-photon imaging. Fig 2.2a shows representative “response maps” from one animal illustrating post-stimulus increases in OGB-1 fluorescence in response to different frequencies of stimulation applied to the cHL for 1s each. In all animals imaged, differences in the Ca^{2+} response amplitude and pattern of cortical activation for lower frequency 3/10 Hz stimuli in comparison to higher frequency 100/200/300 Hz stimuli are noticeable, with higher frequency stimuli appearing to result in a greater Ca^{2+} response (quantified for all animals in Figs 2.2 and 2.3). Fig 2.2b,c depict representative neurons selected from the imaging plane shown in A that display different magnitudes in their Ca^{2+} response to the different stimuli. Notably, the neuron in Fig 2.2b is more responsive to high frequency 100, 200, and 300Hz stimuli, whereas the neuron in Fig 2.2c exhibits a mean response that is transient and most strongly activated by 10Hz stimulation.

Patterns of activation to somatosensory stimuli within S1 cortex are distinct

To evaluate the selectivity of neurons to particular square-wave stimuli across local networks of 100-350 cells in somatosensory cortex, threshold criteria were used to define cells exhibiting a significant response to a particular stimulus. Fig 2.2d depicts a representative color-coded image plane of neurons exhibiting a significant (above threshold) response to each stimulus frequency. Variations in stimulus selectivity are apparent. Neurons selective to a single stimulus frequency are illustrated as a uniformly coloured dot, while neurons responding broadly to multiple frequencies are depicted with 2 or more colors. While individual neurons could be preferentially responsive to particular frequencies of stimulation, a significant main effect of stimulus frequency on the percent of neurons with above threshold responses was observed ($F_{(4, 39)} = 4.713$, $p = 0.0034$) (Fig 2.2e). Notably, high frequency 100 & 200Hz stimuli displayed a significantly greater percentage of above threshold responses relative to 3 & 10Hz stimuli. Consistent with previous research by Hayashi et al., 2018, approximately 15% of neurons exhibited a significant response for the 3Hz or 10Hz stimuli, and approximately 30% of the population exhibited a significant response for each of the 100, 200, or 300Hz stimuli (Fig 2.2e). The majority of neurons with above threshold Ca^{2+} responses were responding to multiple stimuli, with approximately $32.7 \pm 4.2\%$ selective to a single stimulus, $33.2 \pm 1.8\%$ activated by two stimuli, and $34.1 \pm 3.8\%$ activated by three or more stimuli (Fig 2.2f). 60.9% of all neurons that were responsive to 3 or more stimuli were responding to 100, 200, and 300Hz. To further determine the amount of overlap between above threshold responsive neurons for each stimulus, we measured the percentage of cells that demonstrated above threshold responses in common with other stimuli. Consistent with the large population of neurons showing preferential

responses to high frequency 100, 200, & 300Hz stimuli, Fig 2.2g demonstrates that higher frequency stimuli displayed a larger percentage overlap in their responsive cell populations as compared to the percent overlap between lower frequency stimuli.

Mean population Ca²⁺ response characteristics do not scale linearly with the number of oscillations in a stimulus

Sensory-evoked Ca²⁺ transients from neurons in S1 were analyzed to determine whether their response characteristics varied proportionately to the square-wave stimulus frequency. If response intensity were defined by the number of repetitive limb oscillations in a stimulus, it would be predicted that the amplitude and decay of the Ca²⁺ transients would increase with each greater frequency. Fig 2.3a depicts mean Ca²⁺ response traces from all above threshold cHL-responsive cells acquired at a fixed depth of 130um from the cortical surface in the S1HL. A greater overall response for high frequency 100, 200, and 300Hz stimuli relative to 3 and 10Hz stimuli is apparent. Quantification of Ca²⁺ transients from all recorded limb responsive regions across all animals is shown in Fig 2.3b-d. Notably, Fig 2.3b shows that the peak amplitude of the sensory evoked above-threshold Ca²⁺ transient did not vary significantly according to stimulation frequency. However, a significant main effect of frequency was observed on AUC ($F_{(4, 39)} = 4.325, p = 0.0054$), with 200Hz stimuli exhibiting significantly greater AUC than 3 & 10Hz stimuli (Fig 2.3c). No evidence of direct scaling of response properties, such that 10Hz would elicit greater neuron activity than 3Hz, or 200Hz greater activity than 100Hz, was observed.

Because a $\Delta F / F_0$ of greater than 10% (measured using OGB-1) has been associated with firing of multiple action potentials underlying the Ca²⁺ response (Kerr et al., 2005), the

proportion of “strongly responsive” neurons with sensory-evoked Ca^{2+} transient amplitude of greater than 10% $\Delta\text{F}/\text{F}_0$ was determined. The proportion of strongly responsive neurons varied with stimulation frequency ($F_{(4, 38)} = 3.669$, $p = 0.0127$) (Fig 2.3d). Post hoc comparisons confirmed that a larger percentage of neurons exhibited peak amplitude of greater than 10% $\Delta\text{F}/\text{F}_0$ for 100 & 200Hz stimuli compared to 3Hz stimuli.

Stimulus-evoked pairwise correlations vary as a function of the square-wave stimulus frequency

Analysis of the stimulus-evoked correlated activity between neurons was used to further define the structure of pairwise interrelationships of Ca^{2+} fluctuations resulting from the sensory stimulus across populations of up to 350 neurons per optical section. These correlations provide an approximation of neurons that respond similarly, and thus allowed us to examine patterns of cortical neuron activity during different stimulus conditions. Fig 2.4a demonstrates a representative example of a seed-cell based stimulus-evoked correlation map for a 1s 100Hz stimulus where the fluorescence over time of the seed cell (orange) was correlated with fluorescence of all other pixels in the image. Neurons with highly correlated and weakly correlated stimulus-evoked activity are observed. Pairwise stimulus-evoked correlation strength between all neurons was also determined. Data for the stimulus-evoked correlation between all cells within network populations was pooled across animals and sorted by stimulus frequency. The distance between neuron pairs was determined by the Euclidean distance between the centers of mass of their cell bodies within the imaging plane. The stimulus-evoked correlation coefficient decreased as a function of the pairwise distance between neurons for all frequencies tested (mean slope of -0.26), a result predicted based on previous studies within the barrel cortex

of mice that demonstrate higher correlations among nearby cells (Kwon et al., 2018; Sabri et al., 2016). The slope of the line fit for the pairwise correlation as a function of distance was not significantly different between stimuli conditions ($F_{(4, 39)} = 0.4616$, $p = 0.7634$), thereby indicating a similar decrease in the stimulus-evoked correlation by distance for all stimuli. Notably, all stimulus conditions exhibited a significant negative slope (Single sample t-test relative to theoretically slope of 0, $p < .05$ with Bonferroni correction for all stimulus conditions). Although this result may suggest a small degree of similarity in the stimulus related Ca^{2+} measurements for neurons found closer together, the correlation between any two particular neurons is poorly predicted by the distance between them as indicated by very low R^2 values for all stimuli (mean R^2 of 0.029). The R^2 values for all stimuli were not significantly different from each other ($F_{(4, 39)} = 0.3522$, $p = 0.8409$), suggesting that this low degree of predictive value did not vary based on the particular stimulus delivered. Thus, these data do not support spatial clustering in response to distinct stimuli. Fig 2.4b gives a color-coded depiction of the stimulus-evoked pairwise correlation between a population of 74 neurons within the cFL somatosensory cortex of a representative animal. Notably, the pattern of pairwise stimulus-evoked correlations varies between stimuli ($p < 0.001$, using Jennrich test of matrix equality (Jennrich, 1970)), thereby illustrating distinct inter-relationships of network activity resulting from different frequencies of stimulation. We further confirmed the significance of these pairwise cross correlations by running a stationary bootstrapping procedure (see methods). Bootstrapping further supported that the pairwise comparisons meeting the bootstrapping criteria varied as a function of the stimulus (Fig 2.4c,d). Across all animals, mean stimulus-evoked pairwise correlation varied significantly as a function of stimulation frequency ($F_{(4, 39)} = 2.902$, $p = 0.0340$) (Fig 2.4e), with a trend towards greater overall stimulus-evoked correlation for high

frequency stimuli.

Frequency or quantity representations in cortical Ca²⁺ transients

Stronger neuronal activation for high frequency 100, 200, & 300Hz stimuli, compared to 3 & 10Hz stimuli, is shown in previous data. However, because the frequency of oscillatory stimulation was varied but duration of stimulation was constant at 1s, the quantity of limb oscillations varied significantly between stimulus conditions. To clarify if stimulus frequency or absolute number of oscillations was the primary driver of distinct patterns of cortical activity, stimuli with 10 absolute oscillations of the limb during the stimulus period were delivered at two frequencies (0.05s at 200Hz and 0.1s at 100Hz). Selective patterns of evoked neuronal Ca²⁺ responses were still observed with these 10 oscillation stimuli (Fig 2.5a), with minimal overlap between neurons responsive to each stimulus (Fig 2.5b). Notably, when stimuli were restricted to 10 oscillations for these 0.05s at 200Hz and 0.1s at 100Hz trials, the lower percentage of responding neurons show reduced overlap relative to longer 1s at 200Hz and 1s at 100Hz stimuli (Fig 2.5b vs. 2.2g). Fig 2.5c illustrates stimulus-evoked correlation maps between a population of 74 neurons within the cFL somatosensory cortex of a representative animal for these 10 oscillation stimuli (from the same animal as displayed in Fig 2.4b). To determine whether the stimulus-evoked correlations observed for these stimuli were repeated over multiple trials during the length of the imaging session, custom Matlab based routines were used to determine the similarity of these maps across trials to generate “within stimulus” comparisons. Stimulus-evoked correlation maps generated from one stimulus were also compared on a trial by trial basis to those generated from the other stimulus to generate “between stimulus” comparisons (see Fig S2.1 for SSIM method). We observed a statistical trend ($p = 0.0540$) suggesting higher stimulus-

evoked correlation map similarity for within stimulus comparisons as opposed to comparisons between the two different 10 oscillation stimuli (Fig 2.5d). Observing data from all of our animals studied, the percent of neurons responding, area under the curve, neuron response amplitude, and the Ca^{2+} response decay tau was not statistically different between 0.05s 200Hz and 0.1s 100Hz stimuli (Fig 2.5e,f,g,h). Thus, the low percent overlap for these 10 oscillation stimuli and the trend towards dissimilarity when comparing their correlation maps (Fig 2.5a-d) is a better indicator of differences between the population responses to these 10 oscillation stimuli than the averaged response characteristics of these populations (Fig 2.5e-h).

Longer stimuli evoke more consistent patterns of activity in somatosensory neuronal networks

Within the vibrissal sensory cortex of rodents, the perceived intensity of oscillatory stimuli grows over the course of longer stimulus durations (Fassihi et al., 2017). Fig 2.5 shows that two short duration stimuli with different frequency, but a fixed absolute number of limb oscillations, activate largely different populations of neurons in the somatosensory cortex. To determine whether the pattern of cortical activity elicited by short duration stimuli would be consistent for longer duration stimuli of the same frequency, short duration 0.1s 100Hz and 0.05s 200Hz stimuli were compared to longer duration 1s 100Hz and 1s 200Hz stimuli, respectively. Fig 2.6a depicts stimulus-evoked correlation maps from the cFL somatosensory cortex of a representative animal. The structural similarity index was used to compare stimulus-evoked correlational maps between these stimuli of fixed frequency but different duration across multiple trials within the same animals (see Fig S2.1 for an example of this). A significant main effect was found for the 100Hz stimulus condition ($F(2,20) = 4.502$, $p = 0.0243$), with the

“Within 1s 100Hz” condition having significantly greater stimulus-evoked map similarity than the “B/T 0.1s 100Hz and 1s 100Hz” condition in post-hoc comparisons (Fig 2.6b). This effect was not significant for the 200 Hz stimuli, though a similar pattern is apparent (Fig 2.6c). Furthermore, a significant main effect is detected when comparing 1s 100Hz to 1s 200Hz stimulus condition ($F(2,20) = 5.243, p = 0.0148$), with the “Within 1s 100Hz” condition having significantly greater stimulus-evoked map similarity than the “B/T 1s 100Hz and 1s 200Hz” condition in post-hoc comparisons (Fig 2.6d). Thus, stimulus-evoked correlational map structure was more similar for repeated trials within stimuli than for comparisons between stimuli of different duration. Longer duration stimuli also elicited a greater percentage of neurons responding (Fig 2.6e), slightly greater average neuron response amplitude (Fig 2.6f), and more overlap between their responsive cell populations (Fig 2.6g).

To further examine whether short, high frequency stimuli (0.1s 100Hz and 0.05s 200Hz) lead to different cortical responses than long, low frequency stimuli (1s 3Hz and 10Hz), we compared the stimulus-evoked correlational maps of these stimuli across multiple trials within the same animals (Fig S2.2a,b). A significant main effect was found for the cell-cell correlation map similarity for within stimuli comparisons to between stimuli comparisons ($F_{(1.834,18.34)} = 12.53, p = 0.0005$), with multiple post-hoc comparisons indicating significantly greater map similarity for within stimulus trials as compared to between stimulus trial comparisons (Fig S2.2b). These stimuli were not differentiated by the mean neuron response amplitude of their responsive neural populations ($F_{(1.811,16.30)} = 1.353, p = 0.2835$) (Fig S2.2c), nor the area under the curve of neural responses ($F_{(1.912,17.21)} = 2.372, p = 0.1248$) (Fig S2.2e). A significant main effect was however seen for the percent of neurons responding ($F_{(1.829,16.46)} = 5.311, p = 0.0186$)

and for the neuron decay tau ($F_{(2,517,22.66)} = 7.051$, $p = 0.0025$), with 1s 10Hz stimuli showing a higher percent neurons responding than 0.05s 200Hz and greater decay tau than 0.1s 100Hz and 0.05s 200Hz (Fig S2.2d,f). A low percent overlap in the responsive neuronal populations was observed between all stimuli (Fig S2.2g).

Discussion

Calcium imaging is a powerful tool to record sensory-evoked response properties of groups of visually identified neurons in the supragranular cortical layers (Kerr et al., 2005, 2007; Ohki et al., 2005; Stosiek et al., 2003; Winship and Murphy, 2008), particularly in rodents. The present study investigated the sensory-evoked Ca^{2+} response in the primary somatosensory cortex of mice to different frequencies and durations of mechanical square-wave limb stimulation using piezoelectric bending actuators. Bending actuators are often used for the study of cortical excitability during disease or after injury due to their simplicity of use and low cost. Despite having no clear naturalistic equivalent, these stimulators likely provide a highly multimodal input to the somatosensory cortex due to their high oscillation amplitude and method of attachment to the limb. We therefore hypothesized that differential activation of diverse populations of peripheral mechanoreceptors for each stimulus frequency would elicit different patterns of activity in somatosensory cortical neuronal networks, and that these distinct patterns would be apparent when analyzing the activity of neurons in these networks. Consistent with previous studies examining the representation of vibro-tactile stimuli in the mouse primary somatosensory cortex (Hayashi et al., 2018), our data demonstrates that patterns of suprathreshold (i.e. spiking) activity in the local neuronal network in S1 are modulated by the frequency and duration of our square-wave stimuli. Notably, Ca^{2+} responses to square-wave

stimuli do not scale proportionally to the absolute quantity of limb oscillations within a temporal period. Instead, 3Hz and 10Hz stimuli appear to show similar levels of cortical activation but are distinguished by their dissimilar patterns of activity in the neuronal network. High frequency 100Hz, 200Hz and 300Hz stimuli all elicit greater response strength (number of neurons active, AUC and percent of strongly responsive neurons) than lower frequency 3Hz and 10Hz stimuli. However, the percentage of neurons responding, the response amplitude and AUC of responsive neurons did not scale linearly with stimulus frequency within the high frequency range. Notably, a trend of reduced response strength is even apparent for cortical responses to 300Hz relative to 100 and 200Hz. This non-linear scaling is consistent with findings that neurons responding to high frequency stimuli over 100Hz are not temporally entrained, but are instead tuned to selective features of the high frequency stimulus (Prsa et al., 2019). A greater average cross-correlation for high frequency stimuli was observed (Fig 2.4e), potentially due to stronger and more frequent responses within the neural population to these high frequency stimuli. Stimulus-evoked correlation maps were more structurally similar for repeated stimuli of the same frequency as compared to repeated stimuli between different stimulus frequencies, suggesting a degree of representational consistency across stimulus trials within a single imaging session.

The correlation structure for different stimuli are known to be influenced by multiple types of correlation including signal correlation (r_{signal}) and spike-count (noise) correlation (r_{sc}) (Cohen and Kohn, 2011; Kohn et al., 2016). Measured r_{sc} has previously been found to be small when neuron responses are weak (Cohen and Kohn, 2011), and the majority of studies measuring r_{sc} within the primate sensory cortex have indicated low r_{sc} in the range of 0.1-0.2 in pairs of nearby neurons with strong r_{signal} (Cohen and Kohn, 2011). Within the mouse whisker barrel

cortex, r_{sc} is highest among neurons with similar orientation tuning and excitability to single-whisker deflections (Kwon et al., 2018). Recent work examining the representation of vibrotactile stimuli within the limb associated somatosensory cortex of mice has further supported low r_{sc} measures in pairs of excitatory cells with strong r_{signal} , however with higher r_{sc} among pairs of inhibitory interneurons (Hayashi et al., 2018). It has been argued that minimizing correlation within the neural population serves to reduce representational redundancy and improves representational efficiency (Barlow, 2001; Simoncelli and Olshausen, 2001). The stimulus associated cell-cell correlation maps here defined patterns of activity within the network, and demonstrated that these patterns of activity were distinct between stimuli. Although neuronal activity to repeated presentations of the same stimulus is known to vary on a trial by trial basis (Hayashi et al., 2018), our data indicate that the structure of the correlation between neuron pairs remains more consistent across trials of the same stimulus than in comparison of trials between different stimuli. However, Ca^{2+} imaging deconvolution methods, that have greater precision when combined with Ca^{2+} indicators of higher temporal fidelity and larger signal-to-noise ratios (Friedrich et al., 2017; Pachitariu et al., 2018; Pnevmatikakis et al., 2016), were not used in this study to approximate spike times and compute spike-count correlations for the pairwise comparisons. Furthermore, the sparse and discontinuous nature of the five frequencies of stimulation tested does not give sufficient information to determine precise tuning curves for cells within the network. Stimulus-evoked correlation maps also can not define whether cells displayed correlated Ca^{2+} signals due to sensory-evoked Ca^{2+} transients, or due to neural silence during the stimulus period. Future studies could make use of Ca^{2+} indicators with higher temporal fidelity, such as the GCaMP7F Ca^{2+} indicator (Dana et al., 2019) or GEVIs (Knöpfel and Song, 2019), to better deconvolve spike timing and compute both signal and spike-count

correlations and their contribution to the neuronal representation for each stimulus.

A general feature of hierarchical somatosensory systems holds that activity within neural populations along the afferent pathway from the periphery are organized into systematic body maps according to their somatotopically arranged receptive fields. Within this system, stimulus information is parcellated on a hierarchical network level as relevant features from each previous level are selectively represented within the higher-order representation of the next level (Delhaye et al., 2018). Although many of the fundamental mechanisms by which afferent signals arise from peripheral mechanoreceptors have been well studied (Abraira and Ginty, 2013; Brunton et al., 2017; Delhaye et al., 2018; Goodwin and Wheat, 2004; Lesniak et al., 2014; Li et al., 2011; Owens and Lumpkin, 2014; Walsh et al., 2015; Zimmerman et al., 2014), mounting evidence points to a large degree of functional overlap between neurons at multiple levels of the CNS in responding to afferent signals from multiple somatosensory modalities (Bui et al., 2015; Delhaye et al., 2018; Doetsch, 2000; Hayward, 2011; Pei et al., 2009; Saal and Bensmaia, 2014). Recent research strongly indicates that single cells within S1 cortex and below may already hold high-level representations of activity from multiple mechanosensory modalities, multiple receptive field locations, or even higher order features such as those associated with movement direction, velocity, texture, shape, orientation, compliance, slip, and rolling (Delhaye et al., 2018; Doetsch, 2000; Hayward, 2011; Jörntell et al., 2014; Saal and Bensmaia, 2014). A proportion of these multimodal neurons have even been found to reside within the spinal cord and brainstem nuclei as the first synaptic targets for afferent fibers emanating from the limbs (Abraira and Ginty, 2013; Bui et al., 2015; Johansson and Flanagan, 2009; Jörntell et al., 2014; Kim et al., 2015; Li et al., 2011; Shishido and Toda, 2017). It has been recently shown in cats that cells of the cuneate

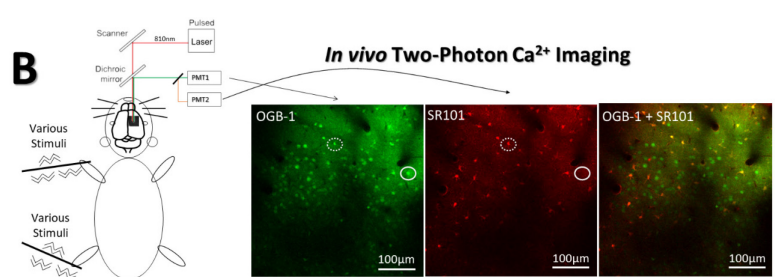
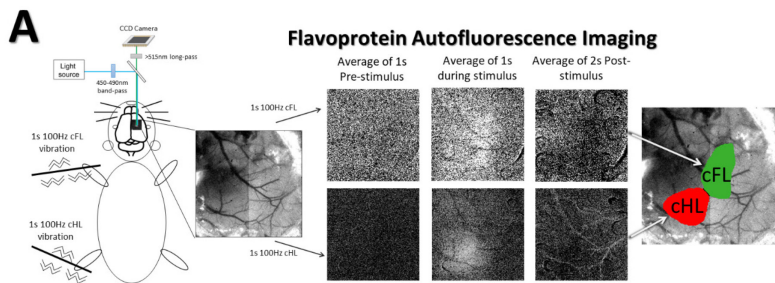
nucleus encode high level information related to unique combinations of contact initiation/cessation, slip, and rolling contact (Jörntell et al., 2014). Thus, even proximal neuronal networks in hierarchical somatosensory pathways may represent complex sensory information within their local neuronal population. It is therefore plausible that the limb-associated S1 cortex in rodents already holds representations of complex stimulus features within its single cell and population code similar to higher mammals. The non-linear differences in response strength to our stimuli, and differences in the cortical representation demonstrated by our 10 oscillation stimuli in comparison to each other and to their longer temporal duration equivalents, both support that mouse S1 cortex is not simply entrained by the stimulus frequency but is instead modulated by the frequency and length of the stimulus. Single cells within S1 barrel cortex have been shown to display tuning related to multi-whisker features such as center-surround feature extraction, angular tuning, and multi-whisker correlations (Estebanez et al., 2018), thereby lending further weight to the prediction that the limb-associated S1 cortex may also represent convergent multimodal stimulus features within the stimulus representations we have depicted here.

This study did not attempt to directly examine the contribution of specific mechanoreceptor populations in the limbs to the afferent signal generated by our square-wave stimuli and their corresponding cortical responses. While it is not possible to give specific predictions on how strongly each modality was represented within the afferent response and cortical activity, peripheral mechanoreceptors are known to have varied activation thresholds at a range of frequencies (Bensmaia, 2008; Muniak et al., 2007), and the overall pattern of evoked activity would therefore reflect mixed afferent signals generated by the stimuli in this study.

Saturation of the calcium response for high frequency limb oscillation could potentially contribute to similarities in the percent of neurons responding (Fig 2.2e) and the average population response magnitude (Fig 2.3) to our high frequency stimuli. However, distinct patterns of cellular responses for neurons responsive to each of the high frequency stimuli (Fig 2.2g), and differences observed in the correlational map structure between different high frequency stimuli (Figs 2.5,2.6), suggest that the calcium response maintained sufficient fidelity to record distinct representations of stimulus frequency. Future studies could make use of measurement methods with higher temporal fidelity and transgenic animals expressing channelrhodopsins in genetically-identified modality specific afferents to further examine the contribution of particular modalities to the cortical response (Li et al., 2011; Prsa et al., 2019). This study also made use of anesthetized animals and passive stimulation. Anesthesia has previously been shown to reduce the magnitude and spread of cortical activation from simple somatic stimuli (Chapin and Lin, 1984; Chen et al., 2005; Lissek et al., 2016). Anesthesia also reduces the potential contribution of corollary discharge and reafference due to voluntary action in modulating sensory input and cortical responses (Crapse and Sommer, 2008). Somatosensory responses are known to be modulated by the relevance of stimuli to behavior and task performance (Dionne et al., 2013; Gomez-Ramirez et al., 2016; Johansen-Berg et al., 2000; Nelson et al., 2004; Scaglione et al., 2014; Staines et al., 2002a), and a combination of responses to artificial and simplified stimuli may not fully predict responses of a sensory system to complex naturalistic stimuli (Kayser et al., 2004; Lehky et al., 1992; Meyer et al., 2016; Sadagopan and Wang, 2009). Within the rodent barrel cortex, for instance, aperiodic stimulus trains associated with naturalistic conditions may have sufficient noise to modulate the response magnitude of cortical networks, especially at higher stimulus frequencies (Lak et al., 2008).

Furthermore, movement-related suppression of self-generated somatosensory activation uses thalamocortical mechanisms in mice to enhance selectivity for touch-related signals (Yu et al., 2016). Although the square-wave stimuli in our study lack the aperiodic, broadband, and re-afferent nature of naturalistic stimuli, our results demonstrate that the limb-associated primary somatosensory cortex of mice differentially represents these distinct mechanical limb stimuli at the level of local neuronal networks in the S1 of anesthetized animals and serves to inform future studies about the relative differences in cortical responses expected between the various stimuli observed herein.

Chapter 2: Figures



C

Stimulus Frequency	3 Hz	10Hz	100 Hz		200Hz		300Hz
Stimulus Duration	1s	1s	0.1s	1s	0.05s	1s	1s

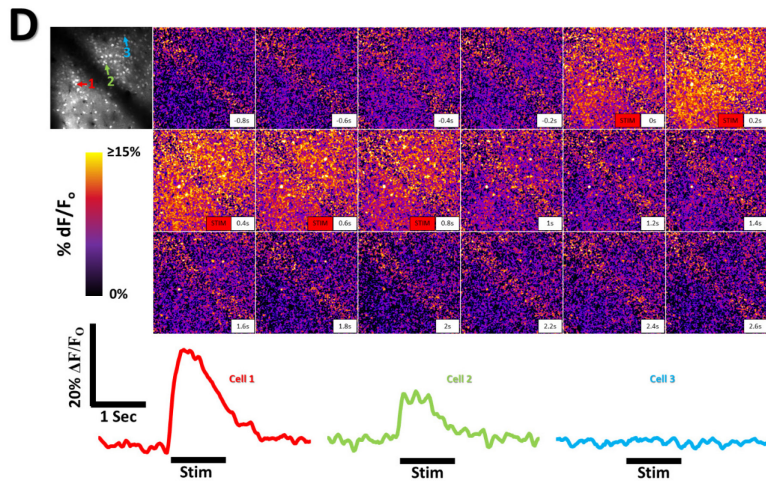


Fig 2.1. Imaging protocols and experimental methods. (A) Oscillatory stimulation (1s, 100 Hz) of the cFL or cHL during imaging of flavoprotein autofluorescence (FA) was used to define S1FL and S1HL limb associated somatosensory regions, respectively. The time course and regional distribution of FA response to cFL (top) and cHL (bottom) stimulation are shown. Each frame displays the averaged $\Delta F/F_0$ fluorescence intensity over the period indicated. FA response maps (see Materials and Methods) were thresholded at 50% of peak response amplitude and merged with an image of the surface vasculature to create color-coded regional maps of cFL and cHL activation. Regional maps from FA imaging were used as guides for membrane-permeant Ca^{2+} indicator OGB-1 AM injection. Astrocyte marker SR101 was bath applied to delineate astrocytes from neurons. (B) Two-photon imaging setup showing OGB-1 and SR101 labelling in the S1HL of one animal. Ca^{2+} imaging in both S1FL and S1HL during oscillatory stimulation was used to assess sensory-evoked single-cell responses. Circle depicts neuron not present on the SR101 astrocyte channel. Dotted circle depicts astrocyte labelling that was omitted from analysis. (C) 5 frequencies of stimulation were applied in random order for each animal. 8 trials of each stimulus were tested for each animal. (D) Cortical Ca^{2+} response to a 1s 200Hz stimulation of the cHL of one example animal. Top left panel depicts an averaged image of the baseline period prior to stimulus onset within the cHL responsive region at 130um depth. Three example cells are indicated on the top left panel with their respective color coded Ca^{2+} signals found below the Ca^{2+} imaging montage.

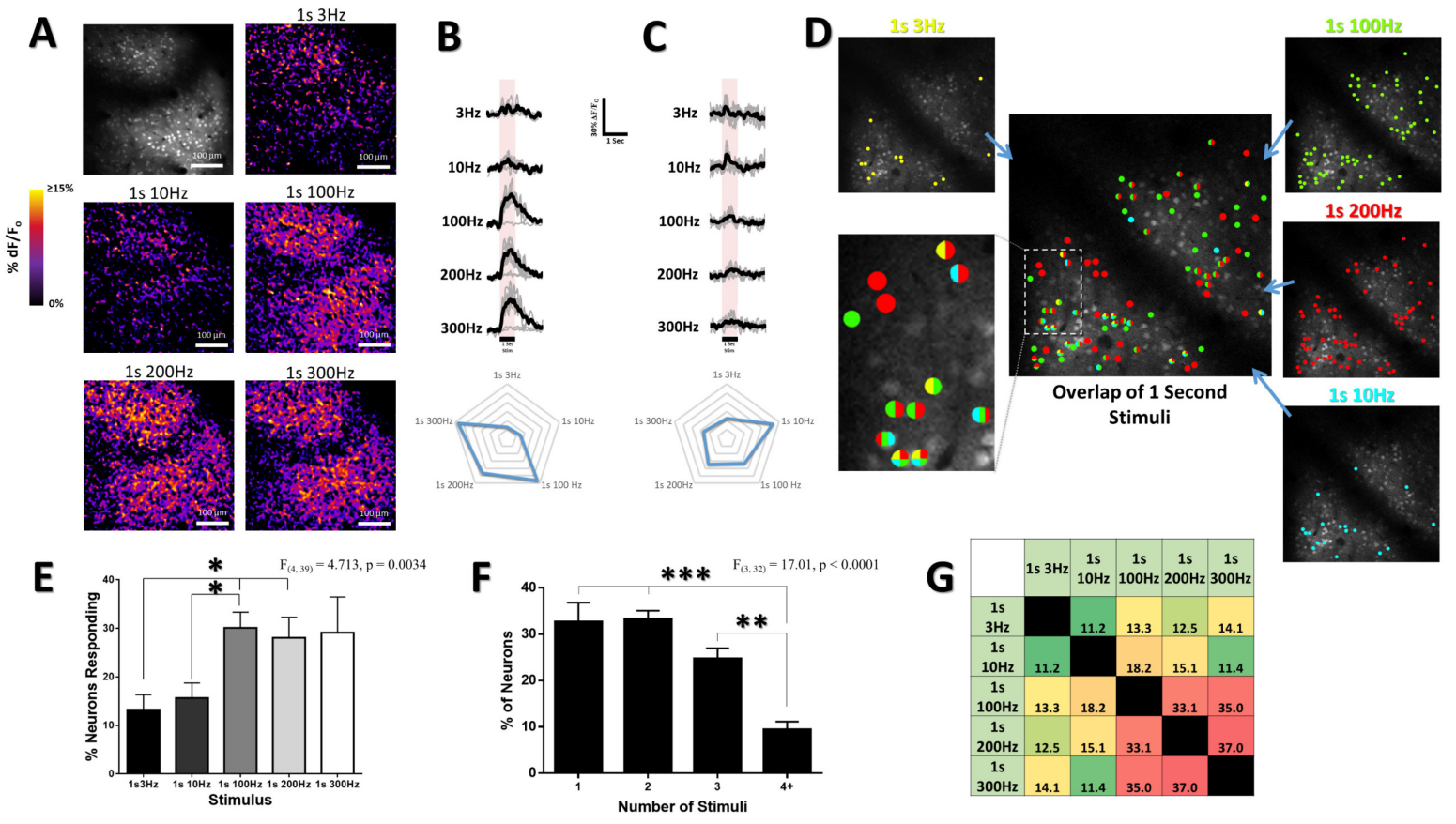


Fig 2.2. Neuronal and population response selectivity to stimulus frequency within the limb associated somatosensory cortex. (A) Difference images illustrating the averaged change in fluorescence $\Delta F/F_0$ from baseline over the 1s stimulus period. Top left panel depicts an averaged image of the baseline period prior to stimulus onset within the cHL responsive region at 130 μ m depth in an example animal. High frequency 100, 200, & 300Hz stimuli elicit greater cortical activation of neurons and neuropil than lower frequency 3 & 10Hz stimuli (quantified in Fig 3). (B,C) Ca^{2+} traces for individual neurons responding to the different stimuli (average of 8 trials of stimulation per limb) are shown for each stimulus for the particular chosen neuron. The neuron in B is more responsive to high frequency 100, 200, & 300Hz stimulation, and displays minimal response to lower frequency 3 and 10Hz stimuli. The neuron in C responds preferentially to 10Hz stimuli. Plots below Ca^{2+} traces indicate peak Ca^{2+} response magnitude for each stimulus (D) Color coded map of responsive neurons superimposed on an optical section at 130 μ m depth in the cHL of an example animal. Neurons were deemed responsive by threshold analysis of somatic responses, with color representing above-threshold responses to stimulation at the particular frequency and duration stated. High frequency stimuli (100 & 200Hz) elicit a greater number of neurons responsive for these stimuli. The inset image displays the same color code used for each particular stimulus and shows how certain cells within this population are selective in their response to particular stimuli, whereas others display overlap in their responsiveness to multiple different stimuli. (E) Mean percent of neurons responding to each of our stimuli across all animals (N=10). (F) Mean percent of neurons within each optical section responsive to 1, 2, 3, or 4+ stimuli across all animals (N=10). (G) Color coded chart displaying the percentage overlap between the neurons responsive to each stimulus for all animals (N=10). High frequency 100, 200, & 300Hz stimuli display greater overlap in their responsive cell populations as compared to the activated cell population overlap for 3Hz and 10Hz stimuli. * $p < 0.05$; ** $p < 0.01$; *** $p < 0.001$

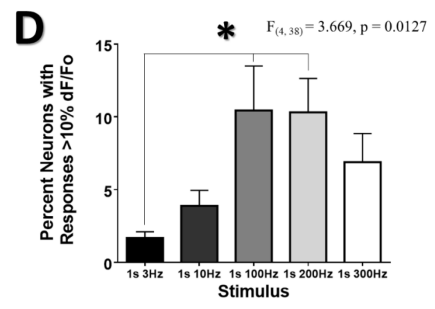
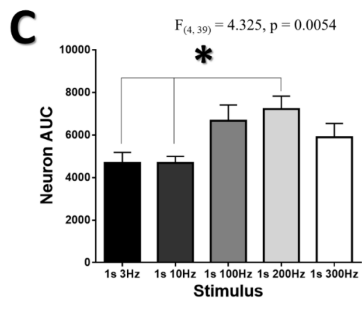
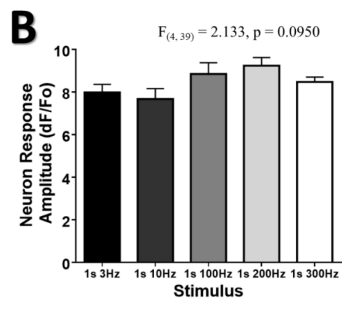
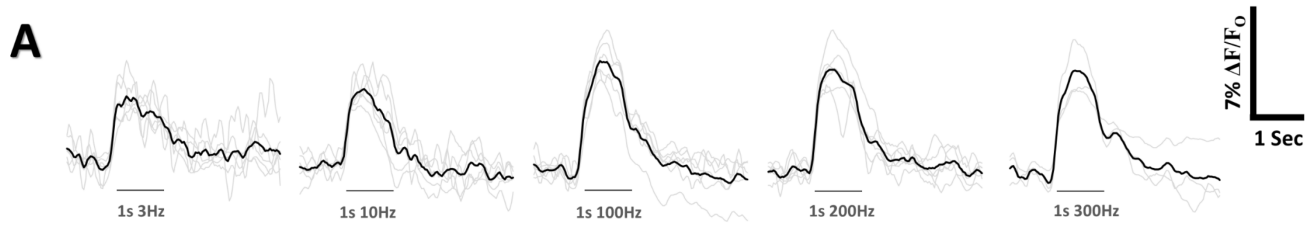


Fig 2.3. Mean population Ca²⁺ response characteristics do not scale linearly with the number of oscillations in a stimulus. (A) Ca²⁺ response traces averaged from all cells at 130μm in the cHL of all animals for each frequency. Grey lines depict individual animal Ca²⁺ responses, black lines are the average of the grey lines from all animals. Average data for b,c,d, & e are taken from all limb representations from all animals. (B) No change in the mean neuron Ca²⁺ response amplitude was observed for any of the stimulus frequencies. A significant effect of frequency was observed for the under the curve (AUC) (C) of neuron responses to the different frequencies of stimulation. (D) A significant effect of frequency was observed on the percentage of neurons with responses greater than 10% ΔF/F₀. *p < 0.05; **p < 0.01; ***p < 0.001

Fig 2.4. Stimulus-evoked pairwise correlations vary as a function of the stimulus frequency.

(A) Example of a seed-cell based correlation technique for a 1s 100Hz stimulus at 130 μ m in the cHL of one animal. The $\Delta F/F_0$ fluorescence over time for the seed cell (orange) was correlated against the fluorescence over time for all other pixels in the imaging frame to generate the correlation map displayed. Example fluorescence traces are shown to the right with an example of a cell with high (blue trace) and low (green trace) correlation to the seed cell. (B) Example heat map matrices of the stimulus-evoked correlation coefficient between a population of 74 neurons within the cFL somatosensory cortex of one example animal. (C) Bootstrapping was used to determine pairwise correlations greater than the 97.5th percentile of the bootstrap and indicated by light blue (see methods). (D) The pairwise correlation values were re-plotted with the correlations that did not meet the bootstrap criteria excluded. (E) A significant effect of stimulus frequency on the mean population correlation coefficient value is observed across all animals (N=10). * $p < 0.05$; ** $p < 0.01$; *** $p < 0.001$

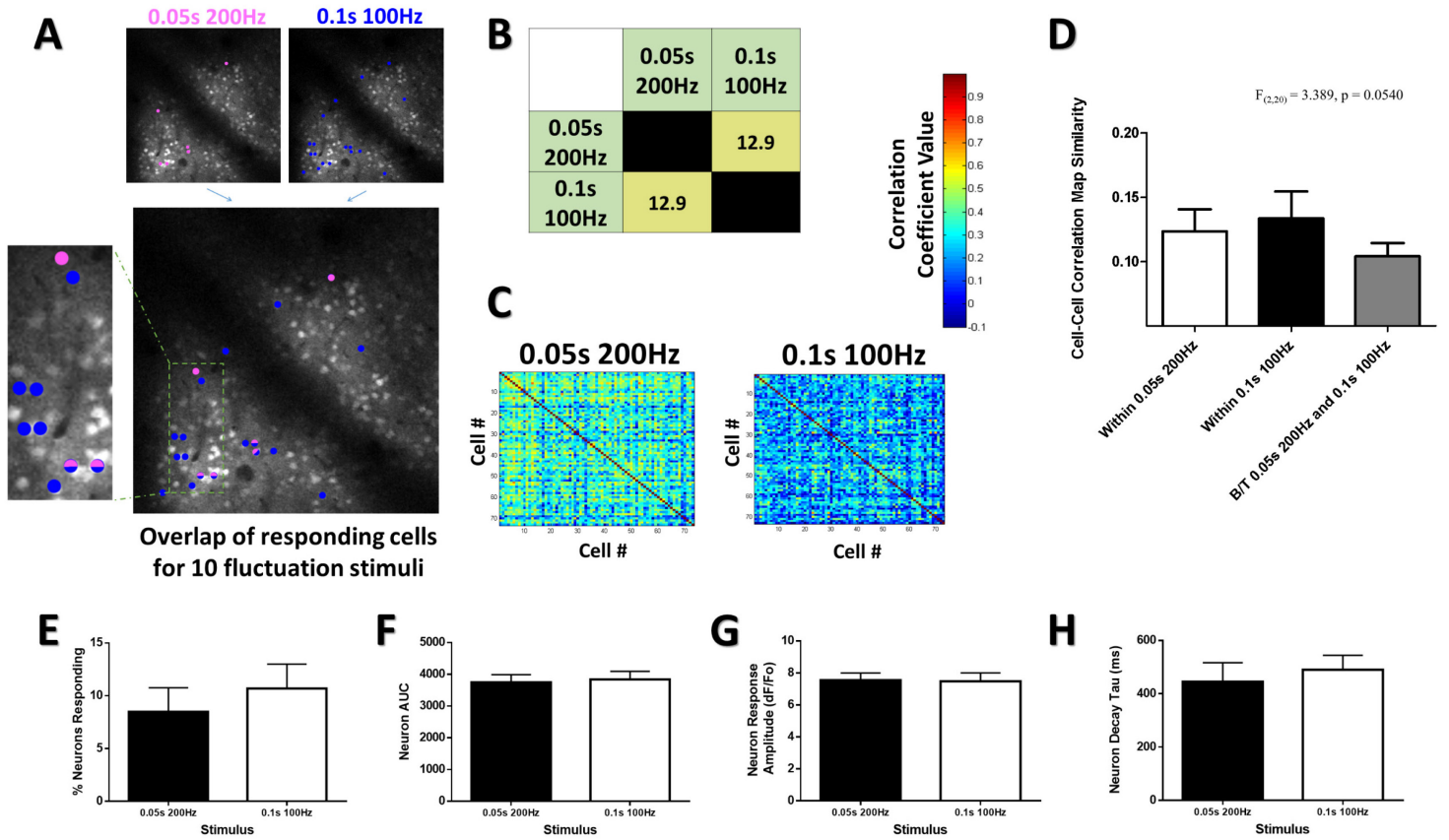
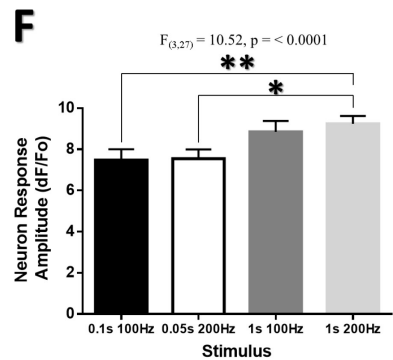
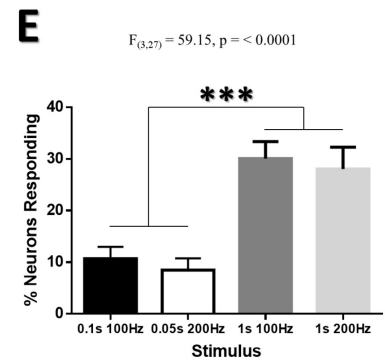
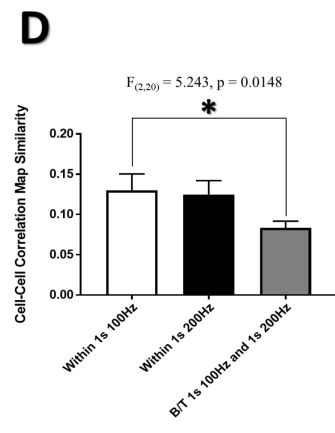
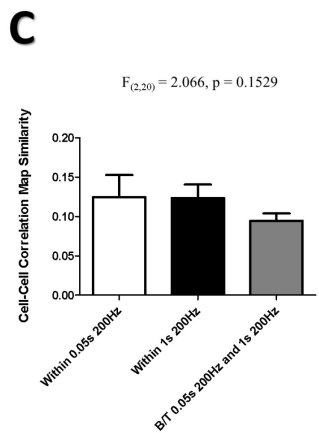
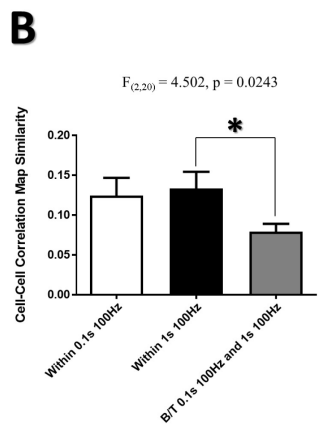
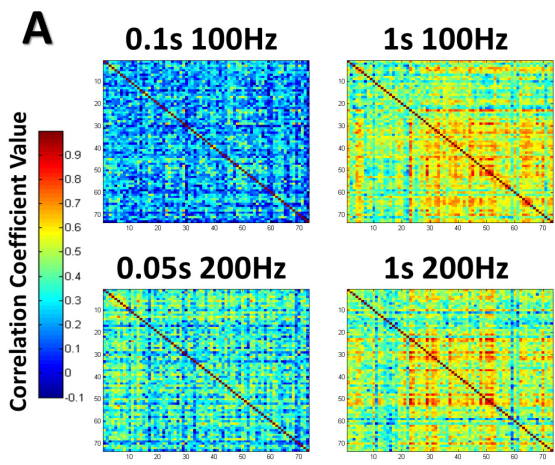


Fig 2.5. Frequency or quantity representations in cortical Ca²⁺ transients. (*A*) Color coded responsive neuron maps superimposed on an optical section at 130 μ m depth in the cHL of an example animal (same animal as in Fig 4). Neurons were deemed responsive by threshold analysis of somatic responses (see methods), with color representing above-threshold responses to stimulation at the particular frequency and duration stated. The overlapping image displays the same color code used for each particular stimulus and shows how certain cells within this population are selective in their response to particular stimuli, whereas others display overlap in their responsiveness to multiple different stimuli, despite all stimuli having the same number of limb oscillations (10 mechanical oscillations of the limb). (*B*) Color coded quantification chart displaying the percentage overlap between the neurons responsive to each stimulus quantified for all animals (N=10). (*C*) Example heat map matrices of the pairwise stimulus-evoked correlation coefficient between a population of 74 neurons within the cFL somatosensory cortex of one example animal at 160 μ m depth for our 10 oscillation stimuli. (*D*) Structural similarity comparison of the maps for all trials depicts a trend towards greater map similarity for within stimulus conditions than between stimulus comparisons. No effect of frequency was seen for the percent of neurons responding (*E*), AUC (*F*), neuron response amplitude (*G*), or decay tau (*H*) for responsive neuron populations. *p < 0.05; **p < 0.01; ***p < 0.001



G

	0.1s 100Hz	0.05s 200Hz	1s 100 Hz	1s 200Hz
0.1s 100Hz		12.9	17.8	14.2
0.05s 200Hz	12.9		11.5	12.4
1s 100 Hz	17.8	11.5		33.1
1s 200Hz	14.2	12.4	33.1	

Fig 2.6. Longer stimuli evoke more consistent patterns of activity in somatosensory neuronal networks. (*A*) Example heat map matrices of the pairwise stimulus-evoked correlation coefficient between a population of 74 neurons within the cFL somatosensory cortex of one example animal at 160 μ m depth for 100 and 200Hz stimuli of different durations. Structural similarity comparison of the maps for all trials depicts greater map similarity for within stimulus conditions than between stimulus for 0.1s 100Hz and 1s 100Hz comparisons (*B*), and a trend for 0.5s 200Hz and 1s 200Hz comparisons (*C*). Significantly less map similarity is seen between 1s 100Hz and 1s 200Hz comparisons than for within stimulus comparisons (*D*). A significant effect of stimulus duration is observed in the percent of neurons responding (*E*) and in the neuron response amplitude (*F*). (*G*) Color coded quantification chart displaying the percentage overlap between neuron populations responsive to each stimulus quantified for all animals (N=10). *p < 0.05; **p < 0.01; ***p < 0.001

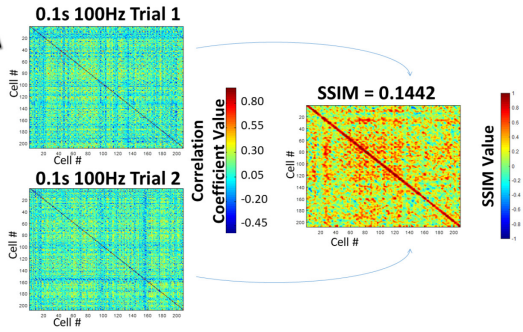
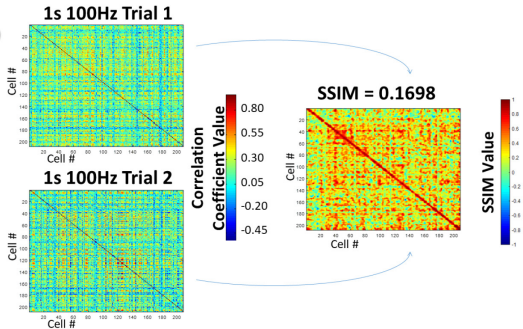
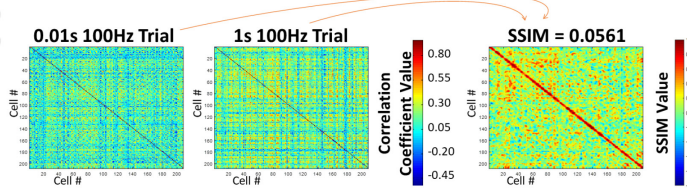
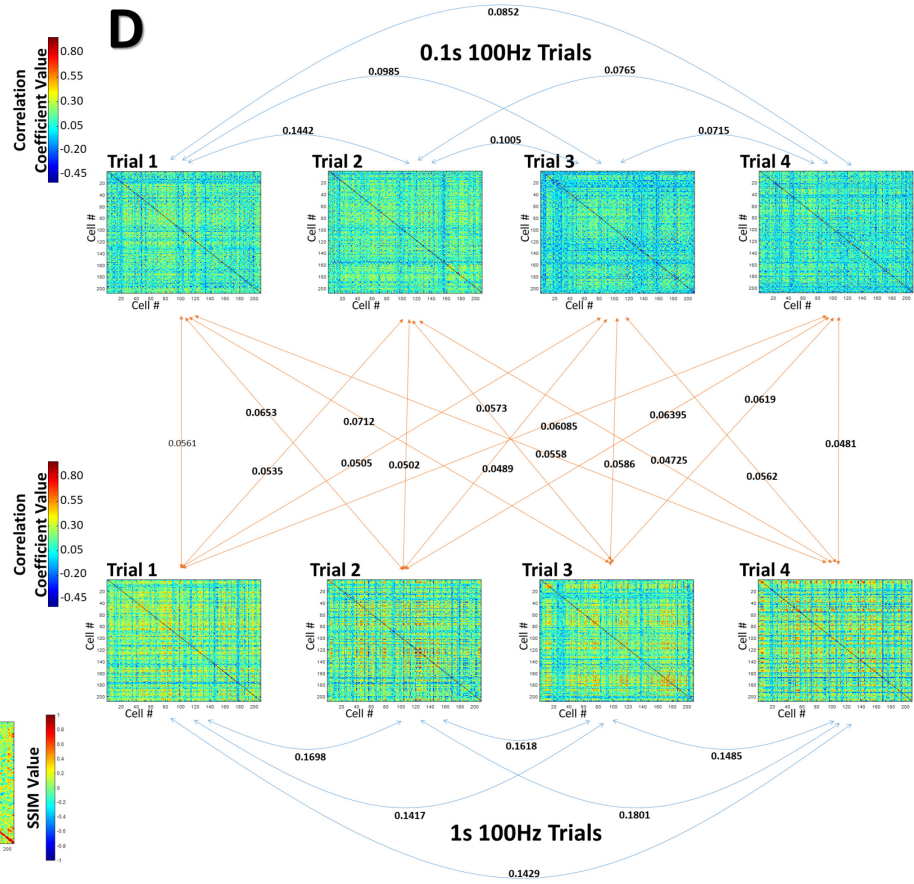
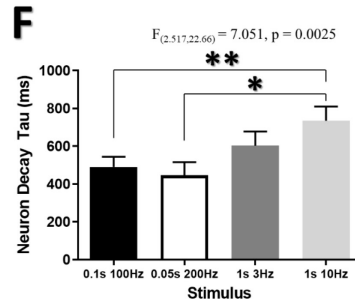
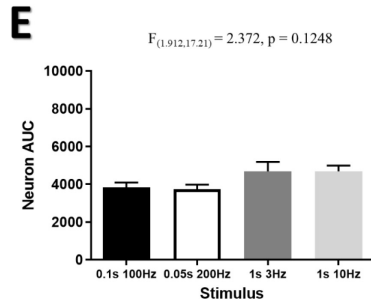
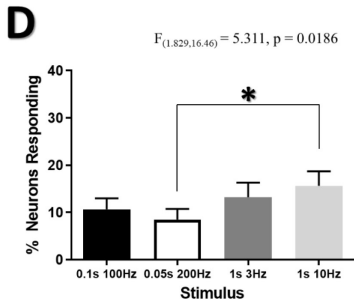
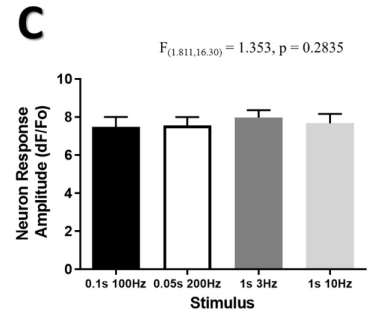
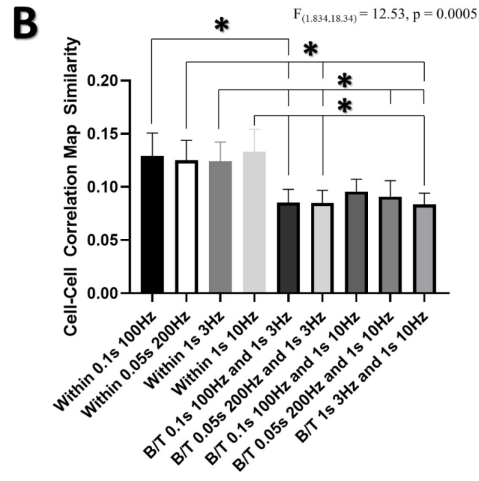
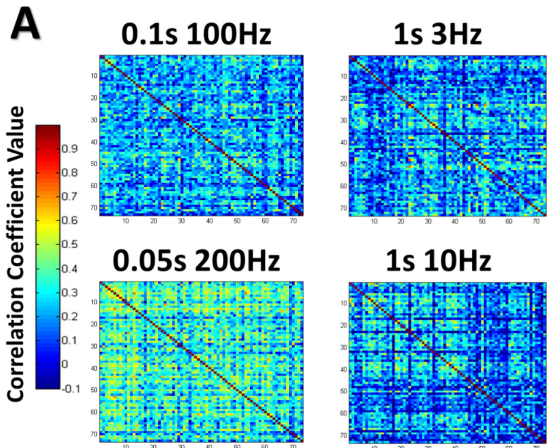
A**B****C****D**

Fig S2.1. Visual example of the structural similarity (SSIM)-based method for trial-by-trial comparisons of correlational map similarity. In this example depicting the stimulus-evoked correlation maps from an example animal in the cHL at 130um depth, the SSIM value and SSIM comparison image display greater similarity for within trials of 0.1s 100Hz (*A*) and within trials for 1s 100Hz (*B*). Comparisons between trials of stimuli with different frequency or temporal durations demonstrate less structural similarity and a lower SSIM value (*C*). To generate the SSIM charts seen in Figs. 5&6, 8 trials of each stimulus were compared for SSIM value within and between stimuli as shown in (*D*) (comparison between 4 trials of each shown here).



G

	0.1s 100Hz	0.05s 200Hz	1s 3Hz	1s 10Hz
0.1s 100Hz		12.9	12.0	13.0
0.05s 200Hz	12.9		11.2	13.3
1s 3Hz	12.0	11.2		11.2
1s 10Hz	13.0	13.3	11.2	

Fig S2.2. Short duration, high frequency stimuli lead to differential cortical activity from long duration, low frequency stimuli. (*A*) Example heat map matrices of the pairwise stimulus-evoked correlation coefficient between a population of 74 neurons within the cFL somatosensory cortex of one example animal at 160 μ m depth for 0.1s 100Hz, 0.05s 200Hz, 1s 3Hz, and 1s 10Hz stimuli. Structural similarity comparison of the maps depicts greater map similarity for within stimulus trial conditions than between stimulus trial comparisons (*B*). A significant effect of stimulus is observed in the percent of neurons responding (*D*) and in the neuron decay tau (*F*), but not in the neuron response amplitude (*C*) or the neuron AUC (*E*). (*G*) Color coded quantification chart displaying the percentage overlap between neuron populations responsive to each stimulus quantified for all animals (N=10). * $p < 0.05$; ** $p < 0.01$; *** $p < 0.001$

Chapter 3: Photothrombotic stroke is associated with reduced cortical activity, deficits in functional connectivity and alterations in neural assembly architecture at early time points within the peri-infarct cortex as measured in awake behaving animals

Abstract

Despite substantial recent progress in mapping the trajectory of network plasticity resulting from focal ischemic stroke, questions remain about the state of neuronal excitability and activity within the peri-infarct cortex of mice. Mounting evidence points to a deficit in sensory-evoked cortical activation after stroke despite multiple markers of impaired inhibitory neurotransmission and a potential for epileptogenic hyperexcitability. However, most of these findings have come from anesthetized animals, acute tissue slices, or immunoassays on extracted tissue, and thus may not reflect cortical activity dynamics in the intact, awake cortex. Here, *in vivo* two-photon calcium imaging of awake head-fixed mobile mice in a floating homecage was used to longitudinally track cortical activity, network functional connectivity, and neural assembly architecture at baseline and for 2 months following photothrombotic stroke targeting the forelimb somatosensory cortex. We demonstrate for the first time a significant loss of neural network functional connectivity and deficits in neuronal assembly architecture concurrent with a trend towards reduced neuronal firing within the peri-infarct cortex. Notably, network dysfunction was highly localized, and these same network deficits could not be detected a short distance outside the peri-infarct cortex, even in regions demonstrated to be a site of forelimb representational remapping. Cortical activity in these distal remapping regions trended towards an increase in firing rate during movement at 4 weeks post-stroke. Finally, we demonstrate that deficits in peri-infarct neural function and network architecture occur concurrently with a behavioral deficit in the tapered beam task and resolve on a timescale consistent with recovery on this task.

Introduction

Previous research examining the post-stroke brain has produced conflicting findings on the state of neuronal activity and excitability within peri-infarct cortical tissue. Data from anesthetized rats suggested elevated spontaneous multiunit firing within the peri-infarct cortex of the post-stroke brain, especially at early time points 3-7 days after stroke (Schiene et al., 1996). Other studies have identified downregulated GABAergic inhibition in peri-infarct cortex (Mittmann et al., 1998; Neumann-Haefelin et al., 1998, 1999; Qü et al., 1998b; Redecker et al., 2002; Schiene et al., 1996), degeneration of parvalbumin-positive inhibitory interneurons (Luhmann et al., 1995; Neumann-Haefelin et al., 1998), decreased paired pulse inhibition (Buchkremer-Ratzmann and Witte, 1997; Domann et al., 1993; Fujioka et al., 2004), increased NMDA receptor mediated excitation (Qü et al., 1998a; Que et al., 1999), and a downregulation of KCC2 (Jaenisch et al., 2016; Jin et al., 2005; Khirug et al., 2021; Martín-Aragón Baudel et al., 2017; Schulte et al., 2018). Together, these changes are believed to contribute to post-stroke cortical hyperexcitability and the potential for epileptogenesis, a common occurrence in the post stroke brain (Jaenisch et al., 2016; Witte and Freund, 1999). However, other studies have indicated that the sensory-evoked responsiveness of the peri-infarct cortex is diminished after focal photothombotic stroke (Brown et al., 2009; Chen et al., 2012; Lim et al., 2014; Sigler et al., 2009; Sweetnam and Brown, 2013; Sweetnam et al., 2012; Winship and Murphy, 2008). Furthermore, even after months of recovery following contralateral forelimb (cFL) representation targeted stroke, the remapped representation of the cFL has been shown to display prolonged modes of activation with lower amplitude (Brown et al., 2009) and reduced temporal fidelity (Sweetnam and Brown, 2013).

To date, no studies have longitudinally tracked changes in the cortical activity of peri-infarct cortical networks after stroke in mobile rodents, and most studies that have examined post-stroke cortical responsiveness have used surgical preparations with anesthetized animals. Anesthesia disrupts cortical activity dynamics and functional connectivity between cortical areas (Cramer et al., 2019; Grandjean et al., 2014; Jonckers et al., 2014; Kalthoff et al., 2013; Nasrallah et al., 2014) and reduces the potential contribution of corollary discharge and reafference due to voluntary action in modulating sensory input and cortical responses (Crapse and Sommer, 2008). Anesthesia has previously been shown to reduce the magnitude and spread of cortical activation from simple somatic stimuli (Chapin and Lin, 1984; Chen et al., 2005; Devonshire et al., 2010; Lissek et al., 2016). It's been noted that at levels of the somatosensory pathway as early as the thalamus, anesthesia in rodents results in modulation in the processing of external sensory stimuli. For example, neurons of the ventroposterior medial area of the thalamus in rodents under anesthesia show small, single-whisker receptive fields (RFs) (Ebner and Kaas, 2015). In contrast, low depths of anesthesia result in multi-whisker RFs (Friedberg et al., 1999), and even up to 14 whisker RFs in awake animals (Faggin et al., 1997; Moore and Nelson, 1998; Nicolelis and Chapin, 1994). These results suggest alterations in sensory processing of external stimuli present in the anesthetized state that are not present in awake animals. While it has recently been shown on a neural population level that the somatosensory cortex of mice is able to differentially represent different frequencies of artificial stimuli under urethane anesthesia (Bandet et al., 2021), other studies have also indicated that a combination of responses to artificial and simplified stimuli under anesthesia may not fully predict responses of a sensory system to complex naturalistic stimuli (Kayser et al., 2004; Lehky et al., 1992; Meyer et al., 2016; Sadagopan and Wang, 2009). It has also recently been shown that the propagation pattern

of cortical activity differs between evoked and spontaneous activity, with spontaneous activity showing more complex trajectories and lower activity amplitudes (Afrashteh et al., 2021). Somatosensory responses are also known to be modulated by the relevance of stimuli to behavior and task performance (Dionne et al., 2013; Gomez-Ramirez et al., 2016; Johansen-Berg et al., 2000; Nelson et al., 2004; Scaglione et al., 2014; Staines et al., 2002a). Likewise, movement-related suppression of self-generated somatosensory activation in mice uses thalamocortical mechanisms to enhance selectivity for touch-related signals (Yu et al., 2016). Within the somatosensory cortex are also a subset of neurons that display activity prior to the onset of voluntary movement (London and Miller, 2013; Nelson, 1987), potentially as a result of corollary signals from central and peripheral inputs modulating the somatic thresholds prior to onset of movement. A subset of neurons within S1 also discharge during limb movements prior to the onset of direct touch, or even during movement without tactile contact, and may even show directional tuning in their activity (Bensmaia and Helms Tillery, 2014). Together, these studies point to a complex, interconnected system that modulates the activity of somatosensory networks in the awake behaving animal that is either not present or is altered in studies of evoked cortical activity under the anesthetized state.

To investigate stroke recovery while avoiding the potential confounds of anesthesia, the present work used Ca^{2+} imaging of imaging regions within and adjacent the peri-infarct area of a focal photothrombotic stroke directed at the cFL somatosensory cortex of mice. We used imaging of awake, freely behaving head-fixed mice in a mobile homecage to longitudinally measure cortical activity, functional connectivity, and neural assembly architecture at baseline and each week for 2 months following stroke onset. We also measured behavioral recovery from

stroke on a tapered beam task, string pull task, and evaluated patterns of movement within the mobile homecage to determine the time course of sensorimotor deficits related to changes in cortical activity and network architecture. Previous research has demonstrated a recovery process for single neuron stimulus selectivity and response properties that begins with a 2-week period of significantly reduced sensory-evoked cortical responses to cFL stimulation, and with extensive plastic changes spanning up to 2 months after stroke (Winship and Murphy, 2008, 2009). We therefore hypothesized that the limb-associated somatosensory cortex would show a deficit in cortical function within the first several weeks after stroke, resulting in a deficit in cortical firing during both moving and resting states, as well as aberrant functional connectivity and neural assembly architecture within the same period. We also predicted that this deficit in cortical function would result in greatest impairment in behavioral measures during the first 2-weeks after stroke, with progressive recovery potentially spanning months. Here, we provide the first evidence of altered neural network functional connectivity and altered architecture of neural assemblies, concurrent with reduced neural activity within the peri-infarct region. In our model, these changes were concentrated to the first week after photothrombotic stroke and localized to the immediate peri-infarct region. We demonstrate that these transient peri-infarct deficits are concurrent with behavioral deficits on the tapered beam task.

Methods

Animals

Three to nine month old Thy1-GCaMP6S mice (Strain GP4.3, Jax Labs) (N=16 stroke (average age: 5.4 months), 5 sham (average age: 6 months)) were used in this study. Mice were group housed in standard laboratory cages in a temperature-controlled room (23°C), maintained on a 12 hr light/dark cycle, and given standard laboratory diet and water *ad libitum*. Cages were randomly assigned to stroke or sham groups such that stroke and sham mice did not co-habitate the same cages. Animal weight was monitored daily during the entirety of the experiment. All experiments were approved by the University of Alberta's Health Sciences Animal Care and Use Committee and adhered to the guidelines set by the Canadian Council for Animal Care. Animals were euthanized through decapitation under deep urethane anesthesia following the end of the final imaging session.

Chronic cranial window implantation

Mice were implanted with a chronic cranial window (Holtmaat et al., 2009) four weeks prior to the first imaging time point (Fig 3.1b). A surgical plane of anesthesia was achieved with 1.5% isoflurane. Body temperature was measured using a rectal probe and maintained at $37\pm 0.5^{\circ}\text{C}$. Mice were administered 0.15 mL of saline subcutaneously to maintain hydration levels. Dexamethasone (2 ug/g) was given subcutaneously to prevent cortical swelling and hemorrhaging during the craniotomy procedure. The skull was exposed by midline scalp incision and the skin retracted. The skull was gently scrapped with a scalpel to remove the periosteum. Grooves were scraped into the skull surface to improve adhesion of dental cement to the skull. A 4 x 4 mm region of the skull overlying the right hemisphere somatosensory region was thinned to

25-50% of original thickness using a high-speed dental drill (~1-5mm lateral, +2 to -2 mm posterior to bregma). A dental drill was used to progressively thin the overlying skull until the bone could be removed with forceps, leaving the dura intact. The exposed cortical surface was bathed in sterile saline solution. A 5mm diameter coverslip was held in place over the craniotomy and its edges attached to the skull using cyanoacrylate glue. A metal headplate was positioned and secured to the skull using dental cement. Animals were injected subcutaneously with buprenorphine (1.0 mg/kg), removed from the isofluorane, and allowed to recovery in a temperature-controlled recovery cage. Mice were returned to their home cage once recovered and monitored daily for weight and post-surgical signs for the duration of the chronic experiment. Mice were allowed to recover for a period of two weeks after window implantation prior to beginning behavior and task habituation (Fig 3.1c). Animals were excluded at the 2 week post-implantation timepoint if their cranial window became cloudy or non-imageable.

Tapered beam task habituation, testing and analysis

Methods for tapered beam habituation and automated recording and analysis have been described previously (Ardesch et al., 2017), with minor modification as follows. Nesting material from the homecage was placed inside of a dark box at the narrow end of the beam to motivate animals to cross the beam. For the first three sessions, mice were placed at the wide end of the beam and allowed to freely explore the beam for a period of 2 minutes, after which the experimenter placed a sheet of paper behind the animal as it crossed the beam to block its return path to the wide end and motivate it to cross to the narrow end with dark box. Once the mouse had reached the dark box with bedding material at the narrow end, they were given 60 seconds within the dark box to associate crossing the beam with reaching the safety of the dark box. The

dark box was transported to their respective homecage for the animal to further associate reaching the dark box with a safe transition to their homecage. On subsequent days, mice were continuously run through the tapered beam for a period of 2 mins each, with a return to their homecage after each crossing. On each of the 3 days prior to the first Ca²⁺ imaging session, mice were tested with three crossings of the beam per day to determine baseline crossing performance. Left and right side slips were captured automatically by Raspberry Pi computer attached to touch sensors on the tapered beam, and Python scripts run to determine number of slips for each side and distance to first slip. Performance on the 9 baseline trials were average to determine a singular average baseline performance level. Mice were tested with three trials on each day prior to each weekly post- imaging timepoint to measure changes in performance.

String pull task habituation, testing and analysis

Methods for string pull habituation and testing have previously been described (Blackwell et al., 2018a; Inayat et al., 2020), with modification as follows. For habituation, mice were individually placed in a transparent rectangular cage without bedding and allowed to freely explore for a period of 5 minutes. 20 strings with variable length were hung over the edge of the cage. Half of the strings were baited with chocolate flavored sucrose pellets. Mice were removed from the apparatus once all of the strings had been pulled into the cage, or once 20 minutes had elapsed. On subsequent days 2 and 3, mice were again placed in the cage with 20 strings to pull. Following this 3-day habituation, from days 4-14 mice were habituated in an alternate transparent string pull box with high sides and transparent front face for video recording. Within this second habituation box, mice received 3 trials with baited strings hung facing the recording camera. The session was terminated when the animal had pulled all three strings or once 20

minutes had elapsed, and the apparatus prepared for the next mouse. On the last day prior to the first Ca^{2+} imaging session, 3 trials of string pull from each mouse were recorded with the use of a GoPro Hero 7 Black (60 fps, 1920×1080 pixels). Mice were re-tested with this same 3 string protocol the day prior to each of their weekly imaging timepoints. Video recordings were analyzed using a semi-automated Matlab string pull package (Inayat et al., 2020). Reach and withdraw movement scaling for the left and right paw was calculated by running a Pearson's correlation between the series of Euclidian distances that the paw travelled during each of the reach or withdraw movements during the string pull and correlating with the peak speed of the paw during each of the respective reaches or withdraws (Blackwell et al., 2018b). A value of 1 indicates a strong linear relationship between longer reach/withdraw paw movement distance and greater peak speed that the paw obtained. Paw reach distance was calculated as the average distance that the paw travelled during each reach movement. Path circuitry is used as a measure of how direct of a path a reach or withdraw movement takes between its starting and end points and is calculated as the total distance travelled divided by the Euclidian distance between the start and end points (Blackwell et al., 2018b). The greater the path circuitry value is above 1, the more the path of the paw deviated from the ideal direct path between the start and end points of the reach/withdraw. A bimanual correlation coefficient was calculated by first detrending the timeseries of Y-axis paw position to remove general changes in the posture of the animal over the course of the string pull attempt, then running a Pearson's correlation between the Y-axis paw position measurements for the right and left paw. A spatial entropy image from each string pull was calculated from the 1D projection of the string pull frames and thresholded at 50% of max to assess the amount of randomness of the animal's movement during the string pull (Fig 3.5g,h). An average standard deviation image for the movement of the paws only was calculated

from the 1D projection of the string pull frames and thresholded at 50% of max standard deviation to determine the amount of variability of hand position during the string pull (Fig 3.5i,j).

Mobile floating homecage habituation and measurement of movement parameters

Methods for floating homecage (Neurotar, Finland) habituation have previously been described (Kislin et al., 2014), with modification as follows. Two weeks after cranial window implantation, each mouse was handled for 5 minutes 3 times per day for the first 2 days to habituate them to handling. For days 3-4, each mouse was handled and repeatedly wrapped and released with a soft cloth for a period of 5 mins 3 times per day in order to habituate to the wrapping procedure. Mice were also given 1 period of 5 minutes each per day to freely explore the floating homecage without being head-restrained. For days 5-8, twice per day the animals were head-restrained in the floating homecage and allowed to move around the floating homecage for a period of 15 minutes with the room lights off before being returned to their cage. For days 8-14, twice per day the mice were head-restrained in the floating homecage for 25 minutes with the floating homecage attached to the microscope in the same conditions in which the animals would be imaged on day 15 onwards. On day 14 (one day prior to their first imaging session) baseline performance on the string pull and tapered beam tasks was measured prior to their last habituation in the floating homecage. Animal movement within the homecage during each Ca^{2+} imaging sessions was tracked to determine animal speed and position. Animal speed was thresholded at 30mm/s to determine periods of time in which the animal was moving and periods of rest were determined as speed below 30mm/s. The amount of time the animal spent in the middle quadrant of the floating homecage was quantified from the tracked position of the

animal and divided by the total time of the recording to determine the tendency of the animal to make central crossings of the floating homecage.

Identification of forelimb and hindlimb somatosensory cortex representations using widefield Ca²⁺ imaging of sensory-evoked responses

On day 10 of habituation, mice were anesthetized with 1.25% isoflurane after they had completed all daily task training and floating homecage habituation. Mice were head-fixed on a stereotaxic frame with continuous isoflurane anesthesia. Body temperature was measured using a rectal probe and maintained at 37±0.5°C. The cortical surface was illuminated with a xenon lamp (excitation band-pass filtered at 450-490nm). Fluorescent emissions were long-pass filtered at 515nm and captured in 12-bit format by a Dalsa Pantera 1M60 camera mounted on a Leica SP5 confocal microscope using a 2.5X objective. The depth of focus was set at 200 µm below the cortical surface. Custom-made piezoceramic mechanical bending actuators were used to elicit oscillatory limb stimulation during widefield Ca²⁺ imaging. The piezo bending actuators comprised a piezo element (Piezo Systems # Q220-A4-203YB) attached to an electrically insulated metal shaft holding a metal U-bend at its end. The palm of the mouse paw was placed within the U-bend, and the U-bend bent to shape to lightly secure the palm. The metal U-bend made contact across a vertical rectangular area of approximately 3x1mm on the palmar and dorsal surface of the hand. Stimulators were driven with square-wave signals from an A-M Systems Model 2100 Isolated Pulse Stimulator. Stimulation alternated between contralateral forelimb (cFL) and contralateral hindlimb (cHL) for up to 40 trials of stimulation of each limb. Placement of actuators was on the glabrous skin of the forepaw or hindpaw, with consistent alignment relative to the flexion of wrist and ankle. Images were captured for 5.0s at 10 Hz (1s

before and 4s after stimulus onset; interstimulus interval = 20s). The trials for each limb were averaged in ImageJ software (NIH). 10 imaging frames (1s) after stimulus onset were averaged and divided by the 10 baseline frames 1s before stimulus onset to generate a response map for each limb. Response maps were thresholded at 95% maximal response to determine limb associated response boundaries, merged, and overlaid on an image of surface vasculature to delineate the cFL and cHL somatosensory areas.

Calcium imaging

On the day following testing for behavioral performance on the string pull and tapered beam tasks, animals were head-restrained within the mobile homecage and Ca^{2+} imaging performed. Awake in-vivo two-photon imaging was performed using a Leica SP5 MP confocal microscope equipped with a Ti:Sapphire Coherent Chameleon Vision II laser tuned to 940 nm for GCaMP6S excitation. A Leica HCX PL APO L 20x 1.0NA water immersion objective was used. Images were acquired using Leica LAS AF using no averaging, a zoom of 1.7x and a frame-rate of 25Hz. Images were acquired at 512x512 pixels over an area of 434x434 μm , yielding a resolution of 0.848 μm per pixel. Two imaging regions were chosen for each animal, with one corresponding to the half-way point between the pre-stroke cFL and cHL somatosensory maps previously determined with widefield Ca^{2+} imaging (the “peri-infarct” imaging region), and the other an imaging region located just lateral to the cHL sensory map (the “distal” imaging region). These regions can be seen in Fig 3.1d and Fig 3.2a. Each imaging region was recorded for 15 minutes while simultaneously tracking the animal’s movement and position within the mobile homecage. Imaging depth was set between 100-180 μm below the cortical surface.

Photothrombotic stroke and sham procedure

After baseline cellular Ca^{2+} imaging, mice were anesthetized using 1.25% isoflurane and head-fixed on a stereotaxic frame with continuous isoflurane anesthesia. Body temperature was measured using a rectal probe and maintained at $37 \pm 0.5^\circ\text{C}$. The mapped cFL area was used as a guide for a targeted photothrombosis procedure. Briefly, a 2mm diameter hole was punched in black electrical tape and attached onto the glass window to block stray light from illuminating cortical areas outside of the desired region. Rose Bengal (a photosensitive dye) was dissolved in 0.01M sterile phosphate buffered saline (Sigma) and injected intraperitoneal (30mg/kg). The cFL cortical area visible through the punched electrical tape was illuminated using a collimated beam of green laser light (532 nm, 17mW) for 20 minutes to photoactivate the Rose Bengal and cause a focal ischemic lesion. Sham controls were treated in the same manner as stroke, however illumination of the laser was omitted.

Two-photon image processing and analysis of neuronal activity

Timeseries images (15 minutes per imaging region, 22500 frames per recording, 25fps) were group averaged in groups of 2, then motion corrected using the TurboReg plugin in FiJi with translation only registration (Schindelin et al., 2012). Z-projections within FiJi of the average and standard deviation were used to define neuronal ROI through manual tracing. Using custom written scripts in Matlab 2020b, ROIs were imported and converted into a format suitable for the Ca^{2+} imaging toolbox used for subsequent steps (Romano et al., 2017). Neuropil for each ROI was determined by expanding an annular donut around each ROI to calculate the neuropil $\Delta F/F_0$ surrounding each ROI. During computation of neuron ROI $\Delta F/F_0$, fluorescence was corrected for neuropil contamination using the formula ($F_{\text{corrected}} = F_{\text{raw}} - \alpha *$

F_{neuropil}) where α was set to 0.4 based on previous studies suggesting that α values between 0.3-0.5 were optimal (Peron et al., 2015), and with F_{neuropil} determined by the peri-somatic donut neuropil fluorescence closely associated with each neuron. A smoothed estimate of the baseline fluorescence was calculated by taking a 30s running average of the 8th percentile of the raw fluorescence, which was then subtracted from the raw fluorescence to remove baseline drift.

Ca²⁺ trace deconvolution to determine neuron firing

To determine significant fluorescent Ca²⁺ transients from the $\Delta F/F_0$ of each neuron, a dynamic threshold implementing a Bayesian odds ratio estimation framework for noise estimation was used to determine transients that met the condition of being greater than 98% of the confidence interval for the calculated fluorescent baseline noise, and were compatible with a tau of ~1.8s for GCaMP6S (Romano et al., 2015, 2017). Determination of firing was performed on the neuronal $\Delta F/F_0$ traces, as implemented in (Romano et al., 2015, 2017), in order to define the Ca²⁺ transient firing rate and to generate raster plots. This information was used to determine neuronal activity “firing rate” as shown in Fig 3.6 and 3.7.

Neuron-neuron correlation analysis and functional connectivity

Using custom written scripts in Matlab, Pearson product-moment correlation coefficients were calculated between the z-scored Ca²⁺ traces derived from each of the neuronal ROIs in a given optical section. Distance between neuron pairs was calculated from the Euclidean distance between the central points of the neuron ROIs of the image frame. Functional connectivity plots (Fig 3.9) were generated by plotting neuron ROI centroids as red dots, and lines between them with line weight and color determined by the strength of the correlation between them.

Stationary variable block bootstrapping (5000 iterations) was performed as a statistical test for the significance of each pairwise correlation and only correlations that were greater than the 99th percentile of the bootstrap were deemed statistically significant and plotted. Average number of significant connections per neuron was calculated by dividing the number of functional connections that met the bootstrapping threshold by the total number of neurons in the population. Average distance between connected neurons was calculated by summing the distance between functional connections that met the bootstrap criteria for significance and dividing by total number of functional connections. Connection density was calculated as percent of max by taking the total number of significant functional connections and dividing by the total potential number of functional connections if every neuron within the population was functionally connected with all other neurons.

Determination of neural assemblies and their activity patterns

To evaluate the co-activity patterns of neurons that form putative neural assemblies, a PCA-Promax procedure was applied as previously described (Romano et al., 2015, 2017), with a zMax threshold manually selected by the first clear minimum in the distribution of z-scored maximal ROI loadings. Notably, the PCA-Promax procedure relaxes the PCA orthogonality condition using a PROMAX oblique rotation of the PC axes (Hendrickson and White, 1964), such that assemblies can contain neurons found within other assemblies. Due to this relaxation of the PCA orthogonality condition, assemblies with high overlap whose dot product exceeded 0.6 were merged. All assemblies were compared to surrogate control datasets, and only those assemblies whose members were significantly correlated and synchronous were kept ($p < 0.05$). To determine the co-activity of neurons within assemblies, a matching index was calculated

(Hilgetag et al., 2002; Romano et al., 2015, 2017; Sporns et al., 2007). The matching index quantifies the proportion of neurons within the assembly that are co-activated simultaneously over the timeseries, with a maximal value of 1 indicating perfect overlap in assembly member activation. The significance of each assembly activation over the timeseries was determined by comparing the activation events to a probability distribution based on the size of the assembly, the size of the total population of N ROIs, and with a threshold p-value of <0.05 considered to be a statistically significant activation. For cross-correlation of assembly activations with speed (Fig 3.12) and assembly-assembly correlations (Fig 3.13), the matching index was first multiplied by the Boolean timeseries of individual assembly activation significance to generate matching index timeseries of significant assembly activations only (presented in Fig 3.12 and 3.13 as percent of maximal assembly activation). ROIs of assembly members were color coded according to their assembly membership, and overlaid on an averaged fluorescence image to generate assembly plots (Fig 3.11).

Statistical analysis

Multivariate comparisons were made using a mixed-effects model for repeated measures based on a restricted maximum likelihood generalized linear mixed model as implemented in Graphpad Prism 9.0.0, with Bonferroni-Sidak corrections used for *post-hoc* comparisons. When there was a significant main effect of group, we performed Bonferroni-Sidak *post-hoc* testing comparing the means of the stroke vs. the sham group at each timepoint. When there was a significant interaction, we performed Bonferroni-Sidak *post-hoc* testing comparing the means of the stroke vs. the sham group at each timepoint, as well as Bonferroni-Sidak *post-hoc* testing to identify within group differences by comparing different timepoints within each group. When

there was a significant main effect of timepoint, but no significant main effect of group or interaction, we performed Bonferroni-Sidak *post-hoc* testing to identify within group differences by comparing different timepoints within each group. Normalized data was analyzed using multivariate mixed-effects models based on a restricted maximum likelihood generalized linear mixed model, with the “pre” timepoint removed from calculation of main effects, interaction, and *post-hoc* statistical testing. All zero time-lag cross-correlations were computed using Pearson’s *r*. A stationary bootstrapping procedure was used as a test of the significance of the calculated Pearson’s *r* of each pairwise timeseries comparison. Within the stationary bootstrapping procedure, 5000 iterations were run and an average block length of 23 frames (1.84s) was used based on previous studies indicating ~1.8s as the decay time for GCaMP6S Ca²⁺ sensor within neurons (Chen et al., 2013; Dana et al., 2019). Pairwise *r* values greater than the 99th percentile of the stationary bootstrap were deemed significant. Non-significant pairwise *r* values were excluded from analyses of average correlation values. For all statistical comparisons, a *p* value of ≤0.05 was considered statistically significant. A *p* value of ≤0.10 was considered a trend, however not statistically significant. Data are expressed as the mean ± SEM.

Results

The experimental timeline is illustrated in Fig 3.1a. Adult Thy1-GCaMP6S mice were implanted with chronic cranial windows and habituated on the floating homecage, tapered beam and string pull task (Fig 3.1a-c). The cFL and cHL somatosensory areas were mapped on the cortex using widefield Ca²⁺ imaging of stimulus-evoked activity (Fig 3.1d, 3.2a, see methods). Imaging regions for longitudinal two-photon Ca²⁺ imaging of cellular activity were chosen based on pre-stroke widefield Ca²⁺ limb mapping (Fig 3.2), with the first region chosen to be between

the pre-stroke cFL and cHL somatosensory maps (termed “peri-infarct” region in this study) and the second region as lateral to the pre-stroke cHL map (termed “distal” region in this study). These regions were imaged at baseline, and each week following photothrombotic stroke. These imaging regions were chosen as they would incorporate predicted areas of remapping for the limb associated somatosensory representations after focal cFL cortex stroke, as has been shown in previous studies (Winship and Murphy, 2008, 2009). Photothrombosis was directed to the cFL somatosensory area of the cortex and induced clearly defined lesions defined by a region of hyperfluorescence 1 week post-stroke (Fig 3.1d, Top). Within the peri-infarct imaging region, cellular dysmorphia and swelling was visually apparent at 1 week after stroke, but partially recovered over the 2 month post-stroke imaging timeframe (Fig 3.1d, Bottom). Morphological change was not apparent in the more distal imaging region lateral to the cHL, likely due to its larger relative distance from the stroke border.

Photothrombotic stroke results in forelimb representation remapping onto adjacent areas of cortex and altered sensory-evoked widefield Ca²⁺ response properties at 8 weeks post-stroke

To elucidate the effect of photothrombotic stroke on the pattern of cortical remapping of the limb-associated somatosensory cortex and to define regional sites for cellular Ca²⁺ imaging, widefield Ca²⁺ imaging of the entire cortical window was performed in combination with piezoelectric stimulation of the contralateral limbs prior to stroke and at the 8 week post-stroke timepoint (Fig 3.2a, see methods). Fig 3.2a shows representative montages from one stroke animal illustrating the cortical cFL and cHL Ca²⁺ responses to 1s, 100Hz limb stimulation of the contralateral limbs at the pre-stroke and 8 week post-stroke timepoints. Notable differences are

observed in the location and magnitude of the cortical responses between timepoints, with the cFL remapping posterior to its pre-stroke location into the area lateral to the cHL map at 8 weeks post-stroke (quantified for all animals in Fig 3.2b-k). Notably, a significant interaction was found in the peak intensity of the cFL sensory-evoked response (Fig 3.2b), with a trend towards a decreased peak cFL response in the stroke group relative to sham at the 8 week timepoint ($p = 0.0805$). Further, a significant main effect of timepoint was seen in the cHL peak response intensity (Fig 3.2c), with the stroke group showing a significant decrease in cHL peak response intensity at the 8 week timepoint compared to pre-stroke ($p = 0.0142$). There was also a significant main effect of group and interaction in the total area of cortical response for cFL evoked Ca^{2+} responses (Fig 3.2d), with the stroke group showing a significant enlargement in the cFL response area at 8 weeks post-stroke compared to sham ($p = 0.0036$). A statistical trend towards a significant main effect of group for the cHL response area was also observed (Fig 3.2e), as well as a trend towards increased cHL response area at the 8 week timepoint compared to sham ($p = 0.0866$). No main effects were seen in the decay constant for the cFL Ca^{2+} response (Fig 3.2f), however a significant main effect of timepoint was observed for the hindlimb decay constant (Fig 3.2g), with *post-hoc* tests indicating a trend towards a decrease for the sham group at the 8 week timepoint relative to the pre timepoint ($p = 0.0995$). Time to peak for the cFL also displayed a significant main effect of timepoint (Fig 3.2h), with a significant decrease in time to peak for the 8 week timepoint in stroke group compared to pre ($p = 0.0178$) and a trend towards a decrease at the 8 week timepoint compared to pre in sham ($p = 0.0918$). No main effect or interaction was seen in the time to peak for the cHL (Fig 3.2i). The stroke group was found to have a significantly larger shift of the cFL map at 8 weeks compared to sham ($p = 0.0002$) (Fig 3.2j), with the majority of that shift due to a significantly larger caudal shift in the cFL map into

the space lateral to the cHL map at the 8 week timepoint in the stroke group compared to sham ($p = 0.0002$) (Fig 3.2k). These results are consistent with previous studies that have observed a decrease in the peak amplitude of the cortical response to limb-stimuli even at timepoints 8 weeks after stroke (Brown et al., 2009; Winship and Murphy, 2008). These results are also consistent with previous studies that have shown a consistent topography of the limb maps in sham animals and a posterior shift in the position of the remapped cFL area after cFL targeted stroke (Winship and Murphy, 2008).

Behavioral tracking in the mobile homecage does not detect a deficit after stroke

To evaluate whether stroke results in a change in the behavior of animals as they were moving within the floating homecage, we quantified the amount of time spent in the middle quadrant of the mobile homecage and the periods of time moving rather than at rest. Fig 3.3a depicts example density maps of time and speed for one example animal at the pre-stroke timepoint. It is visually apparent that the animal spends much of its time near to the walls of the homecage and makes relatively few center crossings. No significant main effect or interaction was seen in the percent of time the animals spent in the middle quadrant between groups or across timepoints (Fig 3.3b). We observed a progressive decline in the percent of time the animals spent moving across all timepoints (Fig 3.3c), with *post-hoc* tests at 2 weeks ($p = 0.0277$), 3 weeks ($p = 0.0072$), 4 weeks ($p = 0.0074$), and 8 weeks ($p = 0.0006$) indicating decreased percent time moving in the stroke group relative to pre-stroke timepoint (Fig 3.3c). This is in partial contrast to a study examining the motor behavior of head-restrained mice on a floating ball after photothrombotic stroke to the sensorimotor cortex that found a decrease in movement at 10 and 20 day post-stroke that partially recovered at 30 days (Latifi et al., 2020).

Tapered beam task depicts a transient behavioral deficit at 1 week post-stroke

To determine if stroke results in a deficit in the gross motor behavior of animals and the time-course of these potential deficits, we quantified the performance of animals on a tapered beam task in terms of the number of left (affected) side slips, right (non-affected) side, and the distance to first slip (Fig 3.4a). Previous research has indicated a transient deficit lasting up to a week for the tapered beam task after focal cortical lesions induced by photothrombosis (Ardesch et al., 2017; Zhao et al., 2005). However, other studies using models of stroke with larger cortical lesions, such as MCAO, have indicated longer lasting deficits on the tapered beam (Lipsanen et al., 2011; Schallert et al., 2002), even at timepoints as long as 450 days after stroke (Schallert et al., 2002). A significant interaction was observed on the number of left side (contralesional) slips in our study (Fig 3.4b), with *post-hoc* tests indicating significant increase in left side slips at the 1 week timepoint for stroke animals compared to sham ($p = 0.0435$). Consistent with the unilateral nature of the photothrombotic damage to the cortex in this study, no main effect or interaction was seen in the number of right side slips (Fig 3.4c). A trend towards a main effect of group was observed in the normalized distance to first slip (fig 3.4d). These results are consistent with a transient deficit in motor behavior on the tapered beam during the first week after stroke induced by focal cortical lesion to the sensorimotor cortex, as has been observed previously (Ardesch et al., 2017; Zhao et al., 2005).

String pull task does not detect a behavioral deficit after stroke

To determine if stroke results in a deficit in a motor behavior that requires the precise and coordinated use of the forelimbs, we quantified the performance of animals on a string pull task in terms of the kinematics of the limbs, the bimanual correlation between the limbs, body

posture, and two measures to quantify the extent of movement within the video recordings: the percent of entropy within the recording window and the standard deviation of paw movement. Fig 3.5a depicts an example animal performing the string pull task from a pre-stroke timepoint. During the task, the animal is upright and performs the task with alternating hand over hand movements as it pulls down the string, with body position and paw kinematic depicted in the timeseries data to the right. A single study has demonstrated that devascularization lesions of the sensorimotor cortex produce deficits in bilateral forelimb coordination as well as direction and distance estimation during forelimb movement (Blackwell et al., 2018c). Contrary to this previous study, we did not detect a significant effect of stroke on any kinematic parameter of motor behavior including left (affected) paw reach movement scaling (Fig 3.5b), left paw reach distance (Fig 3.5c) or left paw reach path circuitry (Fig 3.5d). These same metrics were also measured for the right paw movement and were also not affected by stroke (data not shown). Bimanual correlation between the limbs, an indicator of how well the animal can coordinate the use of both limbs during behavior (Blackwell et al., 2018b, 2018a), was also not affected by stroke (Fig 3.5e), nor was the body angle that the animal had during the string pull (Fig 3.5f). Fig 3.5g depicts an example entropy image from the same pre-stroke animal timepoint as in Fig 3.5a. The percent of total image entropy over threshold (50% of max entropy), a measure of the total randomness of the animal's movement within the recording frame (Inayat et al., 2020), was not found to be affected by stroke (Fig 3.5h). However, a significant main effect of timepoint was seen in image entropy, with *post-hoc* tests showing a significant decrease at the 8 week timepoint relative to pre timepoint in the stroke group ($p = 0.0079$). Similarly, Fig 3.5i depicts an example standard deviation image for paw movement from the same pre-stroke animal timepoint as in Fig 3.5a. A main effect of timepoint and significant interaction was observed in the percent of the

hand movement standard deviation (SD) image over threshold (50% of max SD), with *post-hoc* tests showing a significant decrease at 8 weeks timepoint relative to pre timepoint in the stroke group ($p = 0.0456$), and a trend towards a difference between stroke and sham groups at the 3 week timepoint ($p = 0.0545$). Overall, these results indicate that this analysis of coordinated behavior of the limbs necessary for the string pull task was not sensitive to the focal photothrombotic stroke of the cFL somatosensory cortex in this study.

Neuron firing rate trends towards a transient decrease at 1 week post-stroke in the peri-infarct imaging region

To evaluate whether stroke leads to changes in the firing rate of cortical somatosensory neurons in awake behaving animals, we used an algorithm (Romano et al., 2015, 2017) to determine the mean firing rate of the neural population during periods of movement and periods of rest. Fig 3.6a depicts example Ca^{2+} traces for 40 example neurons at each time point from the imaging region between the forelimb and hindlimb for one example animal in the stroke group. Spike raster plots for all neurons within the population from the same timepoint and animal are shown below the example Ca^{2+} traces (Fig 3.6b). In the peri-infarct imaging region, no main effects or interaction was detected in the average firing rate during movement in non-normalized (Fig 3.7a) or normalized (Fig 3.7b) data, however *post-hoc* analysis of normalized data indicated a trend towards decreased normalized average run firing rate at 1 week in the stroke group relative to sham ($p = 0.0593$). A main effect of group was seen in the non-normalized average firing rate at rest (Fig 3.7c), with *post-hoc* tests showing a significant difference between stroke and sham at the 8 week timepoint ($p = 0.0439$). A significant interaction was also seen in the normalized average firing rate at rest (Fig 3.7d), with *post-hoc* tests showing a trend towards a

decrease in firing rate at rest between the stroke and sham groups at the 1 week post timepoint ($p = 0.0793$). A significant main effect of group was observed in the ratio of firing rate moving to firing rate rest (Fig 3.7e), however no significant differences or trends were observed in *post-hoc* tests, and no main effects or interaction were observed in the normalized ratio of firing rate moving to firing rate rest for the peri-infarct imaging region (Fig 3.7f). In the distal imaging region, a trend towards a main effect of group was seen in the non-normalized average firing rate during movement (Fig 3.7g), but not in the normalized average firing rate during movement (Fig 3.7h), with *post-hoc* tests showing a trend towards an increase in the non-normalized firing rate during movement at the 4 week post timepoint in the stroke group relative to sham ($p = 0.0667$). A trend towards a main effect of group in the average firing rate at rest was observed (Fig 3.7i), with *post-hoc* tests indicating a trend towards an increase in firing rate at rest for the stroke group relative to sham at the 8 week post timepoint ($p = 0.0658$). No main effects or interaction were detected in the normalized average firing rate at rest (Fig 3.7j), or in the non-normalized (Fig 3.7k) and normalized (Fig 3.7l) ratio of firing rate moving to firing rate rest for the distal imaging region. Taken together, these results run contrary to previous reports of increased multi-unit activity as early as 3-7 days after focal photothrombotic stroke (Schiene et al., 1996), and suggest a transient decrease in the average neural firing rate at 1 week post-stroke for cortical sites close to the stroke border prior to a normalization in firing rate at 2 weeks post-stroke. These results further suggest that sites further from the stroke border may trend towards higher firing rates, but at later timepoints of 1-2 months post-stroke.

Average neuron correlation with animal movement is not altered by stroke

To examine whether stroke alters the relationship between the movement of the animal

within the floating homecage and the co-occurring cortical Ca^{2+} activity within the somatosensory cortex, we correlated the Ca^{2+} $\Delta\text{F}/\text{F}_0$ of each neuron with the timeseries of animal speed to determine how correlated the Ca^{2+} activity of neurons is with the speed of the animal. Fig 3.8a depicts an example timeseries of animal speed (green) and Ca^{2+} traces from 20 most active neurons of the population co-recorded with the animal movement. It is apparent that many of these highly active neurons display large Ca^{2+} transients that co-occur along with periods of high activity within the movement timeseries. However, there also appear to be Ca^{2+} transients occurring during periods of relative rest, and periods of neural silence during epochs of high animal activity. For the peri-infarct imaging region, a significant main effect of timepoint was observed in the average correlation coefficient between neurons and speed (Fig 3.8b), however no significant differences were found in *post-hoc* tests between the timepoints. Further, no main effects or interaction were seen in the percent of neurons correlated with movement (Fig 3.8c). In the distal imaging region, no significant main effects or interaction was seen in the average correlation coefficient between neurons and speed (Fig 3.8d), or in the percent of neurons correlated with movement (Fig 3.8e). Together, these results suggest that a large majority of the population is correlated with animal movement, however with relatively low average correlation. Further, these results also suggest that this relationship between the somatosensory Ca^{2+} activity of neurons and animal movement is not disrupted in either the peri-infarct region or the distal region after focal stroke.

Neural population functional connectivity measurements indicate a transient loss of functional connections and connection strength at 1 week post-stroke in the peri-infarct imaging region

Previous studies have shown that stroke leads to a decrease in the functional connectivity of widespread cortical networks (Bauer et al., 2014; Blaschke et al., 2021; Carter et al., 2010, 2012; Cramer et al., 2019; Hakon et al., 2017; Latifi et al., 2020; Longo et al., 2022; Olafson et al., 2021; Rehme and Grefkes, 2013; Siegel et al., 2016; Silasi and Murphy, 2014; Urbin et al., 2014). To examine whether stroke affects functional connectivity on the scale of neural networks within our imaged regions, we plotted the functional connectivity of the neural population in terms of the strength of their correlations (Fig 3.9) and quantified the properties of these connections (Fig 3.10). We observed a significant loss of functional connectivity as early as 1 week after stroke within the peri-infarct imaging region map. This was visually apparent in the stroke group functional connectivity plots at the 1 week timepoint (Fig 3.9a-b) compared to the same location in sham animals (Fig 3.9e-f). No loss of functional connectivity is visually apparent in the distal imaging region map in the stroke or sham groups (Fig 3.9c-d & g-h, respectively). For the peri-infarct imaging region, a trend toward a main effect of group was observed in the normalized average number of significant connections per neuron (Fig 3.10a), with *post-hoc* tests demonstrating a decrease at the 1 week post timepoint in stroke compared to sham ($p = 0.0440$). Further, a significant main effect of group was seen in the normalized number of significant connections per neurons with correlation greater than 0.3 (Fig 3.10b), with *post-hoc* tests indicating a significant decrease at the 1 week post timepoint in the stroke group relative to sham ($p = 0.0363$). A significant main effect of group was also seen in the normalized average distance between connected neurons (Fig 3.10c), with *post-hoc* tests indicating a

significant decrease at 1 week post ($p = 0.0023$) and 8 week post ($p = 0.0218$) timepoints in the stroke group relative to sham. To examine the number of functional connections relative to the total number of possible connections based on the population size, we calculated the connection density (as % of max). No main effects or interactions were seen in the connection density (Fig 3.10d) or in the average correlation coefficient between neurons (Fig 3.10e) for the peri-infarct imaging region. The distal imaging region did not visually display a transient loss of functional connections in the stroke group (Fig 3.9b) in comparison to what was observed in the peri-infarct imaging region maps (Fig 3.9a), and appeared to maintain more consistent functional connectivity graphs with a consistency similar to both imaging areas in the sham group (Fig 3.9c,d). Likewise, no significant main effects or interactions were detected in the normalized number of significant connections per neuron (Fig 3.10f), normalized amount of significant connection with correlation greater than 0.3 (Fig 3.10g), normalized average distance between connected neurons (Fig 3.10h), connection density (Fig 3.10i), or in the average correlation coefficient between neurons (Fig 3.10j) for the distal imaging region map. Together, these results point to a local deficit in functional connectivity within the neuronal population of the peri-infarct imaging region after stroke.

Neural assembly architecture is affected at 1 week post-stroke in the peri-infarct imaging region

Although the use of sophisticated methods for detecting neural assemblies in large populations of neurons has gained increasing popularity with the advent of large population recordings using Ca^{2+} imaging (Mölter et al., 2018), no studies to date have attempted to determine the longitudinal effects of stroke on the architecture of neural assemblies within the

somatosensory cortex of rodents. To determine if focal stroke to the cFL cortex affects the properties of neural assemblies, we used a PCA-Promax procedure (Mölter et al., 2018; Romano et al., 2015, 2017) for neural assembly detection to determine assembly size, population membership, assembly quantity, and overlap in assembly membership. The PCA-Promax method for determining neural assemblies allows neurons to participate in more than a single assembly (Romano et al., 2015, 2017), a property necessary to examine the ability of neural assemblies to dynamically form with varying members of the population for only brief periods of time (Mölter et al., 2018; Romano et al., 2015, 2017). Fig 3.11a shows representative cellular Ca^{2+} fluorescence images with neural assemblies color coded and overlaid for each timepoint for the peri-infarct imaging region and for the distal imaging region for an example stroke and sham animal. For peri-infarct imaging region, a significant main effect of group was found for the number of assemblies (Fig 3.11b), with *post-hoc* tests showing a significant decrease in the number of assemblies at the 1 week and 3 week timepoints for the stroke group compared to sham ($p = 0.0114$ & 0.0058 , respectively), and a trend at the 2 week timepoint for the stroke group compared to sham ($p = 0.0589$). No significant main effect or interaction was, however, seen in the normalized number of assemblies (Fig 3.11c). No significant main effect or interaction was seen in the normalized ratio of assemblies to neurons (Fig 3.11d), potentially suggesting that a decrease in the number of assemblies was coincident with the decreased number of neurons within the peri-infarct imaging region after stroke (data not shown). A trend towards a main effect of group is seen in the normalized number of neurons per assembly (Fig 3.11e), however no trends were observed in *post-hoc* tests. A trend towards a main effect of group was seen in the average percent of the population per assembly (Fig 3.11f), with *post-hoc* tests indicating a trend towards an increased percent of the population per assembly in the stroke

group relative to sham at the 1 week post timepoint ($p = 0.0863$). A trend towards a main effect of group was also seen in the normalized percent of the population within assemblies (Fig 3.11g), with *post-hoc* tests indicating a significant increase in the stroke group relative to sham at the 4 week post timepoint ($p = 0.0177$). No main effects or interactions were seen in the percent of cell overlap between assemblies (Fig 3.11h) or in the percent of assemblies with overlap (Fig 3.11i). Together, these results suggest that in the peri-infarct imaging region, there is a significant disruption to the normal neural assembly architecture, particularly detected at the 1 week timepoint after stroke.

In the distal imaging region, no main effects or interactions are detected in the number of assemblies (Fig 3.11j), normalized number of assemblies (Fig 3.11k), normalized ratio of assemblies to neurons (Fig 3.11l), normalized number of neurons per assembly (Fig 3.11m), average percent of the population per assembly (Fig 3.11n), normalized percent of the population within assemblies (Fig 3.11o), average percent overlap between assemblies (Fig 3.11p), or in the percent of assemblies with overlap (Fig 3.11q). Together, these results indicate that unlike the peri-infarct imaging region, we did not detect the same disruption to the architecture of the distal region neural assemblies, thereby potentially suggesting that cortical networks of the distal cortex may be more resistant to disruption after stroke.

No detectable change in the correlation between assembly activations and movement after stroke

If neural assemblies form the substrate for neural computation during behavior (Buzsáki, 2010), and the spatio-temporal distribution of assembly activity is driven, at least in part, by evoked cortical activity due to stimuli from the external environment during behavior, then we

would predict that the activation of assemblies would be correlated with the behavioral state of the animal, and that stroke could lead to a change in the relationship between animal behavior and assembly activation. To examine whether stroke alters the relationship between the movement of the animal within the floating homecage and activation of neural assemblies within the somatosensory cortex, we correlated the activation timeseries of each assembly with the timeseries of animal speed. Fig 3.12a depicts an example timeseries of animal speed (black) and the timeseries from three example neural assemblies from the population co-recorded with animal movement. It is visually apparent in this example that the blue assembly displays high levels of activation during periods of greatest animal movement, whereas the strong activation periods of the green and orange assemblies do not match as well as that of the blue assembly with animal movement. In the peri-infarct imaging region, no main effects or interactions were detected in the average assembly-speed correlation coefficient (Fig 3.12b), or in the percent of assemblies significantly correlated with movement speed (Fig 3.12c). In the distal imaging region, no main effects or interactions were detected in the average assembly-speed correlation coefficient (Fig 3.12d), or in the percent of assemblies significantly correlated with speed (Fig 3.12e). Together, these results potentially suggest that stroke does not result in changes to how correlated the activation of assemblies are with animal movement for peri-infarct or distal regions.

Correlation among neural assemblies is increased in the peri-infarct imaging region after stroke

If differential activation of neural assemblies in the naïve brain relates to representation of different aspects of the external world (Buzsáki, 2010; Deolindo et al., 2017; Palm et al.,

2014; Romano et al., 2015), then changes in the relationship between the activation patterns of assemblies may predict disrupted processing of sensory information within neural networks. To examine whether focal cortical stroke alters the relationship between the activation patterns of different assemblies within the population, we compared neural assemblies in terms of the correlation between their timeseries activations at each imaging timepoint. Fig 3.13a illustrates three example color coded neural assemblies from a neural population and their corresponding significant time series activations. In the peri-infarct imaging region, a significant main effect of group was seen in the correlation coefficient for significantly correlated assembly-assembly pairs (Fig 3.13b), with post-hoc tests indicating a significantly higher correlation at 2 week ($p = 0.029$) and 4 weeks ($p=0.0253$) in the stroke group relative to sham. No main effect or interaction was detected in the percent of significant assembly-assembly correlations between stroke and sham (Fig 3.13c). In the distal imaging region, no significant main effects or interactions are seen for the correlation coefficient in significantly correlated assembly-assembly pairs (Fig 3.13d), or in the percent of significant assembly-assembly correlations (Fig 3.13e). Together, these results potentially suggest that within the peri-infarct imaging region the relationship between the activations of assemblies is altered, resulting in increased similarity of activations for significantly correlated assemblies.

Discussion

Here, we used longitudinal calcium imaging of awake, head-fixed mice in the mobile homecage to examine how focal photothrombotic stroke to the cFL somatosensory cortex affects cortical activity, functional connectivity, and the architecture and activity of neuronal assemblies, and how these relate to behavioral recovery. First, we demonstrated using sensory-evoked

widefield Ca^{2+} imaging that stroke to the somatosensory cFL area leads to posterior remapping of the cFL representation into the area lateral to the cHL map at 8 weeks post-stroke and an enlargement of the cFL sensory map that was also coupled with reduced peak cFL widefield Ca^{2+} responses. We found that animals displayed a behavioral deficit at 1-week on the tapered beam, but could not detect a deficit in the string pull or in their movement within the mobile homecage. We then illustrated a trend towards a decrease in firing rate within the peri-infarct imaging region at 1 week post-stroke, and an opposite trend towards an increase in firing rate at later time points 1-2 months post-stroke in the more distal imaging region. We also found that the relationship between neuronal Ca^{2+} transients and animal movement, and the relationship between assembly activations and movement, were not detectably affected by stroke. Further, we demonstrated a deficit in the number of functional connections per neuron and in the distance of functional connections for the peri-infarct imaging region that was not detected within the distal imaging region. Lastly, we demonstrated that it was only within the peri-infarct imaging region that we could detect a disruption in neural assembly architecture, including a reduction in number of assemblies, a trend towards an increase in neuron membership within the remaining assemblies, and augmented correlation between the activations of assemblies, and that this was again primarily detected within the first week after stroke.

Plasticity within and between cortical structures leads to partial recovery of function but is proportional to both the extent of damage, as well as the form and quantity of rehabilitative therapy post-stroke (Murphy and Corbett, 2009; Xu et al., 2009). A critical period of highest plasticity begins shortly after the onset of stroke, is greatest during the first few weeks, and progressively diminishes over the weeks to months after stroke (Biernaskie et al., 2004; Brown et

al., 2007, 2009; Carmichael et al., 2005; Cheatwood et al., 2008; Ploughman et al., 2009). Functional recovery after stroke is thought to depend largely on the adaptive plasticity of surviving neurons that reinforce existing connections and/or replace the function of lost networks (Carmichael, 2003b, 2006; Dancause, 2005; Winship and Murphy, 2008, 2009). This neuronal plasticity leads to somatosensory and motor functional remapping to adjacent areas of the cortex and altered topographical organization (Carmichael, 2003b, 2006; Castro-Alamancos and Borrell, 1995; Dancause, 2005; Dijkhuizen et al., 2001, 2003; Frost et al., 2003; Rossini, 2001; Rossini et al., 1998, 2007; Schaechter et al., 2006; Winship and Murphy, 2008, 2009). The driver for this process has largely been ascribed to a complex cascade of intra- and extra-cellular signaling that ultimately leads to plastic re-organization of the microarchitecture and function of surviving peri-infarct tissue (Carmichael, 2003a, 2006; Carmichael et al., 2005; Li and Carmichael, 2006; Li et al., 2010; Murphy and Corbett, 2009; Winship and Murphy, 2009). During this process, the degree to which structural and functional remodeling is driven is dependent on the distance from the stroke core, with closer tissue undergoing more structural and functional re-organization than more distant tissue (for review, see (Winship and Murphy, 2009)). Likewise, dendritic damage is non-uniform within single neurons and is greater with increasing proximity to ischemic zones (Brown and Murphy, 2008; Brown et al., 2008; Enright et al., 2007; Zhang and Murphy, 2007).

Previous research examining the region at the border between the cFL and cHL somatosensory maps has shown this region to be a primary site wherein the cFL representation tends to encroach on the cHL somatosensory territory 1 month after cFL directed photothrombotic stroke, thereby creating a zone of cFL and cHL map overlap (Winship and

Murphy, 2008). Within this overlapping area, neurons have been shown to lose limb selectivity 1 month post-stroke followed by the many of these neurons assuming cFL selective responses 2 months post-stroke as the cFL seizes much of this overlapping territory from the cHL (Winship and Murphy, 2008). In our study, we demonstrate that it's within this same peri-infarct region mapped prior to stroke to border the cFL and cHL somatosensory representations that the most extensive network changes occur. The primary reason for the trend towards reduced firing rate within this peri-infarct border region at 1 week post-stroke in our study is unknown. One potential contributor may simply be a transient loss in blood supply to peri-infarct tissue that is progressively restored as angiogenesis progresses over weeks to months after stroke and re-establishes vascular support for remaining viable tissue (Brown and Murphy, 2008; Brown et al., 2007; Ergul et al., 2012; Greenberg, 2014; Hatakeyama et al., 2020). An alternative contributor may be a loss of synaptic connections that are gradually restored as peri-infarct tissue undergoes a supranormal amount of dendritic remodeling and spine turnover (Brown and Murphy, 2008). Furthermore, the turnover of synaptic contacts may be partially resultant from, or compounded by, a loss of signal propagation through the somatosensory thalamic nuclei due to a reduction in thalamocortical projections after sensorimotor stroke (Carmichael et al., 2001) and a disruption in the functioning of thalamic (Paz et al., 2010; Staines et al., 2002b) and prefrontal (Staines et al., 2002a) circuits for proper gating of sensory information to S1 cortex. This may ultimately result in a deficit in sensory evoked activity in thalamo-cortical projections (Tennant et al., 2017). This may also be compounded by increased transcallosal inhibition from the homotopic contralesional cortex (Koch et al., 2013; Takeuchi and Izumi, 2012). It is also possible that a loss of PV-interneurons after stroke (Luhmann et al., 1995; Neumann-Haefelin et al., 1998), or a disrupted wiring diagram for inhibitory neurons within the peri-infarct cortex (Latifi et al., 2020),

may predispose the peri-infarct networks to aberrant activity patterns. In support of this, therapies that modulate the GABAergic system have shown promise as therapeutics after stroke. For example, augmenting the frequency and amplitude of synaptic GABAergic inhibition with a positive allosteric modulator of phasic GABA_A receptors has been shown to improve behavioral recovery after stroke (Hui et al., 2016). However, the effects of increasing phasic inhibition on whole network activity and functional connectivity have not been shown. Another potential explanation for the reduced cortical responsiveness is the emerging idea that tonic forms of cortical inhibition are augmented after stroke (Cirillo et al., 2020; Clarkson, 2012; Clarkson et al., 2010; Lamtahri et al., 2021; van Nieuwenhuijzen et al., 2021). Likewise, the use of inverse agonists targeted toward reducing excess tonic inhibition mediated by extrasynaptic GABA_A receptors has shown promise in increasing behavioral recovery in animal models of stroke (Clarkson et al., 2010; Lake et al., 2015; Lee and Maguire, 2014). It has also recently been shown that after photothrombotic stroke of the cFL somatosensory cortex, chemogenetic activation of VIP interneurons, that regulate the activity of somatostatin and parvalbumin interneurons (Chamberland et al., 2010; Jackson et al., 2016), enhances sensory-evoked cortical responses to cFL stimulation and improves behavioral recovery (Motaharinia et al., 2021). It has also recently been discovered that the ratio of excitatory to inhibitory neurons is decreased in the motor cortex after focal sensorimotor stroke of the cFL cortex (Latifi et al., 2020). The relative contributions of these different processes to recovery remains to be determined.

It has long been known that stroke results in diaschisis across many areas of the cortex previously connected with the infarcted area (Carmichael et al., 2004; Carrera and Tononi, 2014; Grefkes and Fink, 2014; Silasi and Murphy, 2014). Most studies looking at the functional

connectivity of cortical networks after stroke have focused on connectivity between cortical regions and few have looked at functional connectivity within neural populations at the single neuron level within each region. In humans, fMRI data has revealed that deficits in limb control are highly correlated with decreases in functional connectivity between many regions of the brain (Carter et al., 2010, 2012; Grefkes and Fink, 2014; Guggisberg et al., 2017; Urbin et al., 2014). In animal models of focal sensorimotor stroke, asymmetric decreases in functional connectivity have been found across the lesioned hemisphere particularly at 1 week after stroke that partially recovers by 8 weeks post-stroke and mirrors a similar decrease in cFL stimulation evoked cortical activation at 1 week post-stroke (Lim et al., 2014). Interestingly, research using fMRI in humans has shown that disruption of inter-hemispheric connectivity in the sensorimotor network is more strongly associated with functional impairment than intra-hemispheric connectivity within either the lesioned or unaffected hemisphere (Carter et al., 2012). However, other studies have shown that functional recovery of behavior after stroke is highly correlated with new forms of axonal sprouting within the stroke affected hemisphere (Carmichael, 2003b; Dancause, 2005; Li et al., 2015; Overman et al., 2012), and functional recovery can be boosted with therapies that boost peri-lesional axonal sprouting (Li et al., 2015; Overman et al., 2012). Our findings of decreased number of connections per neuron in the peri-infarct somatosensory cortex are consistent with recent findings by Latifi et al., 2020 that demonstrated a decrease in the total number of functional connections for both inhibitory and excitatory cells in the motor and premotor cortex 10 days after focal sensorimotor stroke (Latifi et al., 2020). However, many of the deficits observed by Latifi et al., 2020 were maintained for up to 30 days after stroke, whereas functional connectivity within the peri-infarct imaging region in our study was not statistically different than sham animals by 2 weeks post-stroke. As the potential number of

functional connections is dependent on the number of cells measured from the population, it is possible that a decrease in the number of connections in both studies simply reflects the loss of neural population within the imaged areas. In this study we also measured connection density (as % of max possible connections) to account for cell loss and surprisingly found no detectable change in connection density due to stroke, potentially suggesting a homeostatic level of connection density that is maintained despite a loss in the total number of functional connections associated with cell loss. We also found no detectable change in the average correlation between neuron pairs across the population, suggesting that there was no detectable decrease in the average magnitude of the coupling between neuronal Ca^{2+} activity across the population after stroke, despite a particularly prominent drop in the number of strong ($r > 0.3$) connections per neuron at the 1 week timepoint. It may also be possible that determining functional connectivity from simple move or rest conditions may not reveal subtle differences in connectivity related to skilled behaviors, however this has not been shown.

The functional connection distance between connected neurons relates to elements of information integration and transmission speed, such that neurons that are spatially close have a higher probability of being connected in order to minimize wiring costs and increase rapid and effective transmission of information (Averbeck and Seo, 2008; Bullmore and Sporns, 2009; Sporns, 2011). However, studies examining functional connections on a macroscopic scale have shown that more costly long distance functional connections are also a necessity in rapid and efficient information transmission between cortical areas, and are known to be affected by stroke (van Meer et al., 2010). On the cellular scale, it's recently been found within the motor cortex of naive mice that excitatory neurons have predominantly shorter range functional connections

whereas inhibitory neurons have predominantly longer range connections, and that this pattern reverses after photothrombotic stroke to the cFL cortex (Latifi et al., 2020). Although we did not differentiate between excitatory and inhibitory neurons within this study, we observed a decrease in the normalized average distance between connected neurons as soon as 1 week post-stroke in the peri-infarct imaging region. This decrease persisted even at 8 weeks after stroke, thereby suggesting a decrease in the number of longer range, more costly connections between neurons.

A highly distributed network of neural circuits forms the basis of information flow in the mammalian brain (Bullmore and Sporns, 2009; Sporns, 2011). Many disease states of the brain are thought to result in disturbances in neural dynamics and connectivity of these networks due to a process of randomization that affects the network nodes and connections, leading to degraded functional performance of the networks (Sporns, 2011; Stam, 2014). According to the cell assembly hypothesis, transient synchronous activation of distributed groups of neurons organize into “neural assemblies” that underly the representation of both external and internal stimuli in the brain (Buzsáki, 2010). These assemblies have been demonstrated in the mammalian (Berkes et al., 2011; Cossart et al., 2003; Harris et al., 2003; Hyman et al., 2013; Malvache et al., 2016; Miller et al., 2014; Sakata and Harris, 2009; See et al.; Truccolo et al., 2010; Villette et al., 2015) and zebrafish (Avitan et al., 2017; Pietri et al., 2017; Romano et al., 2015; Thompson and Scott, 2016) brain, and are often similar in presentation between spontaneous and sensory evoked activations (Berkes et al., 2011; Luczak et al., 2009; MacLean et al., 2005; Miller et al., 2014; Romano et al., 2015). Indeed, the similarity between spontaneous assemblies and sensory evoked assemblies tends to increase during development (Berkes et al., 2011), potentially illustrating the “sculpting” of neural circuits towards commonly encountered

sensory stimuli. To date, no study to our knowledge has examined changes to the architecture of neural assemblies on the level of single cells within neural networks of the somatosensory cortex in the post-stroke brain. A single study examining stroke to the motor cortex in rats has found that stroke leads to an increase in the variability of ensemble spike sequences during a skilled pellet reaching task within both the peri-lesional cortex and the dorsolateral striatum 1-2 weeks after stroke, and subsequently normalizes into consistent neural sequences at later time points post-stroke (Guo et al., 2021). Unfortunately, the use of Ca^{2+} imaging modalities, especially with the use of the slower GCaMP6S variant of Ca^{2+} indicator, does not have sufficient temporal resolution to accurately determine spike sequence timing, and we were therefore not able to determine the variability of spike timing as previously measured (Guo et al., 2021), nor the predictive relationship between assembly activation and neural spike timing that has been depicted in other fields of research (Luczak et al., 2009; Truccolo et al., 2010). We are, however, the first to show a transient decrease in the number of assemblies, a trend towards a higher normalized number of neurons, a trend towards a higher normalized percent of the population per assembly, and an increase in the correlation between the activations of assemblies in the peri-infarct cortex at 1 week post-stroke. If the appearance of each assembly within this peri-infarct somatosensory area correlates with differential processing of distinct elements of sensory experience, then it may be predicted that a loss in the number of assemblies may be predictive of a decrease in the range of sensations that the system can process and may partially explain the loss in sensory range in human stroke patients (Carey and Matyas, 2011; Connell et al., 2008; Kwakkel et al., 2004; Patel et al., 2000; Tyson et al., 2008), however this has not been shown. It has been shown that electrical stimulation of single somatosensory neurons is sufficient to bias animal behavior towards a desired behavioral response (Brecht et al., 2004; Houweling and

Brecht, 2008), thereby suggesting that a sparse neural code may be sufficient for sensation. It has also been argued that minimizing correlation within the neural population serves to reduce representational redundancy and improves representational efficiency (Barlow, 2001; Simoncelli and Olshausen, 2001). In neuronal assembly simulation models, the interplay between excitation and inhibition has been shown to modulate the formation of assemblies such that dominant excitability within networks leads to fast formation of assemblies and less specificity in neuronal activation (Sadeh and Clopath, 2021). Although there have been calculations on the typical size of cell assemblies in several regions of the brain as a percentage of the network population (for review, see (Buzsáki, 2010)), whether there is an optimal number of assemblies or optimal membership size of a neural assembly for a particular neural population is currently unknown. It is possible that a decrease in the number of assemblies and an increase in the membership of neurons in remaining assemblies may signify inefficient or ineffective forms of sensory processing, however this has yet to be shown. Furthermore, it is currently unknown whether increased correlation between the activation time course for different assemblies would be detrimental. It may be possible that co-activation of multiple assemblies simultaneously could decrease the signal-to-noise ratio of assembly activation within the network and affect the propagation of signals to downstream networks, but this has yet to be shown.

Consistent with previous research (Winship and Murphy, 2008), we show that at the 8 week timepoint after cFL photothrombotic stroke the cFL representation is shifted posterior from its pre-stroke location into the area lateral to the cHL map. Notably, our distal imaging region was directly within this remapped cFL area. A trend towards an increase in firing rate at 4 weeks post-stroke for the distal imaging region in this study is consistent with past research that has

indicated an increase in sensory-evoked activity within this area lateral to the cHL representation 1-2 months after focal cFL stroke (Winship and Murphy, 2008). Surprisingly, there was no indication that the cFL remapping into the area lateral to the cHL map in the stroke group resulted in any detectable change to the level of population correlation, functional connectivity, assembly architecture or assembly activations as compared to sham in the distal imaging region. These results support the idea of a very limited spatial distance over which the peri-infarct area surrounding the photothrombotic stroke core results in network functional deficits. These results are also consistent with a spatial gradient of plasticity factors that are generally enhanced with greater proximity to the infarct core (Carmichael, 2003a, 2006; Carmichael et al., 2005; Li and Carmichael, 2006). It has also been noted that rehabilitative training, such as repeated forced use of the impaired limb, prevents the secondary depression of areas functionally connected to the stroke (Nudo, 1997), and may explain the lack of deficit in the distal imaging region, however this has not been shown.

Rehabilitative training after stroke is highly effective in helping to restore motor function for behavior (Bütefisch, 2006; Jones and Adkins, 2015). Studies using other tests of sensorimotor function after photothrombotic stroke such as the grid-walking task, grip strength test, or single pellet reaching test have shown more prolonged deficits of up to 1 month or more after photothrombotic infarct to the cFL sensorimotor area (Longo et al., 2022). Although there was no dedicated rehabilitation protocol for the animals during this experiment, weekly behavioral testing on the string pull and tapered beam, combined with the difficulty of maintaining postural control within the mobile homecage during imaging sessions, may have acted as a mild form of rehabilitation. This mild rehabilitation may have resulted in both compensatory strategy

formation, and/or functional recovery, that resulted in no detectable impairment in the string pull task and in behavior within the floating homecage. However, if compensatory strategy alone was responsible for the degree of behavioral recovery we observed in this study, we would have predicted that analysis of the kinematics of the forelimbs in the string pull task would have elucidated deficits similar to the well-known “learned baduse” phenomenon previously described in rodent reaching behavior after motor cortex devascularization lesions (Alaverdashvili et al., 2008a). It is also possible the lack of any detectable functional impairment on all measures of string pulling performance and of mobile homecage movement relates to the small initial size of the photothrombotic infarcts given in this study. Previous studies in rats have shown that large strokes that encompass most of the motor cortex result in the emergence of compensatory behaviors during recovery (Alaverdashvili and Whishaw, 2008; Alaverdashvili et al., 2008b, 2008a; Metz et al., 2005), whereas small photothrombotic lesions to the motor cortex results not only in compensatory movements, but in functional recovery of original movement patterns (Moon et al., 2009). Likewise, photothrombotic stroke in this study was also performed under isofluorane anesthesia. Exposure to isofluorane during stroke has previously been shown to reduce cortical damage compared to stroke induced in awake animals, and is known to mask the benefits of stroke treatment due to the reduction in stroke severity (Seto et al., 2014).

In summary, in this work we studied the recovery of cortical networks in the peri-infarct cortex directly adjacent to the stroke core, and in distal imaging regions in the area lateral to the cHL map. We demonstrated that the peri-infarct region near to the stroke core displays functional deficits in network functional connectivity and neural assembly architecture, concurrent with a trend towards decreased neuronal activity at 1 week after stroke, and that these

same deficits were not detectable a short distance away in distal imaging region. We also demonstrated that the network deficits were synchronous with a behavioral deficit within the tapered beam task detectable at the same 1 week timepoint. Future studies could make use of stroke models with larger penumbral regions, such as the middle cerebral artery occlusion model, to determine if the same patterns hold true. Further, this study lays the foundation for determining the effects of a dedicated rehabilitation protocol and/or pro-plasticity therapeutic compounds for modulating network activity, functional connectivity, and neural assembly architecture to improve functional recovery and prevent cortical network and behavioral deficits after stroke.

Chapter 3: Figures

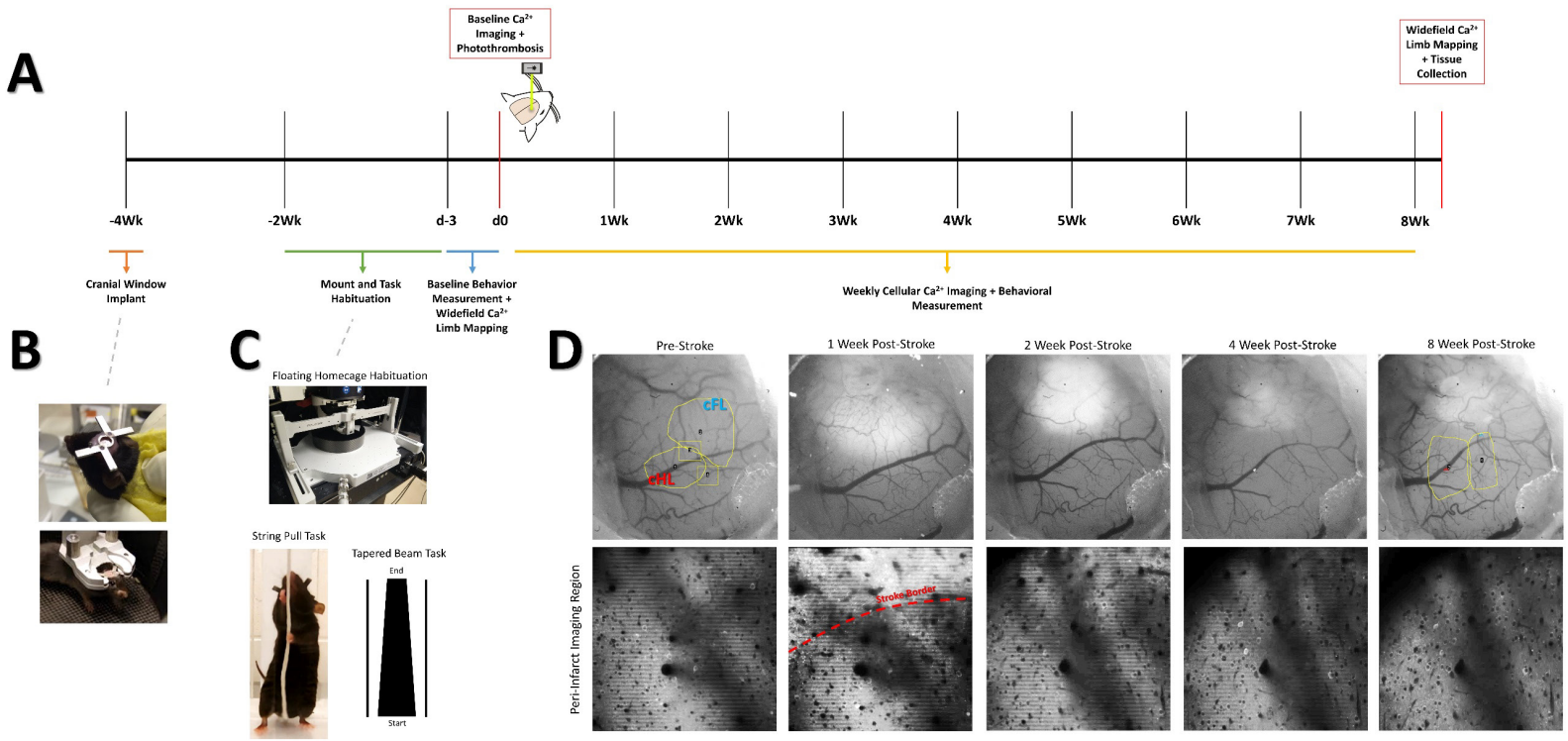
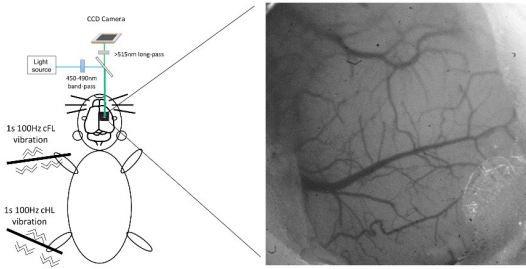
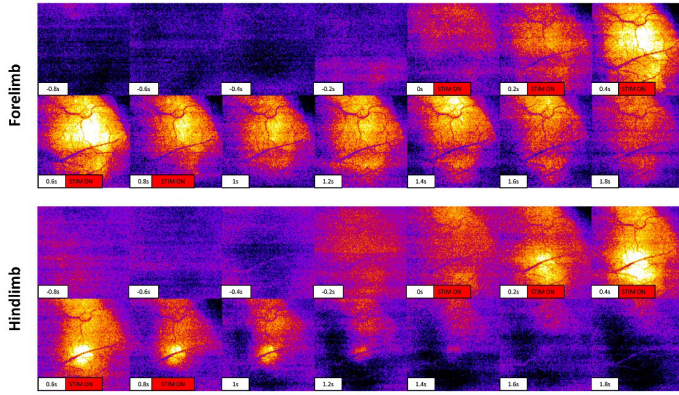
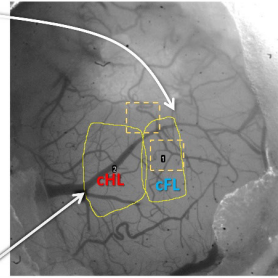
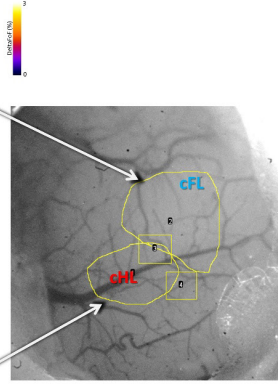
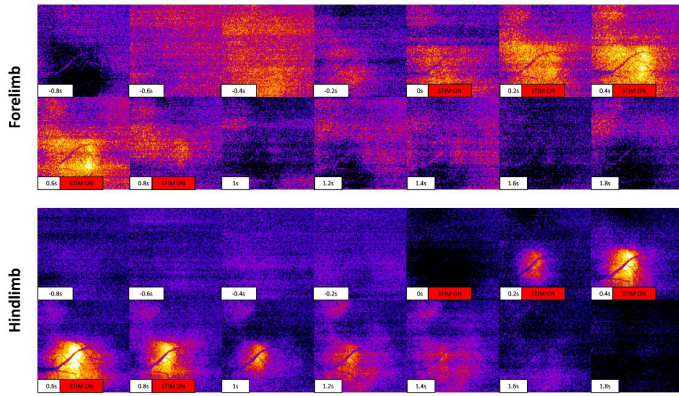
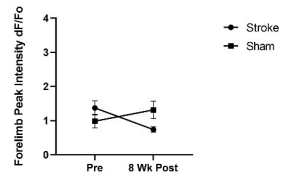


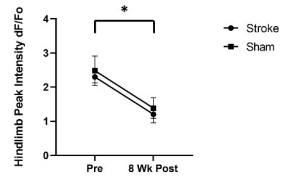
Fig 3.1. Experimental timeline and methods. (A) Timeline of experimental procedures, imaging timepoints, and behavioral tests. (B) Glass cranial windows and headplates were implanted 2 weeks prior to beginning habituation protocols in Thy1-GCaMP6S mice. (C) Mice were habituated on the floating homecage, string pull and tapered beam for a period of 2 weeks prior to baseline measurements for behavior. Along with baseline behavioral measurements, widefield Ca^{2+} limb mapping was performed to determine the location of the contralateral forelimb (cFL) and hindlimb (cHL) somatosensory maps on the cortical surface. Somatosensory response maps were determined by thresholding to 95% of max response amplitude. These maps were used to determine locations for the imaging site located between the cFL and cHL sensory maps at baseline (“peri-infarct” imaging region) and imaging site lateral to the cHL at baseline (“distal” imaging region). For each Ca^{2+} imaging session, both imaging regions were imaged for a period of 15 minutes while simultaneously tracking animal movement within the mobile homecage. After baseline Ca^{2+} imaging, the somatosensory cFL map was targeted with photothrombosis. Behavioral testing on the string pull task and tapered beam task were performed weekly 1 day prior to the Ca^{2+} imaging session. After the final cellular Ca^{2+} imaging session at the 8 week timepoint, stimulus-evoked widefield Ca^{2+} imaging was once again performed to determine the cFL and cHL somatosensory maps. (D) Widefield Ca^{2+} fluorescence images were taken at each weekly timepoint to match Ca^{2+} imaging sites at each timepoint. In the first widefield Ca^{2+} fluorescence image is an example illustrating the locations of the thresholded cFL and cHL somatosensory maps on the cortical surface, as well as the locations of the two imaging regions. The 8 week post-stroke widefield Ca^{2+} fluorescent image depicts the location of the cFL and cHL somatosensory maps determined at the 8 week timepoint from the same animal. The area of hyper-fluorescence due to stroke damage is apparent, with its surface area decreasing over time. Below: Examples of GCaMP6S cellular Ca^{2+} imaging of a peri-infarct imaging region at multiple time points.

A**Pre-Stroke****8 Week Post-Stroke****B**

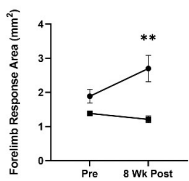
Timepoint $F(1, 12) = 0.8570, p = 0.3728$
 Group $F(1, 12) = 0.2092, p = 0.6556$
 Interaction $F(1, 12) = 8.632, p = 0.0124$

**C**

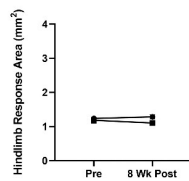
Timepoint $F(1, 12) = 15.02, p = 0.0022$
 Group $F(1, 12) = 0.4267, p = 0.5259$
 Interaction $F(1, 12) = 3.405e-5, p = 0.9954$

**D**

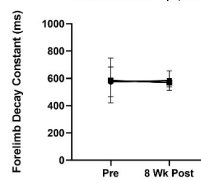
Timepoint $F(1, 12) = 2.273, p = 0.1575$
 Group $F(1, 12) = 7.328, p = 0.0191$
 Interaction $F(1, 12) = 5.372, p = 0.0389$

**E**

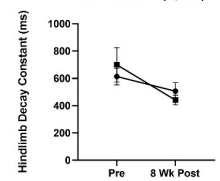
Timepoint $F(1, 12) = 0.06425, p = 0.8042$
 Group $F(1, 12) = 3.929, p = 0.0708$
 Interaction $F(1, 12) = 1.069, p = 0.3217$

**F**

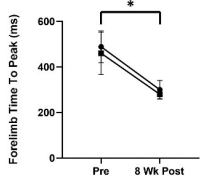
Timepoint $F(1, 12) = 0.0005274, p = 0.9821$
 Group $F(1, 12) = 0.0003909, p = 0.9846$
 Interaction $F(1, 12) = 0.01048, p = 0.9202$

**G**

Timepoint $F(1, 12) = 6.040, p = 0.0302$
 Group $F(1, 12) = 0.01776, p = 0.8962$
 Interaction $F(1, 12) = 1.036, p = 0.3289$

**H**

Timepoint $F(1, 12) = 13.22, p = 0.0034$
 Group $F(1, 12) = 0.1023, p = 0.7545$
 Interaction $F(1, 12) = 0.007679, p = 0.9316$

**I**

Timepoint $F(1, 12) = 0.6944, p = 0.4210$
 Group $F(1, 12) = 1.071, p = 0.3210$
 Interaction $F(1, 12) = 0.3282, p = 0.5773$

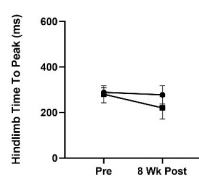
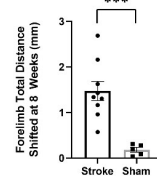
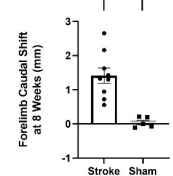
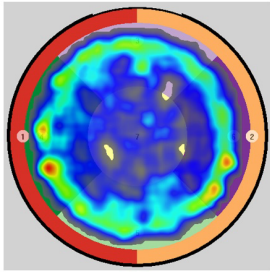
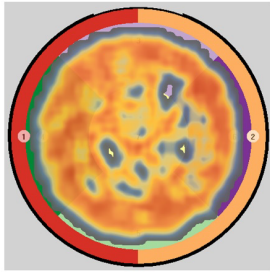
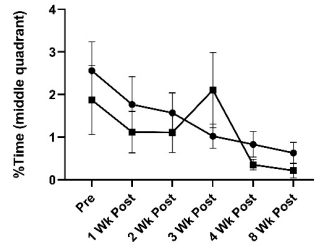
**J****K**

Fig 3.2. Photothrombotic stroke results in forelimb representation remapping onto adjacent areas of cortex and altered sensory-evoked widefield Ca²⁺ response properties at 8 weeks post-stroke. (A) Pseudocolored (%DeltaFoF) montages of representative cFL and cHL responses in S1 of an animal pre-stroke and 8 week post-stroke resulting from oscillatory stimulation (1s, 100 Hz) of the cFL and cHL, respectively. At the 8 week post-stroke timepoint, the cFL map has remapped posterior to its pre-stroke location into the area lateral to the cHL. (B) Mean peak forelimb Ca²⁺ transient response intensity (%DeltaFoF), measured from the thresholded cortical map area of the cFL. A significant interaction is seen, with *post-hoc* tests showing a trend towards lower peak intensity at 8 week post timepoint in the stroke group as compared to sham ($p = 0.0805$). (C) Mean peak hindlimb Ca²⁺ transient response intensity (%DeltaFoF), calculated from the thresholded cortical map area of the cHL. A significant main effect of timepoint was seen, with the stroke group showing a significant decrease in hindlimb peak intensity at 8 weeks compared to pre-stroke timepoint in a *post-hoc* test ($p = 0.0142$). (D) Thresholded cFL response area (mm²). A significant main effect of group and significant interaction is seen, with *post-hoc* tests showing greater response area at 8 weeks in the stroke group compared to sham ($p = 0.0036$). (E) Thresholded hindlimb response area (mm²). A trend towards a main effect of group is seen, with *post-hoc* tests showing a trend towards increased hindlimb response area at 8 weeks for the stroke group relative to sham ($p = 0.0866$). (F) Mean decay constant of the forelimb response (in ms). No significant effects are seen. (G) Mean decay constant of the hindlimb response (in ms). A significant main effect of timepoint is seen, with the sham group showing a trend towards decreased decay time at 8 week post relative to pre in a *post-hoc* test ($p = 0.0995$). (H) Time to peak Ca²⁺ response amplitude for the forelimb (in ms). A significant main effect of timepoint was seen, with *post-hoc* tests showing a significant decrease for the stroke group at 8 weeks post compared to pre ($p = 0.0178$) and a trend in the sham group towards a decrease at 8 weeks post compared to pre ($p = 0.0918$). (I) Time to peak Ca²⁺ response amplitude for the hindlimb (in ms). No significant effects were seen. (J) The stroke group was found to have significantly greater total distance shifted for the forelimb map at the 8 week timepoint compared to sham ($p = 0.0002$), resulting almost completely from a significant caudal shift of the forelimb map at the 8 week timepoint compared to sham ($p = 0.0002$) (K). Stroke N = 9, Sham N = 5. * $p < 0.05$; ** $p < 0.01$; *** $p < 0.001$

A**Density Map of Time****Density Map of Speed****B**

Timepoint F (2, 479, 39.67) = 2.308, $p = 0.1017$
 Group F (1, 16) = 0.4988, $p = 0.4902$
 Interaction F (5, 80) = 0.5858, $p = 0.7108$

**C**

Timepoint F (3, 216, 49.53) = 8.182, $p = 0.0001$
 Group F (1, 16) = 0.2921, $p = 0.5963$
 Interaction F (5, 77) = 1.128, $p = 0.3525$

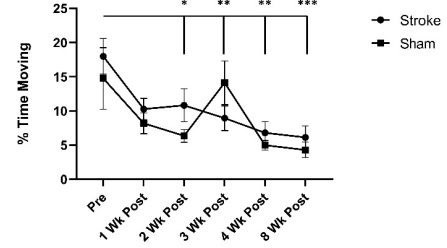


Fig 3.3. Behavioral tracking in the mobile homecage does not detect a deficit after stroke.

(A) Example density maps of time and speed for one example animal at the pre timepoint.

Density maps of time were quantified to determine percent of recording time spent in the middle quadrant. Speed was thresholded at 30mm/s to determine the periods of movement in the mobile homecage and differentiate them from period of rest. **(B)** Percent of time spent in the middle quadrant. No main effects or interactions were seen.

(C) Percent of time spent moving. A significant main effect of timepoint was seen, with *post-hoc* tests at 2 weeks ($p = 0.0277$), 3 weeks ($p = 0.0072$), 4 weeks ($p = 0.0074$), and 8 weeks ($p = 0.0006$) indicating decreased percent time moving in the stroke group relative to pre-stroke timepoint. Stroke N = 13, Sham N = 5. * $p < 0.05$; ** $p < 0.01$; *** $p < 0.001$

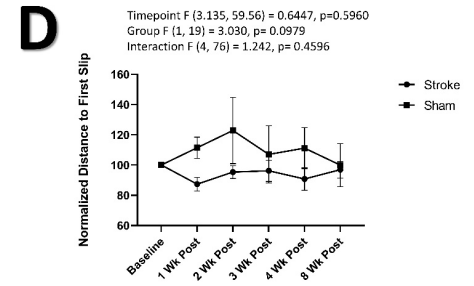
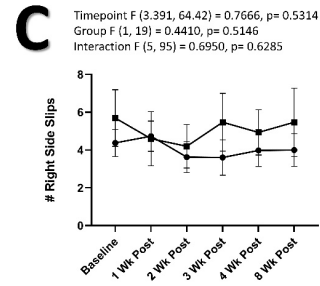
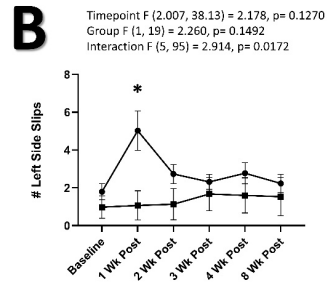
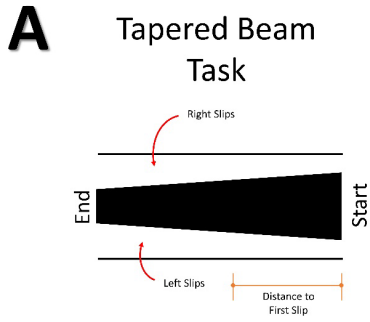
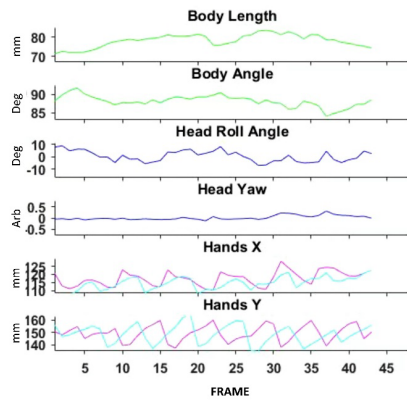
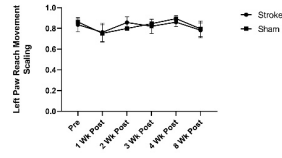


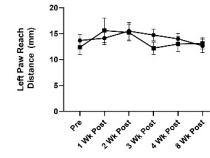
Fig 3.4. Tapered beam task depicts a behavioral deficit at 1 week post-stroke. (A) Illustration of the tapered beam test with the three elements measured; right side slips, left (contralesional) side slips, and distance to first slip. **(B)** Mean number of left side slips. A significant interaction was observed, with *post-hoc* tests showing a greater number of left side slips at 1 week in the stroke group relative to the sham group ($p = 0.0435$). **(C)** Mean number of right-side slips. No main effects or interactions were observed. **(D)** Normalized distance to first slip (as % of baseline). A trend towards a main effect of group was observed, with no trends found in *post-hoc* tests. Stroke N = 16, Sham N = 5. * $p < 0.05$; ** $p < 0.01$; *** $p < 0.001$

A**B**

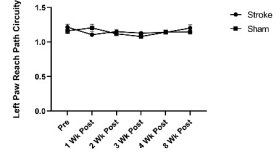
Timepoint F (3.108, 39.16) = 0.9374, $p = 0.4344$
 Group F (1, 13) = 0.005522, $p = 0.9419$
 Interaction F (5, 63) = 0.1498, $p = 0.9794$

**C**

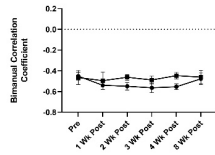
Timepoint F (3.160, 41.08) = 1.606, $p = 0.2008$
 Group F (1, 13) = 0.1172, $p = 0.7376$
 Interaction F (5, 65) = 0.7690, $p = 0.5755$

**D**

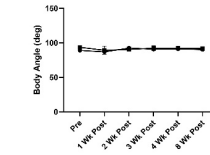
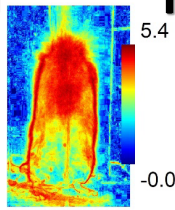
Timepoint F (3.189, 40.19) = 1.217, $p = 0.3169$
 Group F (1, 13) = 0.3888, $p = 0.5437$
 Interaction F (5, 63) = 1.299, $p = 0.2759$

**E**

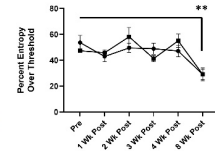
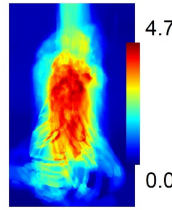
Timepoint F (3.835, 49.85) = 0.6237, $p = 0.6412$
 Group F (1, 13) = 0.5243, $p = 0.4819$
 Interaction F (1, 13) = 2.479, $p = 0.1394$

**F**

Timepoint F (2.313, 30.07) = 0.6222, $p = 0.5660$
 Group F (1, 13) = 0.5243, $p = 0.4819$
 Interaction F (5, 65) = 0.3708, $p = 0.8669$

**G****H**

Timepoint F (3.712, 48.26) = 12.04, $p < 0.0001$
 Group F (1, 13) = 0.03092, $p = 0.8631$
 Interaction F (5, 65) = 1.809, $p = 0.1233$

**I****J**

Timepoint F (3.412, 44.36) = 7.423, $p = 0.0002$
 Group F (1, 13) = 0.03493, $p = 0.8546$
 Interaction F (5, 65) = 2.694, $p = 0.0283$

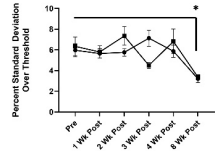


Fig 3.5. String pull task does not detect a behavioral deficit after stroke. (A) Left: Image of example animal performing the string pull task at the pre-stroke timepoint. Right: Data for the animal's body length, body angle, head angle and yaw, and position of the hands is tracked to determine alterations in motor movement between timepoints. No significant main effect or interaction are seen in the left (affected) paw reach movement scaling (B), reach distance (C), reach path circuitry (D), bimanual correlation coefficient (E), or in the animal body angle (F). (G) Example entropy image from the same pre-stroke animal timepoint as in A. (H) A main effect of timepoint is observed in the percent of the entropy image over threshold (50% of max entropy), with *post-hoc* tests showing a significant decrease at the 8 week timepoint relative to pre timepoint in the stroke group ($p = 0.0079$). (I) Example paw movement standard deviation image from the same pre-stroke animal timepoint as in A. (J) A main effect of timepoint and significant interaction is observed in the percent of the hand movement standard deviation (SD) image over threshold (50% of max SD), with *post-hoc* tests showing a significant decrease at 8 weeks timepoint relative to pre timepoint in the stroke group ($p = 0.0456$), and a trend towards a difference between stroke and sham groups at the 3 week timepoint ($p = 0.0545$). Stroke N = 10, Sham N = 5. * $p < 0.05$; ** $p < 0.01$; *** $p < 0.001$

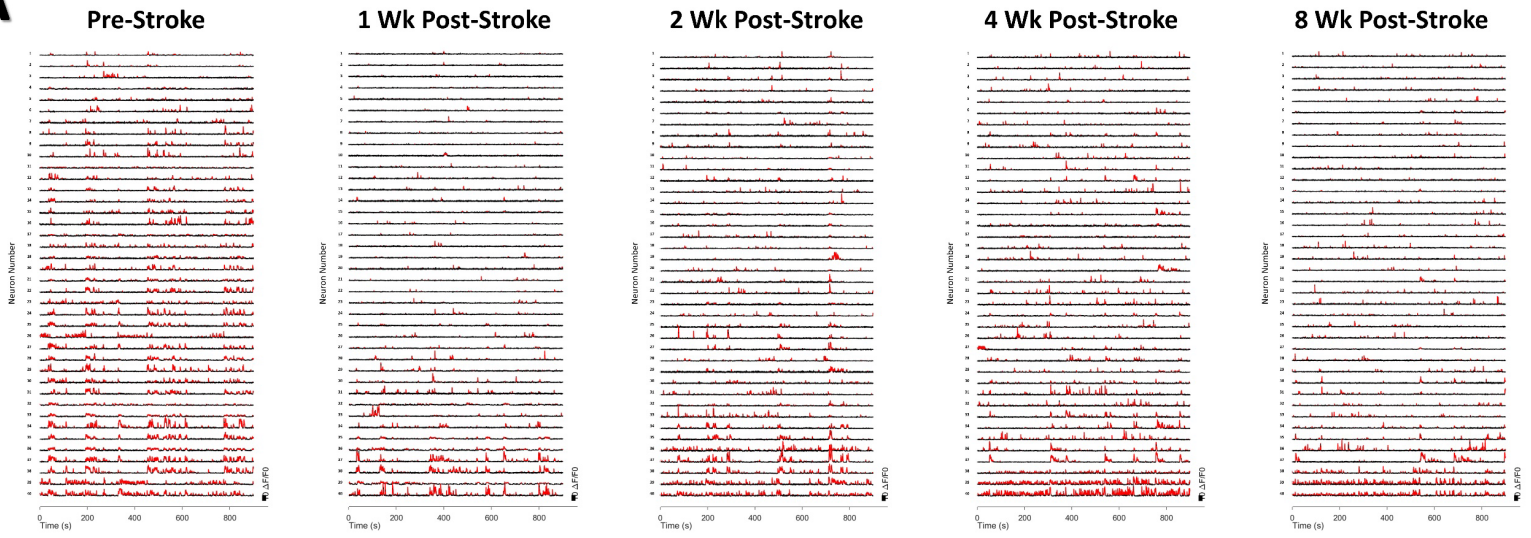
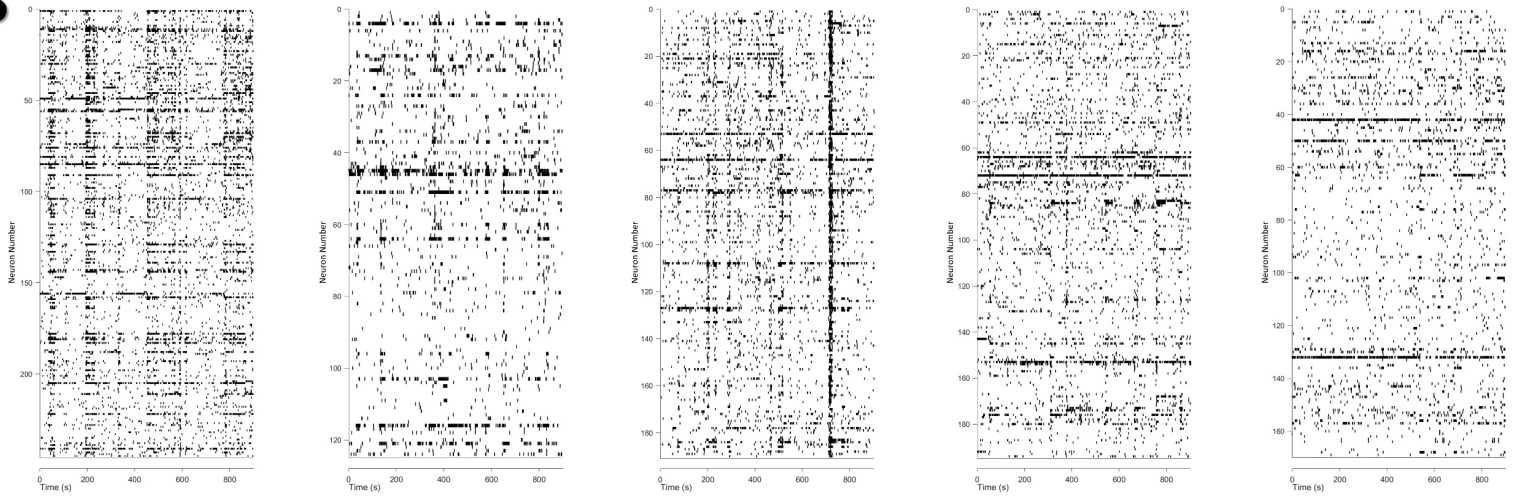
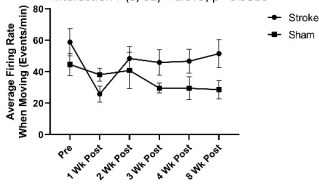
A**B**

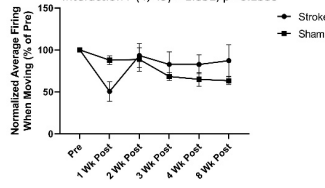
Fig 3.6. Example Ca^{2+} $\Delta\text{F}/\text{F}_0$ traces and spike rasters for a peri-infarct imaging region depicting a decrease in firing at 1 week post-stroke. (A) Example Ca^{2+} traces for 40 example neurons at each time point from the peri-infarct imaging region for one example animal in the stroke group. Significant Ca^{2+} transients are highlighted by red segments. (B) Spike raster plots for all neurons from the same timepoint and animal associated with the Ca^{2+} traces above.

Peri-Infarct Region

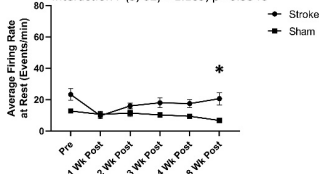
A Timepoint F (3.217, 39.89) = 1.629, p= 0.1953
Group F (1, 13) = 1.106, p= 0.3121
Interaction F (5, 62) = 1.079, p= 0.3810



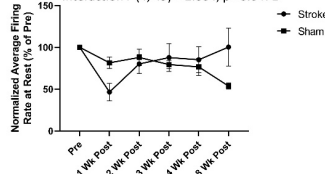
B Timepoint F (2.448, 29.99) = 0.9487, p= 0.4144
Group F (1, 13) = 0.04256, p= 0.8397
Interaction F (4, 49) = 1.852, p= 0.1339



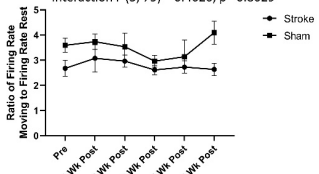
C Timepoint F (2.297, 28.48) = 1.360, p= 0.2742
Group F (1, 13) = 6.058, p= 0.0286
Interaction F (5, 62) = 1.169, p= 0.3346



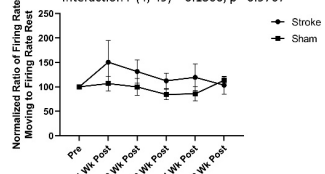
D Timepoint F (2.240, 27.44) = 1.048, p= 0.3712
Group F (1, 13) = 0.006936, p= 0.9349
Interaction F (4, 49) = 2.604, p= 0.0471



E Timepoint F (2.800, 42.00) = 0.6720, p= 0.5642
Group F (1, 13) = 8.958, p= 0.0037
Interaction F (5, 75) = 0.4626, p= 0.8029

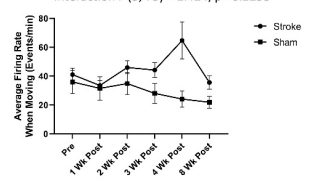


F Timepoint F (1.492, 18.28) = 0.7416, p= 0.4526
Group F (1, 13) = 0.5522, p= 0.4706
Interaction F (4, 49) = 0.1300, p= 0.9707

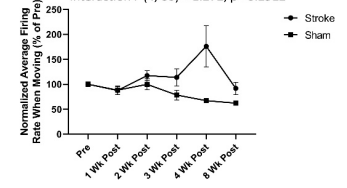


Distal Region

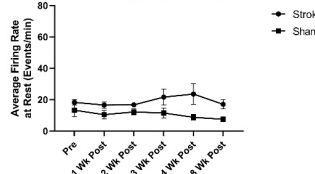
G Timepoint F (1.687, 25.31) = 0.9507, p= 0.3858
Group F (1, 15) = 4.118, p= 0.0606
Interaction F (5, 75) = 1.424, p= 0.2253



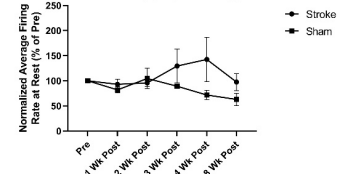
H Timepoint F (1.533, 23.00) = 0.8798, p= 0.4023
Group F (1, 15) = 3.039, p= 0.1017
Interaction F (4, 60) = 1.272, p= 0.2912



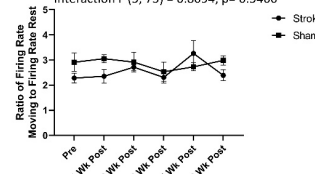
I Timepoint F (1.501, 22.51) = 0.3084, p= 0.6752
Group F (1, 15) = 3.677, p= 0.0744
Interaction F (5, 75) = 0.4139, p= 0.8377



J Timepoint F (1.364, 20.46) = 0.3952, p= 0.6004
Group F (1, 15) = 0.7619, p= 0.3965
Interaction F (4, 60) = 0.5670, p= 0.6875



K Timepoint F (2.584, 38.76) = 0.5792, p= 0.6075
Group F (1, 15) = 1.142, p= 0.3021
Interaction F (5, 75) = 0.8094, p= 0.5466



L Timepoint F (2.448, 36.72) = 0.8441, p= 0.4586
Group F (1, 15) = 0.9175, p= 0.3533
Interaction F (4, 60) = 0.8025, p= 0.5284

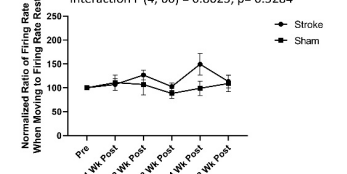
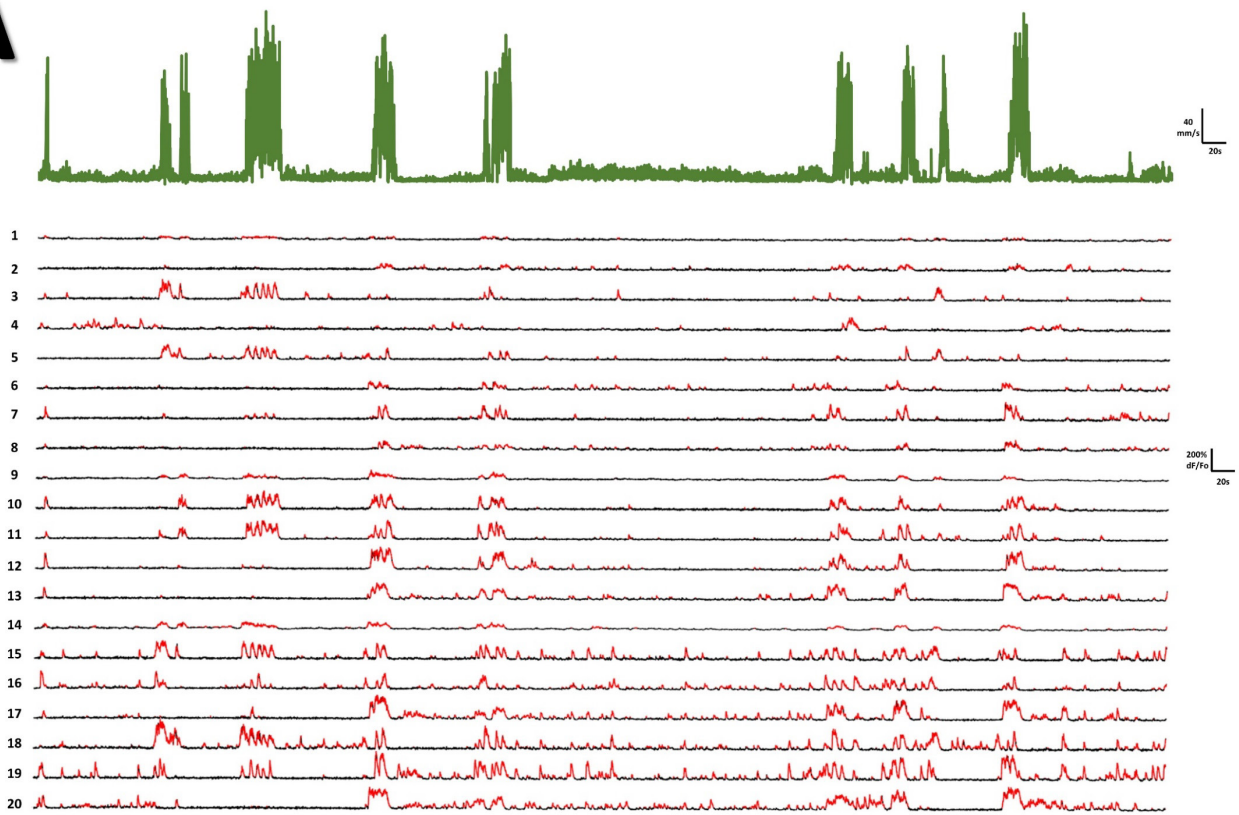
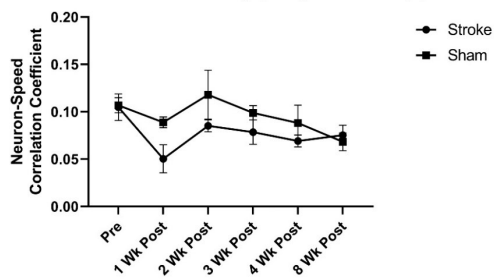


Fig 3.7. Neuron firing rate trends towards a decrease at 1 week in the peri-infarct imaging region after stroke. In the peri-infarct imaging region, no main effects or interaction was seen in the average firing rate during animal movement in non-normalized (A) or normalized (B) data, however *post-hoc* analysis of normalized data indicates a trend towards decreased normalized average firing rate when moving at 1 week in the stroke group relative to sham ($p = 0.0593$). A main effect of group was seen in the non-normalized average firing rate at rest (C), with *post-hoc* tests showing a significant difference between stroke and sham at the 8 week timepoint ($p = 0.0439$). A significant interaction was seen in the normalized average firing rate at rest (D), with *post-hoc* tests showing a trend towards a decrease in firing rate at rest between the stroke and sham groups at the 1 week post timepoint ($p = 0.0793$). A significant main effect of group is observed in the ratio of firing rate moving to firing rate rest (E), however no significant differences or trends are observed in *post-hoc* tests. No main effects or interactions were observed in the normalized ratio of firing rate run to rest for the imaging region between the cFL and cHL (F). In the distal imaging region, a trend towards a main effect of group was seen in the non-normalized average firing rate when moving (G), but not in the normalized average firing rate when moving (H), with *post-hoc* tests showing a trend towards increased non-normalized firing rate during run at 4 week post in the stroke group relative to sham ($p = 0.0667$). A trend towards a main effect of group in the average firing rate at rest is observed (I), with *post-hoc* tests indicating a trend towards an increase in firing rate at rest for the stroke group relative to sham at the 8 week post timepoint ($p = 0.0658$). No main effects or interaction are seen in the normalized average firing rate at rest for the distal imaging region (J). No main effects or interaction were observed for the non-normalized (K) and normalized (L) ratio of firing rate moving to firing rate rest for the distal imaging region. Peri-infarct region Stroke N = 11, Sham N = 4. Distal region Stroke N = 13, Sham N = 4. * $p < 0.05$; ** $p < 0.01$; *** $p < 0.001$

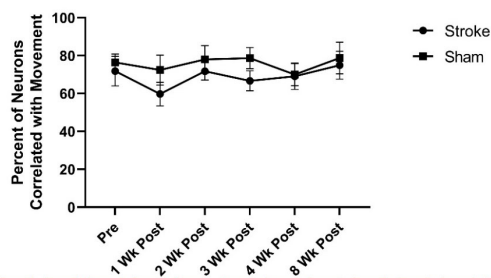
A**B**

Peri-Infarct Region

Timepoint F (3.116, 38.64) = 2.861, $p = 0.0474$
 Group F (1, 13) = 2.296, $p = 0.1536$
 Interaction F (5, 62) = 0.7734, $p = 0.5726$

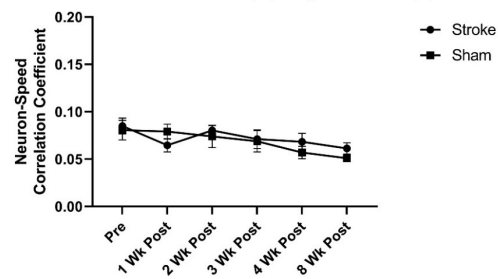
**C**

Timepoint F (3.340, 41.41) = 0.5212, $p = 0.6891$
 Group F (1, 13) = 1.416, $p = 0.2553$
 Interaction F (5, 62) = 0.1813, $p = 0.9686$

**D**

Distal Region

Timepoint F (3.920, 58.80) = 1.862, $p = 0.1304$
 Group F (1, 15) = 0.1935, $p = 0.6663$
 Interaction F (5, 75) = 0.4406, $p = 0.8188$

**E**

Timepoint F (3.539, 53.09) = 1.614, $p = 0.1901$
 Group F (1, 15) = 0.7899, $p = 0.3882$
 Interaction F (5, 75) = 0.7146, $p = 0.6144$

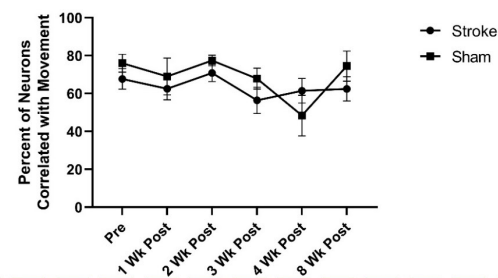


Fig 3.8. Average neuron correlation with animal movement is not detectably altered by stroke. (A) Example time series of animal speed (green) and Ca²⁺ traces from the 20 most active neurons of the population co-recorded with the animal movement speed. Significant Ca²⁺ transients are highlighted by red segments. For the peri-infarct imaging region, a significant main effect of timepoint was observed in the average correlation coefficient between neuron Ca²⁺ traces and speed (B), however *post-hoc* tests did not show a significant difference between any of the timepoints within the stroke and sham groups, respectively. No main effects or interaction was seen in the percent of neurons correlated with movement for the peri-infarct imaging region (C). In the distal imaging region, no significant main effects or interactions were seen in the average correlation coefficient between neuron Ca²⁺ traces and speed (D), or in the percent of neurons correlated with movement (E). Peri-infarct region Stroke N = 11, Sham N = 4. Distal region Stroke N = 13, Sham N = 4. *p < 0.05; **p < 0.01; ***p < 0.001

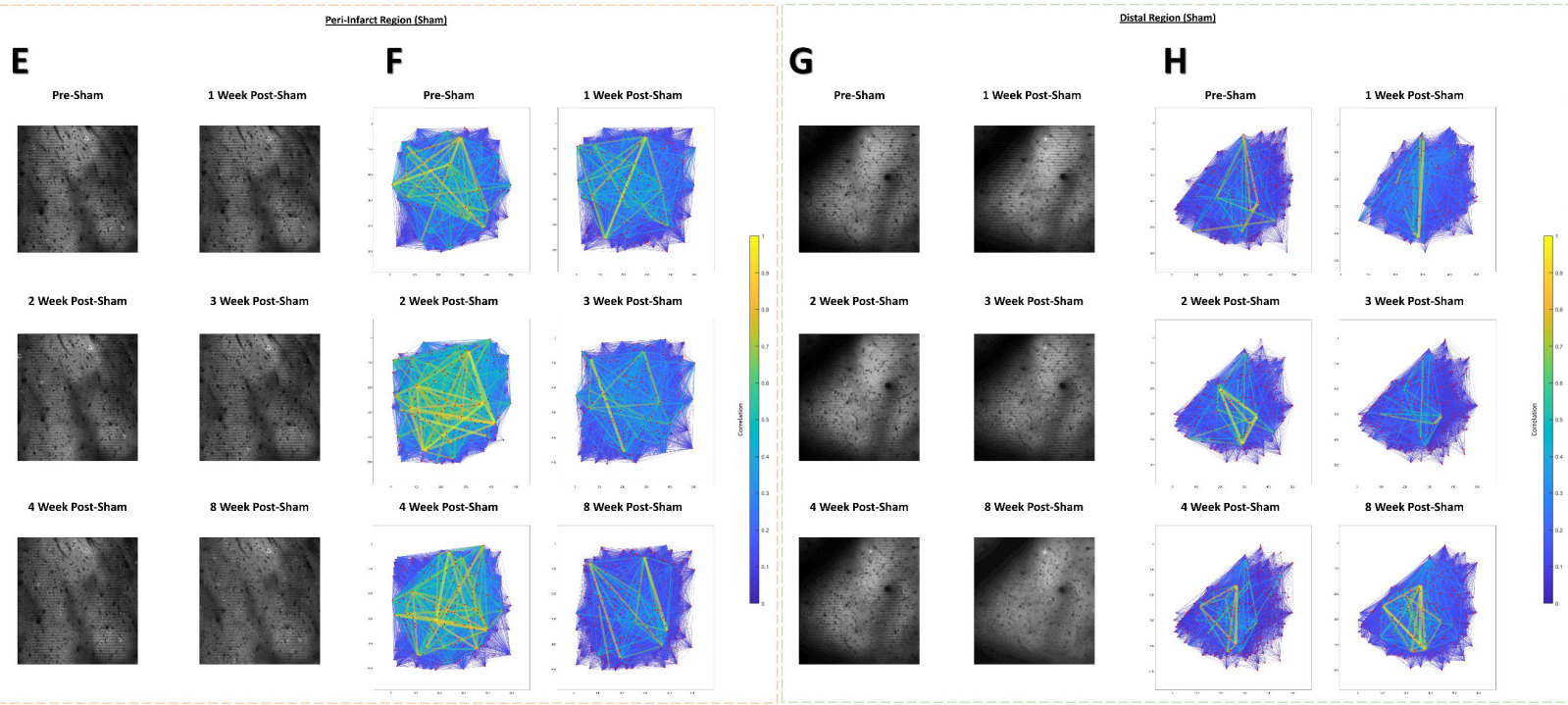
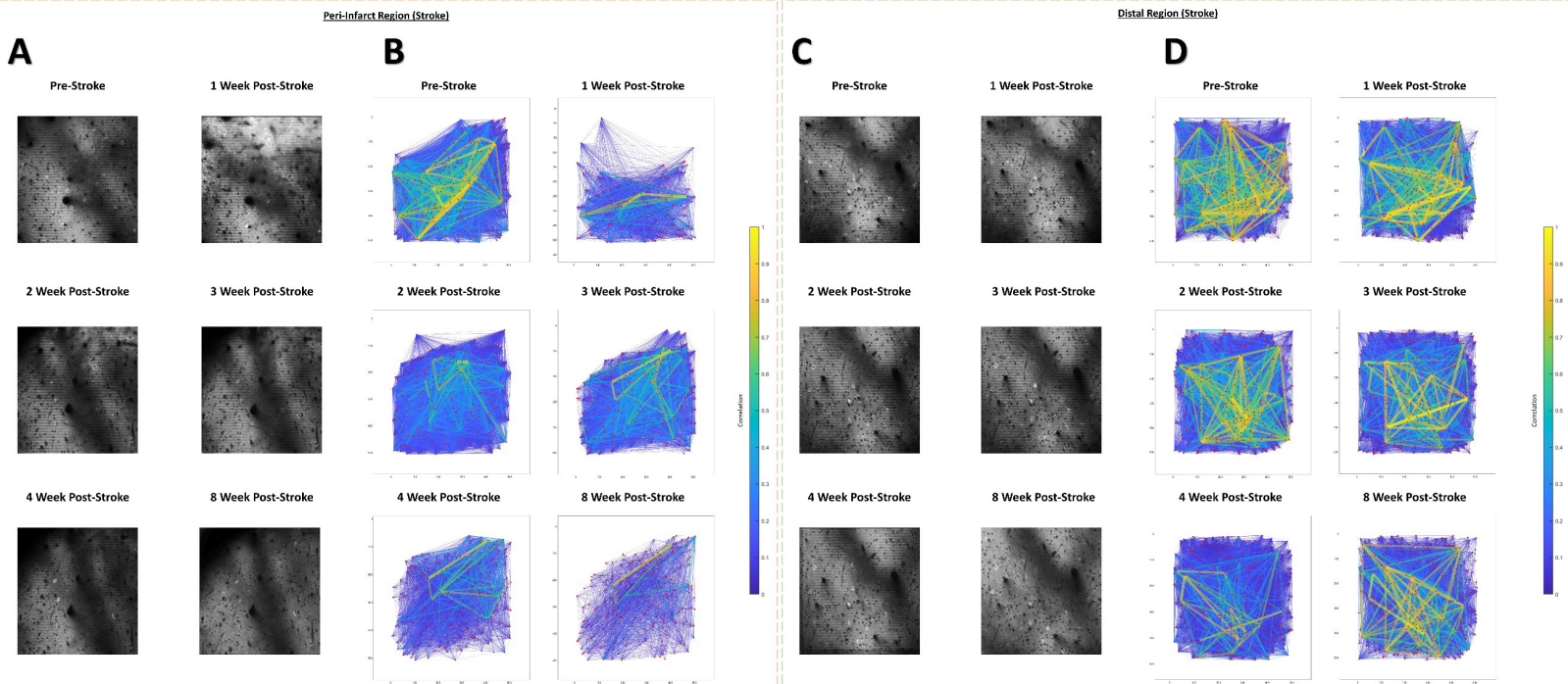
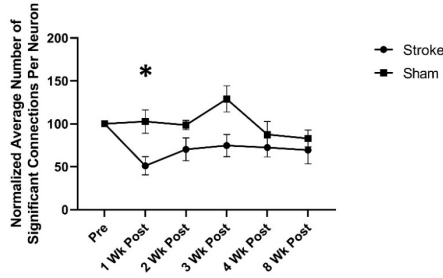


Fig 3.9. Example cellular GCaMP6S Ca²⁺ fluorescence images and population functional connectivity plots. (A-D) Ca²⁺ fluorescence images and functional connectivity plots from the peri-infarct imaging region and the distal imaging region for one example stroke group animal. Population functional connectivity plots demonstrate neurons as red dots, and the functional connection strength as lines with color and line width determined by the strength of the correlation between neurons. Notable cortical damage is visible in the upper portion of the 1 week post-stroke Ca²⁺ fluorescence image in the peri-infarct imaging region (A), which notably improves over the 2-4 week timepoints. A notable loss of functional connections and loss in the number of connections with strong correlation (>0.3) is visible in the functional connectivity plots at 1 week post-stroke in the peri-infarct imaging region (B). In the distal imaging region post-stroke, less structural change is visible in the cellular Ca²⁺ fluorescence images (C), and less change to functional connectivity of the population over time (D). (E-H) Ca²⁺ fluorescence images and functional connectivity plots from the peri-infarct imaging region and the distal imaging region for one example sham group animal. Less structural changes within the cellular Ca²⁺ fluorescence images, and in the functional connectivity plots are visually apparent relative to the example stroke animal. Data quantified in Fig. 3.10.

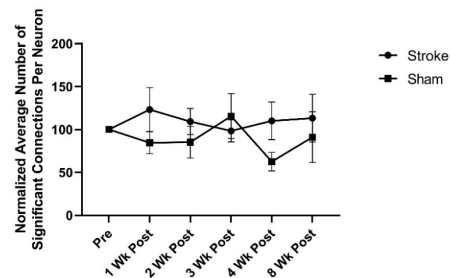
A

Timepoint F (4.132, 47.11) = 2.217, p= 0.1498
 Group F (1, 13) = 4.505, p= 0.0551
 Interaction F (4, 45) = 1.585, p= 0.1947



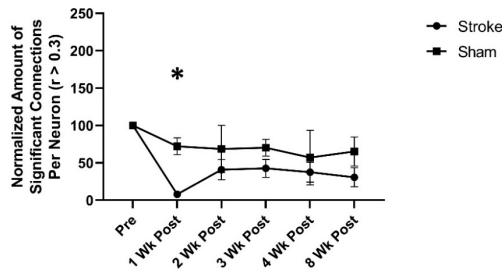
F

Timepoint F (2.041, 30.61) = 0.4766, p= 0.6292
 Group F (1, 15) = 0.4267, p= 0.5235
 Interaction F (4, 60) = 1.124, p= 0.3540



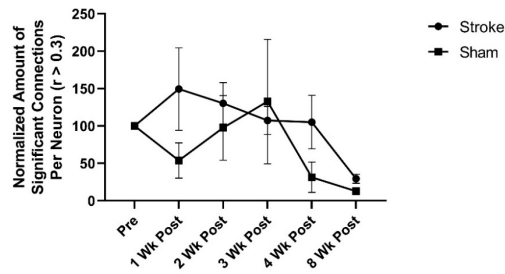
B

Timepoint F (2.102, 22.60) = 0.3885, p= 0.6925
 Group F (1, 13) = 6.423, p= 0.0262
 Interaction F (4, 43) = 0.6512, p= 0.6292



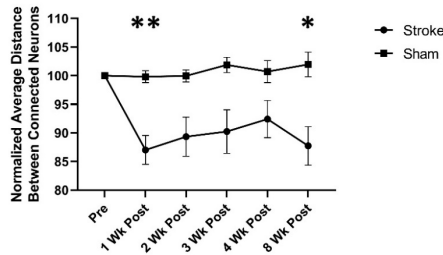
G

Timepoint F (2.228, 32.86) = 2.196, p= 0.1224
 Group F (1, 15) = 1.036, p= 0.3249
 Interaction F (4, 59) = 0.7713, p= 0.5482



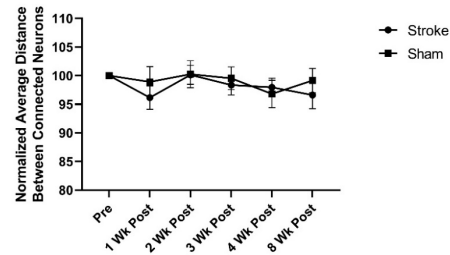
C

Timepoint F (2.613, 32.01) = 0.3434, p= 0.7670
 Group F (1, 13) = 7.989, p= 0.0143
 Interaction F (4, 49) = 0.3439, p= 0.8470



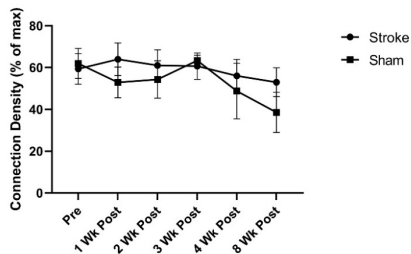
H

Timepoint F (2.794, 41.91) = 0.7835, p= 0.4737
 Group F (1, 15) = 0.1454, p= 0.7083
 Interaction F (4, 60) = 0.3813, p= 0.5018



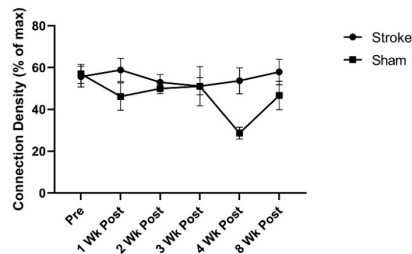
D

Timepoint F (3.251, 40.31) = 0.3546, p= 0.8015
 Group F (1, 13) = 1.257, p= 0.2824
 Interaction F (5, 62) = 1.146, p= 0.3462



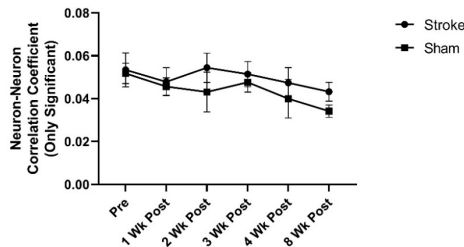
I

Timepoint F (3.467, 52.01) = 1.299, p= 0.2841
 Group F (1, 15) = 2.062, p= 0.1715
 Interaction F (5, 75) = 1.251, p= 0.2942



E

Timepoint F (3.334, 41.34) = 1.083, p= 0.3711
 Group F (1, 13) = 0.5715, p= 0.4631
 Interaction F (5, 62) = 0.1658, p= 0.9742



J

Timepoint F (3.161, 47.41) = 0.4292, p= 0.7430
 Group F (1, 15) = 1.733, p= 0.2078
 Interaction F (5, 75) = 0.4432, p= 0.8169

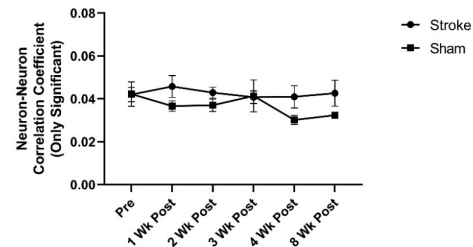
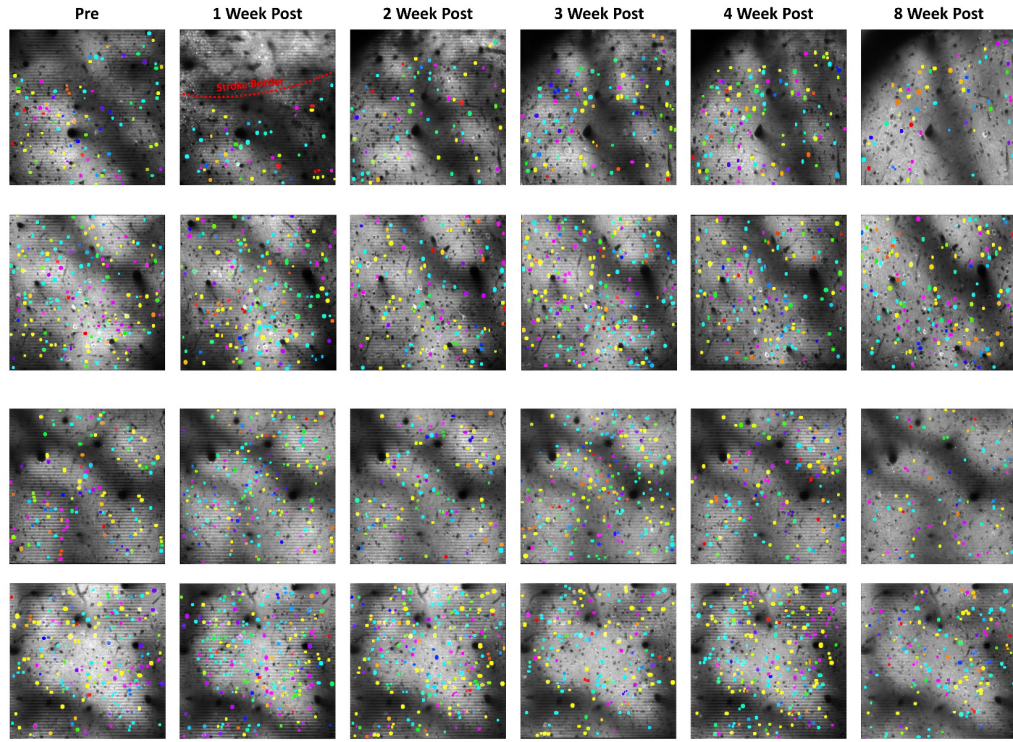
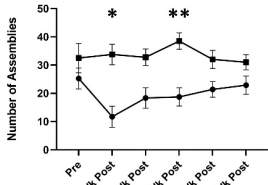


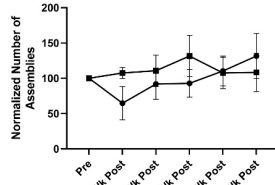
Fig 3.10. Neural population functional connectivity measurements indicate a loss of functional connections and connection strength at 1 week post-stroke in the peri-infarct imaging region. In the peri-infarct imaging region, a trend towards a main effect of group is seen in the normalized average number of significant connections per neuron (**A**), with *post-hoc* tests showing a significant decrease at the 1 week post timepoint in the stroke group relative to sham ($p = 0.0440$). A significant main effect of group is seen in the normalized number of significant connections per neurons with correlation greater than 0.3 (**B**), with *post-hoc* tests indicating a significant decrease at the 1 week post timepoint in the stroke group relative to sham ($p = 0.0363$). A significant main effect of group is seen in the normalized average distance between connected neurons (**C**), with *post-hoc* tests indicating a significant decrease at 1 week post ($p = 0.0023$) and 8 week post ($p = 0.0218$) timepoints in the stroke group relative to sham. No main effects or interactions are seen in the connection density (**D**) or in the average correlation coefficient between neurons with significant connections determined via bootstrapping (**E**) for the peri-infarct imaging region. In the distal imaging region, no significant main effects or interactions are seen in the normalized number of significant connections per neuron (**F**), normalized amount of significant connection with correlation greater than 0.3 (**G**), normalized average distance between connected neurons (**H**), connection density (**I**), or in the average correlation coefficient between neurons with significant connections determined via bootstrapping (**J**). Peri-infarct region Stroke N = 11, Sham N = 4. Distal region Stroke N = 13, Sham N = 4. * $p < 0.05$; ** $p < 0.01$; *** $p < 0.001$

A**B**

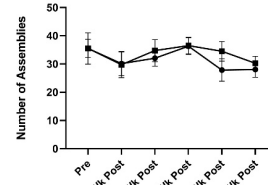
Timepoint F (2.883, 35.75) = 0.8231, $p=0.4857$
 Group F (1, 13) = 11.90, $p=0.0043$
 Interaction F (5, 62) = 1.496, $p=0.2040$

**C**

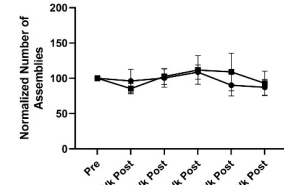
Timepoint F (2.854, 34.96) = 1.389, $p=0.2627$
 Group F (1, 13) = 0.2503, $p=0.6252$
 Interaction F (4, 49) = 1.444, $p=0.2336$

**J**

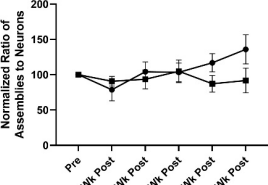
Timepoint F (2.649, 39.73) = 1.433, $p=0.2492$
 Group F (1, 15) = 0.1578, $p=0.6968$
 Interaction F (5, 75) = 0.2838, $p=0.9206$

**K**

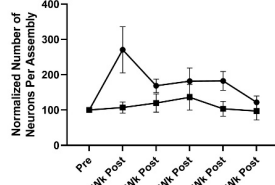
Timepoint F (2.866, 42.99) = 1.755, $p=0.1722$
 Group F (1, 15) = 0.02520, $p=0.8760$
 Interaction F (4, 60) = 0.7060, $p=0.5910$

**D**

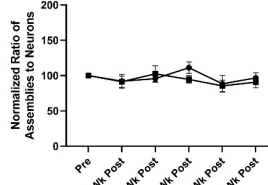
Timepoint F (2.876, 35.23) = 1.132, $p=0.3479$
 Group F (1, 13) = 0.3439, $p=0.5676$
 Interaction F (4, 49) = 1.242, $p=0.3057$

**E**

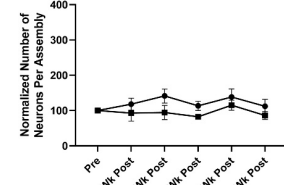
Timepoint F (1.770, 21.68) = 0.9288, $p=0.3995$
 Group F (1, 13) = 3.308, $p=0.0920$
 Interaction F (4, 49) = 0.8614, $p=0.4938$

**L**

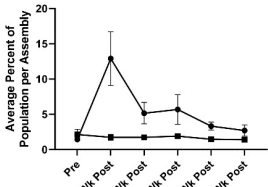
Timepoint F (2.954, 44.31) = 1.030, $p=0.3877$
 Group F (1, 15) = 0.09618, $p=0.7607$
 Interaction F (4, 60) = 0.4769, $p=0.7525$

**M**

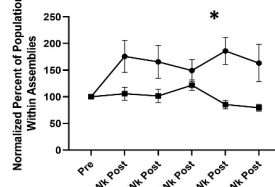
Timepoint F (3.226, 48.40) = 0.8515, $p=0.4795$
 Group F (1, 15) = 0.009268, $p=0.2556$
 Interaction F (4, 60) = 0.1230, $p=0.9737$

**F**

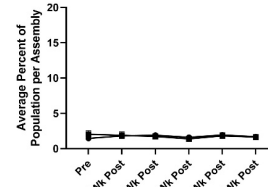
Timepoint F (1.711, 21.22) = 1.738, $p=0.2023$
 Group F (1, 13) = 3.807, $p=0.0729$
 Interaction F (5, 62) = 1.765, $p=0.1333$

**G**

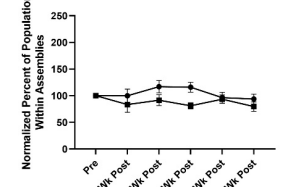
Timepoint F (2.892, 35.42) = 0.2340, $p=0.8655$
 Group F (1, 13) = 3.625, $p=0.0793$
 Interaction F (4, 49) = 0.5076, $p=0.7303$

**N**

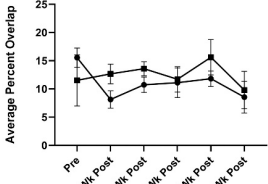
Timepoint F (3.233, 48.50) = 0.4839, $p=0.7088$
 Group F (1, 15) = 0.002991, $p=0.9571$
 Interaction F (5, 75) = 0.5535, $p=0.7352$

**O**

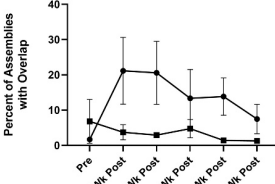
Timepoint F (3.244, 48.66) = 0.8579, $p=0.4766$
 Group F (1, 15) = 1.403, $p=0.2546$
 Interaction F (4, 60) = 0.7031, $p=0.5929$

**H**

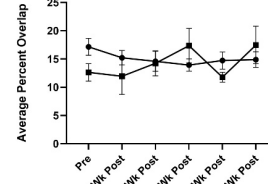
Timepoint F (3.401, 36.06) = 1.189, $p=0.3299$
 Group F (1, 13) = 0.6953, $p=0.4194$
 Interaction F (5, 53) = 0.9927, $p=0.4311$

**I**

Timepoint F (1.910, 23.30) = 0.5114, $p=0.5980$
 Group F (1, 13) = 1.700, $p=0.2150$
 Interaction F (5, 61) = 0.7483, $p=0.5905$

**P**

Timepoint F (3.181, 41.35) = 0.6289, $p=0.6095$
 Group F (1, 15) = 0.3590, $p=0.5580$
 Interaction F (5, 65) = 1.289, $p=0.2795$

**Q**

Timepoint F (3.513, 52.69) = 0.4229, $p=0.7674$
 Group F (1, 15) = 0.009268, $p=0.9246$
 Interaction F (5, 75) = 0.5195, $p=0.7608$

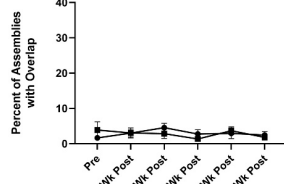
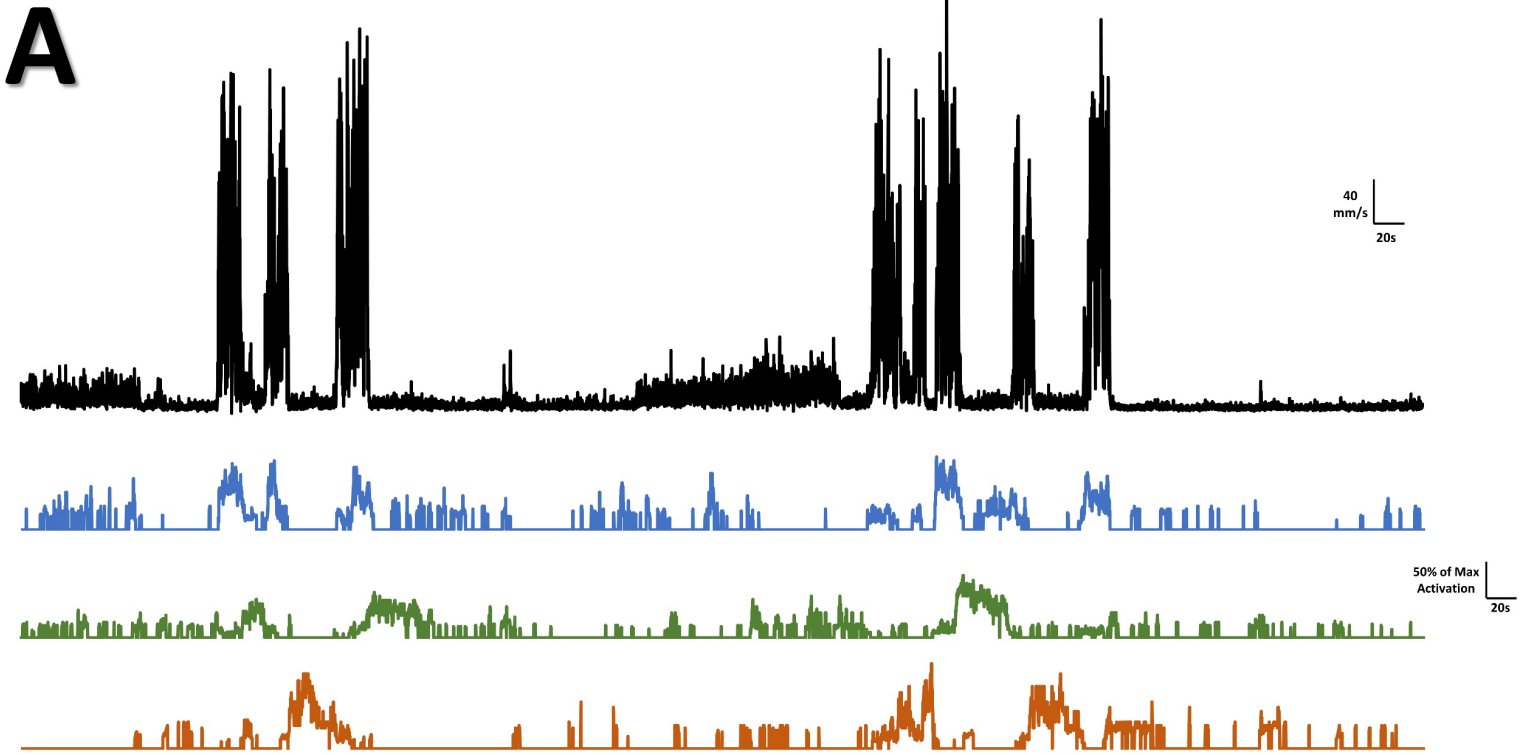
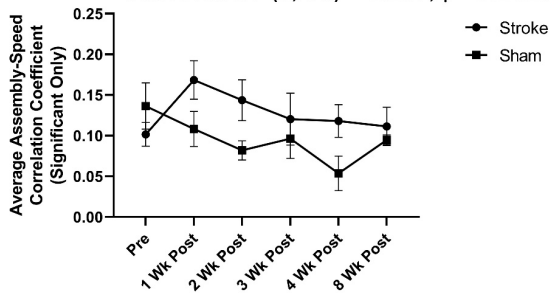


Fig 3.11. Neural assembly architecture is affected at 1 week post-stroke in the peri-infarct region. (A) Representative cellular Ca²⁺ fluorescence images for the peri-infarct imaging region and distal imaging region for an example stroke and sham animal with neural assemblies color coded and overlaid. In the peri-infarct imaging region, a significant main effect of group was found for the number of assemblies (B), with *post-hoc* tests showing a significant decrease in the number of assemblies at the 1 week and 3 week timepoints for the stroke group compared to sham ($p = 0.0114$ & 0.0058 , respectively). A trend is also observed at the 2 week timepoint for the stroke group compared to sham ($p = 0.0589$). However, no main effect or interaction is observed for the normalized number of assemblies (C) or in the normalized ratio of assemblies to neurons (D). A trend towards a main effect of group is seen in the normalized number of neurons per assembly (E), however no significant trends are observed in *post-hoc* tests. A trend towards a main effect of group is seen in the average percent of the population per assembly (F), with *post-hoc* tests showing a trend towards an increase in the stroke group relative to sham at the 1 week post timepoint ($p = 0.0863$). A trend towards a main effect of group is seen in the normalized percent of the population within assemblies (G), with *post-hoc* tests indicating a significant increase at the 4 week post timepoint in the stroke group relative to sham ($p = 0.0177$). No main effects or interactions are detected in the percent of cell overlap between assemblies (H) or in the percent of assemblies with overlap (I). In the distal imaging region, no main effects or interactions are detected in the number of assemblies (J), normalized number of assemblies (K), normalized ratio of assemblies to neurons (L), normalized number of neurons per assembly (M), average percent of the population per assembly (N), normalized percent of the population within assemblies (O), average percent overlap between assemblies (P), or in the percent of assemblies with overlap (Q). Peri-infarct region Stroke N = 11, Sham N = 4. Distal region Stroke N = 13, Sham N = 4. * $p < 0.05$; ** $p < 0.01$; *** $p < 0.001$

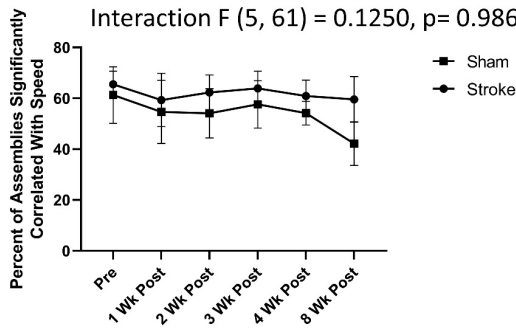


Peri-Infarct Region

B Timepoint F (1.999, 23.99) = 1.099, p = 0.3495
 Group F (1, 13) = 1.356, p = 0.2651
 Interaction F (5, 60) = 1.287, p = 0.2816

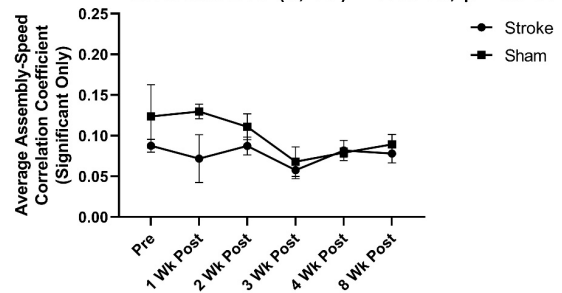


C Timepoint F (2.726, 33.25) = 0.5012, p = 0.6667
 Group F (1, 13) = 0.9432, p = 0.3492
 Interaction F (5, 61) = 0.1250, p = 0.9863



Distal Region

D Timepoint F (2.098, 31.47) = 1.134, p = 0.3368
 Group F (1, 15) = 1.497, p = 0.2399
 Interaction F (5, 75) = 0.5900, p = 0.7076



E Timepoint F (3.689, 55.33) = 1.329, p = 0.2721
 Group F (1, 15) = 0.4223, p = 0.5256
 Interaction F (5, 75) = 0.8646, p = 0.5090

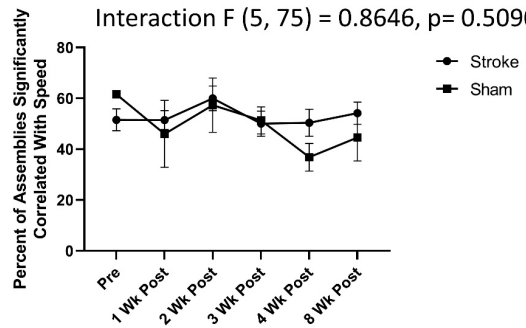
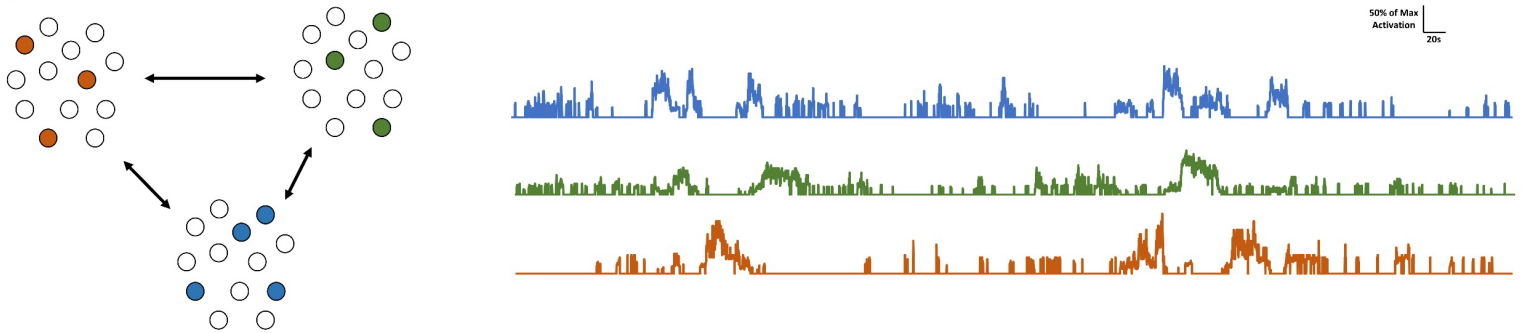
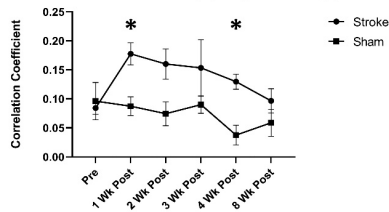


Fig 3.12. Correlation between assembly activations and movement is not detectably affected by stroke. (A) Representative time series of animal movement speed (black) and the assembly activation level for three representative assemblies (blue, green, orange) from the neuron population corresponding to the animal movement speed above. In the peri-infarct imaging region, no main effects or interactions are seen in the average assembly-speed correlation coefficient (B), or in the percent of assemblies significantly correlated with speed (C). In the distal imaging region, no main effects or interactions are seen in the average assembly-speed correlation coefficient (D), or in the percent of assemblies significantly correlated with speed (E). Peri-infarct region Stroke N = 11, Sham N = 4. Distal region Stroke N = 13, Sham N = 4. *p < 0.05; **p < 0.01; ***p < 0.001

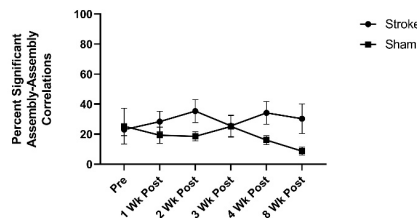
A**B**

Peri-Infarct Region

Timepoint F (2.326, 27.45) = 1.157, $p = 0.3354$
 Group F (1, 13) = 7.247, $p = 0.0185$
 Interaction F (5, 59) = 0.9533, $p = 0.4538$

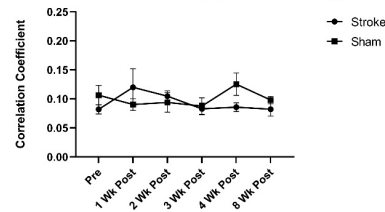
**C**

Timepoint F (3.251, 40.31) = 0.3546, $p = 0.8015$
 Group F (1, 13) = 1.257, $p = 0.2824$
 Interaction F (5, 62) = 1.146, $p = 0.3462$

**D**

Distal Region

Timepoint F (1.632, 24.48) = 0.3879, $p = 0.6409$
 Group F (1, 15) = 0.1774, $p = 0.6796$
 Interaction F (5, 75) = 0.8951, $p = 0.4889$

**E**

Timepoint F (3.533, 53.00) = 0.9293, $p = 0.4452$
 Group F (1, 15) = 0.3359, $p = 0.5708$
 Interaction F (5, 75) = 1.030, $p = 0.4064$

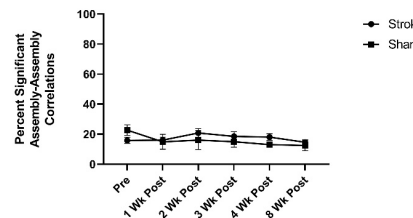


Fig 3.13. Correlation among neural assemblies is increased in the peri-infarct region. (A) Illustration of three example color coded neural assemblies from a neural population and their corresponding time series activations. Assemblies were compared in terms of their overlapping cell population and the correlation between assembly activations. In the peri-infarct imaging region, a significant main effect of group is seen in the correlation coefficient for significantly correlated assembly-assembly pairs (**B**), with *post-hoc* tests indicating a significantly higher correlation at 2 week ($p = 0.029$) and 4 weeks ($p=0.0253$) in the stroke group relative to sham. No main effect or interaction was seen in the percent significant assembly-assembly correlations between stroke and sham groups (**C**). In the distal imaging region, no significant main effects or interactions are seen for the correlation coefficient for significantly correlated assembly-assembly pairs (**D**), or in the percent of significant assembly-assembly correlations (**E**). Peri-infarct region Stroke N = 11, Sham N = 4. Distal region Stroke N = 13, Sham N = 4. * $p < 0.05$; ** $p < 0.01$; *** $p < 0.001$

Chapter 4: Conclusions

It is well recognized in human stroke patients that damage to the sensorimotor cortex leads to impairments in somatosensation, including deficits that may include the inability to sense specific modalities, a loss in stimulus localization, and deficits in stereognosis for objects in the hands (Carey and Matyas, 2011; Connell et al., 2008; Kwakkel et al., 2004; Patel et al., 2000; Tyson et al., 2008). While the fundamental mechanisms of sensory processing within the limb-associated somatosensory cortex have been studied in non-human primates, little information exists on the sensory processing of somatic stimuli within the limb-associated somatosensory cortex of rodents. Furthermore, minimal research exists on how stroke alters patterns of neural activity within the limb-associated somatosensory area in awake, behaving rodents. The main objective of this thesis was to use advanced imaging techniques (widefield Ca^{2+} and flavoprotein imaging, along with cellular Ca^{2+} imaging) to further our scientific knowledge in two ways: First, to determine if different frequencies of artificial mechanical stimuli that are used for the study of sensory-evoked activation of the intact or post-stroke brain are differentially represented within the somatosensory cortex of mice, even when these distinct stimuli have overlapping features. Second, to elucidate plastic changes in neural activity patterns within the limb-associated somatosensory cortex after stroke in awake, behaving animals and evaluate how potential deficits in cortical activity may relate to deficits in animal behavior.

In Chapter 2, we used mechanical limb stimulation to characterize the sensory-evoked response properties of the limb-associated somatosensory cortex in response to square-wave movement with distinct fundamental frequencies but overlapping harmonics. Bending actuators are often used for the study of cortical excitability during disease or after injury due to their simplicity of use and low cost. Despite having no clear naturalistic equivalent, these stimulators

provide a highly multimodal input to the somatosensory cortex due to their high oscillation amplitude and method of attachment to the limb. We therefore hypothesized that differential activation of diverse populations of peripheral mechanoreceptors for each stimulus frequency would elicit different patterns of activity in somatosensory cortical neuronal networks, and that these distinct patterns would be apparent when analyzing the activity of neurons in somatosensory networks. We found that neurons within the limb associated somatosensory cortex responding to various frequencies of square-wave stimuli exhibited stimulus-specific patterns of activity. Subsets of neurons were found to have sensory-evoked activity that was either primarily responsive to single stimulus frequencies or broadly responsive to multiple frequencies of limb stimulation. High frequency stimuli were shown to elicit more population activity, with a greater percentage of the population responding and greater percentage of cells with high amplitude responses. Stimulus-evoked cell-cell correlations within these neuronal networks varied as a function of frequency of stimulation, such that each stimulus elicited a distinct pattern that was more consistent across multiple trials of the same stimulus compared to trials at different frequencies of stimulation. The variation in cortical response to different square-wave stimuli was thus found to be represented by the population pattern of supra-threshold Ca^{2+} transients, the magnitude and temporal properties of the evoked activity, and the structure of the stimulus-evoked correlation between neurons.

According to the “representational framework”, neural assemblies can be identified within neuronal networks by presenting various stimuli of known quantity/quality to the brain, and examining the spatio-temporal attributes of evoked neuronal population responses (Buzsáki, 2010). When this framework is applied to the somatosensory system, some lines of research have

put forth the idea that with a large enough repertoire of diverse stimuli the fundamental mechanisms of stimulus encoding within the system can be elucidated. This idea holds some merit in terms of using stimuli with increasing complexity (e.g. from simple point localized stimuli, to more complex stimuli involving motion, direction, shape, rolling, etc.) to delineate stimulus preference in hierarchical cortical areas (see Chapter 1 for review). Unfortunately, there are questions about whether patterns of activity that are characterized as neural assemblies within each of these hierarchical areas are, in reality, representing what the researcher believe them to be. It is possible that assembly activation may not only relate to the feature of interest, but may also represent a plan for immediate action, corollary information from other brain areas, a high order cognitive or associative process, or even more complex processes not directly related to elementary properties of the stimulus (Buzsáki, 2010). In Chapter 2 we did not examine the contribution of specific afferent fibers to the sensory-evoked somatosensory representations elicited by our mechanical stimuli. With increasing knowledge of genetic markers that identify afferents associated with specific subsets of mechanoreceptors (Handler and Ginty, 2021; Li et al., 2011; Prsa et al., 2019; Wu et al., 2012), there is the potential to specifically target these afferents for optogenetic stimulation and to characterize the response of the limb-associated somatosensory cortex with the intent of determining the contribution that each modality makes. Unfortunately, it is not obvious how to deliver a naturalistic stimulus train to these sensory afferents. Furthermore, increasing evidence points to interactions in the neural processing of different somatosensory modalities as being the norm instead of the exception, and any cortical activity elicited from a single modality in isolation may provide incomplete information as to the true fundamental properties of sensory encoding of naturalistic stimuli. An alternative to determining the sensory-evoked cortical representation of single somatosensory modalities using

optogenetics could instead be to determine the neural representations activated during a behavioral task in which there is naturalistic somatosensation. Indeed, recent research using a vibrissae tactile discrimination task in rats has demonstrated the presence of transiently organizing neural assemblies that hold more information about the tactile stimulus and animal behavior than single neurons alone (Deolindo et al., 2017). Comparing the spatio-temporal evolution of cortical activity with sensory inputs predicted from animal kinematics as it interacts with objects may elucidate neural assemblies related to the behavior, however it comes at the cost of reduced experimental control for the known elemental properties of the stimulus driving the cortical representations. A second difficulty in determining the neural representation of somatic stimuli is the ability to measure large populations of neurons at a high enough temporal resolution to determine the precise temporal procession of neural spiking. Although there is ongoing research into deconvolutional methods for the determination of spike quantity from Ca^{2+} imaging data (Friedrich et al., 2017; Pachitariu et al., 2018; Pnevmatikakis et al., 2016; Romano et al., 2015, 2017; Vogelstein et al., 2010), the low temporal fidelity of Ca^{2+} indicators presents a barrier to determining precise spike timing to resolve the temporal evolution of patterned cell firing on short timescales. A solution may be the use of genetically encoded voltage indicators (GEVIs) that have significantly greater temporal resolution than Ca^{2+} indicators. Unfortunately, GEVIs currently have lower signal-to-noise ratio than Ca^{2+} indicators and are sensitive to photobleaching, qualities that have prevented their more widespread usage (for review, see (Platisa and Pieribone, 2018; Yang and St-Pierre, 2016)). The combined use of more robust future GEVIs along with head-mounted micro-endoscopes to monitor the fast temporal evolution of cortical activity while co-monitoring the animal's naturalistic behavior without head fixation may be one means of better determining cortical activity and neural representations associated

with naturalistic sensory stimuli in the future. In addition, continual advancement in micro-electronic stimulators (for example, see (Jörntell et al., 2014)) may enable the use of sophisticated stimulation techniques that could be applied to the glabrous skin of mice in the awake state in order to determine if the somatosensory cortex of mice has structured inter-regional or intra-regional hierarchical representations of somatic features in some way analogous to the cortical areas 3a, 3b, 1 and 2 observed in the primate brain.

In Chapter 3, we evaluated post-stroke cortical activity, functional connectivity and neural assembly architecture in the peri-infarct and distal cortex in order to further clarify the functional state of the post-stroke cortex. We deemed this necessary in light of observations from other studies indicating a deficit in sensory-evoked cortical activation after stroke despite multiple markers of impaired cortical inhibition and a potential for epileptogenic hyperexcitability. Based on past research in anesthetized mice that had shown a deficit in sensory-evoked somatosensory activation using cellular Ca^{2+} imaging after focal FL stroke (Winship and Murphy, 2008), we hypothesized that we would see decreased sensorimotor cortical activity in awake behaving animals within the first 2 weeks after stroke and that this would be concurrent with behavioral impairments at the same timepoints. We are the first to show that there is a significant reduction in neural network functional connectivity and deficits in neuronal assembly architecture along with a trend towards reduced firing rate detectable in the peri-infarct cortex, but not detectable in the distal cortex, at 1 week after focal FL stroke in awake, behaving animals. Indeed, the distal cortex trended towards an increase in firing rate at 1-2 months post-stroke, suggesting that in our model of focal stroke, detectable deficits may be highly localized to the immediate peri-lesional area. The peak of these detectable deficits in the

peri-infarct cortex was synchronous with a behavioral deficit in the tapered beam task, and was not detected in the string pull task or in behavioral monitoring within the mobile homecage. The lack of detectable behavioral deficits in the string pull task in Chapter 3 was contrary to what we had predicted. Past research has shown a transient deficit lasting up to a week in the string pull task after devascularization lesion of the somatosensory cortex (Blackwell et al., 2018c), similar to the deficit previously observed at 1 week in the tapered beam task after focal FL photothrombosis (Ardesch et al., 2017; Zhao et al., 2005). As the tapered beam can be considered a more gross measure of sensorimotor function, in comparison to the string pull task that measures the kinematics of forelimb movement (Blackwell et al., 2018b, 2018a, 2018c), it is surprising that we would find a detectable deficit on the tapered beam task but not on the string pull task. It may be the case that despite measuring many elements of forelimb kinematics in the string pull, it was still insensitive to the fine deficits resulting from the photothrombotic model of stroke. Indeed, our recording equipment did not have sufficient resolution and framerate to determine the kinematics of the animal's individual digits during the task, and as such we cannot say if even finer aspects of single digit kinematics could have been affected while more gross measures of limb position were unaffected. We were again surprised to find that in both stroke and sham groups animal movement within the mobile homecage decreased over the course of the experiment. This continual decrease may potentially reflect the animal realizing that movement within the mobile homecage did not expedite their return to the homecage or may potentially result from a continual habituation and decrease in anxiety over the 2 month period of weekly imaging.

In Chapter 3, it is also possible that the lack of detectable deficit on the string pull, and

the deficit detected at 1 week on the tapered beam, could relate to the small infarct size and small penumbral area associated with photothrombotic stroke. Indeed, other studies using models of stroke with larger cortical lesions, such as MCAO, have indicated longer lasting deficits on the tapered beam (Lipsanen et al., 2011; Schallert et al., 2002), even at timepoints as long as 450 days after stroke (Schallert et al., 2002). Photothrombotic stroke was chosen for the research in Chapter 3 due to the ability to specifically target the FL somatosensory cortex for infarction and for the ability to use well defined imaging regions with known location relative to the pre-stroke somatotopic FL and HL maps. Unfortunately, the penumbra, an area of hypoperfused tissue surrounding the stroke core in endovascular stroke models such as MCAO (Doyle et al., 2008), is very small in the photothrombotic model of stroke (Carmichael, 2005; Sommer, 2017). If the small penumbral area of the photothrombotic stroke used in Chapter 3 was confined entirely within the peri-infarct imaging region, it may be a strong factor in isolating the detectable deficit to within the peri-infarct area, but not in the distal area. As such, future research could make use of stroke models with a larger stroke size and penumbral area, such as an MCAO model of stroke, to determine if the same deficits measured in Chapter 3 spatially extend across larger areas of the cortex associated with the larger penumbra and if these deficits persist for greater than the first week after stroke. A further opportunity for research would be to combine the measures of cortical function from Chapter 3 with pro-plasticity therapies to determine if these therapies can prevent the deficit in cortical function and behavior, and augment recovery. Likewise, if the MCAO model of stroke demonstrated long lasting functional and behavioral deficits, or spatially extended cortical function deficits within both the peri-infarct and distal cortex, then the MCAO model may serve as good measures of the ability of pro-plasticity therapies to augment functional recovery.

A limitation of the study in Chapter 3 was the age of the animals used. Human patients are typically elderly (primary risk factor for stroke) and may have additional risk factors that include diabetes, hypertension, and coronary disease (Casals et al., 2011). It is well known that the elderly brain has reduced ischemic tolerance (Ay et al., 2005; Bury and Jones, 2002; Joutel et al., 2010; Li et al., 2018; Ma et al., 2020; Popa-Wagner et al., 2007), and aged rodents show more severe behavioral deficits and reduced behavioral recovery after stroke. In Chapter 3, the mice that were used were young adults, healthy, and genetically homogenous, thereby reducing the applicability of the results. The young and healthy status of the mice in Chapter 3 also likely limited the extent of deficits in cortical function and behavior. Future research could re-examine the effects of focal photothrombotic stroke to the FL within aged mice to determine if the same results observed in Chapter 3 hold true.

Similar to the neural representations of stimuli observed in Chapter 2, in Chapter 3 we were unable to determine what sub-modalities of limb-associated mechanosensations were driving cortical activity and leading to the formation of the neuronal assemblies we observed. It is possible that longitudinal measurements of sensory-evoked somatosensory activation using the same artificial mechanical stimuli used in Chapter 2, or the use of modality specific optogenetic stimulation, could provide useful information on a deficit in representational processing of these stimuli at each timepoint after stroke. However, the combined use of GEVIs with simultaneous video monitoring of animal interaction with its sensory environment at each timepoint may be another more significant means of investigating some of the sensory aspects that may have been represented within the cortical networks that we were monitoring in Chapter 3.

In conclusion, the data presented in this thesis illuminates patterns by which different frequencies of artificial sensory stimuli often used in stroke research are represented within the limb-associated somatosensory cortex of mice under anesthetized conditions in the uninjured brain, and reveals longitudinal alterations to cortical network activity and functional network structure within the peri-infarct cortex after focal FL photothrombotic stroke. The data presented in this work could serve as a basis for continued study to better understand the function and plastic re-organization of the limb-associated somatosensory cortex in mice in the uninjured brain and stroke damaged brain in the anesthetized and awake, behaving state.

References

- Abraira, V.E., and Ginty, D.D. (2013). The sensory neurons of touch. *Neuron* 79, 618–639. <https://doi.org/10.1016/j.neuron.2013.07.051>.
- Ackerley, R., Backlund Wasling, H., Liljencrantz, J., Olausson, H., Johnson, R.D., and Wessberg, J. (2014). Human C-tactile afferents are tuned to the temperature of a skin-stroking caress. *J Neurosci* 34, 2879–2883. <https://doi.org/10.1523/JNEUROSCI.2847-13.2014>.
- Adeoye, O., Hornung, R., Khatri, P., and Kleindorfer, D. (2011). Recombinant tissue-type plasminogen activator use for ischemic stroke in the United States: a doubling of treatment rates over the course of 5 years. *Stroke* 42, 1952–1955. <https://doi.org/10.1161/STROKEAHA.110.612358>.
- Adibi, M. (2019). Whisker-Mediated Touch System in Rodents: From Neuron to Behavior. *Front Syst Neurosci* 13, 40. <https://doi.org/10.3389/fnsys.2019.00040>.
- Afrashteh, N., Inayat, S., Bermudez-Contreras, E., Luczak, A., McNaughton, B.L., and Mohajerani, M.H. (2021). Spatiotemporal structure of sensory-evoked and spontaneous activity revealed by mesoscale imaging in anesthetized and awake mice. *Cell Rep* 37, 110081. <https://doi.org/10.1016/j.celrep.2021.110081>.
- Agnew, Z., and Wise, R.J.S. (2008). Separate areas for mirror responses and agency within the parietal operculum. *J Neurosci* 28, 12268–12273. <https://doi.org/10.1523/JNEUROSCI.2836-08.2008>.
- Akay, T., Tourtellotte, W.G., Arber, S., and Jessell, T.M. (2014). Degradation of mouse locomotor pattern in the absence of proprioceptive sensory feedback. *Proceedings of the National Academy of Sciences* 111, 16877–16882. <https://doi.org/10.1073/pnas.1419045111>.
- Akers, R.M., and Killackey, H.P. (1978). Organization of corticocortical connections in the parietal cortex of the rat. *J Comp Neurol* 181, 513–537. <https://doi.org/10.1002/cne.901810305>.
- Alaverdashvili, M., and Whishaw, I.Q. (2008). Motor cortex stroke impairs individual digit movement in skilled reaching by the rat. *Eur J Neurosci* 28, 311–322. <https://doi.org/10.1111/j.1460-9568.2008.06315.x>.
- Alaverdashvili, M., Foroud, A., Lim, D.H., and Whishaw, I.Q. (2008a). “Learned baduse” limits recovery of skilled reaching for food after forelimb motor cortex stroke in rats: a new analysis of the effect of gestures on success. *Behav Brain Res* 188, 281–290. <https://doi.org/10.1016/j.bbr.2007.11.007>.
- Alaverdashvili, M., Moon, S.-K., Beckman, C.D., Virag, A., and Whishaw, I.Q. (2008b). Acute but not chronic differences in skilled reaching for food following motor cortex devascularization vs. photothrombotic stroke in the rat. *Neuroscience* 157, 297–308. <https://doi.org/10.1016/j.neuroscience.2008.09.015>.

- Alia, C., Cangi, D., Massa, V., Salluzzo, M., Vignozzi, L., Caleo, M., and Spalletti, C. (2021). Cell-to-Cell Interactions Mediating Functional Recovery after Stroke. *Cells* *10*, 3050. <https://doi.org/10.3390/cells10113050>.
- Alitto, H.J., and Usrey, W.M. (2003). Corticothalamic feedback and sensory processing. *Curr Opin Neurobiol* *13*, 440–445. [https://doi.org/10.1016/s0959-4388\(03\)00096-5](https://doi.org/10.1016/s0959-4388(03)00096-5).
- Allen, N.J., Rossi, D.J., and Attwell, D. (2004). Sequential release of GABA by exocytosis and reversed uptake leads to neuronal swelling in simulated ischemia of hippocampal slices. *J Neurosci* *24*, 3837–3849. <https://doi.org/10.1523/JNEUROSCI.5539-03.2004>.
- Alloway, K.D., Olson, M.L., and Smith, J.B. (2008). Contralateral corticothalamic projections from MI whisker cortex: potential route for modulating hemispheric interactions. *J Comp Neurol* *510*, 100–116. <https://doi.org/10.1002/cne.21782>.
- Alloway, K.D., Smith, J.B., Beauchemin, K.J., and Olson, M.L. (2009). Bilateral projections from rat MI whisker cortex to the neostriatum, thalamus, and claustrum: forebrain circuits for modulating whisking behavior. *J Comp Neurol* *515*, 548–564. <https://doi.org/10.1002/cne.22073>.
- Angel, A., and Lemon, R.N. (1975). Sensorimotor cortical representation in the rat and the role of the cortex in the production of sensory myoclonic jerks. *J Physiol* *248*, 465–488. <https://doi.org/10.1113/jphysiol.1975.sp010984>.
- Ardesch, D.J., Balbi, M., and Murphy, T.H. (2017). Automated touch sensing in the mouse tapered beam test using Raspberry Pi. *J Neurosci Methods* *291*, 221–226. <https://doi.org/10.1016/j.jneumeth.2017.08.030>.
- Ashby, D.M., LeDue, J., Murphy, T.H., and McGirr, A. (2019). Peripheral Nerve Ligation Elicits Widespread Alterations in Cortical Sensory Evoked and Spontaneous Activity. *Sci Rep* *9*, 15341. <https://doi.org/10.1038/s41598-019-51811-8>.
- Augurelle, A.-S., Smith, A.M., Lejeune, T., and Thonnard, J.-L. (2003). Importance of cutaneous feedback in maintaining a secure grip during manipulation of hand-held objects. *J Neurophysiol* *89*, 665–671. <https://doi.org/10.1152/jn.00249.2002>.
- Averbeck, B.B., and Seo, M. (2008). The Statistical Neuroanatomy of Frontal Networks in the Macaque. *PLoS Comput Biol* *4*, e1000050. <https://doi.org/10.1371/journal.pcbi.1000050>.
- Avitan, L., Pujic, Z., Mölter, J., Van De Poll, M., Sun, B., Teng, H., Amor, R., Scott, E.K., and Goodhill, G.J. (2017). Spontaneous Activity in the Zebrafish Tectum Reorganizes over Development and Is Influenced by Visual Experience. *Curr Biol* *27*, 2407-2419.e4. <https://doi.org/10.1016/j.cub.2017.06.056>.
- Ay, H., Koroshetz, W.J., Vangel, M., Benner, T., Melinosky, C., Zhu, M., Menezes, N., Lopez, C.J., and Sorensen, A.G. (2005). Conversion of ischemic brain tissue into infarction increases with age. *Stroke* *36*, 2632–2636. <https://doi.org/10.1161/01.STR.0000189991.23918.01>.
- Balbinot, G., Schuch, C.P., Jeffers, M.S., McDonald, M.W., Livingston-Thomas, J.M., and

Corbett, D. (2018). Post-stroke kinematic analysis in rats reveals similar reaching abnormalities as humans. *Scientific Reports* 8, 8738. <https://doi.org/10.1038/s41598-018-27101-0>.

Bandet, M.V., Dong, B., and Winship, I.R. (2021). Distinct patterns of activity in individual cortical neurons and local networks in primary somatosensory cortex of mice evoked by square-wave mechanical limb stimulation. *PLoS One* 16, e0236684. <https://doi.org/10.1371/journal.pone.0236684>.

Barlow, H. (2001). Redundancy reduction revisited. *Network* 12, 241–253. .

Battaglia, G., Lizier, C., Colacitti, C., Princivalle, A., and Spreafico, R. (1994). A reticuloreticular commissural pathway in the rat thalamus. *J Comp Neurol* 347, 127–138. <https://doi.org/10.1002/cne.903470110>.

Bauer, A.Q., Kraft, A.W., Wright, P.W., Snyder, A.Z., Lee, J.-M., and Culver, J.P. (2014). Optical imaging of disrupted functional connectivity following ischemic stroke in mice. *NeuroImage* 99, 388–401. <https://doi.org/10.1016/j.neuroimage.2014.05.051>.

Bell, J., Bolanowski, S., and Holmes, M.H. (1994). The structure and function of Pacinian corpuscles: a review. *Prog Neurobiol* 42, 79–128. [https://doi.org/10.1016/0301-0082\(94\)90022-1](https://doi.org/10.1016/0301-0082(94)90022-1).

Bengtsson, F., Brasselet, R., Johansson, R.S., Arleo, A., and Jörntell, H. (2013). Integration of sensory quanta in cuneate nucleus neurons in vivo. *PLoS One* 8, e56630. <https://doi.org/10.1371/journal.pone.0056630>.

Bensmaia, S.J. (2008). Tactile intensity and population codes. *Behav Brain Res* 190, 165–173. <https://doi.org/10.1016/j.bbr.2008.02.044>.

Bensmaia, S., and Helms Tillery, S.I. (2014). Tactile Feedback from the Hand. In *The Human Hand as an Inspiration for Robot Hand Development*, R. Balasubramanian, and V.J. Santos, eds. (Cham: Springer International Publishing), pp. 143–157.

Bensmaia, S.J., Denchev, P.V., Dammann, J.F., Craig, J.C., and Hsiao, S.S. (2008). The representation of stimulus orientation in the early stages of somatosensory processing. *J Neurosci* 28, 776–786. <https://doi.org/10.1523/JNEUROSCI.4162-07.2008>.

Bentivoglio, M., and Rustioni, A. (1986). Corticospinal neurons with branching axons to the dorsal column nuclei in the monkey. *J Comp Neurol* 253, 260–276. <https://doi.org/10.1002/cne.902530212>.

Benveniste, H., Drejer, J., Schousboe, A., and Diemer, N.H. (1984). Elevation of the extracellular concentrations of glutamate and aspartate in rat hippocampus during transient cerebral ischemia monitored by intracerebral microdialysis. *J Neurochem* 43, 1369–1374. <https://doi.org/10.1111/j.1471-4159.1984.tb05396.x>.

Berkes, P., Orbán, G., Lengyel, M., and Fiser, J. (2011). Spontaneous cortical activity reveals hallmarks of an optimal internal model of the environment. *Science* 331, 83–87.

<https://doi.org/10.1126/science.1195870>.

Biernaskie, J., Chernenko, G., and Corbett, D. (2004). Efficacy of rehabilitative experience declines with time after focal ischemic brain injury. *J Neurosci* 24, 1245–1254. <https://doi.org/10.1523/JNEUROSCI.3834-03.2004>.

Biernaskie, J., Szymanska, A., Windle, V., and Corbett, D. (2005). Bi-hemispheric contribution to functional motor recovery of the affected forelimb following focal ischemic brain injury in rats. *European Journal of Neuroscience* 21, 989–999. <https://doi.org/10.1111/j.1460-9568.2005.03899.x>.

Birznieks, I., and Vickery, R.M. (2017). Spike Timing Matters in Novel Neuronal Code Involved in Vibrotactile Frequency Perception. *Curr Biol* 27, 1485–1490.e2. <https://doi.org/10.1016/j.cub.2017.04.011>.

Birznieks, I., Macefield, V.G., Westling, G., and Johansson, R.S. (2009). Slowly adapting mechanoreceptors in the borders of the human fingernail encode fingertip forces. *J Neurosci* 29, 9370–9379. <https://doi.org/10.1523/JNEUROSCI.0143-09.2009>.

Blackwell, A.A., Banovetz, M.T., Qandeel, Whishaw, I.Q., and Wallace, D.G. (2018a). The structure of arm and hand movements in a spontaneous and food rewarded on-line string-pulling task by the mouse. *Behavioural Brain Research* 345, 49–58. <https://doi.org/10.1016/j.bbr.2018.02.025>.

Blackwell, A.A., Köppen, J.R., Whishaw, I.Q., and Wallace, D.G. (2018b). String-pulling for food by the rat: Assessment of movement, topography and kinematics of a bilaterally skilled forelimb act. *Learning and Motivation* 61, 63–73. <https://doi.org/10.1016/j.lmot.2017.03.010>.

Blackwell, A.A., Widick, W.L., Cheatwood, J.L., Whishaw, I.Q., and Wallace, D.G. (2018c). Unilateral forelimb sensorimotor cortex devascularization disrupts the topographic and kinematic characteristics of hand movements while string-pulling for food in the rat. *Behavioural Brain Research* 338, 88–100. <https://doi.org/10.1016/j.bbr.2017.10.014>.

Blaschke, S.J., Hensel, L., Minassian, A., Vlachakis, S., Tscherpel, C., Vay, S.U., Rabenstein, M., Schroeter, M., Fink, G.R., Hoehn, M., et al. (2021). Translating Functional Connectivity After Stroke: Functional Magnetic Resonance Imaging Detects Comparable Network Changes in Mice and Humans. *Stroke* 52, 2948–2960. <https://doi.org/10.1161/STROKEAHA.120.032511>.

Blicher, J.U., Near, J., Næss-Schmidt, E., Stagg, C.J., Johansen-Berg, H., Nielsen, J.F., Østergaard, L., and Ho, Y.-C.L. (2015). GABA levels are decreased after stroke and GABA changes during rehabilitation correlate with motor improvement. *Neurorehabil Neural Repair* 29, 278–286. <https://doi.org/10.1177/1545968314543652>.

Bock, D.D., Lee, W.-C.A., Kerlin, A.M., Andermann, M.L., Hood, G., Wetzel, A.W., Yurgenson, S., Soucy, E.R., Kim, H.S., and Reid, R.C. (2011). Network anatomy and in vivo physiology of visual cortical neurons. *Nature* 471, 177–182. <https://doi.org/10.1038/nature09802>.

Bolanowski, S.J., Gescheider, G.A., Verrillo, R.T., and Checkosky, C.M. (1988). Four channels

mediate the mechanical aspects of touch. *J. Acoust. Soc. Am.* *84*, 1680–1694. .

Bolton, P.S., and Tracey, D.J. (1992). The medullary relay from neck receptors to somatosensory thalamus in the rat: a neuroanatomical study. *Exp Brain Res* *88*, 473–484.
<https://doi.org/10.1007/BF00228177>.

Bourane, S., Grossmann, K.S., Britz, O., Dalet, A., Del Barrio, M.G., Stam, F.J., Garcia-Campmany, L., Koch, S., and Goulding, M. (2015). Identification of a spinal circuit for light touch and fine motor control. *Cell* *160*, 503–515. <https://doi.org/10.1016/j.cell.2015.01.011>.

Brecht, M., Schneider, M., Sakmann, B., and Margrie, T.W. (2004). Whisker movements evoked by stimulation of single pyramidal cells in rat motor cortex. *Nature* *427*, 704–710.
<https://doi.org/10.1038/nature02266>.

Brett-Green, B., Fifková, E., Larue, D.T., Winer, J.A., and Barth, D.S. (2003). A multisensory zone in rat parietotemporal cortex: intra- and extracellular physiology and thalamocortical connections. *J Comp Neurol* *460*, 223–237. <https://doi.org/10.1002/cne.10637>.

Brett-Green, B., Paulsen, M., Staba, R.J., Fifková, E., and Barth, D.S. (2004). Two distinct regions of secondary somatosensory cortex in the rat: topographical organization and multisensory responses. *J. Neurophysiol.* *91*, 1327–1336. <https://doi.org/10.1152/jn.00905.2003>.

Briggs, F., and Usrey, W.M. (2008). Emerging views of corticothalamic function. *Curr Opin Neurobiol* *18*, 403–407. <https://doi.org/10.1016/j.conb.2008.09.002>.

Brisben, A.J., Hsiao, S.S., and Johnson, K.O. (1999). Detection of vibration transmitted through an object grasped in the hand. *J Neurophysiol* *81*, 1548–1558.
<https://doi.org/10.1152/jn.1999.81.4.1548>.

Brooks, J.X., and Cullen, K. (2019). Predictive Sensing: The Role of Motor Signals in Sensory Processing. *Biol Psychiatry Cogn Neurosci Neuroimaging* *4*, 842–850.
<https://doi.org/10.1016/j.bpsc.2019.06.003>.

Brown, C.E., and Murphy, T.H. (2008). Livin’ on the Edge: Imaging Dendritic Spine Turnover in the Peri-Infarct Zone during Ischemic Stroke and Recovery. *The Neuroscientist* *14*, 139–146.
<https://doi.org/10.1177/1073858407309854>.

Brown, C.E., Li, P., Boyd, J.D., Delaney, K.R., and Murphy, T.H. (2007). Extensive turnover of dendritic spines and vascular remodeling in cortical tissues recovering from stroke. *J Neurosci* *27*, 4101–4109. <https://doi.org/10.1523/JNEUROSCI.4295-06.2007>.

Brown, C.E., Wong, C., and Murphy, T.H. (2008). Rapid Morphologic Plasticity of Peri-Infarct Dendritic Spines After Focal Ischemic Stroke. *Stroke* *39*, 1286–1291.
<https://doi.org/10.1161/STROKEAHA.107.498238>.

Brown, C.E., Aminoltejari, K., Erb, H., Winship, I.R., and Murphy, T.H. (2009). In Vivo Voltage-Sensitive Dye Imaging in Adult Mice Reveals That Somatosensory Maps Lost to Stroke Are Replaced over Weeks by New Structural and Functional Circuits with Prolonged Modes of

- Activation within Both the Peri-Infarct Zone and Distant Sites. *J. Neurosci.* 29, 1719–1734. <https://doi.org/10.1523/JNEUROSCI.4249-08.2009>.
- Brown, C.E., Boyd, J.D., and Murphy, T.H. (2010). Longitudinal in vivo imaging reveals balanced and branch-specific remodeling of mature cortical pyramidal dendritic arbors after stroke. *J Cereb Blood Flow Metab* 30, 783–791. <https://doi.org/10.1038/jcbfm.2009.241>.
- Brunton, E., Blau, C.W., and Nazarpour, K. (2017). Separability of neural responses to standardised mechanical stimulation of limbs. *Sci Rep* 7, 11138. <https://doi.org/10.1038/s41598-017-11349-z>.
- Bucci, D.J. (2009). Posterior parietal cortex: an interface between attention and learning? *Neurobiol Learn Mem* 91, 114–120. <https://doi.org/10.1016/j.nlm.2008.07.004>.
- Buchkremer-Ratzmann, I., and Witte, O.W. (1997). Extended brain disinhibition following small photothrombotic lesions in rat frontal cortex. *NeuroReport* 8, 519–522. .
- Buetefisch, C.M. (2015). Role of the Contralesional Hemisphere in Post-Stroke Recovery of Upper Extremity Motor Function. *Front Neurol* 6, 214. <https://doi.org/10.3389/fneur.2015.00214>.
- Bui, T.V., Akay, T., Loubani, O., Hnasko, T.S., Jessell, T.M., and Brownstone, R.M. (2013). Circuits for grasping: spinal dI3 interneurons mediate cutaneous control of motor behavior. *Neuron* 78, 191–204. <https://doi.org/10.1016/j.neuron.2013.02.007>.
- Bui, T.V., Stifani, N., Panek, I., and Farah, C. (2015). Genetically identified spinal interneurons integrating tactile afferents for motor control. *J. Neurophysiol.* 114, 3050–3063. <https://doi.org/10.1152/jn.00522.2015>.
- Bullmore, E., and Sporns, O. (2009). Complex brain networks: graph theoretical analysis of structural and functional systems. *Nat Rev Neurosci* 10, 186–198. <https://doi.org/10.1038/nrn2575>.
- Burke, D., Gandevia, S.C., and Macefield, G. (1988). Responses to passive movement of receptors in joint, skin and muscle of the human hand. *J Physiol* 402, 347–361. <https://doi.org/10.1113/jphysiol.1988.sp017208>.
- Burton, H., and Carlson, M. (1986). Second somatic sensory cortical area (SII) in a prosimian primate, *Galago crassicaudatus*. *J Comp Neurol* 247, 200–220. <https://doi.org/10.1002/cne.902470206>.
- Burton, H., and Fabri, M. (1995). Ipsilateral intracortical connections of physiologically defined cutaneous representations in areas 3b and 1 of macaque monkeys: projections in the vicinity of the central sulcus. *J Comp Neurol* 355, 508–538. <https://doi.org/10.1002/cne.903550404>.
- Burton, H., and Sinclair, R.J. (2000). Tactile-spatial and cross-modal attention effects in the primary somatosensory cortical areas 3b and 1-2 of rhesus monkeys. *Somatosens Mot Res* 17, 213–228. <https://doi.org/10.1080/08990220050117574>.

Burton, H., Fabri, M., and Alloway, K. (1995). Cortical areas within the lateral sulcus connected to cutaneous representations in areas 3b and 1: a revised interpretation of the second somatosensory area in macaque monkeys. *J Comp Neurol* 355, 539–562. <https://doi.org/10.1002/cne.903550405>.

Burton, H., Sinclair, R.J., Hong, S.Y., Pruett, J.R., and Whang, K.C. (1997). Tactile-spatial and cross-modal attention effects in the second somatosensory and 7b cortical areas of rhesus monkeys. *Somatosens Mot Res* 14, 237–267. <https://doi.org/10.1080/08990229770971>.

Bury, S.D., and Jones, T.A. (2002). Unilateral sensorimotor cortex lesions in adult rats facilitate motor skill learning with the “unaffected” forelimb and training-induced dendritic structural plasticity in the motor cortex. *J Neurosci* 22, 8597–8606. .

Bushnell, M.C., and Duncan, G.H. (1987). Mechanical response properties of ventroposterior medial thalamic neurons in the alert monkey. *Exp Brain Res* 67, 603–614. <https://doi.org/10.1007/BF00247291>.

Bütefisch, C.M. (2006). Neurobiological bases of rehabilitation. *Neurol Sci* 27, s18–s23. <https://doi.org/10.1007/s10072-006-0540-z>.

Buzsáki, G. (2010). Neural syntax: cell assemblies, synapse ensembles, and readers. *Neuron* 68, 362–385. <https://doi.org/10.1016/j.neuron.2010.09.023>.

Calautti, C., and Baron, J.-C. (2003). Functional Neuroimaging Studies of Motor Recovery After Stroke in Adults. *Stroke* 34, 1553–1566. <https://doi.org/10.1161/01.STR.0000071761.36075.A6>.

Camarillo, L., Luna, R., Nácher, V., and Romo, R. (2012). Coding perceptual discrimination in the somatosensory thalamus. *Proc Natl Acad Sci U S A* 109, 21093–21098. <https://doi.org/10.1073/pnas.1219636110>.

Carey, L.M., and Matyas, T.A. (2011). Frequency of discriminative sensory loss in the hand after stroke in a rehabilitation setting. *J Rehabil Med* 43, 257–263. <https://doi.org/10.2340/16501977-0662>.

Carey, L.M., Matyas, T.A., and Oke, L.E. (1993). Sensory loss in stroke patients: effective training of tactile and proprioceptive discrimination. *Arch Phys Med Rehabil* 74, 602–611. [https://doi.org/10.1016/0003-9993\(93\)90158-7](https://doi.org/10.1016/0003-9993(93)90158-7).

Carlson, M. (1981). Characteristics of sensory deficits following lesions of Brodmann’s areas 1 and 2 in the postcentral gyrus of *Macaca mulatta*. *Brain Res* 204, 424–430. [https://doi.org/10.1016/0006-8993\(81\)90602-8](https://doi.org/10.1016/0006-8993(81)90602-8).

Carmichael, S.T. (2003a). Gene expression changes after focal stroke, traumatic brain and spinal cord injuries. *Curr Opin Neurol* 16, 699–704. <https://doi.org/10.1097/01.wco.0000102621.38669.77>.

Carmichael, S.T. (2003b). Plasticity of Cortical Projections after Stroke. *The Neuroscientist* 9, 64–75. <https://doi.org/10.1177/1073858402239592>.

- Carmichael, S.T. (2005). Rodent Models of Focal Stroke: Size, Mechanism, and Purpose. *NeuroRx* 2, 396–409. .
- Carmichael, S.T. (2006). Cellular and molecular mechanisms of neural repair after stroke: Making waves. *Annals of Neurology* 59, 735–742. <https://doi.org/10.1002/ana.20845>.
- Carmichael, S.T., Wei, L., Rovainen, C.M., and Woolsey, T.A. (2001). New patterns of intracortical projections after focal cortical stroke. *Neurobiol Dis* 8, 910–922. <https://doi.org/10.1006/nbdi.2001.0425>.
- Carmichael, S.T., Tatsukawa, K., Katsman, D., Tsuyuguchi, N., and Kornblum, H.I. (2004). Evolution of Diaschisis in a Focal Stroke Model. *Stroke* 35, 758–763. <https://doi.org/10.1161/01.STR.0000117235.11156.55>.
- Carmichael, S.T., Archibeque, I., Luke, L., Nolan, T., Momiy, J., and Li, S. (2005). Growth-associated gene expression after stroke: evidence for a growth-promoting region in peri-infarct cortex. *Exp Neurol* 193, 291–311. <https://doi.org/10.1016/j.expneurol.2005.01.004>.
- Carrera, E., and Tsononi, G. (2014). Diaschisis: past, present, future. *Brain* 137, 2408–2422. <https://doi.org/10.1093/brain/awu101>.
- Carter, A.R., Astafiev, S.V., Lang, C.E., Connor, L.T., Rengachary, J., Strube, M.J., Pope, D.L.W., Shulman, G.L., and Corbetta, M. (2010). Resting interhemispheric functional magnetic resonance imaging connectivity predicts performance after stroke. *Ann Neurol* 67, 365–375. <https://doi.org/10.1002/ana.21905>.
- Carter, A.R., Shulman, G.L., and Corbetta, M. (2012). Why use a connectivity-based approach to study stroke and recovery of function? *NeuroImage* 62, 2271–2280. <https://doi.org/10.1016/j.neuroimage.2012.02.070>.
- Casals, J.B., Pieri, N.C., Feitosa, M.L., Ercolin, A.C., Roballo, K.C., Barreto, R.S., Bressan, F.F., Martins, D.S., Miglino, M.A., and Ambrósio, C.E. (2011). The Use of Animal Models for Stroke Research: A Review. *Comp Med* 61, 305–313. .
- Castro-Alamancos, M.A., and Borrell, J. (1995). Functional recovery of forelimb response capacity after forelimb primary motor cortex damage in the rat is due to the reorganization of adjacent areas of cortex. *Neuroscience* 68, 793–805. [https://doi.org/10.1016/0306-4522\(95\)00178-L](https://doi.org/10.1016/0306-4522(95)00178-L).
- Cauna, N. (1956). Nerve supply and nerve endings in Meissner's corpuscles. *Am J Anat* 99, 315–350. <https://doi.org/10.1002/aja.1000990206>.
- Cauna, N., and Ross, L.L. (1960). The fine structure of Meissner's touch corpuscles of human fingers. *J Biophys Biochem Cytol* 8, 467–482. <https://doi.org/10.1083/jcb.8.2.467>.
- Centonze, D., Rossi, S., Tortiglione, A., Picconi, B., Prosperetti, C., De Chiara, V., Bernardi, G., and Calabresi, P. (2007). Synaptic plasticity during recovery from permanent occlusion of the middle cerebral artery. *Neurobiol Dis* 27, 44–53. <https://doi.org/10.1016/j.nbd.2007.03.012>.

Chabriat, H., Bassetti, C.L., Marx, U., Audoli-Inthavong, M.-L., Sors, A., Lambert, E., Watzel, M., Hermann, D.M., and RESTORE BRAIN study investigators (2020). Safety and efficacy of GABAA $\alpha 5$ antagonist S44819 in patients with ischaemic stroke: a multicentre, double-blind, randomised, placebo-controlled trial. *Lancet Neurol* 19, 226–233. [https://doi.org/10.1016/S1474-4422\(20\)30004-1](https://doi.org/10.1016/S1474-4422(20)30004-1).

Chamberland, S., Salesse, C., Topolnik, D., and Topolnik, L. (2010). Synapse-specific inhibitory control of hippocampal feedback inhibitory circuit. *Front Cell Neurosci* 4, 130. <https://doi.org/10.3389/fncel.2010.00130>.

Chapin, J.K., and Lin, C.S. (1984). Mapping the body representation in the SI cortex of anesthetized and awake rats. *J. Comp. Neurol.* 229, 199–213. <https://doi.org/10.1002/cne.902290206>.

Chapin, J.K., Sadeq, M., and Guise, J.L.U. (1987). Corticocortical connections within the primary somatosensory cortex of the rat. *Journal of Comparative Neurology* 263, 326–346. <https://doi.org/10.1002/cne.902630303>.

Chapman, C.E., and Meftah, E.-M. (2005). Independent controls of attentional influences in primary and secondary somatosensory cortex. *J Neurophysiol* 94, 4094–4107. <https://doi.org/10.1152/jn.00303.2005>.

Chapman, C.E., Bushnell, M.C., Miron, D., Duncan, G.H., and Lund, J.P. (1987). Sensory perception during movement in man. *Exp Brain Res* 68, 516–524. <https://doi.org/10.1007/BF00249795>.

Che Has, A.T., Absalom, N., van Nieuwenhuijzen, P.S., Clarkson, A.N., Ahring, P.K., and Chebib, M. (2016). Zolpidem is a potent stoichiometry-selective modulator of $\alpha 1\beta 3$ GABAA receptors: evidence of a novel benzodiazepine site in the $\alpha 1$ - $\alpha 1$ interface. *Sci Rep* 6, 28674. <https://doi.org/10.1038/srep28674>.

Cheatwood, J.L., Emerick, A.J., and Kartje, G.L. (2008). Neuronal plasticity and functional recovery after ischemic stroke. *Top Stroke Rehabil* 15, 42–50. <https://doi.org/10.1310/tsr1501-42>.

Cheema, S., Whitsel, B.L., and Rustioni, A. (1983). The corticocuneate pathway in the cat: relations among terminal distribution patterns, cytoarchitecture, and single neuron functional properties. *Somatosens Res* 1, 169–205. <https://doi.org/10.3109/07367228309144547>.

Chen, L.M., Friedman, R.M., and Roe, A.W. (2005). Optical imaging of SI topography in anesthetized and awake squirrel monkeys. *J. Neurosci.* 25, 7648–7659. <https://doi.org/10.1523/JNEUROSCI.1990-05.2005>.

Chen, S., Raos, V., and Bentivoglio, M. (1992). Connections of the thalamic reticular nucleus with the contralateral thalamus in the rat. *Neurosci Lett* 147, 85–88. [https://doi.org/10.1016/0304-3940\(92\)90780-b](https://doi.org/10.1016/0304-3940(92)90780-b).

Chen, S., Mohajerani, M.H., Xie, Y., and Murphy, T.H. (2012). Optogenetic analysis of neuronal

excitability during global ischemia reveals selective deficits in sensory processing following reperfusion in mouse cortex. *J Neurosci* 32, 13510–13519. <https://doi.org/10.1523/JNEUROSCI.1439-12.2012>.

Chen, T.-W., Wardill, T.J., Sun, Y., Pulver, S.R., Renninger, S.L., Baohan, A., Schreiter, E.R., Kerr, R.A., Orger, M.B., Jayaraman, V., et al. (2013). Ultra-sensitive fluorescent proteins for imaging neuronal activity. *Nature* 499, 295–300. <https://doi.org/10.1038/nature12354>.

Cheney, P.D., and Preston, J.B. (1976). Classification and response characteristics of muscle spindle afferents in the primate. *J Neurophysiol* 39, 1–8. <https://doi.org/10.1152/jn.1976.39.1.1>.

Cirillo, J., Mooney, R.A., Ackerley, S.J., Barber, P.A., Borges, V.M., Clarkson, A.N., Mangold, C., Ren, A., Smith, M.-C., Stinear, C.M., et al. (2020). Neurochemical balance and inhibition at the subacute stage after stroke. *J Neurophysiol* 123, 1775–1790. <https://doi.org/10.1152/jn.00561.2019>.

Clarkson, A.N. (2012). Perisynaptic GABA Receptors The Overzealous Protector. *Adv Pharmacol Sci* 2012, 708428. <https://doi.org/10.1155/2012/708428>.

Clarkson, A.N., Huang, B.S., Macisaac, S.E., Mody, I., and Carmichael, S.T. (2010). Reducing excessive GABA-mediated tonic inhibition promotes functional recovery after stroke. *Nature* 468, 305–309. <https://doi.org/10.1038/nature09511>.

Clarkson, A.N., Overman, J.J., Zhong, S., Mueller, R., Lynch, G., and Carmichael, S.T. (2011). AMPA receptor-induced local brain-derived neurotrophic factor signaling mediates motor recovery after stroke. *J Neurosci* 31, 3766–3775. <https://doi.org/10.1523/JNEUROSCI.5780-10.2011>.

Claxton, G. (1975). Why can't we tickle ourselves? *Percept Mot Skills* 41, 335–338. <https://doi.org/10.2466/pms.1975.41.1.335>.

Cohen, M.R., and Kohn, A. (2011). Measuring and interpreting neuronal correlations. *Nat Neurosci* 14, 811–819. <https://doi.org/10.1038/nn.2842>.

Condylis, C., Lowet, E., Ni, J., Bistrong, K., Ouellette, T., Josephs, N., and Chen, J.L. (2020). Context-Dependent Sensory Processing across Primary and Secondary Somatosensory Cortex. *Neuron* 106, 515-525.e5. <https://doi.org/10.1016/j.neuron.2020.02.004>.

Connell, L.A., Lincoln, N.B., and Radford, K.A. (2008). Somatosensory impairment after stroke: frequency of different deficits and their recovery. *Clin Rehabil* 22, 758–767. <https://doi.org/10.1177/0269215508090674>.

Cossart, R., Aronov, D., and Yuste, R. (2003). Attractor dynamics of network UP states in the neocortex. *Nature* 423, 283–288. <https://doi.org/10.1038/nature01614>.

Costanzo, R.M., and Gardner, E.P. (1981). Multiple-joint neurons in somatosensory cortex of awake monkeys. *Brain Res* 214, 321–333. [https://doi.org/10.1016/0006-8993\(81\)91197-5](https://doi.org/10.1016/0006-8993(81)91197-5).

- Cramer, S.C. (2008). Repairing the human brain after stroke: I. Mechanisms of spontaneous recovery. *Ann Neurol* 63, 272–287. <https://doi.org/10.1002/ana.21393>.
- Cramer, J.V., Gesierich, B., Roth, S., Dichgans, M., Düring, M., and Liesz, A. (2019). In vivo widefield calcium imaging of the mouse cortex for analysis of network connectivity in health and brain disease. *NeuroImage* 199, 570–584. <https://doi.org/10.1016/j.neuroimage.2019.06.014>.
- Crapse, T.B., and Sommer, M.A. (2008). Corollary discharge across the animal kingdom. *Nat Rev Neurosci* 9, 587–600. <https://doi.org/10.1038/nrn2457>.
- Dana, H., Sun, Y., Mohar, B., Hulse, B.K., Kerlin, A.M., Hasseman, J.P., Tsegaye, G., Tsang, A., Wong, A., Patel, R., et al. (2019). High-performance calcium sensors for imaging activity in neuronal populations and microcompartments. *Nature Methods* 16, 649–657. <https://doi.org/10.1038/s41592-019-0435-6>.
- Dancause, N. (2005). Extensive Cortical Rewiring after Brain Injury. *Journal of Neuroscience* 25, 10167–10179. <https://doi.org/10.1523/JNEUROSCI.3256-05.2005>.
- Darian-Smith, C., Darian-Smith, I., Burman, K., and Ratcliffe, N. (1993). Ipsilateral cortical projections to areas 3a, 3b, and 4 in the macaque monkey. *J Comp Neurol* 335, 200–213. <https://doi.org/10.1002/cne.903350205>.
- Dawson, D.R., and Killackey, H.P. (1987). The organization and mutability of the forepaw and hindpaw representations in the somatosensory cortex of the neonatal rat. *Journal of Comparative Neurology* 256, 246–256. <https://doi.org/10.1002/cne.902560205>.
- Deleuze, C., and Huguenard, J.R. (2006). Distinct electrical and chemical connectivity maps in the thalamic reticular nucleus: potential roles in synchronization and sensation. *J Neurosci* 26, 8633–8645. <https://doi.org/10.1523/JNEUROSCI.2333-06.2006>.
- Delhaye, B.P., Long, K.H., and Bensmaia, S.J. (2018). Neural Basis of Touch and Proprioception in Primate Cortex. *Compr Physiol* 8, 1575–1602. <https://doi.org/10.1002/cphy.c170033>.
- Deolindo, C.S., Kunicki, A.C.B., da Silva, M.I., Lima Brasil, F., and Moiola, R.C. (2017). Neuronal Assemblies Evidence Distributed Interactions within a Tactile Discrimination Task in Rats. *Front Neural Circuits* 11, 114. <https://doi.org/10.3389/fncir.2017.00114>.
- Devonshire, I.M., Grandy, T.H., Dommett, E.J., and Greenfield, S.A. (2010). Effects of urethane anaesthesia on sensory processing in the rat barrel cortex revealed by combined optical imaging and electrophysiology. *Eur J Neurosci* 32, 786–797. <https://doi.org/10.1111/j.1460-9568.2010.07322.x>.
- Dhawan, J., Benveniste, H., Nawrocky, M., Smith, S.D., and Biegon, A. (2010). Transient focal ischemia results in persistent and widespread neuroinflammation and loss of glutamate NMDA receptors. *Neuroimage* 51, 599–605. <https://doi.org/10.1016/j.neuroimage.2010.02.073>.
- Dhawan, J., Benveniste, H., Luo, Z., Nawrocky, M., Smith, S.D., and Biegon, A. (2011). A new

look at glutamate and ischemia: NMDA agonist improves long-term functional outcome in a rat model of stroke. *Future Neurol* 6, 823–834. <https://doi.org/10.2217/fnl.11.55>.

DiCarlo, J.J., and Johnson, K.O. (2000). Spatial and temporal structure of receptive fields in primate somatosensory area 3b: effects of stimulus scanning direction and orientation. *J Neurosci* 20, 495–510. .

DiCarlo, J.J., Johnson, K.O., and Hsiao, S.S. (1998). Structure of receptive fields in area 3b of primary somatosensory cortex in the alert monkey. *J Neurosci* 18, 2626–2645. .

Dijkhuizen, R.M., Ren, J., Mandeville, J.B., Wu, O., Ozdag, F.M., Moskowitz, M.A., Rosen, B.R., and Finklestein, S.P. (2001). Functional magnetic resonance imaging of reorganization in rat brain after stroke. *PNAS* 98, 12766–12771. <https://doi.org/10.1073/pnas.231235598>.

Dijkhuizen, R.M., Singhal, A.B., Mandeville, J.B., Wu, O., Halpern, E.F., Finklestein, S.P., Rosen, B.R., and Lo, E.H. (2003). Correlation between Brain Reorganization, Ischemic Damage, and Neurologic Status after Transient Focal Cerebral Ischemia in Rats: A Functional Magnetic Resonance Imaging Study. *J. Neurosci.* 23, 510–517. <https://doi.org/10.1523/JNEUROSCI.23-02-00510.2003>.

Dimitriou, M., and Edin, B.B. (2008a). Discharges in human muscle receptor afferents during block grasping. *J Neurosci* 28, 12632–12642. <https://doi.org/10.1523/JNEUROSCI.3357-08.2008>.

Dimitriou, M., and Edin, B.B. (2008b). Discharges in human muscle spindle afferents during a key-pressing task. *J Physiol* 586, 5455–5470. <https://doi.org/10.1113/jphysiol.2008.160036>.

Ding, Q., Liu, S., Yao, Y., Liu, H., Cai, T., and Han, L. (2021). Global, Regional, and National Burden of Ischemic Stroke, 1990-2019. *Neurology* 10.1212/WNL.0000000000013115. <https://doi.org/10.1212/WNL.0000000000013115>.

Dionne, J.K., Legon, W., and Staines, W.R. (2013). Crossmodal influences on early somatosensory processing: interaction of vision, touch, and task-relevance. *Exp Brain Res* 226, 503–512. <https://doi.org/10.1007/s00221-013-3462-z>.

Disbrow, E., Roberts, T., and Krubitzer, L. (2000). Somatotopic organization of cortical fields in the lateral sulcus of *Homo sapiens*: evidence for SII and PV. *J Comp Neurol* 418, 1–21. [https://doi.org/10.1002/\(sici\)1096-9861\(20000228\)418:1<1::aid-cne1>3.0.co;2-p](https://doi.org/10.1002/(sici)1096-9861(20000228)418:1<1::aid-cne1>3.0.co;2-p).

Doetsch, G.S. (2000). Patterns in the brain: Neuronal population coding in the somatosensory system. *Physiology & Behavior* 69, 187–201. .

Domann, R., Hagemann, G., Kraemer, M., Freund, H.-J., and Witte, O.W. (1993). Electrophysiological changes in the surrounding brain tissue of photochemically induced cortical infarcts in the rat. *Neuroscience Letters* 155, 69–72. [https://doi.org/10.1016/0304-3940\(93\)90675-B](https://doi.org/10.1016/0304-3940(93)90675-B).

Doyle, K.P., Simon, R.P., and Stenzel-Poore, M.P. (2008). Mechanisms of ischemic brain

damage. *Neuropharmacology* 55, 310–318. <https://doi.org/10.1016/j.neuropharm.2008.01.005>.

Dykes, R.W., Rasmusson, D.D., Sretavan, D., and Rehman, N.B. (1982). Submodality segregation and receptive-field sequences in cuneate, gracile, and external cuneate nuclei of the cat. *J Neurophysiol* 47, 389–416. <https://doi.org/10.1152/jn.1982.47.3.389>.

Ebner, F.F., and Kaas, J.H. (2015). Chapter 24 - Somatosensory System. In *The Rat Nervous System (Fourth Edition)*, G. Paxinos, ed. (San Diego: Academic Press), pp. 675–701.

Edin, B.B., and Vallbo, A.B. (1990a). Dynamic response of human muscle spindle afferents to stretch. *J Neurophysiol* 63, 1297–1306. <https://doi.org/10.1152/jn.1990.63.6.1297>.

Edin, B.B., and Vallbo, A.B. (1990b). Muscle afferent responses to isometric contractions and relaxations in humans. *J Neurophysiol* 63, 1307–1313. <https://doi.org/10.1152/jn.1990.63.6.1307>.

Enright, L.E., Zhang, S., and Murphy, T.H. (2007). Fine mapping of the spatial relationship between acute ischemia and dendritic structure indicates selective vulnerability of layer V neuron dendritic tufts within single neurons in vivo. *J Cereb Blood Flow Metab* 27, 1185–1200. <https://doi.org/10.1038/sj.jcbfm.9600428>.

Ergul, A., Alhusban, A., and Fagan, S.C. (2012). Angiogenesis: a harmonized target for recovery after stroke. *Stroke* 43, 2270–2274. <https://doi.org/10.1161/STROKEAHA.111.642710>.

Estebanez, L., Férézou, I., Ego-Stengel, V., and Shulz, D.E. (2018). Representation of tactile scenes in the rodent barrel cortex. *Neuroscience* 368, 81–94. <https://doi.org/10.1016/j.neuroscience.2017.08.039>.

Fabri, M., and Burton, H. (1991). Topography of connections between primary somatosensory cortex and posterior complex in rat: a multiple fluorescent tracer study. *Brain Res* 538, 351–357. [https://doi.org/10.1016/0006-8993\(91\)90455-5](https://doi.org/10.1016/0006-8993(91)90455-5).

Faggin, B.M., Nguyen, K.T., and Nicolelis, M.A. (1997). Immediate and simultaneous sensory reorganization at cortical and subcortical levels of the somatosensory system. *Proc Natl Acad Sci U S A* 94, 9428–9433. <https://doi.org/10.1073/pnas.94.17.9428>.

Fang, M.C., Cutler, D.M., and Rosen, A.B. (2010). Trends in thrombolytic use for ischemic stroke in the United States. *J Hosp Med* 5, 406–409. <https://doi.org/10.1002/jhm.689>.

Farrant, M., and Nusser, Z. (2005). Variations on an inhibitory theme: phasic and tonic activation of GABA(A) receptors. *Nat Rev Neurosci* 6, 215–229. <https://doi.org/10.1038/nrn1625>.

Fassihi, A., Akrami, A., Pulecchi, F., Schönfelder, V., and Diamond, M.E. (2017). Transformation of Perception from Sensory to Motor Cortex. *Curr. Biol.* 27, 1585–1596.e6. <https://doi.org/10.1016/j.cub.2017.05.011>.

Feigin, V.L., Lawes, C.M., Bennett, D.A., Barker-Collo, S.L., and Parag, V. (2009). Worldwide stroke incidence and early case fatality reported in 56 population-based studies: a systematic

review. *The Lancet Neurology* 8, 355–369. [https://doi.org/10.1016/S1474-4422\(09\)70025-0](https://doi.org/10.1016/S1474-4422(09)70025-0).

Feigin, V.L., Forouzanfar, M.H., Krishnamurthi, R., Mensah, G.A., Connor, M., Bennett, D.A., Moran, A.E., Sacco, R.L., Anderson, L., Truelsen, T., et al. (2014). Global and regional burden of stroke during 1990–2010: findings from the Global Burden of Disease Study 2010. *Lancet* 383, 245–254. .

Felleman, D.J., and Van Essen, D.C. (1991). Distributed hierarchical processing in the primate cerebral cortex. *Cereb Cortex* 1, 1–47. <https://doi.org/10.1093/cercor/1.1.1-a>.

Feng, Y.-W., Huang, Y.-Q., Yan, Y., Li, G., He, X.-F., Liang, F.-Y., Pei, Z., Lan, Y., and Xu, G.-Q. (2020). Phasic GABA signaling mediates the protective effects of cTBS against cerebral ischemia in mice. *Neurosci Lett* 715, 134611. <https://doi.org/10.1016/j.neulet.2019.134611>.

Fitzgerald, P.J., Lane, J.W., Thakur, P.H., and Hsiao, S.S. (2004). Receptive field properties of the macaque second somatosensory cortex: evidence for multiple functional representations. *J Neurosci* 24, 11193–11204. <https://doi.org/10.1523/JNEUROSCI.3481-04.2004>.

Fitzgerald, P.J., Lane, J.W., Thakur, P.H., and Hsiao, S.S. (2006). Receptive field (RF) properties of the macaque second somatosensory cortex: RF size, shape, and somatotopic organization. *J Neurosci* 26, 6485–6495. <https://doi.org/10.1523/JNEUROSCI.5061-05.2006>.

Foffani, G., Tutunculer, B., and Moxon, K.A. (2004). Role of spike timing in the forelimb somatosensory cortex of the rat. *J. Neurosci.* 24, 7266–7271. <https://doi.org/10.1523/JNEUROSCI.2523-04.2004>.

Foffani, G., Chapin, J.K., and Moxon, K.A. (2008). Computational Role of Large Receptive Fields in the Primary Somatosensory Cortex. *Journal of Neurophysiology* 100, 268–280. <https://doi.org/10.1152/jn.01015.2007>.

Fortier-Poisson, P., and Smith, A.M. (2016). Neuronal activity in somatosensory cortex related to tactile exploration. *J Neurophysiol* 115, 112–126. <https://doi.org/10.1152/jn.00747.2014>.

Fortier-Poisson, P., Langlais, J.-S., and Smith, A.M. (2016). Correlation of fingertip shear force direction with somatosensory cortical activity in monkey. *J Neurophysiol* 115, 100–111. <https://doi.org/10.1152/jn.00749.2014>.

Frahm, C., Haupt, C., Weinandy, F., Siegel, G., Bruehl, C., and Witte, O.W. (2004). Regulation of GABA transporter mRNA and protein after photothrombotic infarct in rat brain. *J Comp Neurol* 478, 176–188. <https://doi.org/10.1002/cne.20282>.

Francis, J.T., Xu, S., and Chapin, J.K. (2008). Proprioceptive and Cutaneous Representations in the Rat Ventral Posterolateral Thalamus. *Journal of Neurophysiology* 99, 2291–2304. <https://doi.org/10.1152/jn.01206.2007>.

Freeman, A.W., and Johnson, K.O. (1982a). A model accounting for effects of vibratory amplitude on responses of cutaneous mechanoreceptors in macaque monkey. *J Physiol* 323, 43–64. <https://doi.org/10.1113/jphysiol.1982.sp014060>.

- Freeman, A.W., and Johnson, K.O. (1982b). Cutaneous mechanoreceptors in macaque monkey: temporal discharge patterns evoked by vibration, and a receptor model. *J Physiol* 323, 21–41. <https://doi.org/10.1113/jphysiol.1982.sp014059>.
- Fridman, E.A., Hanakawa, T., Chung, M., Hummel, F., Leiguarda, R.C., and Cohen, L.G. (2004). Reorganization of the human ipsilesional premotor cortex after stroke. *Brain* 127, 747–758. <https://doi.org/10.1093/brain/awh082>.
- Friedberg, M.H., Lee, S.M., and Ebner, F.F. (1999). Modulation of Receptive Field Properties of Thalamic Somatosensory Neurons by the Depth of Anesthesia. *Journal of Neurophysiology* 81, 2243–2252. <https://doi.org/10.1152/jn.1999.81.5.2243>.
- Friedman, L.K., Belayev, L., Alfonso, O.F., and Ginsberg, M.D. (2000). Distribution of glutamate and preproenkephalin messenger RNAs following transient focal cerebral ischemia. *Neuroscience* 95, 841–857. [https://doi.org/10.1016/s0306-4522\(99\)00452-2](https://doi.org/10.1016/s0306-4522(99)00452-2).
- Friedrich, J., Zhou, P., and Paninski, L. (2017). Fast online deconvolution of calcium imaging data. *PLoS Comput. Biol.* 13, e1005423. <https://doi.org/10.1371/journal.pcbi.1005423>.
- Fritschy, J.M., and Mohler, H. (1995). GABAA-receptor heterogeneity in the adult rat brain: differential regional and cellular distribution of seven major subunits. *J Comp Neurol* 359, 154–194. <https://doi.org/10.1002/cne.903590111>.
- Frost, S.B., Barbay, S., Friel, K.M., Plautz, E.J., and Nudo, R.J. (2003). Reorganization of remote cortical regions after ischemic brain injury: a potential substrate for stroke recovery. *J Neurophysiol* 89, 3205–3214. <https://doi.org/10.1152/jn.01143.2002>.
- Fujioka, H., Kaneko, H., Suzuki, S.S., and Mabuchi, K. (2004). Hyperexcitability-associated rapid plasticity after a focal cerebral ischemia. *Stroke* 35, e346-348. <https://doi.org/10.1161/01.STR.0000130990.28734.9c>.
- Fyffe, R.E., Cheema, S.S., and Rustioni, A. (1986). Intracellular staining study of the feline cuneate nucleus. I. Terminal patterns of primary afferent fibers. *J Neurophysiol* 56, 1268–1283. <https://doi.org/10.1152/jn.1986.56.5.1268>.
- Ganesh, A., Lindsay, P., Fang, J., Kapral, M.K., Côté, R., Joiner, I., Hakim, A.M., and Hill, M.D. (2016). Integrated systems of stroke care and reduction in 30-day mortality: A retrospective analysis. *Neurology* 86, 898–904. <https://doi.org/10.1212/WNL.0000000000002443>.
- Gardner, E.P., and Costanzo, R.M. (1981). Properties of kinesthetic neurons in somatosensory cortex of awake monkeys. *Brain Res* 214, 301–319. [https://doi.org/10.1016/0006-8993\(81\)91196-3](https://doi.org/10.1016/0006-8993(81)91196-3).
- Garraghty, P.E., Pons, T.P., and Kaas, J.H. (1990). Ablations of areas 3b (SI proper) and 3a of somatosensory cortex in marmosets deactivate the second and parietal ventral somatosensory areas. *Somatosens Mot Res* 7, 125–135. <https://doi.org/10.3109/08990229009144703>.
- Gattringer, T., Posekany, A., Niederkorn, K., Knoflach, M., Poltrum, B., Mutzenbach, S.,

- Haring, H.-P., Ferrari, J., Lang, W., Willeit, J., et al. (2019). Predicting Early Mortality of Acute Ischemic Stroke. *Stroke* 50, 349–356. <https://doi.org/10.1161/STROKEAHA.118.022863>.
- Gescheider, G.A., Bolanowski, S.J., Pope, J.V., and Verrillo, R.T. (2002). A four-channel analysis of the tactile sensitivity of the fingertip: frequency selectivity, spatial summation, and temporal summation. *Somatosens Mot Res* 19, 114–124. <https://doi.org/10.1080/08990220220131505>.
- Ginsberg, M.D. (2008). Neuroprotection for ischemic stroke: past, present and future. *Neuropharmacology* 55, 363–389. <https://doi.org/10.1016/j.neuropharm.2007.12.007>.
- Glykys, J., and Mody, I. (2006). Hippocampal network hyperactivity after selective reduction of tonic inhibition in GABA A receptor alpha5 subunit-deficient mice. *J Neurophysiol* 95, 2796–2807. <https://doi.org/10.1152/jn.01122.2005>.
- Glykys, J., and Mody, I. (2007). Activation of GABAA receptors: views from outside the synaptic cleft. *Neuron* 56, 763–770. <https://doi.org/10.1016/j.neuron.2007.11.002>.
- Goldin, M.A., Harrell, E.R., Estebanez, L., and Shulz, D.E. (2018). Rich spatio-temporal stimulus dynamics unveil sensory specialization in cortical area S2. *Nat Commun* 9, 4053. <https://doi.org/10.1038/s41467-018-06585-4>.
- Gomez-Ramirez, M., Hysaj, K., and Niebur, E. (2016). Neural mechanisms of selective attention in the somatosensory system. *J. Neurophysiol.* 116, 1218–1231. <https://doi.org/10.1152/jn.00637.2015>.
- Goodwin, A.W., and Wheat, H.E. (2004). Sensory signals in neural populations underlying tactile perception and manipulation. *Annu. Rev. Neurosci.* 27, 53–77. <https://doi.org/10.1146/annurev.neuro.26.041002.131032>.
- Grandjean, J., Schroeter, A., Batata, I., and Rudin, M. (2014). Optimization of anesthesia protocol for resting-state fMRI in mice based on differential effects of anesthetics on functional connectivity patterns. *NeuroImage* 102, 838–847. <https://doi.org/10.1016/j.neuroimage.2014.08.043>.
- Green, J.B. (2003). Brain reorganization after stroke. *Top Stroke Rehabil* 10, 1–20. <https://doi.org/10.1310/H65X-23HW-QL1G-KTNQ>.
- Green, A.R., Hainsworth, A.H., and Jackson, D.M. (2000). GABA potentiation: a logical pharmacological approach for the treatment of acute ischaemic stroke. *Neuropharmacology* 39, 1483–1494. [https://doi.org/10.1016/s0028-3908\(99\)00233-6](https://doi.org/10.1016/s0028-3908(99)00233-6).
- Greenberg, D.A. (2014). Cerebral angiogenesis: a realistic therapy for ischemic disease? *Methods Mol Biol* 1135, 21–24. https://doi.org/10.1007/978-1-4939-0320-7_2.
- Grefkes, C., and Fink, G.R. (2014). Connectivity-based approaches in stroke and recovery of function. *The Lancet Neurology* 13, 206–216. [https://doi.org/10.1016/S1474-4422\(13\)70264-3](https://doi.org/10.1016/S1474-4422(13)70264-3).

- Grigg, P., and Greenspan, B.J. (1977). Response of primate joint afferent neurons to mechanical stimulation of knee joint. *J Neurophysiol* *40*, 1–8. <https://doi.org/10.1152/jn.1977.40.1.1>.
- Guggisberg, A.G., Nicolo, P., Cohen, L.G., Schnider, A., and Buch, E.R. (2017). Longitudinal structural and functional differences between proportional and poor motor recovery after stroke. *Neurorehabil Neural Repair* *31*, 1029–1041. <https://doi.org/10.1177/1545968317740634>.
- Guilbaud, G., Peschanski, M., Gautron, M., and Binder, D. (1980). Neurones responding to noxious stimulation in VB complex and caudal adjacent regions in the thalamus of the rat. *PAIN* *8*, 303–318. [https://doi.org/10.1016/0304-3959\(80\)90076-7](https://doi.org/10.1016/0304-3959(80)90076-7).
- Guo, L., Kondapavulur, S., Lemke, S.M., Won, S.J., and Ganguly, K. (2021). Coordinated increase of reliable cortical and striatal ensemble activations during recovery after stroke. *Cell Rep* *36*, 109370. <https://doi.org/10.1016/j.celrep.2021.109370>.
- Gurtubay-Antolin, A., León-Cabrera, P., and Rodríguez-Fornells, A. (2018). Neural Evidence of Hierarchical Cognitive Control during Haptic Processing: An fMRI Study. *ENeuro* *5*, ENEURO.0295-18.2018. <https://doi.org/10.1523/ENeuro.0295-18.2018>.
- Gutrecht, J.A., Zamani, A.A., and Pandya, D.N. (1992). Lacunar thalamic stroke with pure cerebellar and proprioceptive deficits. *J Neurol Neurosurg Psychiatry* *55*, 854–856. <https://doi.org/10.1136/jnnp.55.9.854>.
- Hagemann, G., Redecker, C., Neumann-Haefelin, T., Freund, H.-J., and Witte, O.W. (1998). Increased long-term potentiation in the surround of experimentally induced focal cortical infarction. *Annals of Neurology* *44*, 255–258. <https://doi.org/10.1002/ana.410440217>.
- Hakon, J., Quattromani, M.J., Sjölund, C., Tomasevic, G., Carey, L., Lee, J.-M., Ruscher, K., Wieloch, T., and Bauer, A.Q. (2017). Multisensory stimulation improves functional recovery and resting-state functional connectivity in the mouse brain after stroke. *Neuroimage Clin* *17*, 717–730. <https://doi.org/10.1016/j.nicl.2017.11.022>.
- Hall, R.D., and Lindholm, E.P. (1974). Organization of motor and somatosensory neocortex in the albino rat. *Brain Research* *66*, 23–38. [https://doi.org/10.1016/0006-8993\(74\)90076-6](https://doi.org/10.1016/0006-8993(74)90076-6).
- Handler, A., and Ginty, D.D. (2021). The mechanosensory neurons of touch and their mechanisms of activation. *Nat Rev Neurosci* *22*, 521–537. <https://doi.org/10.1038/s41583-021-00489-x>.
- Harris, K.D., and Mrsic-Flogel, T.D. (2013). Cortical connectivity and sensory coding. *Nature* *503*, 51–58. <https://doi.org/10.1038/nature12654>.
- Harris, K.D., Csicsvari, J., Hirase, H., Dragoi, G., and Buzsáki, G. (2003). Organization of cell assemblies in the hippocampus. *Nature* *424*, 552–556. <https://doi.org/10.1038/nature01834>.
- Harvey, M.A., Saal, H.P., Dammann, J.F., and Bensmaia, S.J. (2013). Multiplexing stimulus information through rate and temporal codes in primate somatosensory cortex. *PLoS Biol.* *11*, e1001558. <https://doi.org/10.1371/journal.pbio.1001558>.

- Hatakeyama, M., Ninomiya, I., and Kanazawa, M. (2020). Angiogenesis and neuronal remodeling after ischemic stroke. *Neural Regen Res* 15, 16–19. <https://doi.org/10.4103/1673-5374.264442>.
- Hayashi, A., Yoshida, T., and Ohki, K. (2018). Cell Type Specific Representation of Vibrotactile Stimuli in the Mouse Primary Somatosensory Cortex. *Front Neural Circuits* 12. <https://doi.org/10.3389/fncir.2018.00109>.
- Hayward, V. (2011). Is there a “plenhaptic” function? *Philos. Trans. R. Soc. Lond., B, Biol. Sci.* 366, 3115–3122. <https://doi.org/10.1098/rstb.2011.0150>.
- Hayward, V., Terekhov, A.V., Wong, S.-C., Geborek, P., Bengtsson, F., and Jörntell, H. (2014). Spatio-temporal skin strain distributions evoke low variability spike responses in cuneate neurons. *J R Soc Interface* 11, 20131015. <https://doi.org/10.1098/rsif.2013.1015>.
- Hendrickson, A.E., and White, P.O. (1964). Promax: A Quick Method for Rotation to Oblique Simple Structure. *British Journal of Statistical Psychology* 17, 65–70. <https://doi.org/10.1111/j.2044-8317.1964.tb00244.x>.
- Hernández, A., Zainos, A., and Romo, R. (2000). Neuronal correlates of sensory discrimination in the somatosensory cortex. *Proc Natl Acad Sci U S A* 97, 6191–6196. <https://doi.org/10.1073/pnas.120018597>.
- Hernández, A., Nácher, V., Luna, R., Zainos, A., Lemus, L., Alvarez, M., Vázquez, Y., Camarillo, L., and Romo, R. (2010). Decoding a perceptual decision process across cortex. *Neuron* 66, 300–314. <https://doi.org/10.1016/j.neuron.2010.03.031>.
- Hihara, S., Taoka, M., Tanaka, M., and Iriki, A. (2015). Visual Responsiveness of Neurons in the Secondary Somatosensory Area and its Surrounding Parietal Operculum Regions in Awake Macaque Monkeys. *Cereb Cortex* 25, 4535–4550. <https://doi.org/10.1093/cercor/bhv095>.
- Hilgetag, C.C., Kötter, R., Stephan, K.E., and Sporns, O. (2002). Computational Methods for the Analysis of Brain Connectivity. In *Computational Neuroanatomy: Principles and Methods*, G.A. Ascoli, ed. (Totowa, NJ: Humana Press), pp. 295–335.
- Hiu, T., Farzampour, Z., Paz, J.T., Wang, E.H.J., Badgely, C., Olson, A., Micheva, K.D., Wang, G., Lemmens, R., Tran, K.V., et al. (2016). Enhanced phasic GABA inhibition during the repair phase of stroke: a novel therapeutic target. *Brain* 139, 468–480. <https://doi.org/10.1093/brain/awv360>.
- Hofer, S.B., Ko, H., Pichler, B., Vogelstein, J., Ros, H., Zeng, H., Lein, E., Lesica, N.A., and Mrsic-Flogel, T.D. (2011). Differential connectivity and response dynamics of excitatory and inhibitory neurons in visual cortex. *Nat Neurosci* 14, 1045–1052. <https://doi.org/10.1038/nn.2876>.
- Holtmaat, A., Bonhoeffer, T., Chow, D.K., Chuckowree, J., De Paola, V., Hofer, S.B., Hübener, M., Keck, T., Knott, G., Lee, W.-C.A., et al. (2009). Long-term, high-resolution imaging in the mouse neocortex through a chronic cranial window. *Nat Protoc* 4, 1128–1144.

<https://doi.org/10.1038/nprot.2009.89>.

Hossmann, K.-A. (2006). Pathophysiology and therapy of experimental stroke. *Cell Mol Neurobiol* 26, 1057–1083. <https://doi.org/10.1007/s10571-006-9008-1>.

Houweling, A.R., and Brecht, M. (2008). Behavioural report of single neuron stimulation in somatosensory cortex. *Nature* 451, 65–68. <https://doi.org/10.1038/nature06447>.

Hoyte, L., Barber, P.A., Buchan, A.M., and Hill, M.D. (2004). The rise and fall of NMDA antagonists for ischemic stroke. *Curr Mol Med* 4, 131–136. <https://doi.org/10.2174/1566524043479248>.

Hsiao, S.S., O’Shaughnessy, D.M., and Johnson, K.O. (1993). Effects of selective attention on spatial form processing in monkey primary and secondary somatosensory cortex. *J Neurophysiol* 70, 444–447. <https://doi.org/10.1152/jn.1993.70.1.444>.

Huerta, M.F., and Pons, T.P. (1990). Primary motor cortex receives input from area 3a in macaques. *Brain Res* 537, 367–371. [https://doi.org/10.1016/0006-8993\(90\)90388-r](https://doi.org/10.1016/0006-8993(90)90388-r).

Huffman, K.J., and Krubitzer, L. (2001). Area 3a: topographic organization and cortical connections in marmoset monkeys. *Cereb Cortex* 11, 849–867. <https://doi.org/10.1093/cercor/11.9.849>.

Humanes-Valera, D., Foffani, G., and Aguilar, J. (2014). Increased cortical responses to forepaw stimuli immediately after peripheral deafferentation of hindpaw inputs. *Sci Rep* 4, 7278. <https://doi.org/10.1038/srep07278>.

Humm, J.L., Kozlowski, D.A., Bland, S.T., James, D.C., and Schallert, T. (1999). Use-dependent exaggeration of brain injury: is glutamate involved? *Exp Neurol* 157, 349–358. <https://doi.org/10.1006/exnr.1999.7061>.

Hummelsheim, H., Wiesendanger, R., Wiesendanger, M., and Bianchetti, M. (1985). The projection of low-threshold muscle afferents of the forelimb to the main and external cuneate nuclei of the monkey. *Neuroscience* 16, 979–987. [https://doi.org/10.1016/0306-4522\(85\)90110-1](https://doi.org/10.1016/0306-4522(85)90110-1).

Husson, T.R., Mallik, A.K., Zhang, J.X., and Issa, N.P. (2007). Functional imaging of primary visual cortex using flavoprotein autofluorescence. *J. Neurosci.* 27, 8665–8675. <https://doi.org/10.1523/JNEUROSCI.2156-07.2007>.

Hyman, J.M., Whitman, J., Emberly, E., Woodward, T.S., and Seamans, J.K. (2013). Action and outcome activity state patterns in the anterior cingulate cortex. *Cereb Cortex* 23, 1257–1268. <https://doi.org/10.1093/cercor/bhs104>.

Hyvärinen, J., and Poranen, A. (1978). Receptive field integration and submodality convergence in the hand area of the post-central gyrus of the alert monkey. *J. Physiol. (Lond.)* 283, 539–556. .

Inayat, S., Singh, S., Ghasroddashti, A., Qandeel, Egodage, P., Whishaw, I.Q., and Mohajerani,

- M.H. (2020). A Matlab-based toolbox for characterizing behavior of rodents engaged in string-pulling. *ELife* 9, e54540. <https://doi.org/10.7554/eLife.54540>.
- Iwamura, Y. (1998). Hierarchical somatosensory processing. *Curr Opin Neurobiol* 8, 522–528. [https://doi.org/10.1016/s0959-4388\(98\)80041-x](https://doi.org/10.1016/s0959-4388(98)80041-x).
- Iwamura, Y., Tanaka, M., Sakamoto, M., and Hikosaka, O. (1985). Diversity in receptive field properties of vertical neuronal arrays in the crown of the postcentral gyrus of the conscious monkey. *Exp Brain Res* 58, 400–411. <https://doi.org/10.1007/BF00235321>.
- Iwamura, Y., Tanaka, M., Sakamoto, M., and Hikosaka, O. (1993). Rostrocaudal gradients in the neuronal receptive field complexity in the finger region of the alert monkey's postcentral gyrus. *Exp Brain Res* 92, 360–368. <https://doi.org/10.1007/BF00229023>.
- Iwamura, Y., Iriki, A., and Tanaka, M. (1994). Bilateral hand representation in the postcentral somatosensory cortex. *Nature* 369, 554–556. <https://doi.org/10.1038/369554a0>.
- Jackson, J., Ayzenshtat, I., Karnani, M.M., and Yuste, R. (2016). VIP+ interneurons control neocortical activity across brain states. *J Neurophysiol* 115, 3008–3017. <https://doi.org/10.1152/jn.01124.2015>.
- Jaenisch, N., Liebmann, L., Guenther, M., Hübner, C.A., Frahm, C., and Witte, O.W. (2016). Reduced tonic inhibition after stroke promotes motor performance and epileptic seizures. *Sci Rep* 6, 26173. <https://doi.org/10.1038/srep26173>.
- Jain, N., Catania, K.C., and Kaas, J.H. (1997). Deactivation and reactivation of somatosensory cortex after dorsal spinal cord injury. *Nature* 386, 495–498. <https://doi.org/10.1038/386495a0>.
- Jenkins, W.M., and Merzenich, M.M. (1987). Chapter 21 Reorganization of neocortical representations after brain injury: a neurophysiological model of the bases of recovery from stroke. In *Progress in Brain Research*, F.J. Seil, E. Herbert, and B.M. Carlson, eds. (Elsevier), pp. 249–266.
- Jennrich, R.I. (1970). An Asymptotic χ^2 Test for the Equality of Two Correlation Matrices. *Journal of the American Statistical Association* 65, 904–912. <https://doi.org/10.2307/2284596>.
- Jiang, W., Tremblay, F., and Chapman, C.E. (1997). Neuronal encoding of texture changes in the primary and the secondary somatosensory cortical areas of monkeys during passive texture discrimination. *J Neurophysiol* 77, 1656–1662. <https://doi.org/10.1152/jn.1997.77.3.1656>.
- Jin, X., Huguenard, J.R., and Prince, D.A. (2005). Impaired Cl⁻ extrusion in layer V pyramidal neurons of chronically injured epileptogenic neocortex. *J Neurophysiol* 93, 2117–2126. <https://doi.org/10.1152/jn.00728.2004>.
- Johansen-Berg, H., Christensen, V., Woolrich, M., and Matthews, P.M. (2000). Attention to touch modulates activity in both primary and secondary somatosensory areas. *Neuroreport* 11, 1237–1241. .

- Johansen-Berg, H., Rushworth, M.F.S., Bogdanovic, M.D., Kischka, U., Wimalaratna, S., and Matthews, P.M. (2002). The role of ipsilateral premotor cortex in hand movement after stroke. *PNAS* *99*, 14518–14523. <https://doi.org/10.1073/pnas.222536799>.
- Johansen-Berg, H., Dawes, H., Guy, C., Smith, S.M., Wade, D.T., and Matthews, P.M. (2002). Correlation between motor improvements and altered fMRI activity after rehabilitative therapy. *Brain* *125*, 2731–2742. <https://doi.org/10.1093/brain/awf282>.
- Johansson, R.S., and Flanagan, J.R. (2009). Coding and use of tactile signals from the fingertips in object manipulation tasks. *Nat. Rev. Neurosci.* *10*, 345–359. <https://doi.org/10.1038/nrn2621>.
- Johansson, R.S., Landström, U., and Lundström, R. (1982a). Sensitivity to edges of mechanoreceptive afferent units innervating the glabrous skin of the human head. *Brain Res* *244*, 27–35. [https://doi.org/10.1016/0006-8993\(82\)90900-3](https://doi.org/10.1016/0006-8993(82)90900-3).
- Johansson, R.S., Landström, U., and Lundström, R. (1982b). Responses of mechanoreceptive afferent units in the glabrous skin of the human hand to sinusoidal skin displacements. *Brain Res* *244*, 17–25. [https://doi.org/10.1016/0006-8993\(82\)90899-x](https://doi.org/10.1016/0006-8993(82)90899-x).
- Johnson, K.O., Yoshioka, T., and Vega-Bermudez, F. (2000). Tactile functions of mechanoreceptive afferents innervating the hand. *J Clin Neurophysiol* *17*, 539–558. .
- Johnston, D.G., Denizet, M., Mostany, R., and Portera-Cailliau, C. (2013). Chronic in vivo imaging shows no evidence of dendritic plasticity or functional remapping in the contralesional cortex after stroke. *Cereb Cortex* *23*, 751–762. <https://doi.org/10.1093/cercor/bhs092>.
- Jonckers, E., Delgado y Palacios, R., Shah, D., Guglielmetti, C., Verhoye, M., and Van der Linden, A. (2014). Different anesthesia regimes modulate the functional connectivity outcome in mice. *Magnetic Resonance in Medicine* *72*, 1103–1112. <https://doi.org/10.1002/mrm.24990>.
- Jones, T.A., and Adkins, D.L. (2015). Motor System Reorganization After Stroke: Stimulating and Training Toward Perfection. *Physiology* *30*, 358–370. <https://doi.org/10.1152/physiol.00014.2015>.
- Jones, E.G., Coulter, J.D., and Hendry, S.H. (1978). Intracortical connectivity of architectonic fields in the somatic sensory, motor and parietal cortex of monkeys. *J Comp Neurol* *181*, 291–347. <https://doi.org/10.1002/cne.901810206>.
- Jörntell, H., Bengtsson, F., Geborek, P., Spanne, A., Terekhov, A.V., and Hayward, V. (2014). Segregation of tactile input features in neurons of the cuneate nucleus. *Neuron* *83*, 1444–1452. <https://doi.org/10.1016/j.neuron.2014.07.038>.
- Joutel, A., Monet-Leprêtre, M., Gosele, C., Baron-Menguy, C., Hammes, A., Schmidt, S., Lemaire-Carrette, B., Domenga, V., Schedl, A., Lacombe, P., et al. (2010). Cerebrovascular dysfunction and microcirculation rarefaction precede white matter lesions in a mouse genetic model of cerebral ischemic small vessel disease. *J Clin Invest* *120*, 433–445. <https://doi.org/10.1172/JCI39733>.

- Julkunen, L., Tenovuo, O., Jääskeläinen, S.K., and Hämäläinen, H. (2005). Recovery of somatosensory deficits in acute stroke. *Acta Neurol Scand* *111*, 366–372. <https://doi.org/10.1111/j.1600-0404.2005.00393.x>.
- Kaas, J.H. (1983). What, if anything, is SI? Organization of first somatosensory area of cortex. *Physiol Rev* *63*, 206–231. <https://doi.org/10.1152/physrev.1983.63.1.206>.
- Kaas, J.H. (2004). Evolution of somatosensory and motor cortex in primates. *Anat Rec A Discov Mol Cell Evol Biol* *281*, 1148–1156. <https://doi.org/10.1002/ar.a.20120>.
- Kaas, J.H., Qi, H.-X., Burish, M.J., Gharbawie, O.A., Onifer, S.M., and Massey, J.M. (2008). Cortical and subcortical plasticity in the brains of humans, primates, and rats after damage to sensory afferents in the dorsal columns of the spinal cord. *Experimental Neurology* *209*, 407–416. <https://doi.org/10.1016/j.expneurol.2007.06.014>.
- Kalisch, R., Holt, B., Petrovic, P., De Martino, B., Klöppel, S., Büchel, C., and Dolan, R.J. (2009). The NMDA agonist D-cycloserine facilitates fear memory consolidation in humans. *Cereb Cortex* *19*, 187–196. <https://doi.org/10.1093/cercor/bhn076>.
- Kalthoff, D., Po, C., Wiedermann, D., and Hoehn, M. (2013). Reliability and spatial specificity of rat brain sensorimotor functional connectivity networks are superior under sedation compared with general anesthesia. *NMR in Biomedicine* *26*, 638–650. <https://doi.org/10.1002/nbm.2908>.
- Karadimas, S.K., Satkunendrarajah, K., Laliberte, A.M., Ringuette, D., Weisspapir, I., Li, L., Gosgnach, S., and Fehlings, M.G. (2020). Sensory cortical control of movement. *Nat Neurosci* *23*, 75–84. <https://doi.org/10.1038/s41593-019-0536-7>.
- Kayser, C., Körding, K.P., and König, P. (2004). Processing of complex stimuli and natural scenes in the visual cortex. *Curr. Opin. Neurobiol.* *14*, 468–473. <https://doi.org/10.1016/j.conb.2004.06.002>.
- Kerlin, A.M., Andermann, M.L., Berezovskii, V.K., and Reid, R.C. (2010). Broadly tuned response properties of diverse inhibitory neuron subtypes in mouse visual cortex. *Neuron* *67*, 858–871. <https://doi.org/10.1016/j.neuron.2010.08.002>.
- Kerr, J.N.D., Greenberg, D., and Helmchen, F. (2005). Imaging input and output of neocortical networks in vivo. *Proc. Natl. Acad. Sci. U.S.A.* *102*, 14063–14068. <https://doi.org/10.1073/pnas.0506029102>.
- Kerr, J.N.D., de Kock, C.P.J., Greenberg, D.S., Bruno, R.M., Sakmann, B., and Helmchen, F. (2007). Spatial organization of neuronal population responses in layer 2/3 of rat barrel cortex. *J. Neurosci.* *27*, 13316–13328. <https://doi.org/10.1523/JNEUROSCI.2210-07.2007>.
- Khan, A.G., Poort, J., Chadwick, A., Blot, A., Sahani, M., Mrsic-Flogel, T.D., and Hofer, S.B. (2018). Distinct learning-induced changes in stimulus selectivity and interactions of GABAergic interneuron classes in visual cortex. *Nat Neurosci* *21*, 851–859. <https://doi.org/10.1038/s41593-018-0143-z>.

Khirug, S., Soni, S., Saez Garcia, M., Tessier, M., Zhou, L., Kuleshkaya, N., Rauvala, H., Lindholm, D., Ludwig, A., Molinari, F., et al. (2021). Protective Role of Low Ethanol Administration Following Ischemic Stroke via Recovery of KCC2 and p75NTR Expression. *Mol Neurobiol* 58, 1145–1161. <https://doi.org/10.1007/s12035-020-02176-x>.

Kim, U., and Lee, T. (2013). Intra-areal and corticocortical circuits arising in the dysgranular zone of rat primary somatosensory cortex that processes deep somatic input. *Journal of Comparative Neurology* 521, 2585–2601. <https://doi.org/10.1002/cne.23300>.

Kim, S.S., Gomez-Ramirez, M., Thakur, P.H., and Hsiao, S.S. (2015). Multimodal Interactions between Proprioceptive and Cutaneous Signals in Primary Somatosensory Cortex. *Neuron* 86, 555–566. <https://doi.org/10.1016/j.neuron.2015.03.020>.

King, V.R., and Corwin, J.V. (1993). Comparisons of hemi-inattention produced by unilateral lesions of the posterior parietal cortex or medial agranular prefrontal cortex in rats: neglect, extinction, and the role of stimulus distance. *Behav Brain Res* 54, 117–131. [https://doi.org/10.1016/0166-4328\(93\)90070-7](https://doi.org/10.1016/0166-4328(93)90070-7).

Kislin, M., Mugantseva, E., Molotkov, D., Kuleshkaya, N., Khirug, S., Kirilkin, I., Pryazhnikov, E., Kolikova, J., Toptunov, D., Yuryev, M., et al. (2014). Flat-floored Air-lifted Platform: A New Method for Combining Behavior with Microscopy or Electrophysiology on Awake Freely Moving Rodents. *JoVE (Journal of Visualized Experiments)* e51869. <https://doi.org/10.3791/51869>.

Klein, A., Sacrey, L.-A.R., Whishaw, I.Q., and Dunnett, S.B. (2012). The use of rodent skilled reaching as a translational model for investigating brain damage and disease. *Neuroscience & Biobehavioral Reviews* 36, 1030–1042. <https://doi.org/10.1016/j.neubiorev.2011.12.010>.

Knibestöl, M. (1975). Stimulus-response functions of slowly adapting mechanoreceptors in the human glabrous skin area. *J Physiol* 245, 63–80. <https://doi.org/10.1113/jphysiol.1975.sp010835>.

Knöpfel, T., and Song, C. (2019). Optical voltage imaging in neurons: moving from technology development to practical tool. *Nature Reviews Neuroscience* 20, 719–727. <https://doi.org/10.1038/s41583-019-0231-4>.

Koch, G., Veniero, D., and Caltagirone, C. (2013). To the Other Side of the Neglected Brain: The Hyperexcitability of the Left Intact Hemisphere. *Neuroscientist* 19, 208–217. <https://doi.org/10.1177/1073858412447874>.

Kohn, A., Coen-Cagli, R., Kanitscheider, I., and Pouget, A. (2016). Correlations and Neuronal Population Information. *Annu Rev Neurosci* 39, 237–256. <https://doi.org/10.1146/annurev-neuro-070815-013851>.

Kolb, B., and Walkey, J. (1987). Behavioural and anatomical studies of the posterior parietal cortex in the rat. *Behav Brain Res* 23, 127–145. [https://doi.org/10.1016/0166-4328\(87\)90050-7](https://doi.org/10.1016/0166-4328(87)90050-7).

Koralek, K.-A., Olavarria, J., and Kellackey, H.P. (1990). Areal and laminar organization of corticocortical projections in the rat somatosensory cortex. *Journal of Comparative Neurology*

299, 133–150. <https://doi.org/10.1002/cne.902990202>.

Krubitzer, L.A., and Kaas, J.H. (1990). The organization and connections of somatosensory cortex in marmosets. *J Neurosci* *10*, 952–974. .

Krubitzer, L.A., and Kaas, J.H. (1992). The somatosensory thalamus of monkeys: cortical connections and a redefinition of nuclei in marmosets. *J Comp Neurol* *319*, 123–140. <https://doi.org/10.1002/cne.903190111>.

Krubitzer, L., Clarey, J., Tweedale, R., Elston, G., and Calford, M. (1995). A redefinition of somatosensory areas in the lateral sulcus of macaque monkeys. *J Neurosci* *15*, 3821–3839. .

Krubitzer, L., Huffman, K.J., Disbrow, E., and Recanzone, G. (2004). Organization of area 3a in macaque monkeys: contributions to the cortical phenotype. *J Comp Neurol* *471*, 97–111. <https://doi.org/10.1002/cne.20025>.

Krubitzer, L., Campi, K.L., and Cooke, D.F. (2011). All Rodents Are Not the Same: A Modern Synthesis of Cortical Organization. *BBE* *78*, 51–93. <https://doi.org/10.1159/000327320>.

Künzle, H. (1977). Projections from the primary somatosensory cortex to basal ganglia and thalamus in the monkey. *Exp Brain Res* *30*, 481–492. <https://doi.org/10.1007/BF00237639>.

Kuriakose, D., and Xiao, Z. (2020). Pathophysiology and Treatment of Stroke: Present Status and Future Perspectives. *Int J Mol Sci* *21*, 7609. <https://doi.org/10.3390/ijms21207609>.

Kwakkel, G., Kollen, B., and Lindeman, E. (2004). Understanding the pattern of functional recovery after stroke: facts and theories. *Restor Neurol Neurosci* *22*, 281–299. .

Kwon, S.E., Tsytsarev, V., Erzurumlu, R.S., and O'Connor, D.H. (2018). Organization of orientation-specific whisker deflection responses in layer 2/3 of mouse somatosensory cortex. *Neuroscience* *368*, 46–56. <https://doi.org/10.1016/j.neuroscience.2017.07.067>.

de Lafuente, V., and Romo, R. (2006). Neural correlate of subjective sensory experience gradually builds up across cortical areas. *Proc Natl Acad Sci U S A* *103*, 14266–14271. <https://doi.org/10.1073/pnas.0605826103>.

Lak, A., Arabzadeh, E., and Diamond, M.E. (2008). Enhanced response of neurons in rat somatosensory cortex to stimuli containing temporal noise. *Cereb. Cortex* *18*, 1085–1093. <https://doi.org/10.1093/cercor/bhm144>.

Lake, E.M.R., Chaudhuri, J., Thomason, L., Janik, R., Ganguly, M., Brown, M., McLaurin, J., Corbett, D., Stanis, G.J., and Stefanovic, B. (2015). The effects of delayed reduction of tonic inhibition on ischemic lesion and sensorimotor function. *J Cereb Blood Flow Metab* *35*, 1601–1609. <https://doi.org/10.1038/jcbfm.2015.86>.

Lamtahri, R., Hazime, M., Gowing, E.K., Nagaraja, R.Y., Maucotel, J., Alasoadura, M., Quilichini, P.P., Lehongre, K., Lefranc, B., Gach-Janczak, K., et al. (2021). The Gliopeptide ODN, a Ligand for the Benzodiazepine Site of GABAA Receptors, Boosts Functional Recovery

- after Stroke. *J Neurosci* *41*, 7148–7159. <https://doi.org/10.1523/JNEUROSCI.2255-20.2021>.
- Latifi, S., Mitchell, S., Habibey, R., Hosseini, F., Donzis, E., Estrada-Sánchez, A.M., Nejad, H.R., Levine, M., Golshani, P., and Carmichael, S.T. (2020). Neuronal Network Topology Indicates Distinct Recovery Processes after Stroke. *Cereb Cortex* *30*, 6363–6375. <https://doi.org/10.1093/cercor/bhaa191>.
- Lazar, R.M., Fitzsimmons, B.-F., Marshall, R.S., Berman, M.F., Bustillo, M.A., Young, W.L., Mohr, J.P., Shah, J., and Robinson, J.V. (2002). Reemergence of stroke deficits with midazolam challenge. *Stroke* *33*, 283–285. <https://doi.org/10.1161/hs0102.101222>.
- Lee, V., and Maguire, J. (2014). The impact of tonic GABAA receptor-mediated inhibition on neuronal excitability varies across brain region and cell type. *Front Neural Circuits* *8*, 3. <https://doi.org/10.3389/fncir.2014.00003>.
- Lee, T., Alloway, K.D., and Kim, U. (2011). Interconnected cortical networks between primary somatosensory cortex septal columns and posterior parietal cortex in rat. *J Comp Neurol* *519*, 405–419. <https://doi.org/10.1002/cne.22505>.
- Lehky, S.R., Sejnowski, T.J., and Desimone, R. (1992). Predicting responses of nonlinear neurons in monkey striate cortex to complex patterns. *J. Neurosci.* *12*, 3568–3581. .
- Lehmann, K., Steinecke, A., and Bolz, J. (2012). GABA through the ages: regulation of cortical function and plasticity by inhibitory interneurons. *Neural Plast* *2012*, 892784. <https://doi.org/10.1155/2012/892784>.
- Lesniak, D.R., Marshall, K.L., Wellnitz, S.A., Jenkins, B.A., Baba, Y., Rasband, M.N., Gerling, G.J., and Lumpkin, E.A. (2014). Computation identifies structural features that govern neuronal firing properties in slowly adapting touch receptors. *Elife* *3*, e01488. <https://doi.org/10.7554/eLife.01488>.
- Li, S., and Carmichael, S.T. (2006). Growth-associated gene and protein expression in the region of axonal sprouting in the aged brain after stroke. *Neurobiology of Disease* *23*, 362–373. <https://doi.org/10.1016/j.nbd.2006.03.011>.
- Li, C.X., Yang, Q., and Waters, R.S. (2012). Functional and structural organization of the forelimb representation in cuneate nucleus in rat. *Brain Research* *1468*, 11–28. <https://doi.org/10.1016/j.brainres.2012.03.048>.
- Li, J., Shan, W., and Zuo, Z. (2018). Age-Related Upregulation of Carboxyl Terminal Modulator Protein Contributes to the Decreased Brain Ischemic Tolerance in Older Rats. *Mol Neurobiol* *55*, 6145–6154. <https://doi.org/10.1007/s12035-017-0826-6>.
- Li, L., Rutlin, M., Abaira, V.E., Cassidy, C., Kus, L., Gong, S., Jankowski, M.P., Luo, W., Heintz, N., Koerber, H.R., et al. (2011). The functional organization of cutaneous low-threshold mechanosensory neurons. *Cell* *147*, 1615–1627. <https://doi.org/10.1016/j.cell.2011.11.027>.
- Li, S., Overman, J.J., Katsman, D., Kozlov, S.V., Donnelly, C.J., Twiss, J.L., Giger, R.J.,

- Coppola, G., Geschwind, D.H., and Carmichael, S.T. (2010). An age-related sprouting transcriptome provides molecular control of axonal sprouting after stroke. *Nat Neurosci* *13*, 1496–1504. <https://doi.org/10.1038/nn.2674>.
- Li, S., Nie, E., Yin, Y., Benowitz, L., Tung, S., Vinters, H., Bahjat, F., Stenzel-Poore, M., Kawaguchi, R., Coppola, G., et al. (2015). GDF10 Is a Signal for Axonal Sprouting and Functional Recovery after Stroke. *Nat Neurosci* *18*, 1737–1745. <https://doi.org/10.1038/nn.4146>.
- Lie, M.E., Gowing, E.K., Clausen, R.P., Wellendorph, P., and Clarkson, A.N. (2018). Inhibition of GABA transporters fails to afford significant protection following focal cerebral ischemia. *J Cereb Blood Flow Metab* *38*, 166–173. <https://doi.org/10.1177/0271678X17743669>.
- Lim, D.H., LeDue, J.M., Mohajerani, M.H., and Murphy, T.H. (2014). Optogenetic mapping after stroke reveals network-wide scaling of functional connections and heterogeneous recovery of the peri-infarct. *J Neurosci* *34*, 16455–16466. <https://doi.org/10.1523/JNEUROSCI.3384-14.2014>.
- Lipsanen, A., Hiltunen, M., and Jolkkonen, J. (2011). Chronic ibuprofen treatment does not affect the secondary pathology in the thalamus or improve behavioral outcome in middle cerebral artery occlusion rats. *Pharmacology Biochemistry and Behavior* *99*, 468–474. <https://doi.org/10.1016/j.pbb.2011.04.019>.
- Lissek, T., Obenaus, H.A., Ditzel, D.A.W., Nagai, T., Miyawaki, A., Sprengel, R., and Hasan, M.T. (2016). General Anesthetic Conditions Induce Network Synchrony and Disrupt Sensory Processing in the Cortex. *Front Cell Neurosci* *10*, 64. <https://doi.org/10.3389/fncel.2016.00064>.
- Liu, B., Liao, M., Mielke, J.G., Ning, K., Chen, Y., Li, L., El-Hayek, Y.H., Gomez, E., Zukin, R.S., Fehlings, M.G., et al. (2006). Ischemic insults direct glutamate receptor subunit 2-lacking AMPA receptors to synaptic sites. *J Neurosci* *26*, 5309–5319. <https://doi.org/10.1523/JNEUROSCI.0567-06.2006>.
- Löken, L.S., Wessberg, J., Morrison, I., McGlone, F., and Olausson, H. (2009). Coding of pleasant touch by unmyelinated afferents in humans. *Nat Neurosci* *12*, 547–548. <https://doi.org/10.1038/nn.2312>.
- London, B.M., and Miller, L.E. (2013). Responses of somatosensory area 2 neurons to actively and passively generated limb movements. *J Neurophysiol* *109*, 1505–1513. <https://doi.org/10.1152/jn.00372.2012>.
- Longo, V., Barbati, S.A., Re, A., Paciello, F., Bolla, M., Rinaudo, M., Miraglia, F., Alù, F., Di Donna, M.G., Vecchio, F., et al. (2022). Transcranial Direct Current Stimulation Enhances Neuroplasticity and Accelerates Motor Recovery in a Stroke Mouse Model. *Stroke* *STROKEAHA121034200*. <https://doi.org/10.1161/STROKEAHA.121.034200>.
- Low, J.S.T., John, L.A.M.-St., and Tracey, D.J. (1986). Nucleus Z in the rat: Spinal afferents from collaterals of dorsal spinocerebellar tract neurons. *Journal of Comparative Neurology* *243*, 510–526. <https://doi.org/10.1002/cne.902430406>.

- Luczak, A., Barthó, P., and Harris, K.D. (2009). Spontaneous events outline the realm of possible sensory responses in neocortical populations. *Neuron* 62, 413–425. <https://doi.org/10.1016/j.neuron.2009.03.014>.
- Luhmann, H.J., Mudrick-Donnon, L.A., Mittmann, T., and Heinemann, U. (1995). Ischaemia-induced long-term hyperexcitability in rat neocortex. *Eur J Neurosci* 7, 180–191. <https://doi.org/10.1111/j.1460-9568.1995.tb01054.x>.
- Luke, L.M., Allred, R.P., and Jones, T.A. (2004). Unilateral ischemic sensorimotor cortical damage induces contralesional synaptogenesis and enhances skilled reaching with the ipsilateral forelimb in adult male rats. *Synapse* 54, 187–199. <https://doi.org/10.1002/syn.20080>.
- Lyden, P.D., and Hedges, B. (1992). Protective effect of synaptic inhibition during cerebral ischemia in rats and rabbits. *Stroke* 23, 1463–1469; discussion 1469-1470. <https://doi.org/10.1161/01.str.23.10.1463>.
- Ma, J., Ma, Y., Shuaib, A., and Winship, I.R. (2020). Impaired Collateral Flow in Pial Arterioles of Aged Rats During Ischemic Stroke. *Transl Stroke Res* 11, 243–253. <https://doi.org/10.1007/s12975-019-00710-1>.
- Mackevicius, E.L., Best, M.D., Saal, H.P., and Bensmaia, S.J. (2012). Millisecond precision spike timing shapes tactile perception. *J Neurosci* 32, 15309–15317. <https://doi.org/10.1523/JNEUROSCI.2161-12.2012>.
- MacLean, J.N., Watson, B.O., Aaron, G.B., and Yuste, R. (2005). Internal dynamics determine the cortical response to thalamic stimulation. *Neuron* 48, 811–823. <https://doi.org/10.1016/j.neuron.2005.09.035>.
- Makous, J.C., Friedman, R.M., and Vierck, C.J. (1996). Effects of a dorsal column lesion on temporal processing within the somatosensory system of primates. *Exp Brain Res* 112, 253–267. <https://doi.org/10.1007/BF00227644>.
- Malvache, A., Reichinnek, S., Villette, V., Haimerl, C., and Cossart, R. (2016). Awake hippocampal reactivations project onto orthogonal neuronal assemblies. *Science* 353, 1280–1283. <https://doi.org/10.1126/science.aaf3319>.
- Martín-Aragón Baudel, M.A.S., Poole, A.V., and Darlison, M.G. (2017). Chloride co-transporters as possible therapeutic targets for stroke. *J Neurochem* 140, 195–209. <https://doi.org/10.1111/jnc.13901>.
- Mascaro, A.L.A., Conti, E., Lai, S., Giovanna, A.P.D., Spalletti, C., Alia, C., Panarese, A., Scaglione, A., Sacconi, L., Micera, S., et al. (2019). Combined Rehabilitation Promotes the Recovery of Structural and Functional Features of Healthy Neuronal Networks after Stroke. *Cell Reports* 28, 3474-3485.e6. <https://doi.org/10.1016/j.celrep.2019.08.062>.
- Massey, J.M., Hubscher, C.H., Wagoner, M.R., Decker, J.A., Amps, J., Silver, J., and Onifer, S.M. (2006). Chondroitinase ABC digestion of the perineuronal net promotes functional collateral sprouting in the cuneate nucleus after cervical spinal cord injury. *J Neurosci* 26, 4406–

4414. <https://doi.org/10.1523/JNEUROSCI.5467-05.2006>.

Matthews, B.H. (1933). Nerve endings in mammalian muscle. *J Physiol* 78, 1–53. <https://doi.org/10.1113/jphysiol.1933.sp002984>.

Mc Larney, B., Hutter, M.A., Degtyaruk, O., Deán-Ben, X.L., and Razansky, D. (2020). Monitoring of Stimulus Evoked Murine Somatosensory Cortex Hemodynamic Activity With Volumetric Multi-Spectral Optoacoustic Tomography. *Front Neurosci* 14, 536. <https://doi.org/10.3389/fnins.2020.00536>.

McKenna, J.E., and Whishaw, I.Q. (1999). Complete Compensation in Skilled Reaching Success with Associated Impairments in Limb Synergies, after Dorsal Column Lesion in the Rat. *J. Neurosci.* 19, 1885–1894. <https://doi.org/10.1523/JNEUROSCI.19-05-01885.1999>.

van Meer, M.P.A., van der Marel, K., Wang, K., Otte, W.M., el Bouazati, S., Roeling, T.A.P., Viergever, M.A., Berkelbach van der Sprenkel, J.W., and Dijkhuizen, R.M. (2010). Recovery of Sensorimotor Function after Experimental Stroke Correlates with Restoration of Resting-State Interhemispheric Functional Connectivity. *J Neurosci* 30, 3964–3972. <https://doi.org/10.1523/JNEUROSCI.5709-09.2010>.

Meftah, E.-M., Shenasa, J., and Chapman, C.E. (2002). Effects of a cross-modal manipulation of attention on somatosensory cortical neuronal responses to tactile stimuli in the monkey. *J Neurophysiol* 88, 3133–3149. <https://doi.org/10.1152/jn.00121.2002>.

Meftah, E.-M., Bourgeon, S., and Chapman, C.E. (2009). Instructed delay discharge in primary and secondary somatosensory cortex within the context of a selective attention task. *J Neurophysiol* 101, 2649–2667. <https://doi.org/10.1152/jn.91121.2008>.

Melzer, P., Champney, G.C., Maguire, M.J., and Ebner, F.F. (2006). Rate code and temporal code for frequency of whisker stimulation in rat primary and secondary somatic sensory cortex. *Exp Brain Res* 172, 370–386. <https://doi.org/10.1007/s00221-005-0334-1>.

Méndez, P., and Bacci, A. (2011). Assortment of GABAergic plasticity in the cortical interneuron melting pot. *Neural Plast* 2011, 976856. <https://doi.org/10.1155/2011/976856>.

Menzel, R.R., and Barth, D.S. (2005). Multisensory and Secondary Somatosensory Cortex in the Rat. *Cerebral Cortex* 15, 1690–1696. <https://doi.org/10.1093/cercor/bhi045>.

Metz, G.A., Antonow-Schlorke, I., and Witte, O.W. (2005). Motor improvements after focal cortical ischemia in adult rats are mediated by compensatory mechanisms. *Behav Brain Res* 162, 71–82. <https://doi.org/10.1016/j.bbr.2005.03.002>.

Meyer, A.F., Williamson, R.S., Linden, J.F., and Sahani, M. (2016). Models of Neuronal Stimulus-Response Functions: Elaboration, Estimation, and Evaluation. *Front Syst Neurosci* 10, 109. <https://doi.org/10.3389/fnsys.2016.00109>.

Michael, N., Bischof, H.-J., and Löwel, S. (2014). Flavoprotein autofluorescence imaging of visual system activity in zebra finches and mice. *PLoS ONE* 9, e85225.

<https://doi.org/10.1371/journal.pone.0085225>.

Miller, J.K., Ayzenshtat, I., Carrillo-Reid, L., and Yuste, R. (2014). Visual stimuli recruit intrinsically generated cortical ensembles. *Proc Natl Acad Sci U S A* *111*, E4053-4061. <https://doi.org/10.1073/pnas.1406077111>.

Mittmann, T., Qü, M., Zilles, K., and Luhmann, H.J. (1998). Long-term cellular dysfunction after focal cerebral ischemia: in vitro analyses. *Neuroscience* *85*, 15–27. [https://doi.org/10.1016/S0306-4522\(97\)00638-6](https://doi.org/10.1016/S0306-4522(97)00638-6).

Mody, I., De Koninck, Y., Otis, T.S., and Soltesz, I. (1994). Bridging the cleft at GABA synapses in the brain. *Trends Neurosci* *17*, 517–525. [https://doi.org/10.1016/0166-2236\(94\)90155-4](https://doi.org/10.1016/0166-2236(94)90155-4).

Mohajerani, M.H., Aminoltejari, K., and Murphy, T.H. (2011). Targeted mini-strokes produce changes in interhemispheric sensory signal processing that are indicative of disinhibition within minutes. *Proc Natl Acad Sci U S A* *108*, E183-191. <https://doi.org/10.1073/pnas.1101914108>.

Mölter, J., Avitan, L., and Goodhill, G.J. (2018). Detecting neural assemblies in calcium imaging data. *BMC Biol* *16*, 143. <https://doi.org/10.1186/s12915-018-0606-4>.

Moon, S.-K., Alaverdashvili, M., Cross, A.R., and Whishaw, I.Q. (2009). Both compensation and recovery of skilled reaching following small photothrombotic stroke to motor cortex in the rat. *Experimental Neurology* *218*, 145–153. <https://doi.org/10.1016/j.expneurol.2009.04.021>.

Moore, C.I., and Nelson, S.B. (1998). Spatio-Temporal Subthreshold Receptive Fields in the Vibrissa Representation of Rat Primary Somatosensory Cortex. *Journal of Neurophysiology* *80*, 2882–2892. <https://doi.org/10.1152/jn.1998.80.6.2882>.

Morales-Botello, M.L., Aguilar, J., and Foffani, G. (2012). Imaging the spatio-temporal dynamics of supragranular activity in the rat somatosensory cortex in response to stimulation of the paws. *PLoS ONE* *7*, e40174. <https://doi.org/10.1371/journal.pone.0040174>.

Motaharinia, M., Gerrow, K., Boghozian, R., White, E., Choi, S.-E., Delaney, K.R., and Brown, C.E. (2021). Longitudinal functional imaging of VIP interneurons reveals sup-population specific effects of stroke that are rescued with chemogenetic therapy. *Nat Commun* *12*, 6112. <https://doi.org/10.1038/s41467-021-26405-6>.

Mountcastle, V.B. (2005). *The Sensory Hand* (Cambridge, Mass: Harvard University Press).

Mountcastle, V.B., Talbot, W.H., Sakata, H., and Hyvärinen, J. (1969). Cortical neuronal mechanisms in flutter-vibration studied in unanesthetized monkeys. Neuronal periodicity and frequency discrimination. *J. Neurophysiol.* *32*, 452–484. <https://doi.org/10.1152/jn.1969.32.3.452>.

Mountcastle, V.B., LaMotte, R.H., and Carli, G. (1972). Detection thresholds for stimuli in humans and monkeys: comparison with threshold events in mechanoreceptive afferent nerve fibers innervating the monkey hand. *J. Neurophysiol.* *35*, 122–136.

<https://doi.org/10.1152/jn.1972.35.1.122>.

Muniak, M.A., Ray, S., Hsiao, S.S., Dammann, J.F., and Bensmaia, S.J. (2007). The Neural Coding of Stimulus Intensity: Linking the Population Response of Mechanoreceptive Afferents with Psychophysical Behavior. *Journal of Neuroscience* 27, 11687–11699. <https://doi.org/10.1523/JNEUROSCI.1486-07.2007>.

Murphy, T.H., and Corbett, D. (2009). Plasticity during stroke recovery: from synapse to behaviour. *Nat Rev Neurosci* 10, 861–872. <https://doi.org/10.1038/nrn2735>.

Murray, E.A., and Mishkin, M. (1984). Relative contributions of SII and area 5 to tactile discrimination in monkeys. *Behav Brain Res* 11, 67–83. [https://doi.org/10.1016/0166-4328\(84\)90009-3](https://doi.org/10.1016/0166-4328(84)90009-3).

Nakatani, M., Maksimovic, S., Baba, Y., and Lumpkin, E.A. (2015). Mechanotransduction in epidermal Merkel cells. *Pflügers Arch* 467, 101–108. <https://doi.org/10.1007/s00424-014-1569-0>.

Nasrallah, F.A., Tay, H.-C., and Chuang, K.-H. (2014). Detection of functional connectivity in the resting mouse brain. *NeuroImage* 86, 417–424. <https://doi.org/10.1016/j.neuroimage.2013.10.025>.

Nelson, R.J. (1987). Activity of monkey primary somatosensory cortical neurons changes prior to active movement. *Brain Res* 406, 402–407. [https://doi.org/10.1016/0006-8993\(87\)90815-8](https://doi.org/10.1016/0006-8993(87)90815-8).

Nelson, R.J. (1996). Interactions between motor commands and somatic perception in sensorimotor cortex. *Curr Opin Neurobiol* 6, 801–810. [https://doi.org/10.1016/s0959-4388\(96\)80031-6](https://doi.org/10.1016/s0959-4388(96)80031-6).

Nelson, A.J., Staines, W.R., Graham, S.J., and McIlroy, W.E. (2004). Activation in SI and SII: the influence of vibrotactile amplitude during passive and task-relevant stimulation. *Brain Res Cogn Brain Res* 19, 174–184. <https://doi.org/10.1016/j.cogbrainres.2003.11.013>.

Neumann-Haefelin, T., Hagemann, G., and Witte, O.W. (1995). Cellular correlates of neuronal hyperexcitability in the vicinity of photochemically induced cortical infarcts in rats in vitro. *Neuroscience Letters* 193, 101–104. [https://doi.org/10.1016/0304-3940\(95\)11677-O](https://doi.org/10.1016/0304-3940(95)11677-O).

Neumann-Haefelin, T., Staiger, J.F., Redecker, C., Zilles, K., Fritschy, J.M., Möhler, H., and Witte, O.W. (1998). Immunohistochemical evidence for dysregulation of the GABAergic system ipsilateral to photochemically induced cortical infarcts in rats. *Neuroscience* 87, 871–879. [https://doi.org/10.1016/s0306-4522\(98\)00124-9](https://doi.org/10.1016/s0306-4522(98)00124-9).

Neumann-Haefelin, T., Bosse, F., Redecker, C., Müller, H.W., and Witte, O.W. (1999). Upregulation of GABAA-receptor alpha1- and alpha2-subunit mRNAs following ischemic cortical lesions in rats. *Brain Res* 816, 234–237. [https://doi.org/10.1016/s0006-8993\(98\)01162-7](https://doi.org/10.1016/s0006-8993(98)01162-7).

Nicolelis, M.A., and Chapin, J.K. (1994). Spatiotemporal structure of somatosensory responses of many-neuron ensembles in the rat ventral posterior medial nucleus of the thalamus. *J.*

Neurosci. *14*, 3511–3532. <https://doi.org/10.1523/JNEUROSCI.14-06-03511.1994>.

van Nieuwenhuijzen, P.S., Parker, K., Liao, V., Houlton, J., Kim, H.-L., Johnston, G.A.R., Hanrahan, J.R., Chebib, M., and Clarkson, A.N. (2021). Targeting GABAC Receptors Improves Post-Stroke Motor Recovery. *Brain Sci* *11*, 315. <https://doi.org/10.3390/brainsci11030315>.

Nimmerjahn, A., Kirchhoff, F., Kerr, J.N.D., and Helmchen, F. (2004). Sulforhodamine 101 as a specific marker of astroglia in the neocortex in vivo. *Nat. Methods* *1*, 31–37. <https://doi.org/10.1038/nmeth706>.

Nishibe, M., Urban, E.T.R., Barbay, S., and Nudo, R.J. (2015). Rehabilitative training promotes rapid motor recovery but delayed motor map reorganization in a rat cortical ischemic infarct model. *Neurorehabil Neural Repair* *29*, 472–482. <https://doi.org/10.1177/1545968314543499>.

Nitz, D. (2009). Parietal cortex, navigation, and the construction of arbitrary reference frames for spatial information. *Neurobiol Learn Mem* *91*, 179–185. <https://doi.org/10.1016/j.nlm.2008.08.007>.

Nolano, M., Provitera, V., Crisci, C., Stancanelli, A., Wendelschafer-Crabb, G., Kennedy, W.R., and Santoro, L. (2003). Quantification of myelinated endings and mechanoreceptors in human digital skin. *Ann Neurol* *54*, 197–205. <https://doi.org/10.1002/ana.10615>.

Nudo, R.J. (1997). Remodeling of cortical motor representations after stroke: implications for recovery from brain damage. *Molecular Psychiatry* *2*, 188–191. <https://doi.org/10.1038/sj.mp.4000188>.

Nudo, R.J., Wise, B.M., SiFuentes, F., and Milliken, G.W. (1996). Neural substrates for the effects of rehabilitative training on motor recovery after ischemic infarct. *Science* *272*, 1791–1794. <https://doi.org/10.1126/science.272.5269.1791>.

Nusser, Z., and Mody, I. (2002). Selective modulation of tonic and phasic inhibitions in dentate gyrus granule cells. *J Neurophysiol* *87*, 2624–2628. <https://doi.org/10.1152/jn.2002.87.5.2624>.

Oh, M.-K., Yoon, K.J., Lee, Y.-T., Chae, S.W., Choi, H.Y., Shin, H.S., Park, Y.H., Chun, S.-W., and Park, Y.S. (2018). Effect of zolpidem on functional recovery in a rat model of ischemic stroke. *J Int Med Res* *46*, 249–257. <https://doi.org/10.1177/0300060517723799>.

Ohki, K., Chung, S., Ch'ng, Y.H., Kara, P., and Reid, R.C. (2005). Functional imaging with cellular resolution reveals precise micro-architecture in visual cortex. *Nature* *433*, 597–603. <https://doi.org/10.1038/nature03274>.

Olafson, E.R., Jamison, K.W., Sweeney, E.M., Liu, H., Wang, D., Bruss, J.E., Boes, A.D., and Kuceyeski, A. (2021). Functional connectome reorganization relates to post-stroke motor recovery and structural and functional disconnection. *Neuroimage* *245*, 118642. <https://doi.org/10.1016/j.neuroimage.2021.118642>.

Overman, J.J., Clarkson, A.N., Wanner, I.B., Overman, W.T., Eckstein, I., Maguire, J.L., Dinov, I.D., Toga, A.W., and Carmichael, S.T. (2012). A role for ephrin-A5 in axonal sprouting,

recovery, and activity-dependent plasticity after stroke. *Proc Natl Acad Sci U S A* *109*, E2230–E2239. <https://doi.org/10.1073/pnas.1204386109>.

Owens, D.M., and Lumpkin, E.A. (2014). Diversification and specialization of touch receptors in skin. *Cold Spring Harb Perspect Med* *4*. <https://doi.org/10.1101/cshperspect.a013656>.

Pachitariu, M., Stringer, C., and Harris, K.D. (2018). Robustness of Spike Deconvolution for Neuronal Calcium Imaging. *J. Neurosci.* *38*, 7976–7985. <https://doi.org/10.1523/JNEUROSCI.3339-17.2018>.

Pack, C.C., and Bensmaia, S.J. (2015). Seeing and Feeling Motion: Canonical Computations in Vision and Touch. *PLoS Biol* *13*, e1002271. <https://doi.org/10.1371/journal.pbio.1002271>.

Padberg, J., Cerkevich, C., Engle, J., Rajan, A.T., Recanzone, G., Kaas, J., and Krubitzer, L. (2009). Thalamocortical connections of parietal somatosensory cortical fields in macaque monkeys are highly divergent and convergent. *Cereb Cortex* *19*, 2038–2064. <https://doi.org/10.1093/cercor/bhn229>.

Palm, G., Knoblauch, A., Hauser, F., and Schüz, A. (2014). Cell assemblies in the cerebral cortex. *Biol Cybern* *108*, 559–572. <https://doi.org/10.1007/s00422-014-0596-4>.

Park, K., Liyanage, A.C., Koretsky, A.P., Pan, Y., and Du, C. (2021). Optical imaging of stimulation-evoked cortical activity using GCaMP6f and jRGECO1a. *Quant Imaging Med Surg* *11*, 998–1009. <https://doi.org/10.21037/qims-20-921>.

Patel, A.T., Duncan, P.W., Lai, S.M., and Studenski, S. (2000). The relation between impairments and functional outcomes poststroke. *Arch Phys Med Rehabil* *81*, 1357–1363. <https://doi.org/10.1053/apmr.2000.9397>.

Paz, J.T., Christian, C.A., Parada, I., Prince, D.A., and Huguenard, J.R. (2010). Focal cortical infarcts alter intrinsic excitability and synaptic excitation in the reticular thalamic nucleus. *J Neurosci* *30*, 5465–5479. <https://doi.org/10.1523/JNEUROSCI.5083-09.2010>.

Pei, Y.-C., Denchev, P.V., Hsiao, S.S., Craig, J.C., and Bensmaia, S.J. (2009). Convergence of submodality-specific input onto neurons in primary somatosensory cortex. *J. Neurophysiol.* *102*, 1843–1853. <https://doi.org/10.1152/jn.00235.2009>.

Peron, S., Chen, T.-W., and Svoboda, K. (2015). Comprehensive imaging of cortical networks. *Current Opinion in Neurobiology* *32*, 115–123. <https://doi.org/10.1016/j.conb.2015.03.016>.

Petersen, C.C.H. (2019). Sensorimotor processing in the rodent barrel cortex. *Nat Rev Neurosci* *20*, 533–546. <https://doi.org/10.1038/s41583-019-0200-y>.

Pfeffer, C.K., Xue, M., He, M., Huang, Z.J., and Scanziani, M. (2013). Inhibition of inhibition in visual cortex: the logic of connections between molecularly distinct interneurons. *Nat Neurosci* *16*, 1068–1076. <https://doi.org/10.1038/nn.3446>.

Phillips, J.R., and Johnson, K.O. (1981). Tactile spatial resolution. II. Neural representation of

Bars, edges, and gratings in monkey primary afferents. *J Neurophysiol* 46, 1192–1203. <https://doi.org/10.1152/jn.1981.46.6.1192>.

Phillips, J.R., Johansson, R.S., and Johnson, K.O. (1992). Responses of human mechanoreceptive afferents to embossed dot arrays scanned across fingerpad skin. *J Neurosci* 12, 827–839. .

Pietri, T., Romano, S.A., Pérez-Schuster, V., Boulanger-Weill, J., Candat, V., and Sumbre, G. (2017). The Emergence of the Spatial Structure of Tectal Spontaneous Activity Is Independent of Visual Inputs. *Cell Rep* 19, 939–948. <https://doi.org/10.1016/j.celrep.2017.04.015>.

Platisa, J., and Pieribone, V.A. (2018). Genetically encoded fluorescent voltage indicators: are we there yet? *Curr Opin Neurobiol* 50, 146–153. <https://doi.org/10.1016/j.conb.2018.02.006>.

Ploughman, M., Windle, V., MacLellan, C.L., White, N., Doré, J.J., and Corbett, D. (2009). Brain-derived neurotrophic factor contributes to recovery of skilled reaching after focal ischemia in rats. *Stroke* 40, 1490–1495. <https://doi.org/10.1161/STROKEAHA.108.531806>.

Pnevmatikakis, E.A., Soudry, D., Gao, Y., Machado, T.A., Merel, J., Pfau, D., Reardon, T., Mu, Y., Lacefield, C., Yang, W., et al. (2016). Simultaneous Denoising, Deconvolution, and Demixing of Calcium Imaging Data. *Neuron* 89, 285–299. <https://doi.org/10.1016/j.neuron.2015.11.037>.

Pons, T.P., and Kaas, J.H. (1986). Corticocortical connections of area 2 of somatosensory cortex in macaque monkeys: a correlative anatomical and electrophysiological study. *J Comp Neurol* 248, 313–335. <https://doi.org/10.1002/cne.902480303>.

Pons, T.P., Garraghty, P.E., Cusick, C.G., and Kaas, J.H. (1985). The somatotopic organization of area 2 in macaque monkeys. *J Comp Neurol* 241, 445–466. <https://doi.org/10.1002/cne.902410405>.

Pons, T.P., Garraghty, P.E., Friedman, D.P., and Mishkin, M. (1987). Physiological evidence for serial processing in somatosensory cortex. *Science* 237, 417–420. <https://doi.org/10.1126/science.3603028>.

Pons, T.P., Garraghty, P.E., and Mishkin, M. (1992). Serial and parallel processing of tactual information in somatosensory cortex of rhesus monkeys. *J Neurophysiol* 68, 518–527. <https://doi.org/10.1152/jn.1992.68.2.518>.

Popa-Wagner, A., Badan, I., Walker, L., Groppa, S., Patrana, N., and Kessler, C. (2007). Accelerated infarct development, cytogenesis and apoptosis following transient cerebral ischemia in aged rats. *Acta Neuropathol* 113, 277–293. <https://doi.org/10.1007/s00401-006-0164-7>.

Poranen, A., and Hyvärinen, J. (1982). Effects of attention on multiunit responses to vibration in the somatosensory regions of the monkey's brain. *Electroencephalogr Clin Neurophysiol* 53, 525–537. [https://doi.org/10.1016/0013-4694\(82\)90065-7](https://doi.org/10.1016/0013-4694(82)90065-7).

- Prsa, M., Morandell, K., Cuenu, G., and Huber, D. (2019). Feature-selective encoding of substrate vibrations in the forelimb somatosensory cortex. *Nature* 567, 384–388. <https://doi.org/10.1038/s41586-019-1015-8>.
- Qi, H.-X., Lyon, D.C., and Kaas, J.H. (2002). Cortical and thalamic connections of the parietal ventral somatosensory area in marmoset monkeys (*Callithrix jacchus*). *J Comp Neurol* 443, 168–182. <https://doi.org/10.1002/cne.10113>.
- Qi, H.-X., Gharbawie, O.A., Wong, P., and Kaas, J.H. (2011). Cell-poor septa separate representations of digits in the ventroposterior nucleus of the thalamus in monkeys and prosimian galagos. *J Comp Neurol* 519, 738–758. <https://doi.org/10.1002/cne.22545>.
- Qü, M., Mittmann, T., Luhmann, H.J., Schleicher, A., and Zilles, K. (1998a). Long-term changes of ionotropic glutamate and GABA receptors after unilateral permanent focal cerebral ischemia in the mouse brain. *Neuroscience* 85, 29–43. [https://doi.org/10.1016/s0306-4522\(97\)00656-8](https://doi.org/10.1016/s0306-4522(97)00656-8).
- Qü, M., Buchkremer-Ratzmann, I., Schiene, K., Schroeter, M., Witte, O.W., and Zilles, K. (1998b). Bihemispheric reduction of GABAA receptor binding following focal cortical photothrombotic lesions in the rat brain. *Brain Res* 813, 374–380. [https://doi.org/10.1016/s0006-8993\(98\)01063-4](https://doi.org/10.1016/s0006-8993(98)01063-4).
- Que, M., Schiene, K., Witte, O.W., and Zilles, K. (1999). Widespread up-regulation of N-methyl-D-aspartate receptors after focal photothrombotic lesion in rat brain. *Neurosci Lett* 273, 77–80. [https://doi.org/10.1016/s0304-3940\(99\)00598-4](https://doi.org/10.1016/s0304-3940(99)00598-4).
- Randolph, M., and Semmes, J. (1974). Behavioral consequences of selective subtotal ablations in the postcentral gyrus of *Macaca mulatta*. *Brain Res* 70, 55–70. [https://doi.org/10.1016/0006-8993\(74\)90211-x](https://doi.org/10.1016/0006-8993(74)90211-x).
- Rao, V.L., Bowen, K.K., and Dempsey, R.J. (2001). Transient focal cerebral ischemia down-regulates glutamate transporters GLT-1 and EAAC1 expression in rat brain. *Neurochem Res* 26, 497–502. <https://doi.org/10.1023/a:1010956711295>.
- Raos, V., and Bentivoglio, M. (1993). Crosstalk between the two sides of the thalamus through the reticular nucleus: a retrograde and anterograde tracing study in the rat. *J Comp Neurol* 332, 145–154. <https://doi.org/10.1002/cne.903320202>.
- Rasmussen, A.T., and Peyton, W.T. (1948). The course and termination of the medial lemniscus in man. *J Comp Neurol* 88, 411–424. <https://doi.org/10.1002/cne.900880304>.
- Rathelot, J.-A., and Strick, P.L. (2006). Muscle representation in the macaque motor cortex: an anatomical perspective. *Proc Natl Acad Sci U S A* 103, 8257–8262. <https://doi.org/10.1073/pnas.0602933103>.
- Redecker, C., Luhmann, H.J., Hagemann, G., Fritschy, J.M., and Witte, O.W. (2000). Differential downregulation of GABAA receptor subunits in widespread brain regions in the freeze-lesion model of focal cortical malformations. *J Neurosci* 20, 5045–5053. .

Redecker, C., Wang, W., Fritschy, J.-M., and Witte, O.W. (2002). Widespread and Long-Lasting Alterations in GABAA-Receptor Subtypes after Focal Cortical Infarcts in Rats: Mediation by NMDA-Dependent Processes. *J Cereb Blood Flow Metab* 22, 1463–1475. <https://doi.org/10.1097/01.WCB.0000034149.72481.BD>.

Reep, R.L., and Corwin, J.V. (2009). Posterior parietal cortex as part of a neural network for directed attention in rats. *Neurobiol Learn Mem* 91, 104–113. <https://doi.org/10.1016/j.nlm.2008.08.010>.

Rehme, A.K., and Grefkes, C. (2013). Cerebral network disorders after stroke: evidence from imaging-based connectivity analyses of active and resting brain states in humans. *J Physiol* 591, 17–31. <https://doi.org/10.1113/jphysiol.2012.243469>.

Reinecke, S., Dinse, H.R., Reinke, H., and Witte, O.W. (2003). Induction of bilateral plasticity in sensory cortical maps by small unilateral cortical infarcts in rats. *European Journal of Neuroscience* 17, 623–627. <https://doi.org/10.1046/j.1460-9568.2003.02459.x>.

Reinert, K.C., Gao, W., Chen, G., and Ebner, T.J. (2007). Flavoprotein autofluorescence imaging in the cerebellar cortex in vivo. *J. Neurosci. Res.* 85, 3221–3232. <https://doi.org/10.1002/jnr.21348>.

Ro, T., Ellmore, T.M., and Beauchamp, M.S. (2013). A neural link between feeling and hearing. *Cereb Cortex* 23, 1724–1730. <https://doi.org/10.1093/cercor/bhs166>.

Rod, M.R., and Auer, R.N. (1989). Pre- and post-ischemic administration of dizocilpine (MK-801) reduces cerebral necrosis in the rat. *Can J Neurol Sci* 16, 340–344. <https://doi.org/10.1017/s031716710002919x>.

Romano, S.A., Pietri, T., Pérez-Schuster, V., Jouary, A., Haudrechy, M., and Sumbre, G. (2015). Spontaneous Neuronal Network Dynamics Reveal Circuit's Functional Adaptations for Behavior. *Neuron* 85, 1070–1085. <https://doi.org/10.1016/j.neuron.2015.01.027>.

Romano, S.A., Pérez-Schuster, V., Jouary, A., Boulanger-Weill, J., Candeo, A., Pietri, T., and Sumbre, G. (2017). An integrated calcium imaging processing toolbox for the analysis of neuronal population dynamics. *PLoS Comput Biol* 13, e1005526. <https://doi.org/10.1371/journal.pcbi.1005526>.

Romo, R., Hernández, A., Zainos, A., Lemus, L., and Brody, C.D. (2002). Neuronal correlates of decision-making in secondary somatosensory cortex. *Nat Neurosci* 5, 1217–1225. <https://doi.org/10.1038/nn950>.

Rossi, D.J., Oshima, T., and Attwell, D. (2000). Glutamate release in severe brain ischaemia is mainly by reversed uptake. *Nature* 403, 316–321. <https://doi.org/10.1038/35002090>.

Rossini, P.M. (2001). Tracking post-stroke recovery with magnetoencephalography. *Annals of Neurology* 49, 136–136. [https://doi.org/10.1002/1531-8249\(200101\)49:1<136::AID-ANA24>3.0.CO;2-P](https://doi.org/10.1002/1531-8249(200101)49:1<136::AID-ANA24>3.0.CO;2-P).

Rossini, P.M., Caltagirone, C., Castriota-Scanderbeg, A., Cicinelli, P., Gratta, C.D., Demartin, M., Pizzella, V., Traversa, R., and Romani, G.L. (1998). Hand motor cortical area reorganization in stroke: a study with fMRI, MEG and TCS maps. *NeuroReport* 9, 2141–2146. .

Rossini, P.M., Altamura, C., Ferreri, F., Melgari, J.-M., Tecchio, F., Tombini, M., Pasqualetti, P., and Vernieri, F. (2007). Neuroimaging experimental studies on brain plasticity in recovery from stroke. *Eura Medicophys* 43, 241–254. .

Roth, M.M., Helmchen, F., and Kampa, B.M. (2012). Distinct functional properties of primary and posteromedial visual area of mouse neocortex. *J Neurosci* 32, 9716–9726. <https://doi.org/10.1523/JNEUROSCI.0110-12.2012>.

Ruben, J., Schwiemann, J., Deuchert, M., Meyer, R., Krause, T., Curio, G., Villringer, K., Kurth, R., and Villringer, A. (2001). Somatotopic organization of human secondary somatosensory cortex. *Cereb Cortex* 11, 463–473. <https://doi.org/10.1093/cercor/11.5.463>.

Ryck, M.D., Van Reempts, J., Duytschaever, H., Van Deuren, B., and Clincke, G. (1992). Neocortical localization of tactile/proprioceptive limb placing reactions in the rat. *Brain Research* 573, 44–60. [https://doi.org/10.1016/0006-8993\(92\)90112-M](https://doi.org/10.1016/0006-8993(92)90112-M).

Saal, H.P., and Bensmaia, S.J. (2014). Touch is a team effort: interplay of submodalities in cutaneous sensibility. *Trends Neurosci.* 37, 689–697. <https://doi.org/10.1016/j.tins.2014.08.012>.

Saal, H.P., Harvey, M.A., and Bensmaia, S.J. (2015). Rate and timing of cortical responses driven by separate sensory channels. *Elife* 4, e10450. <https://doi.org/10.7554/eLife.10450>.

Sabri, M.M., Adibi, M., and Arabzadeh, E. (2016). Dynamics of Population Activity in Rat Sensory Cortex: Network Correlations Predict Anatomical Arrangement and Information Content. *Front Neural Circuits* 10, 49. <https://doi.org/10.3389/fncir.2016.00049>.

Sacco, R.L., Bello, J.A., Traub, R., and Brust, J.C. (1987). Selective proprioceptive loss from a thalamic lacunar stroke. *Stroke* 18, 1160–1163. <https://doi.org/10.1161/01.STR.18.6.1160>.

Sadagopan, S., and Wang, X. (2009). Nonlinear Spectrotemporal Interactions Underlying Selectivity for Complex Sounds in Auditory Cortex. *J Neurosci* 29, 11192–11202. <https://doi.org/10.1523/JNEUROSCI.1286-09.2009>.

Sadeh, S., and Clopath, C. (2021). Excitatory-inhibitory balance modulates the formation and dynamics of neuronal assemblies in cortical networks. *Science Advances* <https://doi.org/10.1126/sciadv.abg8411>.

Sainburg, R.L., Ghilardi, M.F., Poizner, H., and Ghez, C. (1995). Control of limb dynamics in normal subjects and patients without proprioception. *J Neurophysiol* 73, 820–835. <https://doi.org/10.1152/jn.1995.73.2.820>.

Sakata, S., and Harris, K.D. (2009). Laminar structure of spontaneous and sensory-evoked population activity in auditory cortex. *Neuron* 64, 404–418. <https://doi.org/10.1016/j.neuron.2009.09.020>.

Salimi, I., Brochier, T., and Smith, A.M. (1999a). Neuronal activity in somatosensory cortex of monkeys using a precision grip. I. Receptive fields and discharge patterns. *J Neurophysiol* *81*, 825–834. <https://doi.org/10.1152/jn.1999.81.2.825>.

Salimi, I., Brochier, T., and Smith, A.M. (1999b). Neuronal activity in somatosensory cortex of monkeys using a precision grip. II. Responses To object texture and weights. *J Neurophysiol* *81*, 835–844. <https://doi.org/10.1152/jn.1999.81.2.835>.

Salimi, I., Brochier, T., and Smith, A.M. (1999c). Neuronal activity in somatosensory cortex of monkeys using a precision grip. III. Responses to altered friction perturbations. *J Neurophysiol* *81*, 845–857. <https://doi.org/10.1152/jn.1999.81.2.845>.

Salinas, E., Hernandez, A., Zainos, A., and Romo, R. (2000). Periodicity and firing rate as candidate neural codes for the frequency of vibrotactile stimuli. *J. Neurosci.* *20*, 5503–5515. .

Saposnik, G., Kapral, M.K., Liu, Y., Hall, R., O'Donnell, M., Raptis, S., Tu, J.V., Mamdani, M., and Austin, P.C. (2011). IScore. *Circulation* *123*, 739–749. <https://doi.org/10.1161/CIRCULATIONAHA.110.983353>.

Saransaari, P., and Oja, S.S. (2008). GABA release under normal and ischemic conditions. *Neurochem Res* *33*, 962–969. <https://doi.org/10.1007/s11064-007-9499-2>.

Saver, J.L., and Yafeh, B. (2007). Confirmation of tPA treatment effect by baseline severity-adjusted end point reanalysis of the NINDS-tPA stroke trials. *Stroke* *38*, 414–416. <https://doi.org/10.1161/01.STR.0000254580.39297.3c>.

Scaglione, A., Foffani, G., and Moxon, K.A. (2014). Spike count, spike timing and temporal information in the cortex of awake, freely moving rats. *J Neural Eng* *11*, 046022. <https://doi.org/10.1088/1741-2560/11/4/046022>.

Schaechter, J.D. (2004). Motor rehabilitation and brain plasticity after hemiparetic stroke. *Progress in Neurobiology* *73*, 61–72. <https://doi.org/10.1016/j.pneurobio.2004.04.001>.

Schaechter, J.D., Moore, C.I., Connell, B.D., Rosen, B.R., and Dijkhuizen, R.M. (2006). Structural and functional plasticity in the somatosensory cortex of chronic stroke patients. *Brain* *129*, 2722–2733. <https://doi.org/10.1093/brain/awl214>.

Schallert, T., Woodlee, M.T., and Fleming, S.M. (2002). Disentangling multiple types of recovery from brain injury. *Pharmacology of Cerebral Ischemia* 201–216. .

Schiene, K., Bruehl, C., Zilles, K., Qü, M., Hagemann, G., Kraemer, M., and Witte, O.W. (1996). Neuronal hyperexcitability and reduction of GABAA-receptor expression in the surround of cerebral photothrombosis. *J Cereb Blood Flow Metab* *16*, 906–914. <https://doi.org/10.1097/00004647-199609000-00014>.

Schindelin, J., Arganda-Carreras, I., Frise, E., Kaynig, V., Longair, M., Pietzsch, T., Preibisch, S., Rueden, C., Saalfeld, S., Schmid, B., et al. (2012). Fiji: an open-source platform for biological-image analysis. *Nat Methods* *9*, 676–682. <https://doi.org/10.1038/nmeth.2019>.

Schmidt, S., Bruehl, C., Frahm, C., Redecker, C., and Witte, O.W. (2012). Age dependence of excitatory-inhibitory balance following stroke. *Neurobiol Aging* 33, 1356–1363. <https://doi.org/10.1016/j.neurobiolaging.2010.11.019>.

Scholl, B., Pattadkal, J.J., Dilly, G.A., Priebe, N.J., and Zemelman, B.V. (2015). Local Integration Accounts for Weak Selectivity of Mouse Neocortical Parvalbumin Interneurons. *Neuron* 87, 424–436. <https://doi.org/10.1016/j.neuron.2015.06.030>.

Schroeter, A., Grandjean, J., Schlegel, F., Saab, B.J., and Rudin, M. (2017). Contributions of structural connectivity and cerebrovascular parameters to functional magnetic resonance imaging signals in mice at rest and during sensory paw stimulation. *J Cereb Blood Flow Metab* 37, 2368–2382. <https://doi.org/10.1177/0271678X16666292>.

Schulte, J.T., Wierenga, C.J., and Bruining, H. (2018). Chloride transporters and GABA polarity in developmental, neurological and psychiatric conditions. *Neurosci Biobehav Rev* 90, 260–271. <https://doi.org/10.1016/j.neubiorev.2018.05.001>.

Schummers, J., Yu, H., and Sur, M. (2008). Tuned responses of astrocytes and their influence on hemodynamic signals in the visual cortex. *Science* 320, 1638–1643. <https://doi.org/10.1126/science.1156120>.

See, J.Z., Atencio, C.A., Sohal, V.S., and Schreiner, C.E. Coordinated neuronal ensembles in primary auditory cortical columns. *ELife* 7, e35587. <https://doi.org/10.7554/eLife.35587>.

Seelke, A.M.H., Padberg, J.J., Disbrow, E., Purnell, S.M., Recanzone, G., and Krubitzer, L. (2012). Topographic Maps within Brodmann's Area 5 of macaque monkeys. *Cereb Cortex* 22, 1834–1850. <https://doi.org/10.1093/cercor/bhr257>.

Serwanski, D.R., Miralles, C.P., Christie, S.B., Mehta, A.K., Li, X., and De Blas, A.L. (2006). Synaptic and nonsynaptic localization of GABAA receptors containing the alpha5 subunit in the rat brain. *J Comp Neurol* 499, 458–470. <https://doi.org/10.1002/cne.21115>.

Seto, A., Taylor, S., Trudeau, D., Swan, I., Leung, J., Reeson, P., Delaney, K.R., and Brown, C.E. (2014). Induction of ischemic stroke in awake freely moving mice reveals that isoflurane anesthesia can mask the benefits of a neuroprotection therapy. *Front Neuroenergetics* 6, 1. <https://doi.org/10.3389/fnene.2014.00001>.

Shibuki, K., Hishida, R., Murakami, H., Kudoh, M., Kawaguchi, T., Watanabe, M., Watanabe, S., Kouuchi, T., and Tanaka, R. (2003). Dynamic imaging of somatosensory cortical activity in the rat visualized by flavoprotein autofluorescence. *J. Physiol. (Lond.)* 549, 919–927. <https://doi.org/10.1113/jphysiol.2003.040709>.

Shishido, S.-I., and Toda, T. (2017). Temporal Patterns of Individual Neuronal Firing in Rat Dorsal Column Nuclei Provide Information Required for Somatosensory Discrimination. *Tohoku J. Exp. Med.* 243, 115–126. <https://doi.org/10.1620/tjem.243.115>.

Siegel, J.S., Ramsey, L.E., Snyder, A.Z., Metcalf, N.V., Chacko, R.V., Weinberger, K., Baldassarre, A., Hacker, C.D., Shulman, G.L., and Corbetta, M. (2016). Disruptions of network

connectivity predict impairment in multiple behavioral domains after stroke. *Proc Natl Acad Sci U S A* *113*, E4367–E4376. <https://doi.org/10.1073/pnas.1521083113>.

Sieghart, W., Fuchs, K., Tretter, V., Ebert, V., Jechlinger, M., Höger, H., and Adamiker, D. (1999). Structure and subunit composition of GABA(A) receptors. *Neurochem Int* *34*, 379–385. [https://doi.org/10.1016/s0197-0186\(99\)00045-5](https://doi.org/10.1016/s0197-0186(99)00045-5).

Sigler, A., Mohajerani, M.H., and Murphy, T.H. (2009). Imaging rapid redistribution of sensory-evoked depolarization through existing cortical pathways after targeted stroke in mice. *Proceedings of the National Academy of Sciences* *106*, 11759–11764. .

Silasi, G., and Murphy, T.H. (2014). Stroke and the Connectome: How Connectivity Guides Therapeutic Intervention. *Neuron* *83*, 1354–1368. <https://doi.org/10.1016/j.neuron.2014.08.052>.

Simoncelli, E.P., and Olshausen, B.A. (2001). Natural image statistics and neural representation. *Annu. Rev. Neurosci.* *24*, 1193–1216. <https://doi.org/10.1146/annurev.neuro.24.1.1193>.

Sinclair, R.J., and Burton, H. (1993). Neuronal activity in the second somatosensory cortex of monkeys (*Macaca mulatta*) during active touch of gratings. *J Neurophysiol* *70*, 331–350. <https://doi.org/10.1152/jn.1993.70.1.331>.

Smith, M.C., and Deacon, P. (1984). Topographical anatomy of the posterior columns of the spinal cord in man. The long ascending fibres. *Brain* *107 (Pt 3)*, 671–698. <https://doi.org/10.1093/brain/107.3.671>.

Smith, J.B., Chakrabarti, S., Mowery, T.M., and Alloway, K.D. (2022). Convergence of forepaw somatosensory and motor cortical projections in the striatum, claustrum, thalamus, and pontine nuclei of cats. *Brain Struct Funct* *227*, 361–379. <https://doi.org/10.1007/s00429-021-02405-6>.

Sommer, C.J. (2017). Ischemic stroke: experimental models and reality. *Acta Neuropathol* *133*, 245–261. <https://doi.org/10.1007/s00401-017-1667-0>.

Soso, M.J., and Fetz, E.E. (1980). Responses of identified cells in postcentral cortex of awake monkeys during comparable active and passive joint movements. *J Neurophysiol* *43*, 1090–1110. <https://doi.org/10.1152/jn.1980.43.4.1090>.

Sporns, O. (2011). The non-random brain: efficiency, economy, and complex dynamics. *Front Comput Neurosci* *5*, 5. <https://doi.org/10.3389/fncom.2011.00005>.

Sporns, O., Honey, C.J., and Kötter, R. (2007). Identification and Classification of Hubs in Brain Networks. *PLOS ONE* *2*, e1049. <https://doi.org/10.1371/journal.pone.0001049>.

Staines, W.R., Graham, S.J., Black, S.E., and McIlroy, W.E. (2002a). Task-relevant modulation of contralateral and ipsilateral primary somatosensory cortex and the role of a prefrontal-cortical sensory gating system. *Neuroimage* *15*, 190–199. <https://doi.org/10.1006/nimg.2001.0953>.

Staines, W.R., Black, S.E., Graham, S.J., and McIlroy, W.E. (2002b). Somatosensory gating and recovery from stroke involving the thalamus. *Stroke* *33*, 2642–2651.

<https://doi.org/10.1161/01.str.0000032552.40405.40>.

Stam, C.J. (2014). Modern network science of neurological disorders. *Nat Rev Neurosci* *15*, 683–695. <https://doi.org/10.1038/nrn3801>.

Stepniewska, I., Preuss, T.M., and Kaas, J.H. (1993). Architectonics, somatotopic organization, and ipsilateral cortical connections of the primary motor area (M1) of owl monkeys. *J Comp Neurol* *330*, 238–271. <https://doi.org/10.1002/cne.903300207>.

Storchi, R., Zippo, A.G., Caramenti, G.C., Valente, M., and Biella, G.E.M. (2012). Predicting spike occurrence and neuronal responsiveness from LFPs in primary somatosensory cortex. *PLoS ONE* *7*, e35850. <https://doi.org/10.1371/journal.pone.0035850>.

Stosiek, C., Garaschuk, O., Holthoff, K., and Konnerth, A. (2003). In vivo two-photon calcium imaging of neuronal networks. *Proceedings of the National Academy of Sciences* *100*, 7319–7324. .

Suzuki, Y., Gyoba, J., and Sakamoto, S. (2008). Selective effects of auditory stimuli on tactile roughness perception. *Brain Res* *1242*, 87–94. <https://doi.org/10.1016/j.brainres.2008.06.104>.

Sweetnam, D.A., and Brown, C.E. (2013). Stroke induces long-lasting deficits in the temporal fidelity of sensory processing in the somatosensory cortex. *J Cereb Blood Flow Metab* *33*, 91–96. <https://doi.org/10.1038/jcbfm.2012.135>.

Sweetnam, D., Holmes, A., Tennant, K.A., Zamani, A., Walle, M., Jones, P., Wong, C., and Brown, C.E. (2012). Diabetes Impairs Cortical Plasticity and Functional Recovery Following Ischemic Stroke. *J Neurosci* *32*, 5132–5143. <https://doi.org/10.1523/JNEUROSCI.5075-11.2012>.

Tada, M., Takeuchi, A., Hashizume, M., Kitamura, K., and Kano, M. (2014). A highly sensitive fluorescent indicator dye for calcium imaging of neural activity in vitro and in vivo. *Eur J Neurosci* *39*, 1720–1728. <https://doi.org/10.1111/ejn.12476>.

Takeuchi, N., and Izumi, S.-I. (2012). Maladaptive plasticity for motor recovery after stroke: mechanisms and approaches. *Neural Plast* *2012*, 359728. <https://doi.org/10.1155/2012/359728>.

Talbot, W.H., Darian-Smith, I., Kornhuber, H.H., and Mountcastle, V.B. (1968). The sense of flutter-vibration: comparison of the human capacity with response patterns of mechanoreceptive afferents from the monkey hand. *J Neurophysiol* *31*, 301–334. <https://doi.org/10.1152/jn.1968.31.2.301>.

Taoka, M., Toda, T., Iriki, A., Tanaka, M., and Iwamura, Y. (2000). Bilateral receptive field neurons in the hindlimb region of the postcentral somatosensory cortex in awake macaque monkeys. *Exp Brain Res* *134*, 139–146. <https://doi.org/10.1007/s002210000464>.

Taoka, M., Toda, T., Hihara, S., Tanaka, M., Iriki, A., and Iwamura, Y. (2016). A systematic analysis of neurons with large somatosensory receptive fields covering multiple body regions in the secondary somatosensory area of macaque monkeys. *J Neurophysiol* *116*, 2152–2162. <https://doi.org/10.1152/jn.00241.2016>.

- Tennant, K.A., Taylor, S.L., White, E.R., and Brown, C.E. (2017). Optogenetic rewiring of thalamocortical circuits to restore function in the stroke injured brain. *Nat Commun* 8, 15879. <https://doi.org/10.1038/ncomms15879>.
- Thompson, A.W., and Scott, E.K. (2016). Characterisation of sensitivity and orientation tuning for visually responsive ensembles in the zebrafish tectum. *Sci Rep* 6, 34887. <https://doi.org/10.1038/srep34887>.
- Tommerdahl, M., Whitsel, B.L., Favorov, O.V., Metz, C.B., and O'Quinn, B.L. (1999). Responses of contralateral SI and SII in cat to same-site cutaneous flutter versus vibration. *J Neurophysiol* 82, 1982–1992. <https://doi.org/10.1152/jn.1999.82.4.1982>.
- Tommerdahl, M., Favorov, O.V., and Whitsel, B.L. (2005). Effects of high-frequency skin stimulation on SI cortex: mechanisms and functional implications. *Somatosens Mot Res* 22, 151–169. <https://doi.org/10.1080/08990220500084461>.
- Torrealba, F., and Valdés, J.L. (2008). The parietal association cortex of the rat. *Biol Res* 41, 369–377. <https://doi.org/S0716-97602008000400002>.
- Tremblay, N., Bushnell, M.C., and Duncan, G.H. (1993). Thalamic VPM nucleus in the behaving monkey. II. Response to air-puff stimulation during discrimination and attention tasks. *J Neurophysiol* 69, 753–763. <https://doi.org/10.1152/jn.1993.69.3.753>.
- Tremblay, R., Lee, S., and Rudy, B. (2016). GABAergic interneurons in the neocortex: From cellular properties to circuits. *Neuron* 91, 260–292. <https://doi.org/10.1016/j.neuron.2016.06.033>.
- Truccolo, W., Hochberg, L.R., and Donoghue, J.P. (2010). Collective dynamics in human and monkey sensorimotor cortex: predicting single neuron spikes. *Nat Neurosci* 13, 105–111. <https://doi.org/10.1038/nn.2455>.
- Tutunculer, B., Foffani, G., Himes, B.T., and Moxon, K.A. (2006). Structure of the excitatory receptive fields of infragranular forelimb neurons in the rat primary somatosensory cortex responding to touch. *Cereb. Cortex* 16, 791–810. <https://doi.org/10.1093/cercor/bhj023>.
- Tyson, S.F., Hanley, M., Chillala, J., Selley, A.B., and Tallis, R.C. (2008). Sensory loss in hospital-admitted people with stroke: characteristics, associated factors, and relationship with function. *Neurorehabil Neural Repair* 22, 166–172. <https://doi.org/10.1177/1545968307305523>.
- Urbin, M.A., Hong, X., Lang, C.E., and Carter, A.R. (2014). Resting-state functional connectivity and its association with multiple domains of upper-extremity function in chronic stroke. *Neurorehabil Neural Repair* 28, 761–769. <https://doi.org/10.1177/1545968314522349>.
- Vallbo, A.B., Olausson, H., Wessberg, J., and Kakuda, N. (1995). Receptive field characteristics of tactile units with myelinated afferents in hairy skin of human subjects. *J Physiol* 483 (Pt 3), 783–795. <https://doi.org/10.1113/jphysiol.1995.sp020622>.
- Vardar, B., and Güçlü, B. (2017). Non-NMDA receptor-mediated vibrotactile responses of neurons from the hindpaw representation in the rat SI cortex. *Somatosens Mot Res* 34, 189–203.

<https://doi.org/10.1080/08990220.2017.1390450>.

Vardar, B., and Güçlü, B. (2020). Effects of basal forebrain stimulation on the vibrotactile responses of neurons from the hindpaw representation in the rat SI cortex. *Brain Struct Funct* 225, 1761–1776. <https://doi.org/10.1007/s00429-020-02091-w>.

Vázquez, Y., Zainos, A., Alvarez, M., Salinas, E., and Romo, R. (2012). Neural coding and perceptual detection in the primate somatosensory thalamus. *Proc Natl Acad Sci U S A* 109, 15006–15011. <https://doi.org/10.1073/pnas.1212535109>.

Velayos, J.L., Jiménez-Castellanos, J., and Reinoso-Suárez, F. (1989). Topographical organization of the projections from the reticular thalamic nucleus to the intralaminar and medial thalamic nuclei in the cat. *J Comp Neurol* 279, 457–469. <https://doi.org/10.1002/cne.902790310>.

Vemuganti, R. (2005). Decreased expression of vesicular GABA transporter, but not vesicular glutamate, acetylcholine and monoamine transporters in rat brain following focal ischemia. *Neurochem Int* 47, 136–142. <https://doi.org/10.1016/j.neuint.2005.04.015>.

Villette, V., Malvache, A., Tressard, T., Dupuy, N., and Cossart, R. (2015). Internally Recurring Hippocampal Sequences as a Population Template of Spatiotemporal Information. *Neuron* 88, 357–366. <https://doi.org/10.1016/j.neuron.2015.09.052>.

Virani, S.S., Alonso, A., Aparicio, H.J., Benjamin, E.J., Bittencourt, M.S., Callaway, C.W., Carson, A.P., Chamberlain, A.M., Cheng, S., Delling, F.N., et al. (2021). Heart Disease and Stroke Statistics—2021 Update. *Circulation* 143, e254–e743. <https://doi.org/10.1161/CIR.0000000000000950>.

Vogelstein, J.T., Packer, A.M., Machado, T.A., Sippy, T., Babadi, B., Yuste, R., and Paninski, L. (2010). Fast Nonnegative Deconvolution for Spike Train Inference From Population Calcium Imaging. *J Neurophysiol* 104, 3691–3704. <https://doi.org/10.1152/jn.01073.2009>.

Walker, M.C., and Semyanov, A. (2008). Regulation of excitability by extrasynaptic GABA(A) receptors. *Results Probl Cell Differ* 44, 29–48. https://doi.org/10.1007/400_2007_030.

Wallace, M.N. (1987). Histochemical demonstration of sensory maps in the rat and mouse cerebral cortex. *Brain Research* 418, 178–182. [https://doi.org/10.1016/0006-8993\(87\)90977-2](https://doi.org/10.1016/0006-8993(87)90977-2).

Walsh, C.M., Bautista, D.M., and Lumpkin, E.A. (2015). Mammalian touch catches up. *Curr Opin Neurobiol.* 34, 133–139. <https://doi.org/10.1016/j.conb.2015.05.003>.

Wang, Y.-C., Dzyubenko, E., Sanchez-Mendoza, E.H., Sardari, M., Silva de Carvalho, T., Doepfner, T.R., Kaltwasser, B., Machado, P., Kleinschnitz, C., Bassetti, C.L., et al. (2018). Postacute Delivery of GABAA $\alpha 5$ Antagonist Promotes Postischemic Neurological Recovery and Peri-infarct Brain Remodeling. *Stroke* 49, 2495–2503. <https://doi.org/10.1161/STROKEAHA.118.021378>.

Ward, N.S., Brown, M.M., Thompson, A.J., and Frackowiak, R.S.J. (2003). Neural correlates of motor recovery after stroke: a longitudinal fMRI study. *Brain* 126, 2476–2496.

<https://doi.org/10.1093/brain/awg245>.

Weber, A.I., Saal, H.P., Lieber, J.D., Cheng, J.-W., Manfredi, L.R., Dammann, J.F., and Bensmaia, S.J. (2013). Spatial and temporal codes mediate the tactile perception of natural textures. *Proc Natl Acad Sci U S A* *110*, 17107–17112. <https://doi.org/10.1073/pnas.1305509110>.

Weber, B., Burger, C., Wyss, M.T., von Schulthess, G.K., Scheffold, F., and Buck, A. (2004). Optical imaging of the spatiotemporal dynamics of cerebral blood flow and oxidative metabolism in the rat barrel cortex. *Eur. J. Neurosci.* *20*, 2664–2670. <https://doi.org/10.1111/j.1460-9568.2004.03735.x>.

Weber, R., Ramos-Cabrer, P., Justicia, C., Wiedermann, D., Strecker, C., Sprenger, C., and Hoehn, M. (2008). Early Prediction of Functional Recovery after Experimental Stroke: Functional Magnetic Resonance Imaging, Electrophysiology, and Behavioral Testing in Rats. *Journal of Neuroscience* *28*, 1022–1029. <https://doi.org/10.1523/JNEUROSCI.4147-07.2008>.

Welker, C. (1971). Microelectrode delineation of fine grain somatotopic organization of (SmI) cerebral neocortex in albino rat. *Brain Res* *26*, 259–275. .

Welker, C. (1976). Receptive fields of barrels in the somatosensory neocortex of the rat. *J Comp Neurol* *166*, 173–189. <https://doi.org/10.1002/cne.901660205>.

Winship, I.R., and Murphy, T.H. (2008). In vivo calcium imaging reveals functional rewiring of single somatosensory neurons after stroke. *J. Neurosci.* *28*, 6592–6606. <https://doi.org/10.1523/JNEUROSCI.0622-08.2008>.

Winship, I.R., and Murphy, T.H. (2009). Remapping the somatosensory cortex after stroke: insight from imaging the synapse to network. *Neuroscientist* *15*, 507–524. <https://doi.org/10.1177/1073858409333076>.

Winship, I.R., Plaa, N., and Murphy, T.H. (2007). Rapid astrocyte calcium signals correlate with neuronal activity and onset of the hemodynamic response in vivo. *J. Neurosci.* *27*, 6268–6272. <https://doi.org/10.1523/JNEUROSCI.4801-06.2007>.

Witney, A.G., Wing, A., Thonnard, J.-L., and Smith, A.M. (2004). The cutaneous contribution to adaptive precision grip. *Trends Neurosci* *27*, 637–643. <https://doi.org/10.1016/j.tins.2004.08.006>.

Witte, O.W., and Freund, H.J. (1999). Neuronal dysfunction, epilepsy, and postlesional brain plasticity. *Adv Neurol* *81*, 25–36. .

Woolsey, T.A. (1967). Somatosensory, auditory and visual cortical areas of the mouse. *Johns Hopkins Med J* *121*, 91–112. .

Wu, H., Williams, J., and Nathans, J. (2012). Morphologic diversity of cutaneous sensory afferents revealed by genetically directed sparse labeling. *ELife* *1*, e00181. <https://doi.org/10.7554/eLife.00181>.

- Xie, Y., Chen, S., Wu, Y., and Murphy, T. (2014). Prolonged Deficits in Parvalbumin Neuron Stimulation-Evoked Network Activity Despite Recovery of Dendritic Structure and Excitability in the Somatosensory Cortex following Global Ischemia in Mice. *J Neurosci* 34, 14890–14900. <https://doi.org/10.1523/JNEUROSCI.1775-14.2014>.
- Xu, J., and Wall, J.T. (1996). Cutaneous representations of the hand and other body parts in the cuneate nucleus of a primate, and some relationships to previously described cortical representations. *Somatosens Mot Res* 13, 187–197. <https://doi.org/10.3109/08990229609052575>.
- Xu, J., and Wall, J.T. (1999). Functional organization of tactile inputs from the hand in the cuneate nucleus and its relationship to organization in the somatosensory cortex. *J Comp Neurol* 411, 369–389. .
- Xu, X., Ye, L., and Ruan, Q. (2009). Environmental enrichment induces synaptic structural modification after transient focal cerebral ischemia in rats. *Exp Biol Med (Maywood)* 234, 296–305. <https://doi.org/10.3181/0804-RM-128>.
- Yang, H.H., and St-Pierre, F. (2016). Genetically Encoded Voltage Indicators: Opportunities and Challenges. *J Neurosci* 36, 9977–9989. <https://doi.org/10.1523/JNEUROSCI.1095-16.2016>.
- Yau, J.M., Connor, C.E., and Hsiao, S.S. (2013). Representation of tactile curvature in macaque somatosensory area 2. *J Neurophysiol* 109, 2999–3012. <https://doi.org/10.1152/jn.00804.2012>.
- Yu, J., Gutnisky, D.A., Hires, S.A., and Svoboda, K. (2016). Layer 4 fast-spiking interneurons filter thalamocortical signals during active somatosensation. *Nat. Neurosci.* 19, 1647–1657. <https://doi.org/10.1038/nn.4412>.
- Yumiya, H., Kubota, K., and Asanuma, H. (1974). Activities of neurons in area 3a of the cerebral cortex during voluntary movements in the monkey. *Brain Res* 78, 169–177. [https://doi.org/10.1016/0006-8993\(74\)90544-7](https://doi.org/10.1016/0006-8993(74)90544-7).
- Zhang, S., and Murphy, T.H. (2007). Imaging the impact of cortical microcirculation on synaptic structure and sensory-evoked hemodynamic responses in vivo. *PLoS Biol* 5, e119. <https://doi.org/10.1371/journal.pbio.0050119>.
- Zhang, S., Boyd, J., Delaney, K., and Murphy, T.H. (2005). Rapid reversible changes in dendritic spine structure in vivo gated by the degree of ischemia. *J Neurosci* 25, 5333–5338. <https://doi.org/10.1523/JNEUROSCI.1085-05.2005>.
- Zhao, C., Puurunen, K., Schallert, T., Sivenius, J., and Jolkkonen, J. (2005). Effect of cholinergic medication, before and after focal photothrombotic ischemic cortical injury, on histological and functional outcome in aged and young adult rats. *Behavioural Brain Research* 156, 85–94. <https://doi.org/10.1016/j.bbr.2004.05.011>.
- Zimmerman, A., Bai, L., and Ginty, D.D. (2014). The gentle touch receptors of mammalian skin. *Science* 346, 950–954. <https://doi.org/10.1126/science.1254229>.
- Zimny, M.L. (1988). Mechanoreceptors in articular tissues. *Am J Anat* 182, 16–32.

<https://doi.org/10.1002/aja.1001820103>.